Calcium signalling in atrial myocytes and potential targets for atrial fibrillation

Emily Claudie Leigh Akerman

Linacre College

University of Oxford

Submission for the degree of Doctor of Philosophy

Michaelmas 2024

Thesis was supervised by:

Professor Rebecca Ann Beatrice Burton
Department of Pharmacology

And

Professor Manuela Zaccolo
Department of Physiology, Anatomy & Genetics

Acknowledgements:

I would like to thank my thesis director Prof. Rebecca Burton, who has supervised me since my master's internship and until today. I learned so much thanks to her scientific skills and expertise in the field of cardiac physiology which always stimulated my scientific curiosity. Thank you for the training you gave me, your availability, and your wise advice. You taught me to be independent from the start and that nothing is impossible.

I would like to thank Prof. Manuela Zaccolo for welcoming me into her lab. The FRET work was carried out in the Department of Physiology, Anatomy and Genetics at the University of Oxford. I thank you for your kindness and your very, very precious advice throughout this body of work.

A very special thank you to Dr Rebecca Capel and Dr Sam Bose, with whom I shared the first half of my project in the lab with, precious time filled with experiments and discussions. Thank you very much for your support in shaping my thesis from the start. It was always a pleasure to learn and improve my skills from the both of you thanks to your expertise and advice. You both were always ready to listen to all my doctoral questions.

To Dr Thamali Ayagama, Qianqian and Matt, who brought me all their respective knowledge and sympathy during these years of collaboration. Thank you for our long, more or less serious discussions, our laughter, our snack breaks and our great cohesion. I am delighted to have met you and to have shared these good times with you.

I will now thank my family, who are very dear to me: my parents, my grandparents, my brother. It wasn't always easy for you to understand exactly what I was doing, but you all always showed great interest, and support.

Massive thanks to my friends Muji, Laure, Phyphy, Sasha, Leo, and Jeyson for always bringing a little more laughter and craziness into my life. Thank you all for filling my time out of the lab with wonderful memories.

To all the collaborators that I had the pleasure of meeting and who participated, directly or indirectly, in the development of the articles presented in this thesis. May they find here all my gratitude. Thank you to all the members of the Department of Pharmacology who made this adventure very much enjoyable.

Abstract:

Atrial fibrillation (AF) is the most common sustained cardiac arrhythmia (incidence 1-2%). Age-related increases in the risk for AF contribute to 14% of strokes in the UK, which is a significant health burden. Certain treatment modalities, like catheter ablation, have some associated morbidity/mortality concerns and are not always 100% effective. Traditional antiarrhythmic drugs do not have specific intracellular targets; hence it is critical to comprehend the molecular pathophysiology of AF. Calcium homeostasis is a vital signalling mechanism in the heart and alterations in the intracellular concentration of calcium have been shown to lead to arrhythmias. My thesis involves investigations of calcium handling pathways through adrenoceptor stimulation, using isoprenaline for β-adrenergic stimulation and phenylephrine for α-adrenergic stimulation.

I investigated the very potent lysosomal calcium releasing molecule nicotinic acid adenine dinucleotide phosphate (NAADP) and I present evidence that lysosomal calcium, acting through NAADP-mediated stimulation of two-pore channels 2 (TPC2), makes a significant contribution to atrial function and pacemaking. My experiments reveal that lysosomal calcium release directly modulates cyclic adenosine monophosphate (cAMP) upstream to the previously reported effects on sarcoplasmic reticulum (SR) calcium content and calcium handling in neonatal rat atrial myocytes and human induced pluripotent stem cell derived cardiomyocytes. Electron *microscopy* measurements highlight a close spatial relationship between lysosomes and the SR to be altered in human AF tissue samples. In addition to NAADP signalling, I investigated inositol 1,4,5-trisphosphate (IP_3) signalling. The work presented here brings together two major aspects of calcium handling: NAADP signalling and IP_3 signalling and for the first-time probes these pathways in human cells. The experiments investigate the interplay between IP_3-mediated calcium release from the SR and NAADP-mediated calcium release from lysosomes in atrial cells.

In conclusion, my thesis provides evidence that IP_3 and NAADP regulate the release of calcium from intracellular stores in atrial myocytes and influence cardiac function including pacemaking and presents the translational value of my research by investigating these pathways in humans.

Publications list:

Bose SJ, Read MJ, **Akerman E**, Capel RA, Ayagama T, Russell A, Terrar DA, Zaccolo M, Burton RAB. Inhibition of adenylyl cyclase 1 by ST034307 inhibits IP_3-evoked changes in sino-atrial node beat rate. Front Pharmacol. 2022 Aug 29;13:951897. doi: 10.3389/fphar.2022.951897. PMID: 36105228; PMCID: PMC9465815. Chapter 4

Capel RA*, **Akerman E***, Rog-Zielinska EA, Winbo A, Aston D, Mu-u-min RBA, et al. "Lysosomal signalling pathways influence heart rhythm and regulate atrial function. 2024. bioRxiv: 2024.2006.2010.597905. Chapter 3

Akerman E*, Read MJ*, Bose SJ*, Koschinski A, Capel RA, Chao YC, Folkmanaite M, Hester S, Fischer R, Ayagama T, Broadbent SD, Ahamed R, Simon JN, Terrar DA, Zaccolo M, Burton RAB. Activation of IP_3R in atrial cardiomyocytes leads to generation of cytosolic cAMP. bioRxiv: 2024.03.28.583721; doi: https://doi.org/10.1101/2024.03.28.583721. Chapter 4 and 5.

In preparation:

Akerman E, Read MJ, Bose SJ, Capel RA, Song Q, Winbo A, Koschinski A, Calamaio S, Melgari D, Prevostini R, Rivolta I, Zaccolo Z, Terrar DA, Burton RAB. Lysosomal calcium signalling contributes to the acute α-adrenergic response. Chapter 5

Akerman E, Daniel Aston, Eva A. Rog-Zielinska, Barry Boland, Ulrich Schotten, Sander Verheule, Rebecca A Capel, Rebecca A.B. Burton. Atrial Granules in Atrial Cardiomyocytes as Acidic Calcium Stores.

Abbreviations:

α-AR	α-adrenergic receptor
AC	Adenylyl cyclases
AF	Atrial fibrillation
ANS	Autonomic nervous system
AP	Action potential
APD	Action potential duration
ATP	Adenosine triphosphate
AVN	Atrioventricular node
β-AR	β-adrenergic receptors
BPM	Beats per minute
CaMKII	Calcium/calmodulin-stimulated protein kinase II
cAMP	Cyclic adenosine monophosphate
cDNA	Complementary DNA
cGMP	Cyclic guanine monophosphate
CI	Confidence interval
CICR	Calcium induced calcium release
Cx	Connexins
DADs	Delayed afterdepolarizations
DAG	Diacylglycerol
DKO	Double knockout
DNA	Deoxyribonucleic Acid
EADs	Early afterdepolarizations
ECC	Excitation-contraction coupling
ECG	Electrocardiogram
EM	Electron microscopy
ER	Endoplasmic reticulum
FRET	Fluorescence resonance energy transfer
HCN	Hyperpolarization-activated Cyclic Nucleotide-gated channels
hiPSCs	Human induced pluripotent stem cells
hiPSC-aCMs	Human induced pluripotent stem cell derived atrial cardiomyocytes
hiPSC-CMs	Human induced pluripotent stem cell derived cardiomyocytes
IP_3	1,4,5-trisphosphate
IP_3R	1,4,5-trisphosphate receptor
KO	Knockout
LAMP	Lysosome-associated membrane protein
LKB1	Cardiac-specific liver kinase B1
LTCC	L-type calcium channel
PE	Phenylephrine
PLC	Phospholipase C
PKA	Protein kinase A
POPDC	Popeye domain containing protein
MP	Membrane potential
mRNA	Messenger RNA

NAADP	Nicotinic acid adenine dinucleotide phosphate
NCX	Sodium/calcium exchanger
NMAMs	Neonatal mouse atrial myocytes
NRAMs	Neonatal rat atrial myocytes
NRVMs	Neonatal rat ventricular myocytes
PMCA	Plasma Membrane Calcium-ATPase
RNA	Ribonucleic acid
RP	Resting potential
RT-PCR	Reverse transcriptase polymerase chain reaction
RyR	Ryanodine receptors
SD	Standard deviation
SERCA2	Sarcoplasmic/endoplasmic reticulum calcium ATPase
SEM	Standard error of the mean
SR	Sarcoplasmic reticulum
SAN	Sinoatrial node
TTCC	T-type calcium channel
TPC	Two-pore channel
TRPML	Transient receptor potential cation channel mucolipin
V-ATPase	ATP-dependent vacuolar-type proton pump
WT	Wild type

Table of Figures:

Table of Contents

1 Introduction: A general introduction

1.1 Structure of the heart

The heart is a four-chambered muscular organ located in the thoracic cavity divided into two upper chambers (left and right atria) and two lower chambers (left and right ventricles) (Figure 1.1). The human heart is protectively located in the thoracic region between two lungs posterior to the sternum and resting on the superior surface of the diaphragm (Bittihn 2014). The heart is surrounded by the pericardium.

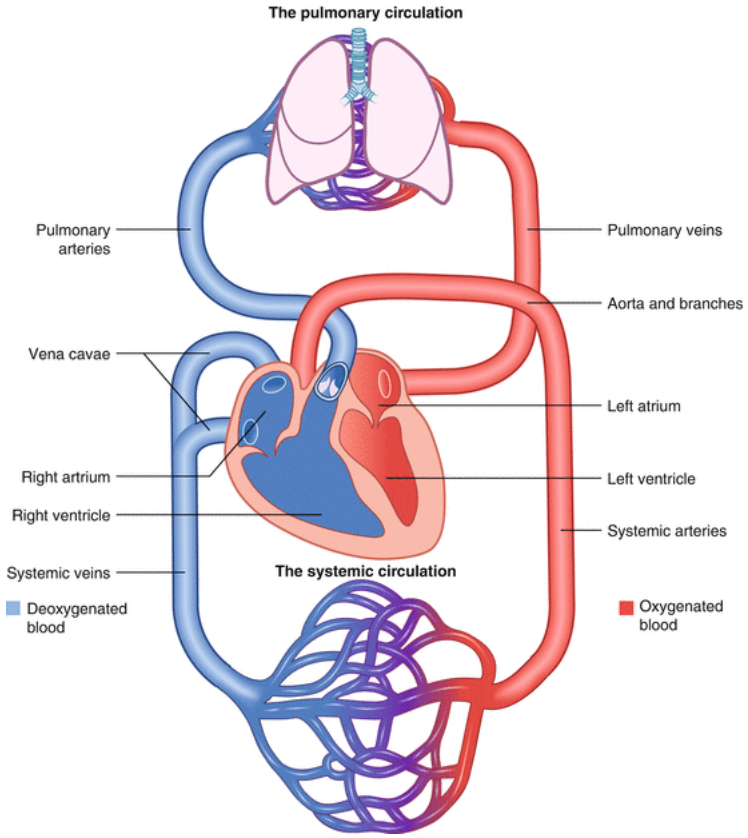

Figure 1.1: Illustration of the heart anatomy and cardiovascular system divided into systemic and pulmonary circulation. Figure obtained with permission from (Rehfeld, Nylander, and Karnov 2017).

A double pump ensures a rapid distribution of oxygen, nutriments, heat, and elimination of waste to support tissue function. There are two circulations in this system: [1] The systemic circulation and [2] the pulmonary circulation (Figure 1.1). This double-circulatory system is divided completely, the one from the other and consists of two chambers, an atrium, and a ventricle. The systemic circulation (left atrium and left ventricle) is responsible for delivering oxygenated blood and nutrients throughout the body through the aorta, arteries and arterioles, and transports waste products to the liver and kidneys. Organs and tissues are irrigated with oxygen and nutrients by capillaries. After supplying the organs and tissues, the blood is

depleted in oxygen and needs to return to the lungs. This is the pulmonary circulation, the blood returns to the heart via the right atrium and right ventricle to be then sent to the lungs to be oxygenated and get rid of excess carbon dioxide.

There are four valves in the heart that allow blood flow in the same direction and prevent backward flow of blood (Bittihn 2014). Blood enters the heart from the inferior and superior vena cava, passes through the right atrium and is ejected through the right ventricle. In the same way, the blood reaches the left heart via the pulmonary veins, transits to the left atrium and is expelled towards the body by the left ventricle. The tricuspid valve prevents backflow of blood from the right ventricle to the right atrium and the pulmonary valve prevents backflow from the pulmonary artery to the right ventricle. The mitral valve plays the same role as the tricuspid valve between the left ventricle and the left atrium while the aortic valve plays the same role as the pulmonary valve between the aorta and the left ventricle (Bittihn 2014).

1.1.1 Anatomical structure of atria

The fibrous structure of the atria makes a complex tissue and is difficult to distinguish even at a microscopic level during imaging. In addition, the anatomy of the atria differs from one patient to another creating complexity and variability in studies. The atria can be seen as two conjoined half-spheres linked together by complex fibre bundles (Katz 2010). The wall between these two half-spheres is commonly referred to as the septal wall. The right atrium has a triangular appendage with an inhomogeneous texture. The inferior and superior vena cava insert into the right atrium. The sinoatrial node (SAN), the starting point of the depolarization wave, is located along the crista terminalis, at the junction between the atrial tissue and vena cava. The left atrium appears as homogeneous tissue in contrast to the right atrium. The transverse (t)-tubule system in the atria c of small mammals is relatively underdeveloped compared to that of the ventricles (Frisk et al. 2014), however recent observations highlight a more extensive t-tubule network in horse, cow and human atrial myocytes (Richards et al. 2011). The t-tubule system is an integral part of the surface membrane that allows the placement of voltage-gated L-type calcium channels (LTCC) in close proximity to clusters of ryanodine receptors (RyR), calcium release channels in the sarcoplasmic reticulum (SR) membrane (Blatter 2017).

The septum of the atria allows the 4 chambers of the heart to be electrically isolated from each other. However, there are inter-atrial connections. The three main connections observed are: the Bachmann bundle, the fossa-ovalis and the coronary sinus (Das, Banerjee, and Mandal

2016). The Bachmann bundle is a network of fibres that inserts into the right atrium at the base of the crista terminalis, below the superior vena cava. It passes through the septal wall of both atria to insert into the septal portion of the left atrium in two places. This bundle ensures rapid electrical conduction from the sinus node, via the crista terminalis, to the anterior wall of the left atrium. The fossa ovalis is a trans-septal cavity, in both the left and right atrium, blocked by a piece of non-conductive tissue allowing slow trans septal conduction. Finally, the coronary sinus is a venous structure opening into the lower part of the right atrium. The muscle fibres of the right atrium wrap around it and can sometimes intertwine with the circumferential bundle of the vestibule of the left atrium (Katz 2010).

1.1.2 Anatomical structure of ventricles

The adult ventricular myocardium is a muscle made of a three-dimensional network of myocardial cells forming a thick-walled pressure vessel. This highly structured network has been described as a multi-layered structure where each layer of myocardial cells has a preferred orientation and notable variations in the curvature and the thickness of the wall both regionally and temporally through the cardiac cycle (Sanchez-Quintana et al. 1995). The myocardium is present in the walls of all four chambers of the heart but is thicker in the ventricles compared to the atria and is thicker in the left ventricle than in the right ventricle. The difference in thickness is due to the difference in the generation of the force of contraction needed to eject blood out of the chamber, with the left ventricle requiring much more power. This ensures that each chamber generates the appropriate amount of pressure for its specific function without overworking.

1.2 Cardiac electrical activity: muscle and cell structure

To assure blood flow throughout the heart and body, a continuous and regulated contraction and relaxation of the heart is essential, this is the cardiac contraction-relaxation cycle (Bittihn 2014). This contraction is triggered by automatic cardiac electrical activity.

1.2.1 Cardiac muscle

The electrical activity of the heart is a complex phenomenon strongly linked to its architecture. The muscle wall, called myocardium, is made up of elongated muscle cells called myocytes, organised into fibres and then into overlapping layers from the innermost part of the wall, the endocardium, to the outer part, the epicardium. This fibrous structuring has two main effects: an optimisation of the mechanical function of the heart and an anisotropic propagation of the

electrical activity. Electrical activity is generated spontaneously by pacemaker cells in the SAN, the centre of rhythm generation and cardiac automatism located in the right atrium. These cells will spontaneously depolarise which will trigger an action potential (AP). This depolarisation will be the origin of the contraction of the cardiomyocytes. From the SAN, the AP created propagates through the atria to reach the atrioventricular node (AVN) and be slowed. The propagation enters the ventricular walls and transmits the depolarization to myocytes. The AP then takes different conduction pathways throughout the ventricles which will ultimately lead to the contraction of the heart. The AP travels through an order: the bundles of His, the Tawara fibres and the Purkinje fibres, which contracts from the apex to the base of the ventricles and from the endocardium to the epicardium to ensure synchronous contraction of the ventricles (Anderson et al. 2013). Contraction of cardiac muscle involves the co-ordination of multiple, precisely regulated signalling pathways, summarised by the process of excitation-contraction coupling (ECC).

The spread of electrical activity within the heart can be recorded using an electrocardiogram (ECG), invented by Willem Einthoven (Fye 1994), which uses electrodes placed on the surface of the body to observe the propagation of AP in the heart (Figure 1.2A). The electrocardiographic trace is broken down into different waves and intervals, which are characteristic of the electrical activity of different regions of the heart. The P wave corresponds to the depolarisation and contraction of the atria (the repolarisation is not visible), the PR interval represents the AVN conduction time more precisely, the depolarisation of the AVN and the bundle of His and its branches. The QRS complex corresponds to the depolarisation and contraction of the ventricles, the ST segment represents phase 2 of AP plateau and the T wave corresponds to the depolarisation and relaxation of the ventricles (Katz 2010). Atrial repolarisation is not visible but takes place during the QRS complex. The QT interval represents the average duration of depolarisation and repolarisation of the ventricles. In the clinic, the ECG is used in the diagnosis of heart rhythm disorders such as atrial fibrillation (AF). The cardiac conduction of a normal heart and an AF heart can be distinguished through an ECG (Figure 1.2B and C). An ECG of AF patients has distinct features, such as the absence of the P wave due to the interruption caused by the uncoordinated depolarisations of atrial myocytes (Husser et al. 2007).

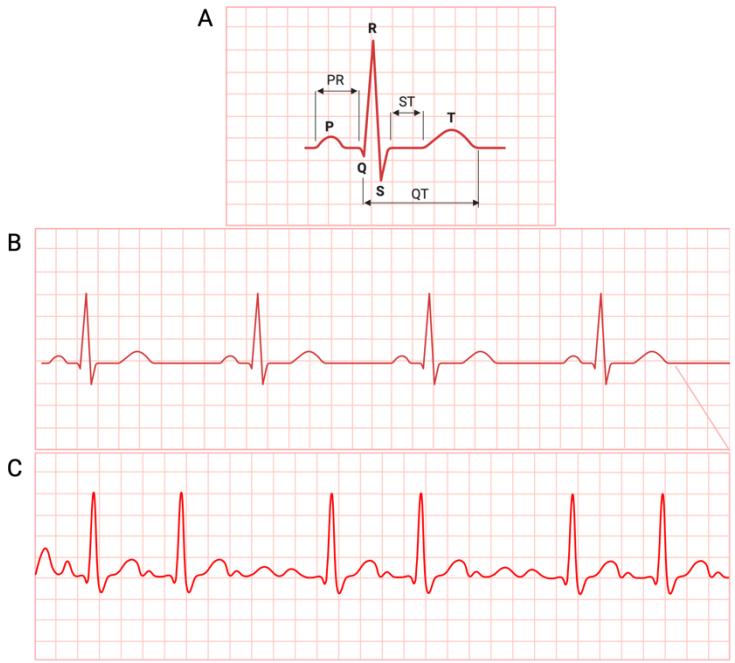

Figure 1.2: Illustration of a normal Electrocardiogram. Representation of the QRS complex (A), an ECG of a (B) normal sinus rhythm and (C) atrial fibrillation. Image created with Biorender.com.

1.2.2 Cardiomyocyte

The heart is composed of 3 main types of cell populations: cardiomyocytes, fibroblasts, and endothelial cells. Cardiomyocytes constitute around 30 to 40% of mammalian heart cells (Zhou and Pu 2016; Pinto et al. 2016). However, in terms of cell count even if cardiomyocytes are not the most abundant they still occupy approximately 70 to 85% of the volume of the heart (Zhou and Pu 2016). These cells are vital for the proper functioning of the heart by their ability to contract.

Adult atrial cardiomyocytes are thin, spindle-shaped, and vary from 100 to 150 microns in length. The main structural constituents of a cardiomyocyte are the sarcolemma (plasma membrane), t-tubules, SR, myofilaments, mitochondria and nuclei. Cardiac myocyte cytoplasm is highly rich in contractile proteins, under a light microscope cardiac muscle appears striated due to the presence of two overlapping myofilaments: fine filaments (actin) and thick filaments (myosin) organised into sarcomeres. Sarcomeres are the contractile unit of cardiac muscle. Within cardiomyocytes, the sarcomere repeats over the entire cell to form myofibrils. Cardiomyocytes are connected end-to-end by intercalated discs. They are junctions expressing high levels of desmosomes and communicating junctions (gap junctions). Desmosomes

provide strong adhesion between cells as gap junctions allow ionic fluxes ensure coordinated contraction of sarcomeres.

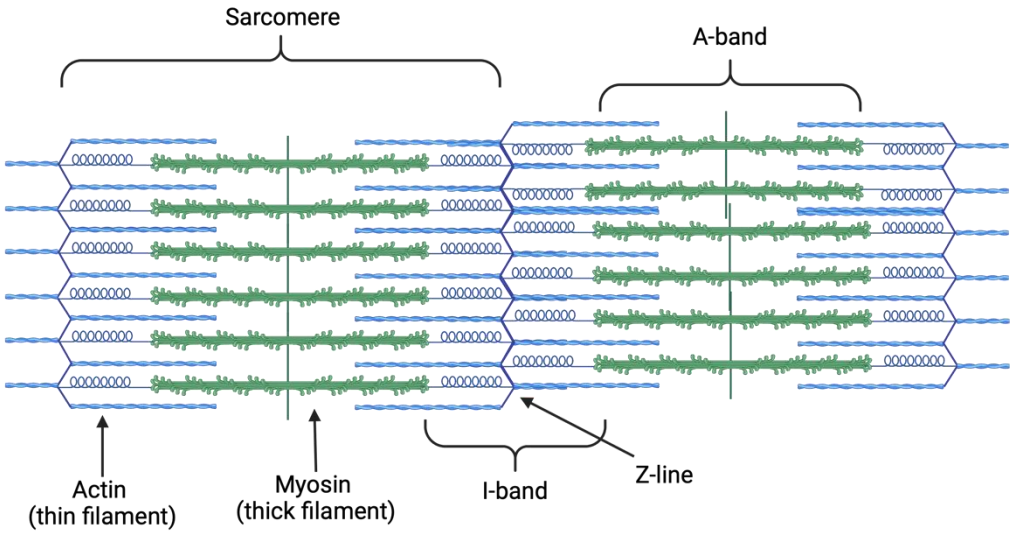

Figure 1.3: Illustration of structure of the fundamental contractile unit of the cardiac muscle: the sarcomere. These units are about 2 μm long and are defined at each end by the Z line which is formed from the protein α-actinin. Attached to the Z lines are the thin filaments made from actin which are joined together to form the thin filament. These actin thin filaments are arranged in a parallel structure with the protein myosin (thick filament). Under polarised light microscopy the arrangement of the actin and myosin protein creates a striated (striped) appearance in which the A band is generated by the myosin filaments and the I band is composed mainly of actin. Image created with Biorender.com based on an image from (Lehman, Crocini, and Leinwand 2022).

The function of the nucleus is to serve as a receptacle of deoxyribonucleic Acid (DNA) for gene expression, terminally differentiated cardiomyocytes are bi- or multi-nucleated or have polyploid nuclei (Kirillova et al. 2021). The heart, as in all striated muscles, requires a large amount energy to succumb to the body's needs which is generated in the form of adenosine triphosphate (ATP) by the mitochondria. The ECC mechanism consumes a lot of ATP at the level of the myofilaments for contraction and also to ensure the transport of ions during excitation. This explains the significant volume occupied by mitochondria in cardiac myocytes. These mitochondria are mainly grouped around the myofilaments, but a population of mitochondria are also located under the sarcolemma. The SR is a specialisation of the smooth endoplasmic reticulum (ER) typical of muscle cells and is rich in calsequestrin, a calcium-binding protein that acts as a calcium buffer within the SR, making the organelle possible to store significant quantities of calcium during relaxation and releases part of it to trigger contraction. The SR has located on the surface two proteins essential for ECC process, the

sarcoplasmic/endoplasmic reticulum calcium ATPase (SERCA2) pump and the RyR type 2. The plasma membrane is where AP spreads. It presents deep invaginations, the t-tubules, which are aligned with the Z striations of the sarcomere. These t-tubules can be connected to each other by longitudinal tubules and forms a complex network which varies according to the stage of development, the region of origin of the cardiomyocytes (atrial or ventricular), and the species considered (Richards et al. 2011). In the majority of species, t-tubules are absent in embryonic myocytes, and fewer and less organised in atrial myocytes, or Purkinje fibres cells compared to ventricular cardiomyocytes which have the most developed transverse tubule system and the most mature. T-tubules propagate depolarization inside cardiomyocytes and play a vital role in the ECC. The t-tubules are rich in ion channels and in voltage-gated LTCC which constitute the "trigger" allowing cardiac contraction to be initiated (Setterberg et al. 2021).

1.3 Myocyte contraction:

The mechanical component which corresponds to the cardiac cycle is, in a simplified manner, composed of two phases: a relaxation phase called diastole during which the heart chambers fill with blood; a contraction phase corresponding to systole which is characterised by an increase in intra-cavitary pressure and by the ejection of blood into the circulatory network (Hall 2019).

1.3.1 Action potential

The membrane potential (MP) of a cardiac cell is determined by all the ionic currents across the cell membrane. Ion channels, transmembrane proteins across the plasma membrane, are responsible for the passage of different ions such as sodium, potassium, calcium and even chloride. The MP can be defined in two main states: the resting potential (RP) and the AP which alternate during the cardiac cycle. The RP corresponds to a balance of ionic currents and has a value of approximately -80 mV. The AP of a cardiomyocyte is broken down into five successive phases (Figure 1.4) (Bers 2002):

Phase 0 represents a rapid phase of depolarisation across the membrane, where the MP, following external stimulation, reaches the activation threshold of the voltage-gated sodium channels which will generate an incoming current sodium.

Phase 1 is an early repolarisation phase which begins with the rapid inactivation of sodium channels and at the same time the voltage-gated potassium channels open and close rapidly, creating a brief outward flow of potassium ions (this phase is not present in pacemaker cells).

Phase 2 corresponds to a plateau phase (more pronounced in ventricular myocytes than in atrial myocytes) due to MP remaining constant. During this phase, efflux of potassium ions through voltage-gated potassium channels and influx of calcium ions with activation of voltage gated LTCC are counterbalanced.

Phase 3 corresponds to terminal repolarisation, LTCC close with activation of delayed rectifier voltage-gated potassium channels open generating an outward positive current, corresponding to negative change in MP.

Phase 4 corresponds to the RP (diastole) with activation of the inward rectifying potassium channels for a return to a MP between -60 and -90mV. For atrial and ventricle cardiomyocytes this phase is stable, the efflux of sodium and calcium and the influx of potassium in balanced; unlike nodal cells which will present a slow phase of spontaneous diastolic depolarisation linked to the activation of a funny current (If) mediated by Hyperpolarization-activated Cyclic Nucleotide-gated channels (HCN). SAN cardiomyocytes are the primary pacemaker cells that initiates the heartbeat. SA node cells naturally depolarise during diastole, creating a rhythmic, spontaneous impulse that sets the pace for the rest of the heart. AVN cardiomyocytes also exhibit some pacemaker activity, much slower than SAN cardiomyocytes and act as a secondary pacemaker if the SAN fails. Purkinje fibres are specialised conduction fibres located in the ventricles and have pacemaker activity but depolarise more slowly than the SAN or AVN. They can generate spontaneous AP in the absence of faster pacemaker signals (Levick 2013).

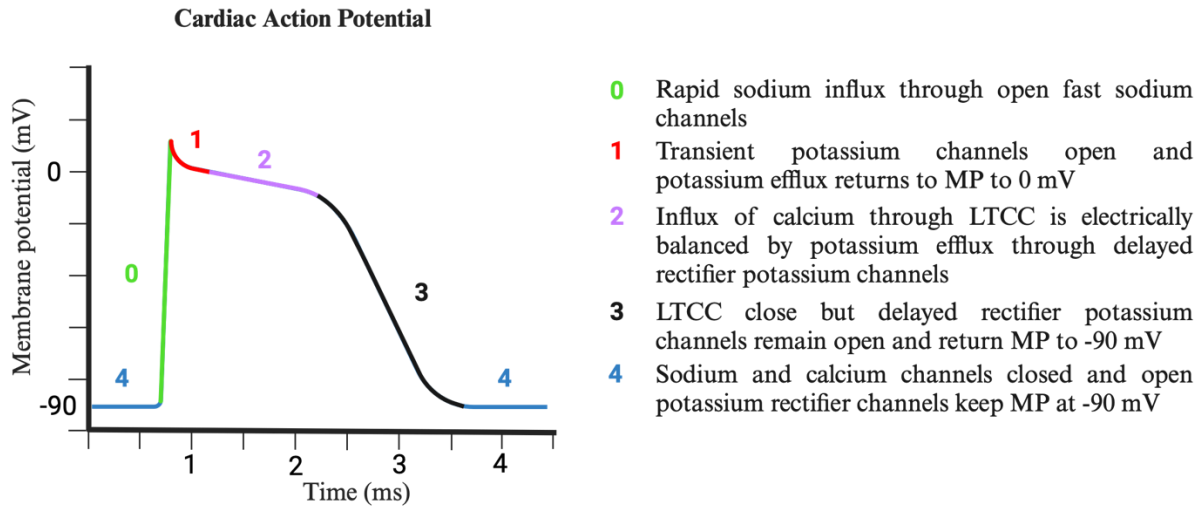

Figure 1.4: Illustration of cardiac AP phases. Image created with Biorender.com based on an image from (Bers 2002).

1.3.2 Automaticity

Unlike atrial or ventricular cells, SAN cells are characterised as having no true resting potential (DiFrancesco 1993). Phase 0 (the rapid initial depolarization of the action potential) is mostly mediated by L-type calcium currents and occurs at a slower rate than in ventricular tissue, making sodium currents less prominent as the primary drivers of depolarisation compared to other regions of the heart in small rodent and humans. The notch and plateau phases (phases 1 and 2) of the ventricular action potential are lacking in the SAN action potential (Aziz, Li, and Tinker 2018). SAN exhibits a slow diastolic depolarisation (known as the pacemaker potential, Figure 1.5). Mediated in the initial phase by sodium influx via I_f, largely constituted by the HCN4 subunit. Depolarisation occurs progressively by T-type calcium channels and finally L-type calcium channels, specifically $Ca_v1.3$, just prior to threshold and initiation of phase 0. L-type calcium currents are inactivated, and many potassium channels are opened, causing repolarisation the action potential.

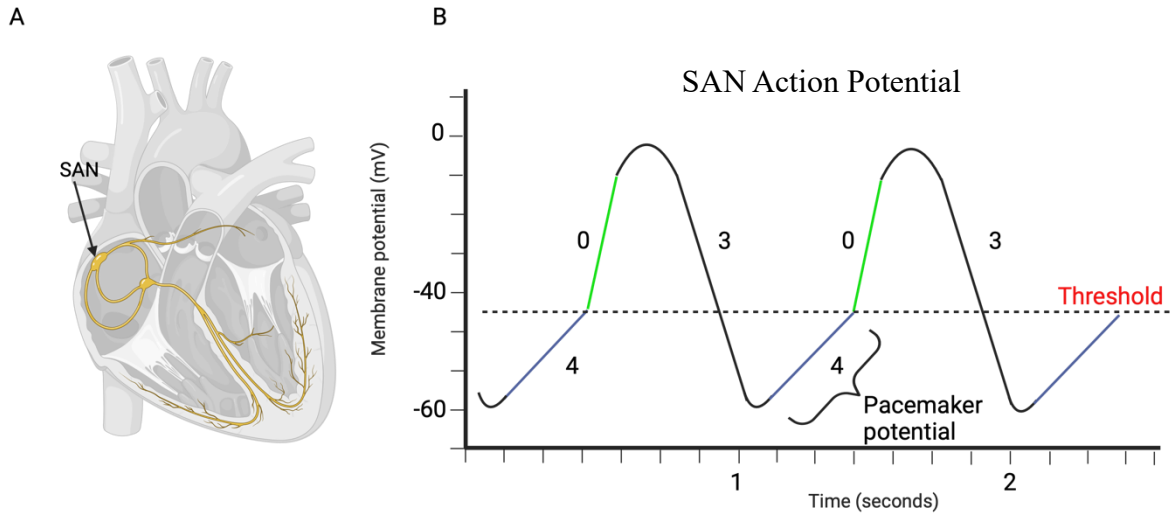

Figure 1.5: Illustration of the heart and location of SAN (A) and AP phases (B). Maximum resting potential is -60 mV and are SAN AP is divided into three phases and have a triangular shape. Phase 4 is the spontaneous depolarisation (the physiological pacemaker) that triggers the action potential once the membrane potential reaches a threshold between -40 and -30mV). Phase 0 is the depolarisation phase of the action potential, dependent on the slow calcium-sodium channel. This is followed by phase 3 repolarisation. Once the cell is completely repolarised at about -60mV, the cycle is spontaneously repeated. Image created with Biorender.com (Noble 1960).

At a molecular level in a pacemaker cells, it is debated that an AP is generated by a coupling system between two "clocks", a membrane clock, and a calcium clock (Lakatta and DiFrancesco 2009). The membrane clock is the first theory to be put forward and postulates, AP is initiated by channels located on the plasma membrane including the If, the transient (TTCC) and slow (LTCC) forming calcium currents, and several outgoing potassium currents but also by currents generated by the sodium/calcium exchanger (NCX) and the sodium/potassium ATPase pump (Noble 1960). The more recent proposed calcium clock postulates that the SR itself acts as a pace regulator (Bogdanov, Vinogradova, and Lakatta 2001) by the presence RyR type 2 and SERCA2 anchored in the membrane of the SR. It is very likely that neither clocks work in the absence of the other, they entrain each other to generate the automaticity of cardiac pacemaker cells (Maltsev and Lakatta 2012). In order to generate spontaneous AP, SAN cells must depolarise spontaneously and sufficiently to the excitation threshold of LTCC (around –40mV) for initiation of a new AP in an automatic and rhythmic contraction (Seyama 1976).

1.3.3 Propagation

The electrical activity which originates in the pacemaker cells of the SAN is transmitted to the entire myocardium due to the communicating junctions of the cardiac cells allowing the coupling of the cells between them (Alexander and Goldberg 2003). These junctions or also called Gap junctions are composed of six transmembrane proteins, the connexins (Cx), constituting the connexon and which, by associating with neighbouring Cx, will form pores through the plasma membranes to ensure electrical continuity between cells (Saez et al. 2003). The composition of Cx is different depending on the heart region considered, thus leading to differences in the speed of propagation of electrical activity throughout the heart. For example, the atria (0.6 m/s) are essentially composed of Cx40 and Cx43, unlike the SAN (0.03 m/s) and AVN (0.05 m/s) only composed of Cx45 (Desplantez et al. 2007; Severs et al. 2008).

At the cellular level, AP transmission occurs in a linear manner, whereas at the tissue level, cells have two types of conduction: longitudinal and transverse. These conductions result from the elongated shape of the cells which give them an anisotropic architecture. Furthermore, the propagation of electrical activity takes place two to three times faster in the longitudinal direction than in the transverse direction, because of the presence of gap junctions preferably located at the end of the cells (Alexander and Goldberg 2003).

1.3.4 Excitation–contraction coupling (ECC)

Since Ringer's discovery of the role of calcium (Ringer 1883), calcium ions have been shown to play an essential role in diverse physiological mechanisms and cellular processes in many species. As a result of its many signalling roles, the level of free calcium in the cytosol of a cell is tightly controlled. In cardiomyocytes, the resting cytoplasmic calcium concentration is kept extremely low at 100 nM and its diffusion is limited by the crowded environment and high number of calcium buffering substances (Smith and Eisner 2019). Calcium handling in the heart plays a major role pacemaker activity, it is a driving force in the ECC process, representing an essential second messenger. With every contraction, ECC converts the passage of electrical excitation across the myocardium to contraction via a rapid rise and subsequent recovery of cytosolic calcium, the calcium transient (Bers 2002). It is important to keep in mind that this process depends not only the properties of calcium channels and transporters but also on precise intracellular arrangement of organelles to ensure maximum efficiency.

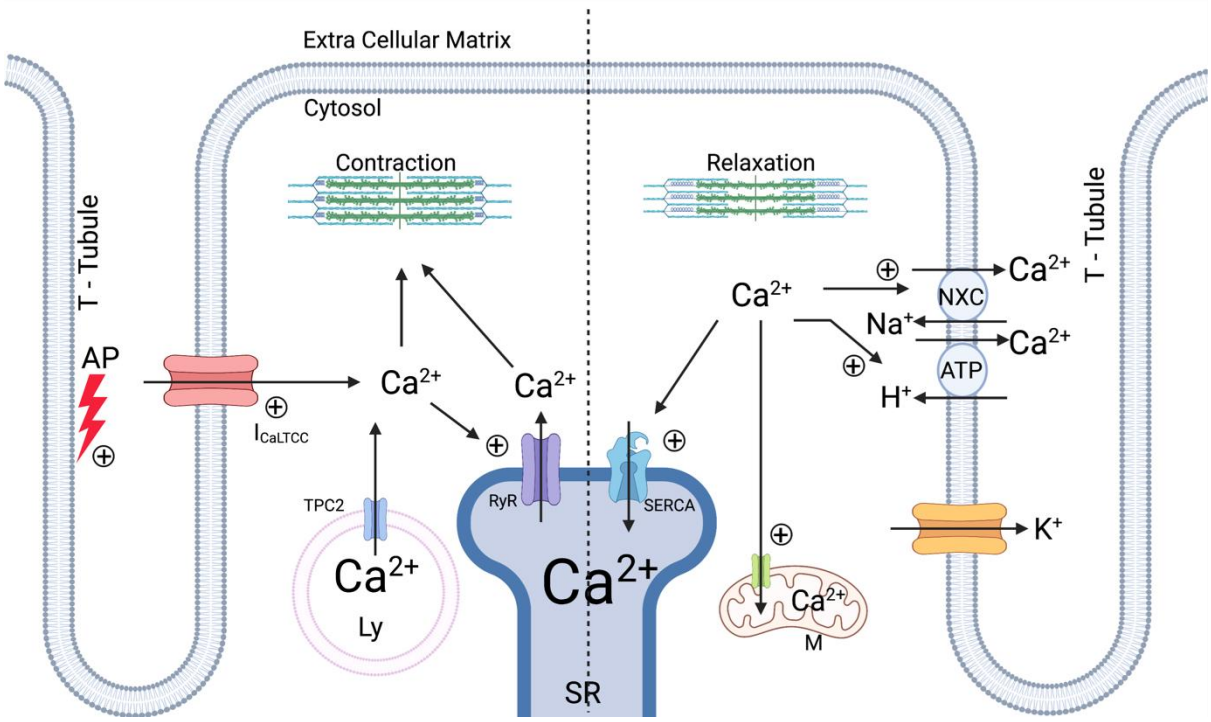

Figure 1.6: Schematic representation of calcium transport in myocytes during an action potential. Image created with Biorender.com based on an image from (Bers 2002).

1.3.5 Calcium induced calcium release (CICR)

Calcium enters the cytosol via voltage gated LTCC and is sensed at the cytosolic face of RyR, which then open, leading to extensive calcium release from the SR. The SR maintains free calcium concentration between 100 – 500 µM (Berridge 2002). As the RyR open, calcium is then driven by a concentration gradient increasing the cytosolic calcium from 100 nM to 10 µM. Once the contraction has been completed, a relaxation stage takes place to prepare for the next contraction. For this to occur, intracellular calcium must decrease, thus allowing calcium to dissociate from the myofilaments. This requires a pumping back of most of the calcium into the SR via the SERCA2 pump and an efflux of the little remaining calcium by the NCX exchanger (Na^+/Calcium exchanger, exchanging 3 sodium ions for one calcium ion) and the calcium-ATPase pump PMCA (Plasma Membrane Calcium-ATPase). The speed and quantity of calcium pumping by SERCA2 is dependent on its inhibitor phospholamban (Figure 1.6).

It should be noted that the amount of calcium extruded from the cell during relaxation must be the same as the amount of calcium entered, to maintain balance (Bers 2002).

1.4 Adrenergic signalling in the heart

The different systems and organs of the human body are influenced by the autonomic nervous system (ANS). Its function is to regulate and modulate their activities and takes place automatically and unconsciously. The ANS is divided into two different subsystems working in parallel, in opposite directions and on similar target organs: The parasympathetic nervous system is responsible for the "rest and digest" part of our activities, its main role is to reduce energy consumption and manages basal activities such as digestion. The sympathetic nervous system in which during emergency or dangerous situations, prepares the body "fight-or-flight" responses (Cannon and Rosenberg 1932). Its responsible for all the mechanisms that increase energy consumption and prepare the body for action such as increased blood pressure, tachycardia or peripheral vasoconstriction. This system operates according to a two-neuron model. A first short pre-ganglionic neuron, located in the thoracolumbar part of the spinal cord, releases acetylcholine in the para- or pre-vertebral ganglion, which activates the nicotinic receptors located on the second post-ganglionic neuron. To in turn release norepinephrine, which activates adrenergic receptors in peripheral target tissues. Adrenergic receptors are divided into two groups: α-adrenergic receptor (α-AR1 and (α-AR2) and β-adrenergic receptors (β-AR1, β-AR2, β-AR3) (Pfleger, Gresham, and Koch 2019).

1.4.1 α-adrenergic signalling in the heart

There are two subtypes of α-AR: α1-AR and α2-AR. α1-AR are highly expressed on vascular smooth muscle cells and cardiomyocytes and α2-AR are mainly found in the central nervous system. α1-ARs exist as three distinct molecular subtypes, named α1A, α1B, and α1D. α1-AR are coupled to stimulatory heterotrimeric Gq/11 (Gαq) proteins that activate the enzyme phospholipase C (PLC) by binding of endogenous catecholamines, norepinephrine, and epinephrine. Activation of PLC leads to hydrolysis of membrane-bound phosphatidylinositol 4,5-bisphosphate (PIP_2) and the cytosolic release of the second messenger inositol 1,4,5-trisphosphate (IP_3) and diacylglycerol (DAG, Figure 1.9). IP_3 induces release of intra-cytosolic calcium from the SR. DAG activates PKC, a serine/threonine kinase; this leads to phosphorylation of enzymes and alteration of ion channels leading to electrolyte transfer in and out of cells, vasoconstriction, increased blood pressure and gene expression. Even if α1-AR have had lest investigation over β-AR, emerging evidence regarding the importance of α1-AR in myocyte physiology has shown much prominence (Motiejunaite, Amar, and Vidal-Petiot 2021).

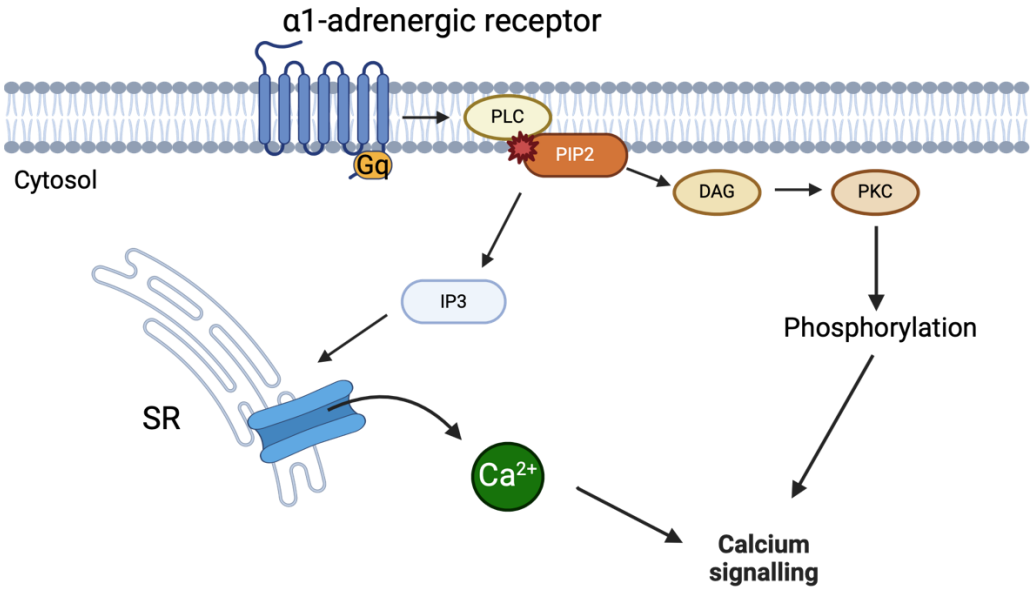

Figure 1.7: Illustration of α-adrenergic signalling pathway. Norepinephrine or epinephrine binds to the extracellular domain of the α1-AR, coupled to Gq protein. Upon ligand binding, the receptor undergoes a conformational change, which activates the Gq protein by exchanging GDP for GTP on its α-subunit. The activated Gq protein stimulates PLC. PLC catalyses the hydrolysis of PIP_2 into two second messengers: IP_3 and DAG. IP_3 diffuses into the cytoplasm and binds to IP_3 receptor type 2 (IP_3R2) located on the SR. This triggers the release of calcium into the cytosol. Simultaneously, DAG remains in the membrane and activates PKC. The increase in cytosolic calcium and activation of PKC leads to a variety of downstream effects. Image created with Biorender.com.

1.4.2 β-adrenergic signalling in the heart

β-AR belong to the GPCR superfamily and are coupled to heterotrimeric G proteins. β-AR are monomeric proteins characterised by 7 transmembrane α helices linked together by 3 extracellular loops and 3 intracellular loops. They have an extracellular N-terminus and a cytoplasmic C-terminus(Ji, Grossmann, and Ji 1998). There are three subtypes of β-AR: β1-AR, β2-AR and β3-AR. All three are expressed in the myocardium. β1-ARs account for approximately 80% of total β-ARs, while β2-ARs and β3-ARs represent the remaining 17% and 3%, respectively. The signalling pathway of β1-AR and β2-AR is constituted by Gs proteins, activation of these receptors (fixation of an agonist leads to a change of conformation) stimulates adenylyl cyclases (ACs) that catalyse conversion of ATP into cyclic adenosine monophosphate (cAMP). This important production of cAMP leads to the activation of protein kinase A (PKA) (Steinberg 1999). Activated PKA can phosphorylate key ECC proteins which stimulates important positives inotropic and chronotropic event the heart such as LTCCs

enhancing calcium influx during the AP, phospholamban at serine-16 which relieves its inhibitory effect on the SERCA2a, RyR2 leading to an increase in calcium release during systole, troponin I reducing the sensitivity of the contractile proteins to calcium, facilitating faster relaxation and enhancing diastolic function and voltage-gated potassium channels which affects AP duration and refractoriness (Xiao 2001).

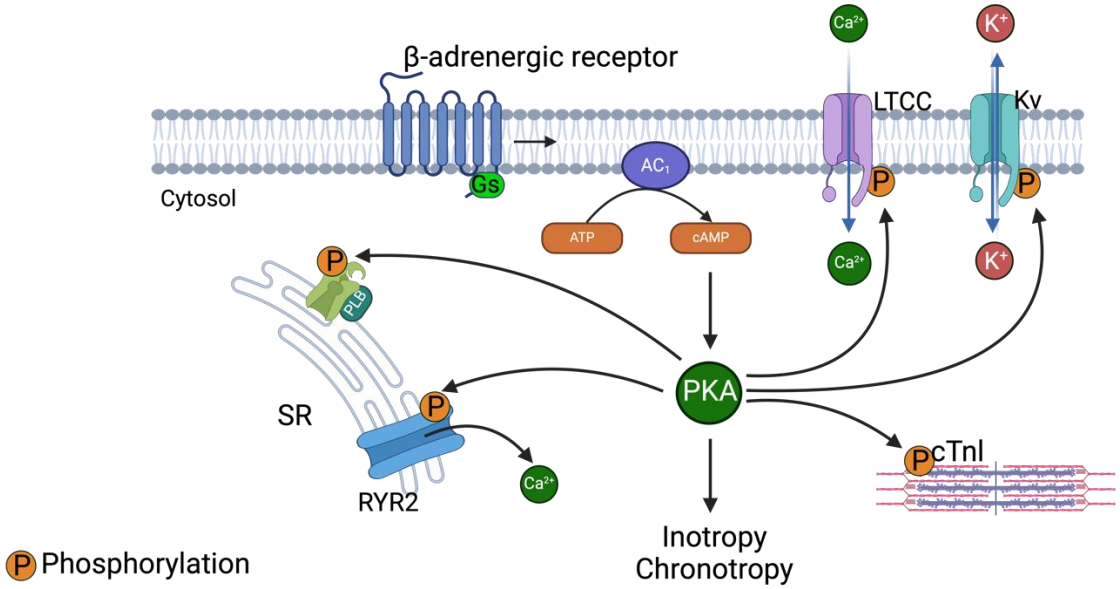

Figure 1.8: Illustration of β-adrenergic signalling pathway. Catecholamines bind to the extracellular domain of the β-AR, coupled to Gs protein. Upon ligand binding, the receptor undergoes a conformational change, activating the Gs protein by causing the exchange of GDP for GTP on its α-subunit. The Gs α-subunit with bound GTP dissociates from the β and γ subunits and activates ACs, an enzyme located on the inner side of the plasma membrane. Activated ACs catalyse the conversion of ATP into cAMP and cAMP binds to the regulatory subunits of PKA, leading to the dissociation and activation of its catalytic subunits. Activated PKA phosphorylates various target proteins, leading to a wide range of physiological effects. cTnI; cardiac troponin I. Image created with Biorender.com.

1.5 Calcium mobilising second messengers

Second messengers are defined based on several criteria: they must be produced in response to the binding of an extracellular agonist to its plasma-membrane receptor, an intracellular target on which they will act, and participate in a physiological function by a rapid cytosolic concentration increase to an its activating stimulus. Calcium-releasing secondary messengers act on channel receptors located on intracellular stores to release calcium.

1.5.1 IP_3

1.5.1.1 IP_3 and IP_3R discovery and structure

(Streb et al. 1983) first discovered that IP_3 evokes an increase in the intracellular level of calcium in pancreatic acinar cells. IP_3 receptor (IP_3R) were later described in 1988, purified from rat cerebellum (Supattapone et al. 1988) showing it's high affinity with IP_3 (Kd= 100 nM). IP_3R activation requires the binding of both IP_3 and calcium to have the highest open probability during calcium transients. Electron *microscopy* (EM) immunocytochemical studies of rat cerebellar Purkinje cells, localised IP_3R to the ER (Ross et al. 1989). In humans, IP_3R are in 3 different isoforms encoded by 3 different genes, presenting 60% homology: IP_3R type 1 (IP_3R1), the first isoform identified and cloned (Supattapone et al. 1988), IP_3R type 2 (IP_3R2) and IP_3R type 3 (IP_3R3). The IP_3R is expressed ubiquitously, but each isoform presents its own expression profiles that can vary depending on the physiological or pathological context (Taylor, Genazzani, and Morris 1999). IP_3R is a intracellular calcium channel and formed a tetramer with the 4 homologue subunits, of approximately 2700 amino acids and 310 kDa each linked by non-covalent bonds (Maeda et al. 1991). The IP_3 receptor is made up of three regions: an N-terminal cytosolic domain where is located IP_3 binding sequence as well as other regulatory factors, a hydrophobic region composed of 6 transmembrane helices containing the part which forms the ionic pore and a short C-terminal cytosolic sequence (Foskett et al. 2007) (Figure 1.11).

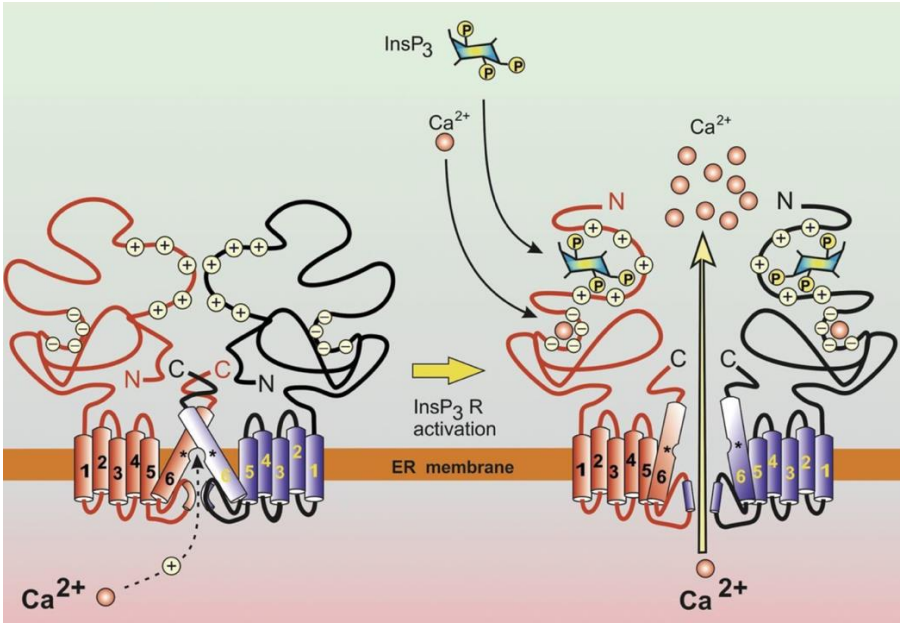

Figure 1.9: Illustration of IP_3 receptor. IP_3 diffuses through the cytoplasm and binds to the IP_3R and allows the release of calcium stored in the SR in cardiomyocytes. Figure obtained with permission from (Berridge 2016)

1.5.1.2 IP_3 signalling

Calcium release from the SR is mediated by two forms of intracellular calcium release channels: the RyRs, responsible for CICR, and the IP_3R. The involvement of IP_3 signalling in cardiac cellular calcium handling is less well understood. The IP_3R are activated by IP_3 and calcium (Berridge 1984). IP_3 is a second messenger resulting from the synthesis of PIP_2 into DAG (Sandow et al.). Three endogenous isoforms have been described: IP_3R1, IP_3R2 and IP_3R3. The RyRs, with great homologies with IP_3R, are also composed of three isoforms, RyR1, RyR2 and RyR3. They are activated by low concentrations of ryanodine (Husser et al.) or calcium (µM) and inactivated by high concentrations. ryanodine (100 µM) or calcium (mM) (Inui, Saito, and Fleischer 1987; Meissner 1986).

As cited above, the main known ligand of IP_3R leading to the intracellular release of calcium is IP_3 via the intracellular signalling pathway involving PLC. Extracellular stimuli of tyrosine kinase receptors or Gq/11 protein-coupled receptors (including α-AR), leads to the cleavage of PIP_2 into IP_3, as well as DAG. DAG remains at the plasma membrane due to its hydrophobicity and activates protein kinase C (PKC), via stimulation of PLC to activate a cascade of protein phosphorylations. Hydrophilic IP_3 diffuses into the cytoplasm and binds to each protein binding domain of IP_3R subunits leading to a change in receptor conformation (Berridge and Irvine 1989; Berridge 1984). In cardiomyocytes, binding of IP_3 to IP_3R on the SR leads to SR calcium release into the cytosol (Berridge, Lipp, and Bootman 2000) enhancing cellular calcium oscillations (Zhu and Nosek 1991). Calcium, regarding the IP_3R, exhibits biphasic activity, by activating or inhibiting the channel. The calcium release mechanism is dependent on calcium itself (CICR), notably via voltage-dependent calcium entry. At low intracellular calcium concentrations (100-300 nM), the channel is activated, while high calcium concentrations above 300 nM inhibit IP_3R activity. But this inhibitory effect of calcium can be controlled in the presence of high concentrations of IP_3, which allows the opening the receptor even in high calcium concentrations (Bootman and Lipp 1999).

1.5.1.3 Physiological implications

IP_3-dependent calcium signalling participates in the regulation of different cellular processes in excitable and non-excitable cells. IP_3 is a ubiquitous second messenger in response to neurotransmitters, hormones and growth factors (Berridge 2009). The IP_3 signalling pathway plays direct roles via the generation of calcium signals but also indirect roles by modulating calcium signals induced by multiple signalling pathways and impact widespread physiological

functions such as fertilization, proliferation, metabolism, and secretion. The isoform IP_3R type 2 first described by (Südhof et al. 1991) is the predominant form in isolated atrial myocytes and is also expressed in ventricular myocytes at a lower level (Lipp et al. 2000). Additionally, Lipp and colleagues used a membrane-permeant IP_3 ester (IP_3-BM) to activate IP_3R resulting in spontaneous calcium release events and increased the calcium transient amplitudes, highlighting a role for IP_3 in cardiac excitation-contraction coupling. IP_3R therefore have the ability and potency to modulate cardiac ECC and evidence has shown that IP_3 has a positive chronotropic and inotropic effect in atrial SAN preparations. The SAN expresses three IP_3R mRNA isoforms, the type IP_3R2 was the predominant protein isoform detected by Western blot and Immunohistochemistry studies also showed that IP_3R2 was expressed and localised with a similar distribution to SERCA2 in the central SAN region. Functional studies were also conducted and IP_3-BM increased calcium spark frequency and the pacemaker firing rate in single isolated pacemaker cells and were absent in the SAN from transgenic IP_3R2 knockout mice (Ju et al. 2011). Knockout of NCX in SAN cells were used to study the influence of IP_3 signalling on cardiac pacemaking creating a system where periodic intracellular calcium cycling persists despite the absence of depolarization or calcium flux across the sarcolemma. Recordings of confocal line scans of spontaneous calcium release in WT and NCX KO SAN cells in the presence of an IP_3R blockers decreased the frequency of spontaneous calcium transients and waves in WT and NCX KO cells. Alternatively, increased IP_3 production induced by phenylephrine (PE) increased calcium transient and wave frequency (Kapoor et al. 2015) making the IP_3 signalling pathway a potential target for the treatment of AF.

1.5.1.4 Pathophysiological implications

As, IP_3R play important physiological roles, they are also involved in several pathologies. Neuronal disorders such as bipolar disease (Schlecker et al. 2006), Alzheimer disease, Huntington disease and in brain ischemia where expression of IP_3R is selectively downregulated in the brain (Haug et al. 1996; Zhang et al. 1995). In Diabetes, loss or malfunction of the β-cell is linked to dysregulation of levels of IP_3 (Barker and Berggren 2013). IP_3 mediated calcium signalling mechanism has also been implicated in cardiac pathophysiology. Calcium signals were recorded in response to IP_3-BM in isolated rat atrial myocytes recorded and induced arrhythmogenicity (Mackenzie et al. 2002). Changes in the expression of IP_3R have been linked with cardiac diseases, IP_3R expression has been shown to be increased in right atrial tissue from patients with chronic AF (Yamda et al. 2001) as well as over-expressing IP_3R2 in transgenic mice displayed a cardiac hypertrophy phenotype with an

increase in heart weight and expression of hypertrophy-related genes (Nakayama et al. 2010). As the activation of Gq\11 coupled GPCRs in the atria have been shown to lead to enhance calcium signalling via IP_3 generation via electrical events they are potentially proarrhythmic (Tinker et al. 2016). IP_3-dependent calcium release involvement and downstream actions are not fully elucidated and additional studies must be carried out for a better understanding of not only physiological mechanisms but also pathophysiological mechanisms.

1.5.2 Adenylyl cyclases

1.5.2.1 Description

Adenylyl cyclases (ACs) are activated by the Gαs protein released during stimulation of a GPCR and constitute the main sources of cAMP in cardiomyocytes. ACs are enzymes that catalyse the conversion of adenosine triphosphate (ATP) into cAMP. ACs play an important role for the inotropic and chronotropic response of cardiac muscle to adrenergic stimulation by G-protein-coupled receptors (Mons et al. 1998) (Zaccolo, Zerio, and Lobo 2021). The first AC isoform (AC1) was cloned in 1989 (Krupinski et al. 1989). So far, 10 isoforms of ACs have been identified in mammals, 9 closely related transmembrane (AC 1 to 9) and one soluble (AC10, I will not be describing properties of AC10 throughout this manuscript). The molecular structure of the 9 transmembrane ACs consists of two hydrophobic domains comprising six transmembrane helices each and two cytoplasmic domains which form the catalytic site (Hanoune and Defer 2001).

1.5.2.2 Regulation

Gαs protein activates ACs while Gαi inhibits them. Additionally, forskolin (diterpene extracted from the *Coleus forskohlii* plant) is an activator of all mammalian ACs. Many inhibitors of ACs have been synthesised, some of which appear to work well *in vitro* but many are modified nucleotides or nitrogen bases aimed at targeting the catalytic site of the enzyme, a highly conserved region between isoforms (Seifert et al. 2012). Unfortunately, this leads to difficulties with isoform specificity and selectivity compared to inhibitors of other proteins.

1.5.2.3 ACs in the heart

These isoforms are differentially expressed across tissues. In the heart, AC5 and AC6 are the predominant AC isoforms and the main AC isoforms responsible for cAMP synthesis (Guellich, Mehel, and Fischmeister 2014). However, high basal cAMP levels have been measured in isolated rabbit SAN myocytes (Vinogradova et al. 2006). AC8 and AC1 are

calcium- stimulated isoforms were shown to be expressed in atrial and SAN myocytes (Mattick et al. 2007). Functional studies presented the importance of AC activity was investigated by monitoring activation of I_f. Inhibition of AC activity (by MDL-12,330A) shifted activation in the hyperpolarizing direction, while inhibition of phosphodiesterases (by IBMX) shifted I_f activation in the depolarising direction (Mattick et al. 2007). Unlike AC5/6 which are inhibited by calcium, AC1 and AC8 are calcium activated and contribute to the generation of rhythmic action potentials by regulating the LTCC current (Younes et al. 2008). AC1 and AC8 may play a major role in initiation and regulation of the heartbeat and IP_3 signalling in cardiac atria and sinoatrial node involves stimulation of calcium-activated AC1 and AC8 by IP_3-evoked calcium release from junctional SR (Capel et al. 2021). Excessive stimulation of other ACs, such as AC5, has been shown to promote proarrhythmic effects by inducing SR calcium overload and hyperactivation of RyR, which in turn induces spontaneous calcium waves and afterdepolarizations (Zhao et al. 2015). The link between IP_3 pathway and downstream activation of calcium stimulated ACs has been relatively understudied. Understanding the possible interaction between IP_3R pathways and calcium stimulated ACs therefore has the potential to provide important insights concerning acute mechanisms for initiation of atrial arrhythmias and may provide a novel atrial specific therapeutic approach for arrhythmias. Additional studies must be carried out for a better understanding of the mechanism, in particular the nature of the molecular interactors which participate in it. In addition, their location is decisive in the spatial organisation of cAMP signals.

1.5.3 cAMP:

1.5.3.1 Discovery of cAMP

cAMP was discovered in the late 1950s by Earl W. Sutherland. Earl W. Sutherland observed that when separating a liver homogenate by centrifugation, the fraction and the supernatant communicated not directly with the help of hormones but via a second messenger, cAMP. the hormones he studied (adrenaline and glucagon) led to the production of cAMP in the fraction of the liver homogenate capable of stimulating glycogen phosphorylase in the supernatant (Rall and Sutherland 1958). Sutherland quickly identified cAMP in tissues other than the liver, such as the brain, skeletal muscle and heart, suggesting its ubiquitous nature (Sutherland and Rall 1958). He had just discovered a major mechanism of action of hormones which earned him the Nobel Prize in Medicine 15 years later. The production of cAMP is initiated when a first extracellular messenger (hormones, neurotransmitters) binds to a GPCR (Zaccolo 2009). The

cytosolic level of cAMP is determined by the dynamic equilibrium between production by ACs and degradation by phosphodiesterases (Beavo et al. 1971).

1.5.3.2 Targets of cAMP

1.5.3.2.1 Protein kinase A: major target

PKA is a ubiquitous cellular kinase which phosphorylates a range of intracellular targets and is modulated by the local concentration of cAMP. PKA is a major player in cAMP signalling pathways and plays an essential role in the regulation of cardiac function. In the absence of cAMP, the PKA holoenzyme is a heterotetramer consisting of two catalytic (C) subunits that are linked and inhibited by a dimer of regulatory (R) subunits. Cooperative binding of two cAMP molecules to both the A and B sites of each R subunit causes dissociation and activation of the C subunits, which as previously described, allows PKA to phosphorylate multiple protein targets in various subcellular compartments (Bers 2002). PKA have been described into two groups, named PKA-I and PKA-II, due to differences in their R subunits, RI and RII, respectively, each being subdivided into α and β subtypes (Hofmann et al. 1975). PKA-RII is known to be the main isoform responsible for the inotropic effects of β-AR stimulation. RIIα represents the major isoform expressed in the heart (Skalhegg and Tasken 2000). The spatial and temporal organisation of cAMP/PKA signalling is achieved by a carefully ordered balance between local effector activation and signal termination assembled and targeted by A-Kinase Anchoring Protein (AKAP). More than 50 AKAPs have been identified and, although they belong to a structurally diverse family, they all share the ability to enable tightly regulated phosphorylation of substrates anchored or located near PKA (Calejo and Taskén 2015).

1.5.3.2.2 Exchange Protein Activated by cAMP

The intracellular effects of cAMP were first thought to be exclusively attributed to PKA activation. However, in 1998, a family of new cAMP effector proteins, called Exchange Protein Activated by cAMP (EPAC) was discovered (de Rooij et al. 1998; Kawasaki et al. 1998). A discovery hinting at the complexity of the cAMP signalling mechanism. The EPAC family is composed of EPAC1 and EPAC2, they bind with a high affinity to cAMP to activate a family of small G-proteins, Rap1 and Rap2, the Ras family (de Rooij et al. 2000). Binding of cAMP to EPAC promotes GDP to GTP exchange, thereby inducing activation of the small G protein Rap (Gloerich and Bos 2010). On the other hand, proteins activating the GTPase-activating proteins (GAPs) reinforce the intrinsic GTP hydrolysis activity of Rap, which leads to the inactivation of the GTPase (Lezoualc'h et al. 2008). Alongside the research of EPAC signalling

pathway, much work on EPAC's regulation was being conducted in the heart. It was first discovered that in primary cardiomyocytes, EPAC induces hypertrophy through activation of Rac and calcineurin signalling pathway making EPAC a positive regulator of cardiac growth (Morel et al. 2005), this novel finding opened a field of research of EPAC in the heart. It was later confirmed in adult rat ventricular cells, where EPAC, downstream of β-AR signalling, leads to diastolic calcium leak from the SR by activating calcium/calmodulin-stimulated protein kinase II (CaMKII) which phosphorylates RyR2. (Pereira et al. 2007). EPAC proteins also were showed to constitute important effectors of cAMP compartmentation and calcium handling (Lezoualc'h et al. 2016). More particularly, the EPAC2 isoform is localised at the level of T-tubules (Z streak of the cardiomyocyte) and its activation by β1-AR signalling results in calcium leak from the SR via CaMKIIδ-dependent phosphorylation of RyR2-S2814 (Pereira et al. 2007). This lab later showed, this pathway leads to the occurrence of β-AR-induced arrhythmias and reduced cardiac function (Pereira et al. 2013). In 2004 the first EPAC based fluorescence resonance energy transfer (FRET) reporter for the detection of cAMP was developed (Ponsioen et al. 2004) (Figure 1.12).

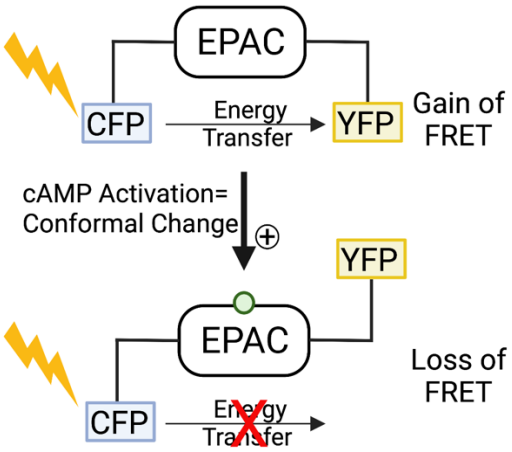

Figure 1.10: Cytosolic FRET-based reporter EPAC-S^{H187}(Klarenbeek et al. 2015). Image created with Biorender.com.

1.5.3.2.3 Hyperpolarization-activated Cyclic Nucleotide-gated channels (HCNs)

In mammals, HCNs ion channels are tetramers belonging to the family of hyperpolarisation-activated cyclic nucleotide-gated ion channels (Scicchitano et al. 2012). Four isoforms have been identified, namely HCN1-4 and are at the origin of the I_f current in the SAN which is a current controlling heart rate (DiFrancesco 1991). These channels are modulated by cyclic nucleotides and are non-cation selective. They are permeable to both potassium and sodium.

The four isoforms are expressed differently in the heart. In particular, the HCN4 isoform constitutes the main isoform expressed in the SAN, followed by HCN1 and HCN2 (Scicchitano et al. 2012). HCN2 is mainly present in the ventricle while HCN3 expression is negligible in all tissues (Chandler et al. 2009). Binding of cAMP to HCNs channels increases the probability of channel opening during membrane hyperpolarisation by inducing a conformational change of the protein. In addition, Ivabradine is a heart rate-reducing pharmacological agent from a selective and specific block of HCN channels. This action is selective for pacemaker cells in the SAN and does not impact other ion channels or conduction pathways making the I_f current an interesting therapeutic target (Bucchi et al. 2006). Ivabradine has been studied in clinical trials, the SHIFT (Systolic Heart Failure Treatment with the IF Inhibitor Ivabradine Trial) trial involved over 6,500 patients with moderate to severe heart failure and a heart rate ≥70 bpm. Results showed that ivabradine reduced the combined outcome of cardiovascular death or heart failure hospitalisation by slowing heart rate, especially in patients with higher baseline rates. It was also linked to reduced hospitalisations for heart failure but did increase rates of bradycardia (Swedberg et al. 2010).

1.5.3.2.4 Popeye domain containing protein (POPDC)

A fourth class of cAMP effectors was discovered and corresponds to the family of membrane proteins containing the Popeye domain (Reese et al. 1999). These proteins are encoded by the *Popdc* genes (Popdc1, Popdc2 and Popdc3) and are abundantly expressed in the heart and skeletal muscles. It was only reported in 2012 that conserved Popeye domains of POPDC isoforms, located at the cytosolic C-terminal extremity, has a high affinity binding sites for cAMP (Froese et al. 2012), and have regulatory function in heart rate dynamics through cAMP binding. POPDC proteins can also interact with caveolin-3 in t-tubule caveolae highlighting its importance structural integrity and POPDC1-null hearts indicated lower recovery from ischemia injury indicating a role in heart protection (Alcalay et al. 2013). Furthermore, *Popdc1* and *Popdc2* are strongly expressed in cardiac tissue and more particularly in the conduction system, at the level of the SAN and AVN (Froese et al. 2012), indicating POPDC proteins have an important regulatory function in heart rate dynamics that is mediated, at least in part, through cAMP binding.

1.5.3.3 Degradation of cAMP

The degradation of cyclic nucleotides (cAMP and cyclic guanine monophosphate [cGMP]) is uniquely carried out by a superfamily of enzymes called phosphodiesterases (PDEs). This superfamily is subdivided into eleven families, PDE1 to PDE11, PDE3 and PDE4 being the major families controlling cAMP and ECC in the heart (Conti and Beavo 2007). PDEs are the only cyclic nucleotide degrading enzymes and so they are critical regulators of cAMP homeostasis. They achieve this by specifically cleaving the 3'-5'-cyclic phosphate moiety from cAMP or cGMP to leave the corresponding 5'-nucleotide (Fischmeister et al. 2006). They are characterised by their primary structure, their catalytic properties, their capacity to degrade cAMP and/or cGMP, as well as their regulatory mechanisms. Among the eleven families of PDEs, seven are expressed in the heart to degrade cAMP and/or cGMP with different affinities: PDE1-5, PDE8 and PDE9. PDE1-3 can hydrolyse cAMP and cGMP while PDE5 and PDE9 can only hydrolyse cGMP and PDE4 and 8 only cAMP (Keravis and Lugnier 2012).

1.5.3.4 Compartmentation of cAMP in the heart

Compartmentation refers to the mechanisms by which multiple spatially separated cAMP/PKA and cGMP/PKG signalling pathways exert different, or even opposing, functional effects in distinct subcellular microdomains of the same cell (Zaccolo 2011). Compartmentation and compartmentalization are often used interchangeably to describe this process. The term compartmentation became more popular in the 20th century and will be used throughout the rest of this manuscript (Steinberg and Brunton 2001). Mechanisms that limit its diffusion are necessary, these can be physical barriers such as organelle membranes or mitochondrial networks, to create a physical block of the binding of cAMP to its effectors and to the degradation of cAMP by PDEs. Important contributors to cAMP compartmentation are AKAPs, by localising PKA close to its substrates (Dodge-Kafka, Langeberg, and Scott 2006). The first evidence of compartmentation of cAMP signalling in the heart was revealed through experiments showing that β-AR stimulation, increases cAMP, contraction force and activates the pellet and soluble fraction of PKA, while after application of prostaglandin E1, no modification of contractile activity was observed despite an increase in cAMP and activation of PKA in the pellet after cell lysis (Buxton and Brunton 1983), demonstrating the hormonal specific compartmentation of cAMP.

1.5.4 Nicotinic acid adenine dinucleotide phosphate

Nicotinic acid adenine dinucleotide phosphate (NAADP) mediated calcium signalling is highly specific (Galione 2011). Calcium-releasing secondary messengers act on channel receptors located on intracellular stores to release calcium. NAADP is puzzling since in many cells it appears to act via a distinct calcium release mechanism, which resides not on the ER/SR but on acidic organelles and will be described below.

1.5.4.1 Discovery

NAADP is a endogenous calcium-mobilizing second messenger in many cells and species, first shown to mobilise calcium in sea urchin eggs in 1995 (Lee and Aarhus 1995). A few years later, it was shown that NAADP mobilises calcium release from acidic stores of the cell, rather than the ER (Churchill et al. 2002). This study provided evidence that these acidic stores, are lysosomal organelles that function as calcium stores to mobilise calcium in response to NAADP in sea urchin eggs. These experiments made it possible to identify the main characteristics of the reserve sensitive to NAADP.

Additionally, emptying the ER with thapsigargin did not abolish the response to NAADP (Churchill and Galione 2001). The intracellular reserve responsible for calcium signals due to NAADP can be pharmacologically separated from that responding to IP_3. A cellular model allowed separation of intracellular organelles by sucrose gradient centrifugation, which made it possible to prove that the reserves mobilised by IP_3 are also physically separated from those mobilised by NAADP. These cell fractionation experiments also showed the fraction releasing calcium in response to NAADP is distinct from the fraction containing mitochondria, insensitive to thapsigargin, and did not present CICR, unlike those mobilised by IP_3 (Lee and Aarhus 2000).

In addition, a body of evidence favoured the existence of a specific NAADP receptor (Capel et al. 2015; Pitt et al. 2010; Calcraft et al. 2009). Solubilization in sea urchin egg homogenate shows that the isolated protein, which binds NAADP, was much smaller (470 kDa) than IP_3R and RyR (respectively 1000 and 2000 kDa) and made it possible to confirm the pathway of NAADP as being a calcium signalling pathway in its own right, with synthesis enzyme, messenger, receptor, and sensitive reserve (Galione and Petersen 2005).

1.5.4.2 Synthesis and metabolism

The first enzyme discovered to catalyse the synthesis of NAADP was ADP- ribosyl cyclase and was purified from the sea slug (Hellmich and Strumwasser 1991). Sequence comparisons with mammalian tissue revealed that there are mammalian homologues, the lymphocyte antigen CD38 (States, Walseth, and Lee 1992). The CD38 enzyme is a 45 kDa transmembrane glycoprotein with a short cytoplasmic N terminus and a long extracellular C terminal domain (Jackson and Bell 1990). In addition to synthesising cADPR, CD38 can also synthesise NAADP in the presence of NA and NADP, this reaction occurs at an acidic pH (Aarhus et al. 1995)

1.5.4.3 Two-pore channels as NAADP receptors

Two-pore channels (TPCs) are members of the superfamily of voltage-gated ion channels, these cation channels are activated by NAADP. TPCs were first cloned from the rat kidney and consist of two domains that each have the S1 – S6 segments that are usually found in voltage gated cation channels (Ishibashi, Suzuki, and Imai 2000). TPC1 and TPC2 channels, encoded by TPCN1 and TPCN2, respectively, are localised on endosomal and lysosomal membranes. Some studies showed TPCs are sodium-selective with limited calcium permeability (Wang et al. 2012; Cang et al. 2013). TPC1 and TPC2 were linked to the endo-lysosomal pathway by being co-expressed with various organelle markers. They found significant colocalisation of TPC1 with markers for both lysosomes/late endosomes (LAMP1) and endosomes (endo-GFP) but not the ER while TPC2 only colocalised with LAMP-1 (Brailoiu et al. 2009). TPC2 is the isoform most present within the lysosome membrane, TPC2 was tested to see if the channel mediates calcium release from lysosomes by flash photolysis of caged-NAADP on intracellular calcium concentration in wild type (Südhof et al.) HEK293 and tagged TPC2 cells by Fluo3 fluorescence and provoked an initial intracellular calcium rise dependent on acidic organelles but independent of the ER (Calcraft et al. 2009). Other evidence has shown TPC2 to be the major lysosomal targeted isoform able to act as a calcium release channel in the cellular environment by (Pitt et al. 2010). The group reported NAADP to open TPC2 channels in a concentration-dependent manner with binding to high affinity activation sites and low affinity inhibition sites regulated by the pH of the luminal environment of the channel (Pitt et al. 2010). Increased TPC expression was demonstrated to lead to enlarged lysosomes and trafficking dysfunction by assessing endolysosomal transport via the fate of Alexa Fluor 594-conjugated

cholera toxin B, implicating a role for NAADP in the regulation of vesicular trafficking and to be physiologically significant (Ruas et al. 2010).

1.5.4.4 The influence of NAADP on cardiac physiology/pathology

Cytosolic application of NAADP was shown to increase myocyte contraction and the frequency and amplitude of calcium sparks, and this response was inhibited by addition of bafilomycin A1, a vacuolar H^+-ATPase inhibitor acting on acidic calcium stores (Macgregor et al. 2007). Intact Langendorff-perfused hearts upon β-adrenergic stimulation showed increased NAADP levels (Lewis et al. 2012). Photorelease of NAADP and direct application of NAADP-AM, a cell permeant form of NAADP in atrial myocytes increased amplitude and frequency of calcium transients (Collins et al. 2011). Evidence then showed that Tpcn2$^{-/-}$ cardiac myocytes show a reduced response to β -AR stimulation and chronically reduced cardiac hypertrophy and arrhythmogenesis, demonstrating that NAADP/TPC2 signalling plays a major role in cardiac β-AR stimulation (Capel et al. 2015), making TPC2 the most promising candidate receptors for NAADP.

1.5.4.5 Lysosomes

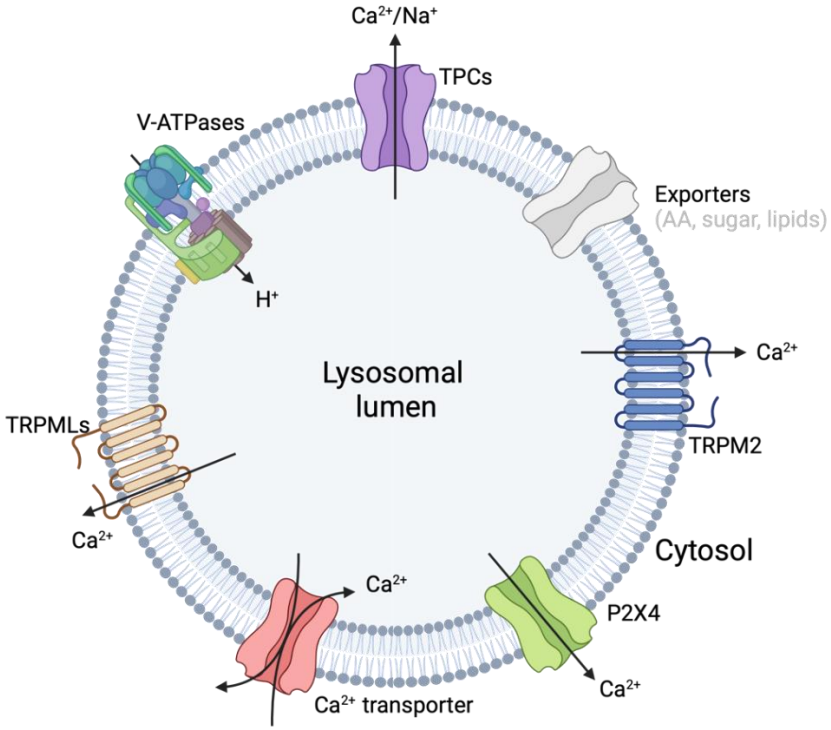

Figure 1.11: Schematic representation of the localisation of lysosomal ion channels and the direction of movement of their respective ions. Image created with Biorender.com and adapted from (de Araujo et al. 2020).

1.5.4.5.1 Physiology

Lysosomes are intracellular organelles measuring a few hundred nanometers in diameter. They were described for the first time in 1955 by Christian de Duve (De Duve et al. 1955) who was able to demonstrate their existence through the use of centrifugation techniques coupled with the detection of the enzyme activity. Lysosomes are spherical, single membrane bound organelles and are found in all cell types. Lysosomal proteins are targeted by phosphorylation of mannose in Golgi apparatus to bind to mannose-6-phosphate receptors to become lysosomes. Lysosomes are acidic membrane-bound organelles responsible for degrading macromolecules from both intracellular and extracellular sources. Around 50 different enzymes capable of degrading proteins, lipids, sugars, or nucleic acids are contained in lysosomes. Lysosomal membranes are covered with many different proteins, which are responsible for various functions such as the acidification of the lumen, transport of degradation products to the cytoplasm, and the fusion of the lysosomal membrane with endosomes, phagosomes and other organelles. LAMP1 and LAMP2 proteins represent half of the total proteins in this membrane (Eskelinen 2006). The pH of the lysosome lumen is extremely tightly regulated by a proton pump (V-ATPase, Figure 1.13) which allows the establishment of an acidic pH (~4-5) necessary for the proper functioning of the lysosomes, low pH provides an optimal environment for the function of luminal hydrolases (Ohkuma, Moriyama, and Takano 1982). The role of lysosomes as an intracellular calcium reservoir was described in the early 2000s (Christensen, Myers, and Swanson 2002; Churchill et al. 2002; Patel and Docampo 2010). Lysosomes maintain their calcium levels at a higher concentration than the cytoplasm, with a calcium concentration in the lumen of these organelles would be around 500µM, which is close to that of the SR (Lloyd-Evans et al. 2008). For many years, lysosomes were considered almost exclusively as vesicles filled with digestive enzymes whose unique role is the degradation of proteins, lipids and sugars.

1.5.4.5.2 Lysosomes and signalling pathways

However, in more recent years, numerous labs have studied these acidic stores to appreciate these organelles in their greatest complexity (Bose, Ayagama, and Burton 2022). It is increasingly clear that lysosomes are very dynamic and participate in the regulation of major signalling pathways and do not only have a digestion role. Calcium signals are involved in the functions of lysosomes but also involved in more global calcium signals at a whole cell to organ

level. Several calcium channels also reside in the lysosomal membrane. Lysosomes are equipped with a set of channels and pumps allowing them to release and capture calcium.

Over the last two decades, lysosomes have been accepted to participate in calcium homeostasis regulation, acting as calcium stores in the heart (Burgoyne, Patel, and Eden 2015) (Ogunbayo et al. 2018). Recent research has shown that lysosomes associate with ER and dwell at regions populated by IP_3R clusters and that lysosomes sequester calcium released by IP_3R (Atakpa et al. 2018), suggesting the involvement of IP_3R in regulating calcium exchange between the SR and lysosomes. Lysosomes are involved in the autophagic process, autophagy is the cellular survival mechanism that leads a self-degradative pathway. As lysosomes are a driving force in the pathway as they are involved in the final step of degradation. Findings have suggested that atrial autophagic flux is activated in patients with AF and autophagy induces atrial electrical remodelling (Yuan et al. 2018).

1.5.4.5.3 Other lysosomal calcium release channels

Only TPCs have been presented in detail and will studied in this manuscript but other calcium channels have been reported. Transient receptor potential cation channel mucolipin subfamily TRPML. There are 3 types TRPMLs, TRPML1, TRPML2 and TRPML3. They are calcium-permeable cation channels expressed in endosome and lysosome membrane (Xu and Ren 2015; Cheng et al. 2010). TRPML1, the best studied of the three, is a cation channel that passes calcium non-selectively and is activated by IP_3 (Dong et al. 2010). Many lipids accumulate in the lysosomes of cells when TRPML1 loses function. Calcium signals from TRPML1 are involved in numerous functions of lysosomes such as exocytosis, plasma membrane repair, autophagy or even lysosome reformation (Li et al. 2016). P2X4 is a trimeric channel that is permeable to both sodium and calcium when activated by luminal ATP and is dually localised on both lysosomal and plasma membranes (Li, Gu, and Xu 2019).

1.5.4.5.4 Calcium uptake

The molecular identity of the pump(s) involved in calcium uptake by lysosomes is not known. The process could be dependent on the pH gradient established by VATP-ase (Morgan et al. 2011). Studies show the inhibition of this pump, and consequently the loss of the pH gradient, induces a strong decrease in the quantity of calcium in the lysosomes (Lloyd-Evans et al. 2008; Christensen, Myers, and Swanson 2002). In addition, yeasts have a calcium/H^+ exchanger in vacuoles (equivalent to lysosomes in yeast) (Morgan et al. 2011) and a study suggests that

lysosomes can replenish their calcium stores in the absence of the pH gradient by inhibiting the V-ATPase H^+ pump (Garrity et al. 2016). According to this study, depletion of calcium from the ER prevents lysosomes from filling with calcium meaning calcium from the ER is essential for lysosomes to be replenished with calcium. Additional studies must be carried out to hope for a better understanding of the phenomenon, in particular the nature of the molecular interactors which participate in it. Calcium channels and pumps are still relatively unknown and additional studies are necessary to understand the mechanisms involved and their regulation.

1.6 Aims of this thesis

Calcium homeostasis plays a vital role in the heart and alterations in the intracellular concentration of calcium have been shown to lead to arrhythmias. Additionally, excessive stimulation of the IP_3 signalling pathway has been linked to AF through abnormal calcium handling. However, little is known about the mechanisms involved in this process and the role of IP_3 signalling in contributing to calcium handling remains unclear. Lysosomes have been identified as calcium stores although a role for lysosomal calcium signals in pacemaker activity, or in the atria has not been established. This thesis adds to the cardiovascular research field, specifically to cytosolic calcium handling in the atria as well as the physiological and pathological function in pacemaking. I postulate that interactions between two major calcium handling pathways (IP_3-mediated release from the SR and NAADP-mediated release from lysosomes) are involved in the modulation of atrial calcium signalling in response to α-adrenergic and β-adrenergic stimulation under physiological conditions, involving the stimulation/modulation of cAMP synthesis via calcium-sensitive AC1 and/or AC8. Furthermore, I propose that this interaction may be relevant for the pathogenesis of pacemaking dysfunctions such as AF. As current treatments are less than optimal, it is therefore vital to better understand the molecular mechanisms, to identify specific atrial drug targets and biomarkers to promote more effective treatments and better disease identification.
The hypothesis for the current study is therefore as follows:

Hypothesis: IP_3-mediated calcium release from the SR and NAADP-mediated calcium release from lysosomes lead to activation of calcium sensitive ACs and contribute to atrial function and pacemaking.

To test my hypothesis and answer my biological question as to how these two major calcium handling pathways (IP_3 and NAADP) contribute to atrial function and pacemaking. My project provides insight on the role of cytosolic calcium modulation in physiological conditions as well as a disease in the atria. In brief, Chapter 3 describes a role for NAADP signalling in response to β-adrenergic signalling, Chapter 4 investigates IP_3 signalling and its role in activating calcium-sensitive AC1 and AC8, Chapter 5 describes a role for NAADP signalling in response to α-adrenergic signalling, highlighting the relevance of these mechanisms in AF and in humans, Chapter 6 summarises the complexity of calcium handling between the SR and lysosomes and the functional implications of these major second messengers in the heart.

2 Methods

2.1 Animals

All work detailed complies with the "Principles and standards for reporting animal experiments" (Grundy, 2015) and the Animal (Scientific Procedures) Act 1986. All experimental protocols (Schedule 1) were approved by the University of Oxford, Procedures Establishment License Number XEC303F12 and under BMS service licence PP0574716 and 303301. All animals were housed maintained in a 12-h light/dark cycle with *ad libitum* access to standard diet and sterilised water.

2.1.1 Mice

From collaborators in the USA (Conti Lab), our lab obtained a global double knock out for AC1 and AC8 mouse colony. Disruption of the *Adcy1* gene in mice was first performed by Wu et al. 1995 (Wu et al. 1995) to generate KO of AC1 mice. KO *Adcy8* in mice were generated by (Muglia et al. 1999), by deletion of exon 1 and exon 2 of the 5'-flanking region of *Adcy8* gene and disruption was confirmed by assay of AC8 activity. AC1 and AC8 homozygote KO (DKO) mice were mated to obtain doubly heterozygotic F1 progeny. F1 mice were then backcrossed to AC1 homozygous mice to afford an F2 progeny with a 1:1 (heterozygote: homozygote) distribution at the *Adcy1* allele and a 1:1 (WT: heterozygote) distribution at the AC8 allele. F2 mice heterozygous for the *Adcy8* allele and homozygous for the AC1 allele were backcrossed to afford 25% doubly homozygous mice (DKO mice) (Wong et al. 1999). In 2020, mice (female and male) from this global DKO line was sent to us by Conti Laboratory from Wayne State University, unfortunately once the animals reached Oxford and that we are able to start the animal breeding process, AC1/8 DKO females were too old to be able to breed (due to lockdown). In order to generated a DKO colony, we backcrossed AC1/8 DKO male mice with WT females and proceeded with same method described above. In the process of generating AC1/8 DKO mice, heterozygous (Het) and homozygous (Hom) genotypes were generated: AC1/8 mice, Het AC1/HomAC8 and HomAC1/HetAC8 mice and used for left and right atrial preparations, an experimental method described below. The C57BL/6 and CD1 mice were obtained from Charles River (UK).

2.1.2 Rats and guinea pigs

Sprague Dawley neonatal rat litters at P3 and adult guinea pigs were obtained from Envigo (UK).

2.2 Human tissue permissions

Biopsies of the atrial appendage were obtained from 2 patients (Frisk et al.) undergoing on-pump cardiac surgery at the John Radcliffe Hospital (Oxford, United Kingdom). The study was approved by the Research Ethics Committee (reference no. 07/Q1607/38), and all patients gave written, informed consent.

2.3 Imaging techniques

2.3.1 Immunostaining

Cardiomyocytes were fixed with 2 % paraformaldehyde for 15 minutes. The cells were washed 3 times with PBS. Cells were then blocked with 10 % Donkey serum, 0.3 % BSA and 0.1 % triton X100 in PBS for 1 hour. Following the removal of the blocking buffer, cells were incubated overnight in 4°C with primary antibodies (listed below). Cells were then washed 3 times with PBS and incubated in the dark at room temperature for 4 hours with the secondary antibodies (1:400) donkey anti-mouse IgG conjugated to Alexa Fluor 564 and (A10040, Invitrogen), goat anti-rabbit IgG conjugated to Alexa Fluor 488 (SA510166, Invitrogen). Cells were washed 3 times in PBS and coverslips were mounted on slides with Vectashield™ with DAPI to stain the nuclei. The slides were viewed using a Nikon eclipse Ti inverted confocal microscope (Nikon) with a 63x/1.2 water objective Plan Apo VC 60xA WI DIC N2 lens. NIS-Element viewer (Nikon) was used to acquire multichannel fluorescence images. For detection of DAPI, fluorescence excitation was 350nm with absorption detected at 460nm. For detection of AlexaFluor 488, fluorescence excitation was at 488nm with emission collected 515nm. Excitation at 561nm was collected at 595nm for detection of AlexaFluor 568nm and imaged sequentially at 2048 × 2048 (12 bits).

PRIMARY ANTIBODY	CAT NO.	CONCENTRATION
Mouse anti-IP_3R2	sc-398434	1:50
Rabbit anti-AC1	55067-1-AP	1:100
Rabbit anti-AC8	55065-1-AP	1:100
Rabbit anti-LAMP2	PA1-655	1:100

Table1: Primary antibodies used for immunostaining.

2.3.2 Lysosomal live imaging

For the staining of acidic compartments (lysosomes) in live cardiac myocytes, LysoTracker™ red was used from Thermo Fisher Scientific (L12492). LysoTracker™ probes are fluorescent acidotrophic probes used for labelling and tracking acidic organelles in live cells. LysoTracker™ dyes consist of a fluorophore linked to a weak base that is only partially protonated at neutral pH, are freely permeant to cell membranes and typically concentrate in spherical organelles. To label atrial myocytes, 50nM LysoTracker™ red was incubated with the cells at room temperature in the dark for 20 minutes in Tyrode (Chapter 2, 2.11 Recipe for solutions, page 59) to allow it to partition into the acidic organelles. Myocytes were then washed twice and left in Tyrode for live imaging using Nikon Eclipse Ti Inverted Fluorescence Microscope with a 40x oil-immersion objective with illumination light at 546 nm.

2.3.3 4PI-SMS microscopy

4Pi-single-molecule switching (SMS) microscopy is an interference-based wide-field imaging method. I prepared NRAMs coverslips (same protocol than immunostaining described in 2.3.1, page 47, secondary antibodies include CF®680 (Biotum) and goat anti-rabbit IgG conjugated to Alexa Fluor 488 (SA510166, Invitrogen)). Imaging was conducted by Dr Jingyu Wang from Department of Engineering Science, Oxford, UK. In brief, fluorescence emitted by a single molecule (fluorophore) is collected by two opposing objectives with a common focus and follows two identical, but separate, beam paths until it is combined with a beam splitter cube and interferes. After combination, the fluorescence emission is relayed onto a camera, with appropriate optics, where it forms four images representing different interference phases. These images are recorded and later analysed to reconstruct a 3D super-resolution image (Wang, Allgeyer, et al. 2021).

2.3.4 High Resolution Episcopic Microscopy

High Resolution Episcopic Microscopy (HREM) was conducted on murine WT and DKO hearts in collaboration with the Sparrow Lab (Department of Physiology, Anatomy and Genetics, Oxford). Whole were fixed overnight at room temperature using Bouin's fixative (HT10132, Merck), then thoroughly rinsed in PBS and subjected to gradual dehydration in a methanol series, starting at 10 % + 10 % between each step, up to 90 % and then 90 %, 95 %, 100 % for 2 hours each step on a rocker at room temperature. Hearts were then embedded using a JB-4 kit (Catalogue number 00226-1, Polysciences), hearts overwent an overnight infiltration

at 4 °C with a 50:50 mixture of methanol and infiltration solution (JB-4 Solution A plus 1.25% (w/v) Benzoyl Peroxide Plasticizer). Hearts were rinsed in 100% infiltration solution for 1 hour in the dark at room temperature on rocker to help minimise residual methanol, the samples were left to incubate for up to 1 week at 4 °C in fresh infiltration solution. The embedding process involved the addition of 6 % (v/v) JB-4 solution B to the infiltration solution to initiate polymerization. Subsequently, analysis was carried out using a 3D Optical HREM imaging system (Indigo Scientific). HREM data were evaluated using Horos 3.3.6 (https://horosproject.org), and Amira for Life & Biomedical Sciences version 2019.4 (Thermo Fisher Scientific).

2.4 Whole tissue functional experiments

2.4.1 Mouse atrial preparations

Male mice (between 28-35g) were terminated by concussion followed by cervical dislocation, the chest cavity was opened, and the heart was rapidly excised and placed in warm, oxygenated physiological saline solution (PSS, Chapter 2, 2.11 Recipe for solutions, page 59) oxygenated with 95 % O_2/5% CO_2) containing heparin (10U/mL). Hearts were transferred to a dissection chamber under a microscope, ventricular tissue was discarded, and the atria were cleared of any overlying tissue such as cardiovascular tubing and adipose tissue. The right and left atria were separated, and loops of thin suture were tied to the lateral edges of each atrium by knotting around a small area of the tissue before mounting them onto a force transducer in an organ bath. One loop was anchored to a hook, and the other tied to the tension transducer with a resting tension between 0.22-0.24 g, a correct weight to visualise contraction without adding a strain to the atrium. The preparation was hung in an organ bath filled with PSS, maintained at 37^{o}C and oxygenated with 95 % O_2/5 % CO_2. Tension data were digitised using a PowerLabs bridge amplifier and recorded on LabChart5 software (all from AD Instruments, UK). Chronotropic effect was measured from the time interval between contraction of spontaneously beating right atrium and beating rate was calculated in real-time from the upstroke of the tension signal using the Chart5 Ratemeter function. Inotropic effect was measured from stimulated left atrium at 5 hertz during these experiments.

2.4.2 Phenylephrine dose-response curves

Phenylephrine (PE) was prepared in PSS (Chapter 2, 2.11 Recipe for solutions, page 59). After the frequency force of right atrial contractions and force of contraction of left atrial contractions

had stabilised (variation of no more than 2 beats per minute (BPM) and 0.2 g over a 10 minute period in the right and left atrium respectively) the effects of PE were investigated over a cumulatively increasing concentration range of 0.1 μM to 30 μM. Preparations were excluded if stabilised beating rate under control conditions only in the presence of PSS was under 300 BPM or if preparations were arrhythmic. Agonist doses were administered every 4 minutes using Gilson pipettes into the organ baths, with the tips submerged in the PSS. Atrial preparations were pre-treated with 1 μM metoprolol 1 hour before the first dose of PE to avoid any interference from β-adrenoceptors. Inhibitors were administered 30 minutes prior to the first dose of PE, allowing sufficient time for these pharmacological agents to penetrate the multicellular preparations.

2.4.3 Isoprenaline dose-response curves

Isoprenaline was prepared in PSS with 4X the amount of isoprenaline weighed of ascorbic acid. Similar to the PE dose response curves, after the frequency of right and left atrial contractions had stabilised, the effects of Isoprenaline were investigated over a cumulatively increasing concentration range of 0.1 nM to 1000 nM. Preparations were also excluded if stabilised beating rate under control conditions only in the presence of PSS was under 300 BPM or if preparations were arrhythmic. Agonist doses were administered every 3 minutes using Gilson pipettes into the organ baths, with the tips submerged in the PSS. Inhibitors were administered 30 minutes prior to the first dose of PE, allowing sufficient time for these pharmacological agents to penetrate the multicellular preparations.

2.5 Neonatal isolations

2.5.1 Neonatal rat ventricle myocytes isolation

Hearts were isolated from neonatal Sprague–Dawley rat pups (P3–P4), atria were dissected and discarded, and the ventricles were cut into small 1 to 2 mm^2 blocks and subjected to enzymatic digestion in trypsin (1mg/ml, Worthington) for 3 hours at 4°C on a rocker, following trypsinisation, the tissue was rinsed with cold Hank's buffered salt solution (HBSS, Sigma Aldrich) for 3 minutes. After the wash, a series of collagenase type IV (1mg/ml, Sigma Aldrich digestions were performed, 5 ml of collagenase was added to the tissue and stirred in a water bath at 37°C for 2 minutes. The first supernatant was discarded, and the process was repeated. Following each collagenase treatment, the tissue was gently agitated with a wide-tip pipette. The supernatant containing myocytes was transferred to a conical tube containing 3 ml of

HBSS and stored on ice. This collagenase digestion step was repeated 4 times. The tubes were balanced using HBSS and centrifuged at 2000 revolutions per minutes (rpm) for 8 minutes. After centrifugation, the supernatant was discarded and HBSS was added to the pellet and gently agitated. Centrifugation was repeated once again (1000 rpm for 10 minutes). The supernatant was then discarded and culture medium (68 % DMEM, 17 % M199, 10 % horse serum, 5 % FBS and 1 % penicillin/streptomycin, all from Sigma Aldrich) was added. The cell suspension was then strained using a 0.7µm sterile cell strainer. The isolated cells were pre-plated in an incubator (37°C, 5% CO2) for an hour to allow fibroblasts to attach to the plastic bottom of the dish. The ventricular myocytes in the supernatant were then carefully removed from the dish and a cell count was performed using a haemocytometer and trypan blue to avoid counting dead myocytes. The neonatal rat ventricle myocytes (NRVMs) were plated on a 24 mm glass coverslip pre-coated with laminin (40 µg/ml, Merck, UK) at a density of 30000 myocytes in culture medium and changed every 48 hours.

2.5.2 Neonatal rat atrial myocytes isolation

Neonatal rat atrial myocytes (NRAMs) were isolated using a modified protocol based on previous methods used to isolate neonatal rat ventricular myocytes (NRVMs) from (Burton et al. 2020; Burton et al. 2015). Hearts were isolated from 3-day-old Sprague Dawley rat pups, culled by cervical dislocation followed by exsanguination. Following dissection, atria were separated from the ventricles, transferred to 2 ml Dulbecco's Modified Eagle's Medium (DMEM) and cut into 1-2 mm^2 pieces. Atrial myocytes were enzymatically isolated by a series of enzymatic digestions; in trypsin (1 mg/ml, Merck, UK, rocked at 4°C for 2 hours) followed by collagenase (type IV, 1mg/ml, Merck, UK). For the collagenase digestions, the trypsin was replaced by 4 ml collagenase solution and tissue was gently triturated using a plastic pipette for 1 minute. The tissue plus collagenase solution was then stirred gently in a bath at 37 °C for 2 minutes and the first supernatant was discarded. A further 4 ml collagenase solution was added to the tissue pellet and triturated for 1 minute using a wide bore pipette. This solution was then stirred gently in a bath at 37°C for 2 minutes and the supernatant (4 ml) added to 3 ml HBSS and stored in a 15 ml centrifuge tube. This process was repeated a further 3 times to produce a total of 4x7 ml cell suspensions. Tubes were centrifuged at 2000 rpm for 8 minutes. Supernatant was then removed, and the cells were resuspended in 2 ml cardiomyocyte plating media (CPM: 85 % DMEM, 17 % M199, 10 % horse serum, 5 % FBS, 1 % penicillin/streptomycin) before being centrifuged at 1000 rpm for 10 minutes. All samples were then strained using a cell strainer and pooled into a single 50 ml centrifuge tube. Isolated cells

were pre-plated and incubated at 37°C (95% O_2, 5% CO_2) for 1 hour to allow separation of fibroblasts. Supernatant containing suspended atrial myocytes was then removed and cell density measured using a haemocytometer and trypan blue. Myocytes were seeded onto 24 mm laminin (40µg/ml, Merck, UK) coated glass coverslips in 35 mm 6-well plates at a density of 15000 cells per ml in CPM. Cell media was changed every 48 hours.

2.5.3 Neonatal mouse atrial myocytes isolation

For isolation of neonatal mouse atrial myocytes (NMAMs), a similar protocol was followed. Enzymatic digestion was shorter due to smaller size and less amount of tissue. Enzymatic digestions: in trypsin rocked at 4 °C for 1.5 hours instead of 2 hours. The collagenase digestions, atria were stirred gently in a bath at 37 °C for 1 minute instead of 2 minutes.

Hearts were isolated from 3-day-old CD1 mice pups, culled by cervical dislocation followed by exsanguination. Following dissection, atria were separated from the ventricles, transferred to 2 ml Dulbecco's Modified Eagle's Medium (DMEM) and cut into 1 mm^2 pieces. Atrial myocytes were enzymatically isolated by a series of enzymatic digestions; in trypsin (1 mg/ml, Merck, UK, rocked at 4°C for 1 hour) followed by collagenase (type IV, 1 mg/ml, Merck, UK). For the collagenase digestions, the trypsin was replaced by 4ml collagenase solution and tissue was gently triturated using a plastic pipette for 30 seconds. The tissue plus collagenase solution was then stirred gently in a bath at 37°C for 1 minute and the first supernatant was discarded. A further 4ml collagenase solution was added to the tissue pellet and triturated for 1 minute using a wide bore pipette. This solution was then stirred gently in a bath at 37°C for 30 seconds and the supernatant (4 ml) added to 3 ml HBSS and stored in a 15 ml centrifuge tube. This process was repeated a further 3 times to produce a total of 4x7 ml cell suspensions. Tubes were centrifuged at 2000 rpm for 8 minutes. Supernatant was then removed, and the cells were resuspended in 2 ml cardiomyocyte plating media before being centrifuged at 1000 rpm for 10 minutes. All samples were then strained using a cell strainer and pooled into a single 50 ml centrifuge tube. Isolated cells were pre-plated and incubated at 37°C (95 % O_2, 5 % CO_2) for 1 hour to allow separation of fibroblasts. Supernatant containing suspended atrial myocytes was then removed and cell density measured using a haemocytometer and trypan blue. Myocytes were seeded onto 24 mm laminin (40 µg/ml, Merck, UK) coated glass coverslips in 35 mm 6-well plates at a density of 30000 cells per ml in CPM. Cell media was changed every 48 hours.

2.5.3.1 NRAMs monolayer recordings

Recordings are done on day 5 of culture. Cells were loaded for 30 minutes with FluoVolt™ Membrane Potential Kit as per manufacturer's instructions (Invitrogen™, Catalog number: F10488). Monolayers were washed twice in HBSS to be replaced by modified Tyrode (Chapter 2, 2.11 Recipe for solutions, page 59) at room temperature. Recordings were done on a Leica DMIRB inverted fluorescence microscope connected to LED lights (FITC) with a prime 95B sCMOS camera at a minimum acquisition frame rate of 80 frames per second using MicroManager software (v2.0, Exposure time = 12.5ms).

2.6 Adult myocyte isolations

2.6.1 Guinea pig atrial myocyte isolation

Guinea pig hearts were dissected and washed in heparin-containing PSS (20 IU per mL) to prevent blood clots forming and mounted on a Langendorff setup for retrograde perfusion via the aorta. The heart was fist perfused in a modified Tyrode (Chapter 2, 2.11 Recipe for solutions, page 59) gassed with 95 % O_2/5 % CO_2 to maintain a pH of 7.4 at 37°C for 3 minutes. Solution was switched to a digestion solution: the modified Tyrode above containing 100 µM $CaCl_2$ and 0.04 mg/ml Liberase™ TH (Roche, Penzberg, Germany) and no ethylene glycol-bis-(beta-aminoethylether)-N,N,N',N'-tetraacetic acid (EGTA). After 25 minutes of enzymatic digestion, the heart was removed. The right atrium was separated from ventricles and left atria in a dissection bath, the tissue was cut into small pieces (around 4x4 mm) followed by 2 minutes of gentle trituration and stored in a high potassium medium SANKB (Chapter 2, 2.11 Recipe for solutions, page 59) at 4°C. Myocytes were left for 30 minutes at 4°C in SANKB before fixing for imaging or functional experiments (calcium transient recordings), and were used up to 4 hours.

2.6.2 Mouse atrial myocyte isolation

WT or DKO C57BL/6 mice hearts were dissected and washed in heparin-containing PSS (20 IU per ml) on a Langendorff setup for retrograde perfusion via the aorta. The heart was first perfused in a modified Tyrode (Chapter 2, 2.11 Recipe for solutions, page 59) gassed with 95 % O_2/5 % CO_2 to maintain a pH of 7.4 at 37°C for 1 minute. Solution was switched to a digestion solution: the modified Tyrode above containing 100 µM $CaCl_2$ and 0.02 mg/ml Liberase™ TH (Roche, Penzberg, Germany) and no EGTA. After 25 minutes of enzymatic digestion, the heart was removed. The atria were separated from ventricles in a dissection bath,

the tissue was cut into small pieces (around 2x2 mm) followed by 1 minute of gentle trituration and stored in a high potassium medium SANKB (Chapter 2, 2.11 Recipe for solutions, page 59) at 4°C. Myocytes were left for 30 minutes at 4°C in SANKB before fixing for imaging or functional experiments (calcium transient recordings), and were used up to 4 hours.

2.7 Single cell functional experiments

2.7.1 Calcium transient imaging

Single cell isolated atrial myocytes were incubated with 3µM Fluo-5F-AM (Invitrogen™) in SAN KB (Chapter 2, 2.11 Recipe for solutions, page 59) for 10 minutes at 37ºC in the dark. Cells were then plated to a glass coverslip for 10 minutes to adhere before imaging. Carbon fibre electrodes were used to field-stimulate calcium transients at 1hertz. All recordings were at 37ºC under gravity-fed superfusion of Tyrode (Chapter 2, 2.11 Recipe for solutions, page 59). Cells were visualised using a Zeiss Axiovert 200 with attached Nipkow spinning disk confocal unit (CSU-10, Yokogawa Electric Corporation, Japan). Excitation light, transmitted through the CSU-10, was provided by a 488-nm diode laser (Vortran Laser Technology Inc., Sacramento, CA). Emitted light was passed through the CSU-10 and collected by an iXON897 EM-CCD camera (Oxford Instruments, UK) at 60 frames per second with 2×2 binning (pixel size = 0.66667 μm^2). To avoid dye bleaching, video recordings were 10-20 seconds long (between 1000-2500 images) every minute to not continually be exposed to 488nm light. Calcium transients were measured using regions of interests (ROIs) in Andor iQ software (version 1.7) to record average whole cell fluorescence. Normalised calcium transient amplitude is expressed as change in mean cell fluorescence (F-F0)/F0 in the cell where F is the fluorescent value at a given time and F0 is the resting fluorescence value.

2.7.2 Fluorescence resonance energy transfer (FRET)

FRET imaging experiments were performed on day 4 of culture and 24 h after infection of the NRAMs with adenovirus carrying EPAC-S^{H187} cytosolic biosensor (Klarenbeek et al. 2015) at a multiplicity of infection of 1000 virus particles per cell. During experiments, cells were maintained at room temperature in a modified Ringer solution (Chapter 2, 2.11 Recipe for solutions, page 59). Dynamic measurements were done using an inverted microscope attached to a cool SNAP HQ2 camera and an optical beam splitter (Photometrics) for simultaneous recording of YFP and CFP emissions. FRET changes were measured as changes in the background-subtracted 480nm/545nm fluorescence emission intensity on excitation at 430 nm.

For recording, cells were left to settle for 4 minutes before any additions of pharmacological agents. Saturation levels were ensured by addition of 10µM of forskolin that activates ACs and increases intracellular levels of cAMP and 100µM of 3-isobutyl-1-methylxanthine (IBMX) a competitive non-selective phosphodiesterase inhibitor which raises intracellular cAMP, activates PKA was added for maximum response, FRET change responses are given as a percentage of the saturating FSK/IBMX response. FRET ratio changes were measured as changes of the background-subtracted 480 nM/545 nM fluorescence (cyan/yellow) emission intensity on excitation at 430 nM and expressed as R/R_0 where R is the ratio at time t and R_0 is the average ratio of the first 240 s. For each plate of cells, multiple cells were analysed individually within the field of view, and the mean FRET ratio (n=1) was calculated as the average for all cells within the field of view. Data are represented as *n*=number of biological replicates and N=number of litters from different rat mothers used for neonatal isolations (10-14 pups per litter), representing the number of independent isolations conducted from litters. Between n=1-3 biological replicates were conducted for N=1 neonatal isolation. The number of technical and biological replicates is indicated in the Figure legends.

2.8 Human iPSC culture

2.8.1 hiPSC-CMs culture and cardiomyocyte differentiation (Winbo protocol)

The cardiomyocytes derived from human-induced pluripotent stem cells (hiPSC-CMs) were obtained from Dr Winbo as previously described (Winbo et al. 2020), reprogrammed from peripheral blood mononuclear cells from a healthy adult male using an integration-free kit (CytoTune-iPS 2.0 Sendai Reprogramming Kit, Invitrogen, Life Technologies, now Thermo Fisher, Cat. Nos. A16517 and A16518) (Winbo et al. 2020). The hiPSC-CMs were differentiated into cardiomyocytes using previously published methods (Sharma et al. 2015; Winbo et al. 2020). Briefly, thawed hiPSC-CMs were plated on Geltrex-covered 12-well plates (0.3 x 10^6 cells/well) and cultured in StemFlex medium. On day 0, at ~85% confluency, the culture medium was changed to RPMI/B27- insulin medium with 6µM GSK3-β inhibitor CHIR9902, followed by RPMI/B27-insulin medium with 5µM Wnt inhibitor IWR1 on day 3. From day 7, the cells were grown in RPMI/B27+insulin medium, replaced every 72 hours. Spontaneously beating cardiomyocytes were further matured to a minimum of 2X days post hiPSC-CMs stage, then dissociated (Accutase (200 µl/ well) for FRET or Collagenase B (1 mg/ml in RPMI) for 18 hours at 37°C for calcium transient imaging) and replated on 12 mm Geltrex-covered glass coverslips before experiments. Calcium transient recordings were

conducted by Dr Winbo in New Zealand, and I analysed the raw recordings in Oxford. FRET work was conducted by myself while Dr Winbo cultured the hiPSC-CMs while she visited Oxford.

2.8.2 hiPSC-aCMs cardiac culture (Calamaio protocol)

Both atrial cardiomyocytes derived from human-induced pluripotent stem cells (hiPSC-aCMs) lines used for all experiments were derived from healthy donors. In particular, one from a female donor with no diagnosed diseases (https://hpscreg.eu/cell-line/TMOi001-A, purchased from Thermo Fisher Scientific) (Calamaio et al. 2023) and the other, previously characterised and published from a 62-year-old male not affected by AF or other cardiac pathologies (Benzoni et al. 2020). hiPSC-aCMs lines were maintained on human Biolaminin 521 LN-coated dishes in TeSR-E8™ medium (Thermo Fisher Scientific).

Cardiac differentiation was carried out by monolayer culture on Matrigel™ hESC-qualified Matrix (Corning, Corning, NY, USA) coated dishes using the PSC Cardiomyocytes Differentiation Kit (Thermo Fisher Scientific), following manufacturer instructions. To induce atrial differentiation, an adaptation of the method previously described (Devalla et al. 2015) was used. Briefly, cells were treated with 1 µmol/L atRA (Sigma) starting from day 3 of differentiation, and the medium was changed every day until day 7. Then, cells were maintained in Cardiomyocytes Maintenance Medium, changing the medium every other day. On the 21st day of differentiation, hiPSC-aCMs culture was enriched using the PSC-Derived Cardiomyocyte Isolation Kit (Miltenyi Biotech) following manufacturer instructions, which allows magnetic separation with highly specific CM surface markers. Immediately after magnetic separation, iPSC-CMs were collected and cryopreserved in liquid nitrogen. For the experiments, atrial differentiated hiPSC-aCMs were thawed on Matrigel-coated dishes and maintained at 37°C (95% O_2, 5% CO_2) with Cardiomyocyte Maintenance Medium with B-27 Supplement 50X and penicillin/streptomycin 100X (Thermo Fisher Scientific). Cells were cultured until 28 days before running FRET or live imaging.

2.8.3 Thaw of hiPSC-aCMs vials

Vials of hiPSC-aCMs were sent by our Italian collaborators and these cells were thawed and cultured until 28 days before conducting FRET work. Vials of hiPSC-aCMs were 21 days old and vials had a concentration from 1 to 1.5 million cells. Before thawing of the vials, dishes were coated with Matrigel (Corning Matrigel™ hESC-qualified Matrix, 5 mL vial CATALOG

NUMBER: 354277), 1 hour before seeding cells and dishes were left in the incubator at 37°C. Matrigel™ (253 µL) was diluted in in 25 mL of DMEM-F12 (Dulbecco's modified Eagle Medium; F-12 Nutrient Mixture (Ham), REF: 21331-020). 500 µL of diluted Matrigel™ was added to cover 24 mm dishes. Cardiomyocytes are thawed by placing the vial in a heated bath at 37°C until only a small cube of ice remains (2-3 mins) and then gently transfer the cellular suspension to a 15 mL collecting tube. The suspension was diluted 5X with DMEM-F12 to dilute DMSO and serum present in the thawing medium. Cells are centrifuged for 5 minutes at 200 g at RT. The cell pellet was then gently resuspended in Cardiomyocyte Maintenance Medium (Thermo Fisher), REF: A29208-01) with B-27TM Supplement (50X, serum free, Thermo Fisher, REF: 17504044), Y27632 Rock Inhibitor (10 µM, STEMCELL TECHNOLOGIES, CAT #72304) and penicillin/streptomycin (100X, Thermo Fisher, REF: 15140148) to be counted with a haemocytometer and trypan blue. Dishes were taken out of the incubator and just before adding the cells the top layer of Matrigel™ was removed ensuring that the coated surface didn't dry up and avoiding scratching the coated surface. Atrial hiPSCs were seeded at 30 000 cells per dish for all experiments.

2.8.4 Culture

During culture hiPSC-aCMs were incubated at 37°C (95% O_2, 5% CO_2). 24 hours after thawing, media is replaced with Cardiomyocyte Maintenance Medium with B-27 Supplement 50X and penicillin/streptomycin 100X. Cells are washed with DMEM-F12 before adding new media as Rock Inhibitor becomes toxic if left for longer periods of time. Media was then changed every 48 hours. Cells were cultured until 28 days before running FRET or live imaging.

2.9 Molecular experiments

2.9.1 RT-qPCR

Extraction and purification of total RNA from cultured NRAMs were conducted using RNeasy Plus Mini Kit (Qiagen). RNA concentration was measured before RNA is reverse transcribed to cDNA using a High-Capacity cDNA Reverse Transcription Kit (Applied Biosystems™). Polymerase Chain Reaction (PCR) Master Mix TaqMan™ Fast Advanced (Thermo Fischer Scientific) was performed. Primers used were *Adcy1* (Rn02115682_s1), *Adcy8* (Rn00567592_m1), *Itpr2* (Rn00579067_m1), *Adcy6* (Rn00563162_m1) and *Gapdh* was used

as reference gene to allow for normalisation of the expression levels of target genes across our different samples.

2.9.2 Western blots

Cultured NRAMs underwent lysate with RIPA and 1% anti-protease cocktail. Protein concentration in lysates were measured using a Pierce™ BCA Protein Assay Kits (Thermo Scientific™) and denatured using 5% 2-mercaptoethanol (Sigma-Aldrich). Proteins were loaded separated by gel electrophoresis (NW04120BOX, NuPAGE 4%–12% Bis-Tris protein gels, 20X MES buffer). The gel was transferred to a nitrocellulose membrane (NC) (Bio-Rad) for protein transfer (X-cell-II blot module, Thermo Fischer Scientific). NC membrane was blocked by incubation in 5% skimmed milk for 1 hour at room temperature on a rocker. The primary antibodies were incubated at 4 °C overnight on a rocker. Donkey anti-mouse IgG conjugated to Alexa Fluor 564 (1:400) and goat anti-rabbit IgG conjugated to Alexa Fluor 488 (1:400) were used as the secondary antibody. The secondary antibodies were detected via fluorescence using Invitrogen™ iBright™ Imagers.

2.10 Statistics

For atrial preparations, [agonist] vs. response (three parameters) was used to form graphs and Log(concentration)-response curves were used to calculate EC50s and maximum responses by fitting an agonist-response curve with a fixed slope to normalised response data. Normalised data were used to compare responses as inhibitors were expected to significantly affect the control beating rate or tension. Dose-response curve maximums and EC50 which are given as mean ± 95 % confidence interval (CI) of best-fit value. Fitted values were compared using ANOVA with Dunnett's multiple comparisons test. For FRET analysis, data was normalised and are presented as mean ± standard error of the mean (SEM) of recorded values. Datasets in this manuscript were tested for normality distribution, using Shapiro Wilk normality test. If datasets passed normality test multiple-group comparison, a one-way analysis of variance (ANOVA) followed by multiple comparison testing was performed or for comparison between two groups, an unpaired, two-tailed Student's t-test was used. If not, datasets were analysed using Kruskal Wallis followed by Dunn's multiple comparison or non-parametric Mann-Whitney U test. Datasets are presented as mean ± SEM. Differences were considered statistically significant at values of $P < 0.05$, *P<0.05, ** P<0.01, *** P<0.001, **** P<0.0001. Statistical methods used are given in the legend of each figure. Statistical analyses

were performed using Prism 10 (GraphPad, CA, USA) . Differences were considered statistically significant at values of $P < 0.05$.

2.11 Recipe for solutions

PSS in mM: NaCl 125, $NaHCO_3$ 25, KCl 5.4, NaH_2PO_4 1.2, $MgCl_2$ 1, glucose 5.5, $CaCl_2$ 1.8, pH to 7.4 with NaOH

Tyrode in mM: NaCl 136, KCl 5.4, $NaHCO_3$ 12, sodium pyruvate 1, NaH_2PO_4 1, $MgCl_2$ 1, EGTA 0.04, glucose 5.

SANKB in mM: KCl 70, $MgCl_2$ 5, K^+ glutamine 5, taurine 20, EGTA 0.04, succinic acid 5, KH_2PO_4 20, HEPES 5, glucose 10; pH to 7.2 with KOH

Extracellular solution (E1) in mM: NaCl 140, KCl 3, MgCl2 2, CaCl2 2, glucose 15, HEPES 10, pH 7.2 with NaOH

3 Chapter 3: Lysosomal signalling in response to beta-adrenergic stimulation in atrial and sino-atrial node myocytes

3.1 Summary of contribution:

This chapter presents a paper investigating the role of lysosomal calcium signalling in atrial and for the first time in SAN myocytes in response to β-AR stimulation. I am joint first author with Dr Rebecca Capel. I carried out atrial preparations, FRET work (on NRAMs and hiPSCs), hiPSC-CMs calcium transient analysis and conducted human lysosomal analysis on EM. Additionally, I did conceptualisation, methodology, and writing of the paper. Figures reproduced from the paper were my own work.

3.2 Introduction

Calcium is a universal intracellular signal, implicated in diverse roles. Extracellular agonist such as hormones and neurotransmitters trigger complex calcium signals through entry of extracellular calcium or calcium release from organelles acting as intracellular calcium stores. To ensure a tight regulation of such a process, cells have significant concentration gradients between the cytoplasm, the different cellular compartments, and the extracellular environment (Berridge, Lipp, and Bootman 2000). The main intracellular calcium reservoir in cardiomyocytes is the SR but other organelles have shown to participate in calcium handling.

NAADP is a potent calcium releasing second messenger releasing calcium from acidic stores first discovered in sea urchin eggs (Lee and Aarhus 1995). The same group proposed later that lysosomes are the targeted calcium store by NAADP. They ran experiments demonstrating the presence of calcium stores in sea urchin eggs mobilised by NAADP and is dependent on a proton gradient maintained by an ATP-dependent vacuolar-type proton pump (V-ATPase) (Churchill et al. 2002). This discovery opened a field of research in cellular physiology for calcium release from intracellular organelles such as lysosome in many different cell types. In the early 2000s, NAADP binding sites were reported in the brain (Patel et al. 2000) and administered NAADP in cultured neocortical neurons caused a release of calcium from acidic stores and potentiates neurite extension (Brailoiu et al. 2005) revealing not only the presence of functional NAADP receptors but also a role for NAADP calcium release in the brain.

NAADP action in ventricular myocytes in guinea pig were first described by (Macgregor et al. 2007). Cytosolic application of "caged" NAADP which is released by a pulse of ultraviolet light caused an increase in resting (diastolic) calcium concentrations and an increased stimulated calcium transient amplitude. This effect was inhibited by bafilomycin A1 (V-ATPase inhibitor), desensitising concentrations of NAADP or by inhibiting SR function by ryanodine and thapsigargin (SERCA pump inhibitor). Evidence later showed that in Langendorff-perfused whole hearts, β-AR stimulation also increased NAADP levels but also increased heart rate and force that was mediated by NAADP (Lewis et al. 2012).

Alongside these studies, NAADP receptors were shown to be distinct from the other calcium second messengers such as IP_3 and cADPR, by removal of functional ER calcium stores (Churchill et al. 2002; Churchill and Galione 2001). TPCs first emerged as a novel intracellular calcium release channel in plants (Peiter et al. 2005). This discovery led (Brailoiu et al. 2009)

to locate TPCs on endosomal and lysosomal membranes by significant colocalisation of TPC1 with endo-GFP and LAMP1 and colocalisation of TPC2 only with LAMP1. Moreover, NAADP-mediated calcium signals were enhanced by overexpression of TPC1 and attenuated after knockdown of TPC1 in human breast cancer cell line (SKBR3) (Brailoiu et al. 2009). TPC2 then became the specific target for NAADP as it also was shown to be specifically expressed on lysosomal membranes and form calcium permeable channels that can bind NAADP with a high affinity (Calcraft et al. 2009). Experiments also showed that responses to NAADP were abolished by disrupting the lysosomal proton gradient and by ablating TPC2 expression, but only attenuated responses by depleting ER calcium stores or blocking IP_3R (Calcraft et al. 2009). The lines above present evidence of TPC2 forming NAADP receptors that release calcium from acidic organelles, lysosomes, which can trigger additional calcium signals from the SR or ER. Around the same time (Zong et al. 2009) also demonstrated TPC2 to display lysosomal NAADP mediated calcium release and was almost completely abolished when the capacity of lysosomes for storing calcium is pharmacologically blocked by bafilomycin A1.

Similar work to Macgregor et al. was conducted in atrial myocytes by Collins et al. (Collins et al. 2011). Photorelease of "caged" NAADP also increased the amplitude of calcium transients without affecting the L-type calcium current and this increase in calcium transients amplitude was accompanied by an increase in the amount of calcium stored in the SR (Collins et al. 2011). NAADP response was eliminated in the presence of bafilomycin A1, confirming the role for lysosomes as important calcium stores the relevancy of NAADP pathway in atrial myocytes.

So far, research has reported a functional role for NAADP in heart physiology, no findings have been made on the potential implication in heart pathophysiology. In 2013, (Nebel et al. 2013) published first reporting of NAADP implications in arrhythmias evoked by β-adrenergic stimulation. They investigated NAADP effects on spontaneous diastolic calcium transients in cardiac myocytes and arrhythmias in awake mice. Results indicated that BZ-194 (a small molecule inhibitor of NAADP action that inhibits NAADP-mediated calcium signalling) blocked spontaneous diastolic calcium transients caused by high concentrations of the β-adrenergic agonist isoproterenol in electrically paced primary cardiomyocytes, as seen with bafilomycin A1 in previous reporting. BZ-194 also reduced isoproterenol-induced arrhythmic events in awake mice. Providing evidence that NAADP modulation plays a role for triggering arrhythmias. Additionally, (Capel et al. 2015) by investigating the importance of TPC2 proteins

in heart physiology discovered in *Tpcn2*$^{-/-}$ mice, NAADP-AM, cell-permeant analogue of NAADP, failed to enhance calcium transients in single myocytes and were also reduced in response to β-adrenergic stimulation contrary to WT mice. They also investigated the physio-pathological implications of NAADP, isolated whole hearts from *Tpcn2*$^{-/-}$ mice showed to be less prone to arrhythmias induced by isoproterenol exposure compared to WT mice. Providing further evidence that ablation of NAADP signalling shows protective properties against isoprenaline exposure induced arrhythmias. More recent studies showed endolysosomes-specific proteins to be upregulated in biopsies from AF goat model and structural anomalies, were also observed from electron tomograms such as autophagic-vacuole formation suggesting that endolysosomes may play a role AF development (Ayagama et al. 2024). Work has shown NAADP pathway to be a modulator of β-adrenergic stimulation and implicated in arrhythmias, raising questions that it could play a role in initiation and even maintenance of atrial arrhythmias effects from adrenergic stimulation.

Arrhythmias are a major health problem; AF is the most common form of arrhythmias worldwide. Current treatments for AF are for rhythm, rate control and anticoagulation to reduce the risk of stroke and restore normal heart rhythm ('Global, regional, and national age-sex-specific mortality for 282 causes of death in 195 countries and territories, 1980-2017: a systematic analysis for the Global Burden of Disease Study 2017' 2018). Unfortunately, these treatment options are insufficient due to the ability of fibrillation itself to sustain AF (re-entrant drivers, fibrosis), named “AF begets AF” (Wijffels et al. 1995) or have major significant undesirable effects on the ventricles due to a lack in specific targets to the atria. A need for novel AF treatments or therapy options is critical due to significant limitations of existing treatments. A role for NAADP signalling as a contribution to SAN pacemaker rate has not previously been studied.

3.3 Aim of Chapter 3

Observations regarding the importance of NAADP in atrial signalling have, thus far, focused solely on the effects of a single dose of isoprenaline in isolated myocytes, and studies in intact tissue are lacking. The aim of this chapter is to further investigate the role of lysosomal calcium signalling in atrial and for the first time in SAN myocytes in response to β-AR stimulation. Additionally, this chapter will present first evidence of the relevance NAADP pathway in humans, in functional work and in cellular structural remodelling analysis as part of AF.

3.4 Methods

The methods used in this chapter have been detailed in Chapter 2. In brief, For the study of intact atrial tissue, CD-1 mice were sacrificed. Left and right atrium were dissected and separated to be mounted on to a force transducer in an organ bath at 37°C in PSS (Chapter 2, 2.11 Recipe for solutions, page 59). Atria were mounted separately to study SAN activity in spontaneously beating right atrium and to study the force of contraction in left atrium paced at 5 hertz. Chronotropic and inotropic responses were measured in real time using LabChart5 software. After stabilisation of each atrium, cumulatively increasing doses of isoprenaline at a concentration range of 0.1 nM to 1000 nM were administered every 3 minutes into the organ bath and 0.001 % DMSO, 500 nM bafilomycin A1 or 3 µM *trans*-Ned-19 were added 45 minutes before first addition of isoprenaline.

Neonatal Sprague-Dawley rat pups were culled between 3-5 days old, ventricles were dissected and discarded. The atria were cut into small pieces and subjected to enzymatic digestion in trypsin (2 hours at 4°C on a shaker, 1 mg/mL), followed by series of collagenase digestion (type II, 2 minutes, 1 mg/mL). NRAMs were plated 30,000 cells per well (35 mm Petri dish) and cultured for 3 days before infection of FRET biosensor.

The development of FRET-based reporters has made it possible to directly monitor concentration changes in cAMP in live cells. FRET technique is a non-radiative energy transfer from a donor to a suitable acceptor fluorophore and occurs only when the donor and acceptor fluorophores are in proximity (less than 10 nm). The untargeted FRET reporter EPAC-S^{h187} was used to measure bulk cytosolic cAMP signals in response to 1 nM isoprenaline in NRAMs and in human induced pluripotent stem cell derived cardiomyocytes (hiPSC-CMs) and in human induced pluripotent stem cell derived atrial cardiomyocytes (hiPSC-aCMs). FRET imaging was performed 24 h after infection of adenovirus carrying EPAC-S^{h187} and cells were maintained at room temperature during experimental protocol. For recording, myocytes were left to settle for 4 min and inhibitor, or saline control were then added, bafilomycin A1 at 100 nM or 0.1 % of DMSO for control. A concentration of 1 nM isoprenaline was administered, this concentration induced global cAMP response without saturation. Isoprenaline was added after 5 mins and left for 10 mins. After the 10 mins, 10 µM of forskolin that activates adenylyl cyclases (ACs) and increases intracellular levels of cAMP and 100 µM of IBMX (3-isobutyl-1-methylxanthine) a competitive non-selective phosphodiesterase inhibitor which raises

intracellular cAMP to ensure saturation of the FRET signal. These FRET changes imply an increase in cAMP, results are given as a percentage of the saturating FSK/IBMX response.

Human calcium transient work in this chapter was conducted on 3 different differentiations of healthy cardiomyocyte hiPSC-CMs line (Winbo et al. 2020) reprogrammed from peripheral blood mononuclear cells from a healthy adult male, described in methods (Chapter 2, hiPSC-CMs culture and cardiomyocyte differentiation (Winbo protocol), page 55). Dr Winbo ran calcium transient experiments from my protocol in New Zealand and sent me raw data for me to analyse and generate presented Figures. Human FRET work was conducted on 3 hiPSC-CMs lines, 1 from (Winbo et al. 2020) described above and from 2 atrial specific hiPSC-CMs lines derived from healthy donors, one from a female donor (Calamaio et al. 2023) the other, from a 62-year-old male not affected by AF or other cardiac pathologies (Benzoni et al. 2020).

Statistical analyses in this Chapter were performed using Prism 10 (Graphpad). Differences were considered statistically significant at values of non-significant (ns)$P>0.05$, *$P<0.05$, ** $P<0.01$, *** $P<0.001$, **** $P<0.0001$. Statistical methods used are given in the legend of each figure.

3.5 Results

3.5.1 Lysosomal calcium forms part of the β-adrenergic response in intact SAN pacemaker tissue

To evaluate the impact of NAADP pathway in atrial function I recorded intact, spontaneously beating right atrial preparations to measure SAN activity through the measurement of beating rate. Figure 3.1A shows dose response curves of spontaneous beating rate in right atria generated in response to cumulative doses from 0.1 to 1000 nM of isoprenaline to measure the effect of NAADP in response to β-stimulation.

Intact SAN preparations responded to isoprenaline with an increase in rate in the expected sigmoidal pattern. In the presence of 0.001 % DMSO as a solvent control, the maximum response to isoprenaline was 80 (79 – 82) % with an EC50 of 2.2 (1.9 – 2.5) nM (n=6, Figure 3.1). In the presence of 500 nM bafilomycin A1, as a method to abrogate acidic store calcium loading, the maximum beating rate increase during cumulative isoprenaline additions was not changed (85 [83 – 89] %) however there was a significant rightward shift in EC50, to 9.5 (7.9 – 11.6) nM (n=7, P<0.01, Figure 3.1). NAADP binding site antagonist *trans*-Ned-19 (3 μM) led to both a significant rightward shift in the EC50 for isoprenaline (P<0.05), to 3.7 (3.2 – 4.4) nM and a significant reduction in maximum beating rate increase, to 63 (61 – 65) % (n=8, P<0.05, Figure 3.1).

No significant differences were seen in starting beating rate before inhibitor additions, starting rate in solvent control with DSMO condition started with 374 ± 10.9 BPM (n=6), preparations with bafilomycin A1 or *trans*-Ned-19 started at 372 ± 16.8 BPM (n=7) and 366 ± 7.9 BPM (n=8) respectively (Figure 3.2A). Addition of either inhibitor showed no significant affect to spontaneous beating rate in the absence of stimulation with isoprenaline, DMSO (0.1 %) condition showed a decrease of 4.5 ± 2.7 % (n=6) and conditions with bafilomycin A1 or *trans*-Ned-19 showed a decrease of 5.3 ± 3.1 % (n=7) and 4.5 ± 3.1 % (n=8) respectively (Figure 3.2B).

1.1.1 Lysosomal calcium forms part of the β-adrenergic response in intact cardiac left atrial tissue

Intact left atria were dissected from CD1 outbred mice to investigate the effect of lysosomal signalling inhibitors on the dose-response curve to isoprenaline (Figure 3.3). In the presence of 0.001 % DMSO as a solvent control, application of cumulative doses of isoprenaline led to a

maximum 170 (154 – 186) % increase in contractile force with an EC50 of 4.2 (2.4 – 7) nM (n=7, Figure 3.3). After incubation with 500 nM bafilomycin A1, the maximum contractile response to isoprenaline was significantly reduced to 99 (88 – 110) % (n= 9, P<0.001) without change in the EC50 (Figure 3.3). In the presence of *trans*-Ned-19 at 3 µM presented a significant reduction in the maximum response to isoprenaline, to 142 (129 – 154) % (P<0.05) and a significant right-shift in the EC50, to 8.8 (5.5-14) nM (n= 6, P<0.01, Figure 3.3). No significant differences were seen in starting beating force before inhibitor additions, tension in solvent control with DSMO condition started with 0.074 ± 0.014 g (n=7), preparations with bafilomycin A1 or trans-Ned-19 started at 0.127 ± 0.017 g (n=9) and 0.097 ± 0.013 g (n=6 respectively (Figure 3.4A). Addition of either inhibitor showed no significant affect to tension in the absence of stimulation with isoprenaline, DMSO condition showed a decrease of 17.5 ± 4.6 % (n=7) and conditions with bafilomycin A1 or *trans*-Ned-19 showed a decrease of 21.4 ± 3.8 % (n=9) and 15.6 ± 4.1 % (n=6) respectively (Figure 3.4B).

3.5.2 Lysosomal calcium makes significant contribution to cellular cAMP levels in response to β-adrenergic stimulation in NRAMs

We measured cellular cAMP in cultured NRAMs expressing the cytosolic Fluorescence resonance energy transfer (FRET)- based reporter EPAC-S^{H187}. In the presence of 0.1 % DMSO as a solvent control, 1 nM isoprenaline led to a FRET change of 30.05 ± 3.6 % (n=11, N=5). This increase in cellular cAMP in response to β-adrenergic stimulation was significantly reduced if carried out in the presence of 100 nM bafilomycin A1 (8.5 ± 2.3 %, n=4, N=4, P<0.01, Figure3.5A). Application of 1 nM isoprenaline to NRAMs in a 0-calcium solution caused a FRET change of 11.39 ± 0.9 % (n=4, N=4). This was significantly reduced if isoprenaline was added in the presence of 100 nM bafilomycin A1 (4.34 ± 0.6 %, n=4, N=4, P<0.001, Figure3.5B). These observations suggest that lysosomes make a significant contribution to the cellular cAMP increase but whether calcium from the SR could still be contributing to this response is investigated below.

A lysosomal contribution to cellular cAMP could feasibly occur downstream of changes in SR and cytosolic calcium levels or in the vicinity of the lysosome itself. After 45 min incubation with ryanodine and thapsigargin (both 2 µM) to empty SR stores, and in the absence of extracellular calcium, 1 nM isoprenaline caused a 17.47 ± 1.2 % (n=6, N=5) FRET change. The presence of 100 nM bafilomycin A1 continued to significantly inhibit (3.7 ± 1 %, n=7, N=5, P<0.0001, Figure 3.5C) the cellular cAMP response to isoprenaline. Taken together these

observations suggest that lysosomal signalling, stimulated following β-adrenergic stimulation, can modulate cellular cAMP levels by a mechanism which does not require calcium arising from the SR.

3.5.3 Lysosomal calcium makes significant contribution to cellular cAMP levels in response to β-adrenergic stimulation in hiPSC-CMs

FRET experiments were carried out on hiPSC-CMs and hiPSC-aCMs to investigate cAMP levels in response to isoprenaline in the presence or absence of bafilomycin A1. I conducted experiments on multiple differentiation replicates on hiPSC-CMs and hiPSC-aCMs to ensure reliability and statistical validity of the results to provide stronger evidence for validating the NAADP pathway in a human cardiomyocyte model. Live cell imaging with Lysotracker^{TM} was conducted to confirm presence of lysosomes in hiPSC-CMs (**i**) and hiPSC-aCMs (**ii**) are presented in Figure 3.6A). Peak in cAMP levels were significantly lower in the presence of bafilomycin A1 with a FRET change of 19.42 ± 2.2 % (n=8, N=4) in response to isoprenaline compared to the control condition (42.51 ± 4.5 %, n=7, N=4, P<0.01, Figure 3.6B).

3.5.4 Bafilomycin A1 inhibits the beating rate response to β-adrenergic stimulation in hiPSC-CMs

The observations presented previously are the first to suggest a role for lysosomal calcium signalling in pacemaker physiology. Here, experiments were conducted at single cell level in cultured spontaneously beating hiPSC-CMs myocytes to confirm the effect of bafilomycin A1 in response to isoprenaline. A concentration of 3 μM Fluo-5F-AM was used to monitor the generation of spontaneous calcium transients in control conditions (Figure 3.7A) and in the presence of 100 nM bafilomycin A1 (Figure 3.7B) and Snapshots of hiPSC-CMs loaded with Fluo-5F-AM are presented in Figure 3.7C. Addition of DMSO or bafilomycin A1 did not differ the beating rate between the 2 conditions with a baseline rate in the presence of DMSO of 47 BPM (n=14, N=4) and 50 BPM (n=11, N=3) in the presence of bafilomycin A1 (Figure 3.8A). A wider spread of baseline calcium transient amplitude was observed in DMSO control conditions compared to the bafilomycin A1 conditions, datapoints were collected from 4 different cell differentiations all scattered throughout the graph not forming a separate group. Cells exhibited an adequate baseline rate with no morphological or anatomical reasons to exclude and survived throughout the duration of the protocol, therefore they were not excluded from the dataset.

Superfusion of 3 nM isoprenaline had an increase in beating rate over 4 minutes with a maximum of 35.4 ± 7.1 % (*n*=14, *N*=4, Figure 3.8B). Whereas the presence of bafilomycin A1 showed a maximum increase of 8.7 ± 5.3 % after 1 minute of exposure to 3 nM of isoprenaline to then decreased over the rest of the 4 min of exposure to isoprenaline with a -3.5 ± 3.2 % at the 4-minute mark (*n*=11, *N*=3, *P*<0.0001, Figure 3.8B). Calcium transient amplitude showed no significance between DMSO and bafilomycin A1 prior any stimulation with isoprenaline (Figure 3.9A), amplitude decreased over 3 nM isoprenaline exposure in both conditions. In the presence of bafilomycin A1 amplitude decreased faster over the 4 minutes of isoprenaline exposure presenting a significant difference at 4 minutes with a decrease of 47.75 ± 5.3 % (*n*=11, *N*=3) compared to 24.92 ± 6 % (*n*=14, *N*=4) to control (*P*<0.001, Figure 3.9B).

A

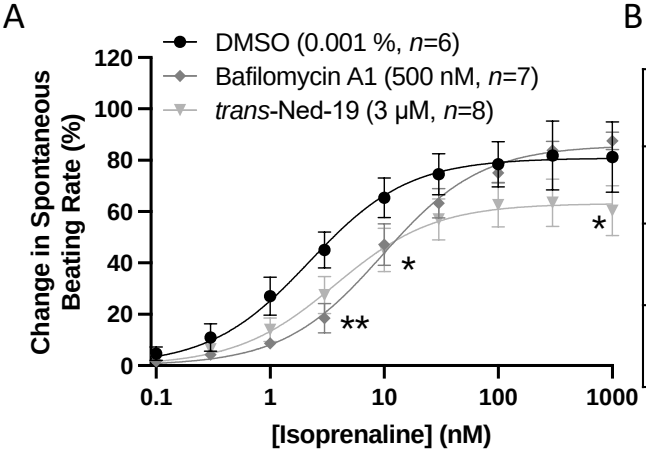

B

	EC50 (nM)	Max (% change)
DMSO (0.001 %)	2.2 (1.9 – 2.5)	80.8 (79.2 – 82.5)
Bafilomycin A1 (500 nM)	9.5 ** (7.9 – 11.6)	85.9 (82.6 – 89.2)
***trans*-Ned-19 (3 µM)**	3.7 * (3.2 – 4.4)	63.2 * (61.3 – 65)

Figure 3.1: Lysosomal calcium contributes to the isoprenaline chronotropic response in intact right atria.

A, Dose-response curves show change in beating rate on cumulative addition of isoprenaline (0.1 nM – 1000 nM) to spontaneously beating murine right atria preparations under control conditions (circles, *n*=6) and in the presence of either 100 nM bafilomycin A1 (squares, *n*=7) or 3 µM *trans*-Ned-19 (triangles, *n*=8).
B, Table indicating EC50 and maximum rate increase measure from dose-response curve in A.

Dose-response curves were fitted using log(agonist) vs. response (three-parameter model). Asterisks indicate significance level for effect of bafilomycin A1 and *trans*-Ned-19 compared to control at individual concentrations, determined using 2-way repeated measures ANOVA followed by Dunnett's multiple comparisons test. Data on graph are represented as mean ± SEM; *, $p<0.05$; **, $p<0.01$.

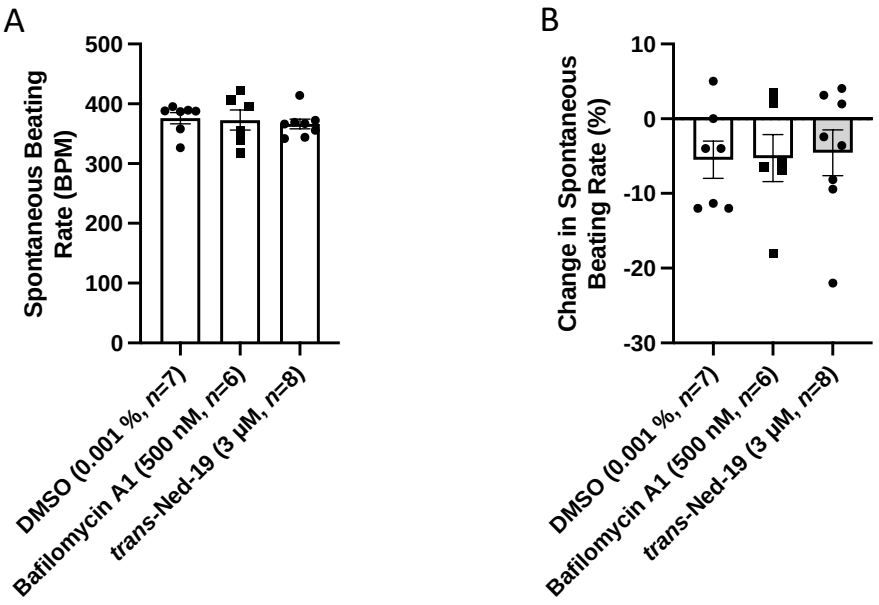

Figure 3.2: Baseline beating rates show no significant changes before addition of isoprenaline.

A, Comparison of spontaneously beating rate in intact murine right atrial preparations in PSS prior to addition of DMSO (*n*=7, circles), 100 nM bafilomycin A1 (*n*=6, diamonds) or 3 µM *trans*-Ned-19 (*n*=8, triangles) before stimulation with isoprenaline.
B, Comparison of change in spontaneously beating rate (in %) in murine right atrial preparations in PSS on addition of DMSO (*n*=7, circles), 100 nM bafilomycin A1 (*n*=6, diamonds) or 3 µM *trans*-Ned-19 (*n*=8, triangles), prior to stimulation with isoprenaline.

No significance for effect of bafilomycin A1 and *trans*-Ned-19 compared to control at individual concentrations was observed, determined using 2-way repeated measures ANOVA followed by Dunnett's multiple comparisons test. Data are represented as mean ± SEM.

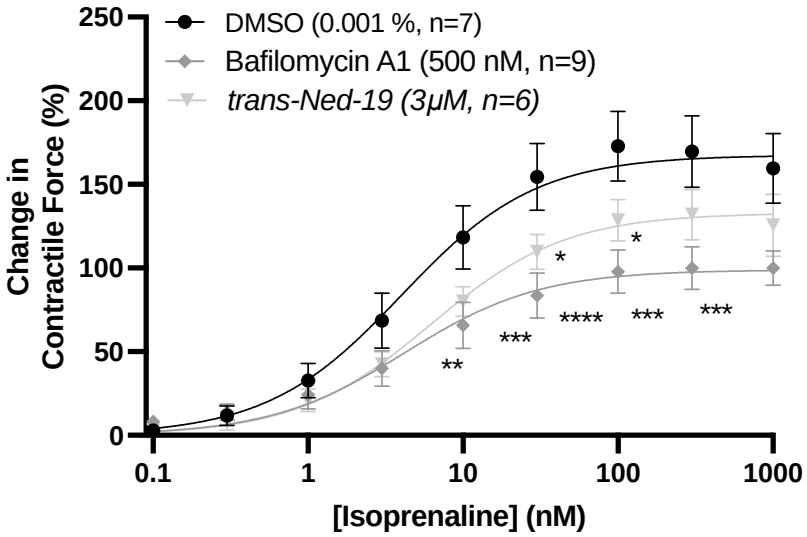

Figure 3.3: Lysosomal calcium contributes to the isoprenaline inotropic response in intact left atria.

Dose-response curves to show change in tension on cumulative addition of isoprenaline to spontaneously beating murine right atria preparations under control conditions (circles, *n*=7) and in the presence of either 100 nM bafilomycin A1 (diamonds, *n*=9) or 3 μM *trans*-Ned-19 (triangles, *n*=6).

Dose-response curves were fitted using log(agonist) vs. response (three-parameter model). Asterisks indicate significance level for effect of bafilomycin A1 and *trans*-Ned-19 compared to control at individual concentrations, determined using 2-way repeated measures ANOVA followed by Dunnett's multiple comparisons test. Data on graph are represented as mean ± SEM; *P<0.05, ** P<0.01, *** P<0.001, **** P<0.0001.

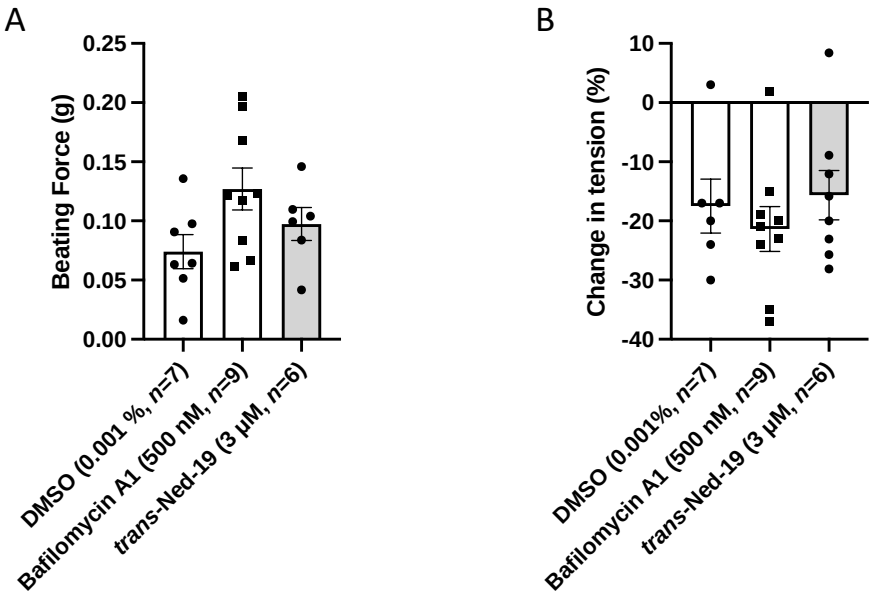

Figure 3.4: Baseline tensions show no significant changes before addition of isoprenaline.

A, Comparison of tension in intact murine stimulated (5 hertz) left atrial preparations in PSS prior to addition of DMSO (*n*=7), bafilomycin A1 (*n*=9) or *trans*-Ned-19 (*n*=6) or stimulation with isoprenaline.
B, Comparison of change in tension (in %) in intact murine stimulated (5 hertz) left atrial preparations in PSS on addition of DMSO (*n*=7), 100 nM bafilomycin A1 (squares, *n*=9) or 3 µM *trans*-Ned-19 (*n*=6) prior to stimulation with isoprenaline.

No significance for effect of bafilomycin A1 and *trans*-Ned-19 compared to control at individual concentrations was observed, determined using 2-way repeated measures ANOVA followed by Dunnett's multiple comparisons test. Data are represented as mean ± SEM.

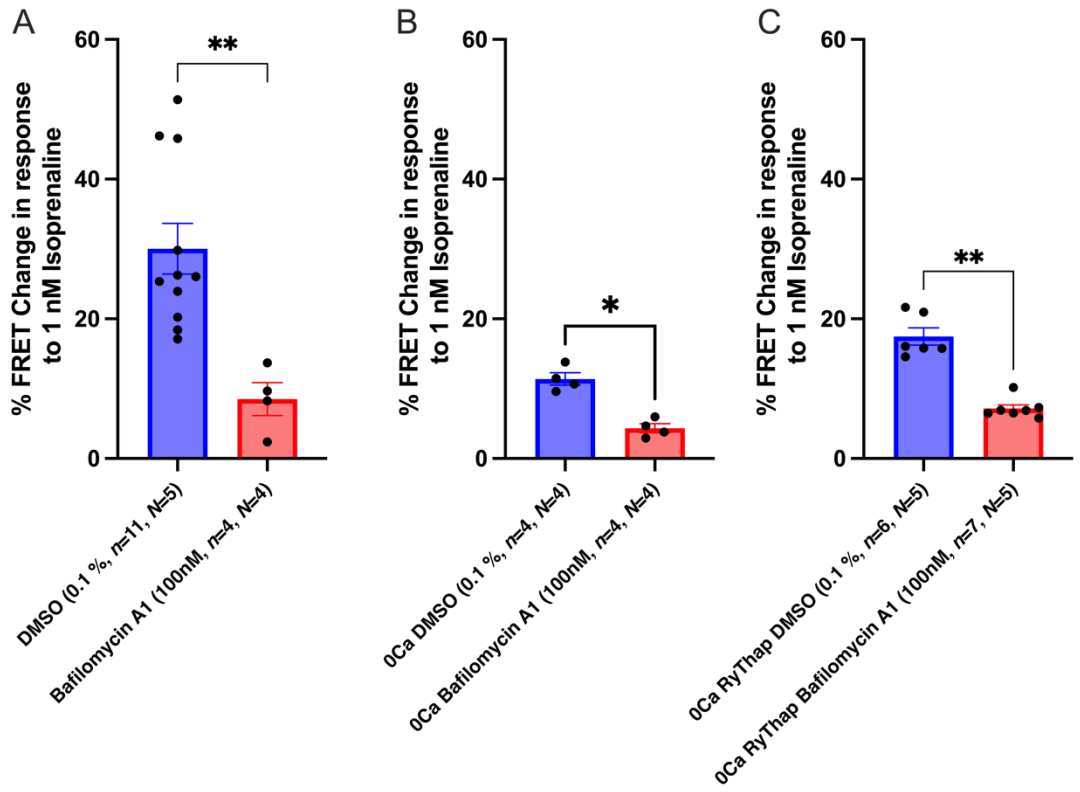

Figure 3.5: Lysosomal signalling contributes to FRET response to isoprenaline in NRAMs.

A, Quantification of the peak FRET change in response to 1 nM isoprenaline in NRAMs in the presence of either DMSO (*n*=11, *N*=5) or 100 nM bafilomycin A1 (*n*=4, *N*=4) in E1 buffer.
B, Quantification of the peak FRET change in response to 1 nM isoprenaline in NRAMs in the presence of either DMSO (*n*=4, *N*=4) or 100 nM bafilomycin A1 (*n*=4, *N*=4) in 0 calcium (0Ca) E1 buffer.
C, Quantification of the peak FRET change in response to 1 nM isoprenaline in NRAMs pre-incubated for 45 minutes with 2 µM ryanodine (Ry) and 2 µM thapsigargin (Thap) in the presence of either DMSO (*n*=6, *N*=5) or 100 nM bafilomycin A1 (*n*=7, *N*=5) in 0 calcium (0Ca) E1 buffer.

Data are represented as mean ± SEM and were analysed using non-parametric Mann-Whitney U test. *n*=experiments; *N*=neonatal isolations. *P<0.05, **P<0.01.

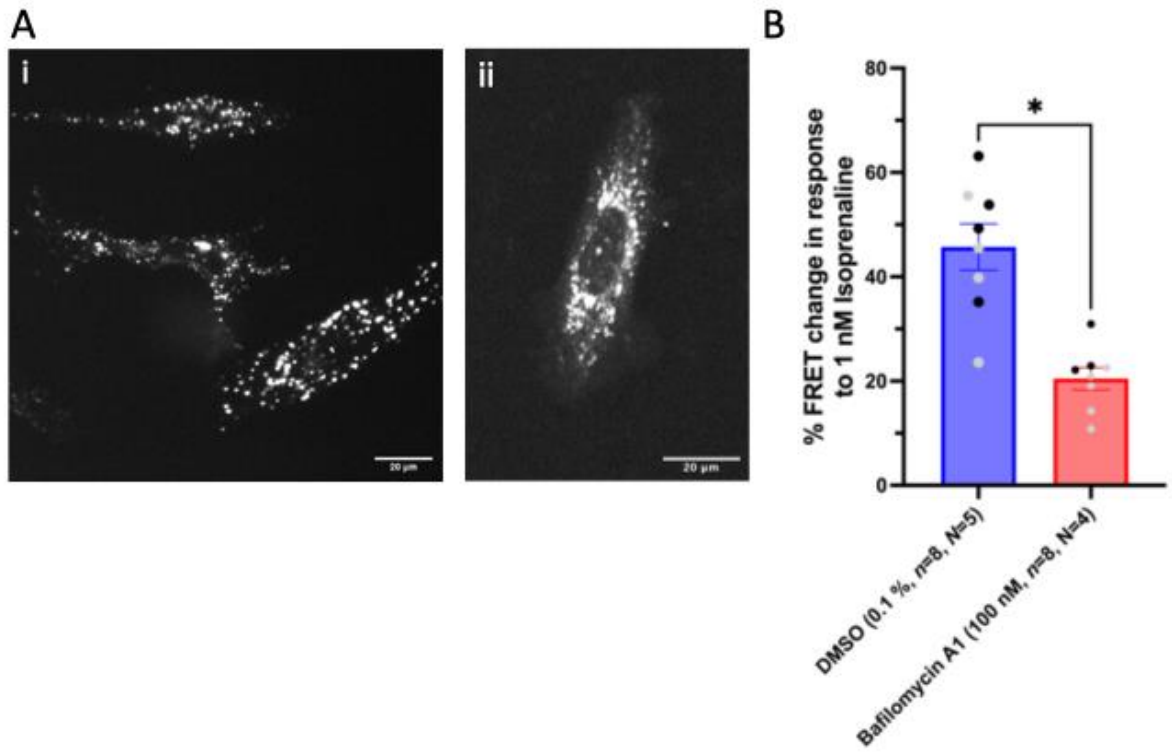

Figure 3.6: Lysosomal signalling contributes to FRET response to isoprenaline in hiPSC-CMs and hiPSC-aCMs.

A, Representative live image of hiPSC-CMs (**i**) and hiPSC-aCMs (**ii**) loaded with Lysotracker™.
B, Quantification of the peak FRET change in response to 1 nM isoprenaline in hiPSC-CMs (grey, Winbo differentiation protocol) and hiPSC-aCMs (black, Calamaio differentiation protocol) in the presence of either DMSO (*n*=7, *N*=4) or 100 nM bafilomycin A1 (*n*=8, *N*=4).

Data are represented as mean ± SEM and were analysed using non-parametric Wilcoxon signed-rank test. *n*=experiments; *N*=neonatal isolations. *P<0.05. A nested t-test indicated no significant difference in means between the subgroups, hiPSC-CMs and hiPSC-aCMs (P= 0,6547).

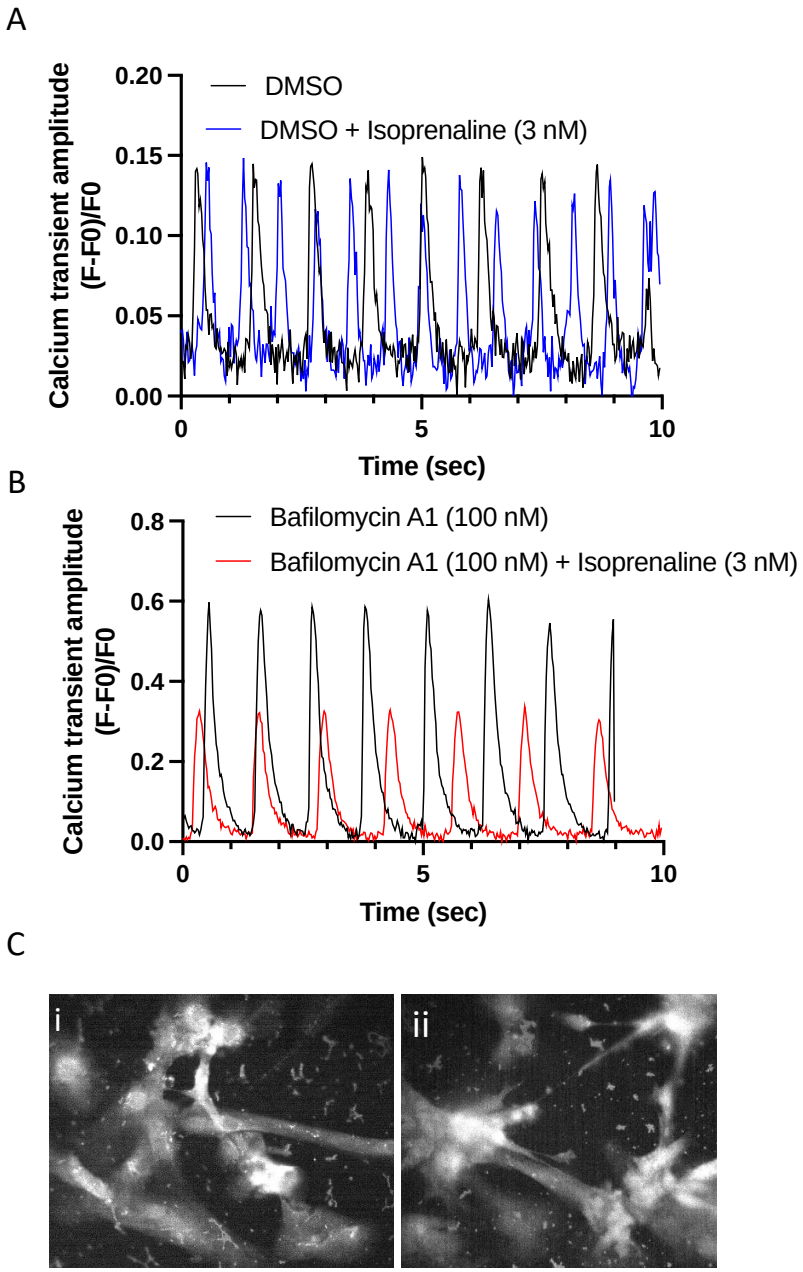

Figure 3.7: Representative traces of calcium transients in hiPSC-CMs.

A, Representative traces to show spontaneously generated calcium transients in hiPSC-CMs in the presence of a solvent control DMSO and after exposure to 3 nM isoprenaline.
B, Representative traces to show spontaneously generated calcium transients in isolated hiPSC-CMs in the presence of 100 nM bafilomycin A1 and after exposure to 3 nM isoprenaline.
C, Snapshots (i, ii) of hiPSC-CMs loaded with Fluo-5F-AM.

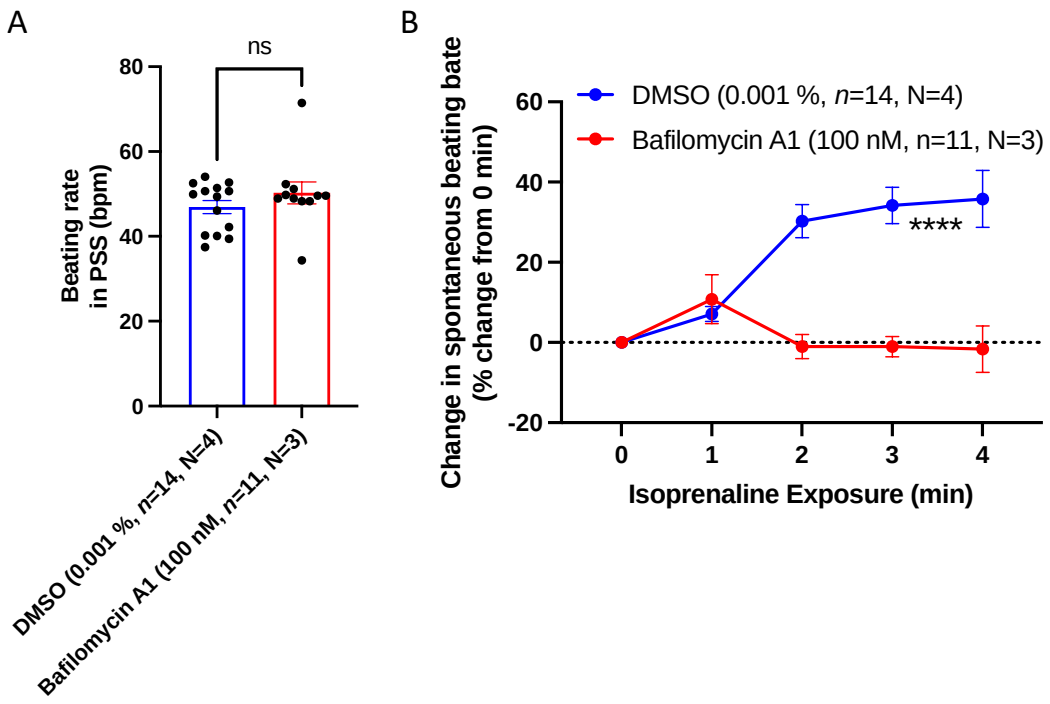

Figure 3.8: Bafilomycin A1 inhibits beating rate response to 3 nM isoprenaline in hiPSC-CMs.

A, Beating rate of hiPSC-CMs in the presence of either DMSO (*n*=14, *N*=4) or 100 nM bafilomycin A1 (*n*=11, *N*=3) in PSS before exposure of isoprenaline.
B, Beating rate response (in %) of human iPSC myocytes in the presence of either DMSO (*n*=14, *N*=4) or 100 nM bafilomycin A1 (*n*=11, *N*=3) after exposure of 3 nM isoprenaline over 4 minutes.

Data are represented as mean ± SEM. Asterisks indicate significance level for effect of 100 nM bafilomycin A1 compared to DMSO control determined using 2-way repeated measures ANOVA followed by Šídák's multiple comparisons test.; not significant (ns); ****P< 0.0001.

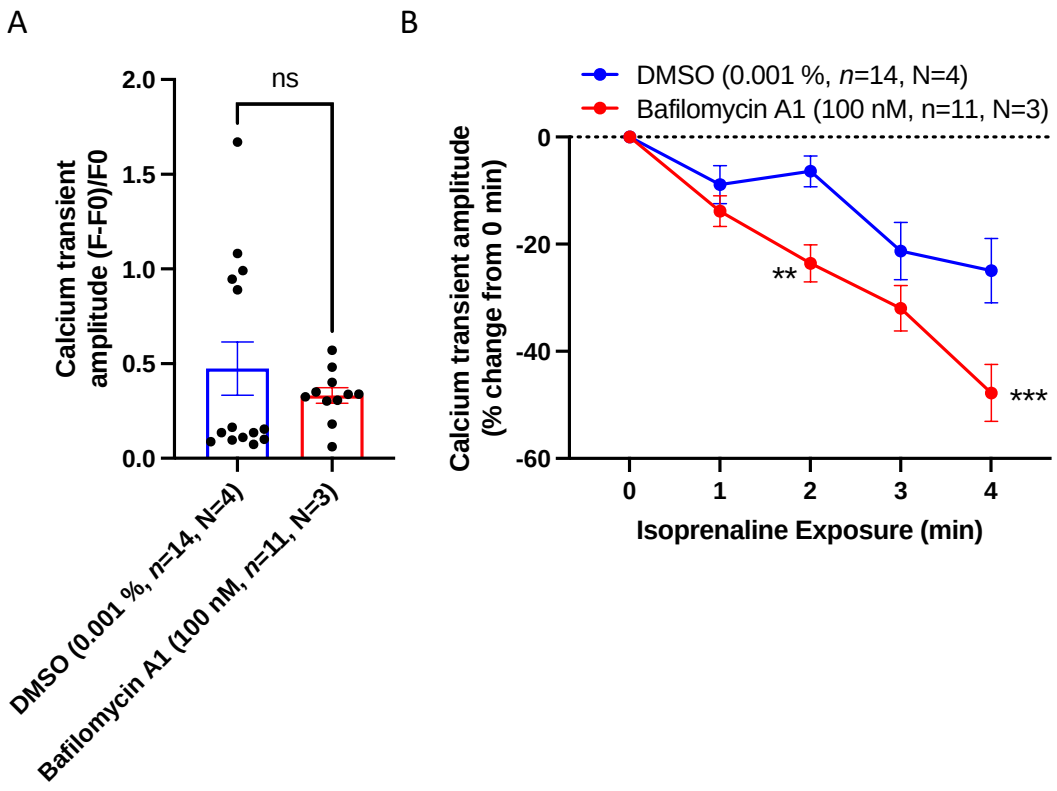

Figure 3.9: Bafilomycin A1 inhibits calcium transient amplitude in response to 3 nM isoprenaline in hiPSC-CMs.

A, Calcium transient amplitude of hiPSC-CMs in the presence of either DMSO (*n*=14, *N*=4) or 100 nM bafilomycin A1 (*n*=11, *N*=3) in PSS.
B, Calcium transient amplitude response (in %) of hiPSC-CMs in the presence of either DMSO (*n*=14, *N*=4) or 100 nM bafilomycin A1 (*n*=11, *N*=3) after exposure of 3 nM isoprenaline over 4 minutes.

Data are represented as mean ± SEM. Asterisks indicate significance level for effect of 100 nM bafilomycin A1 compared to DMSO control determined using 2-way repeated measures ANOVA followed by Šídák's multiple comparisons test.; not significant (ns); **p< 0.01, ***p< 0.001.

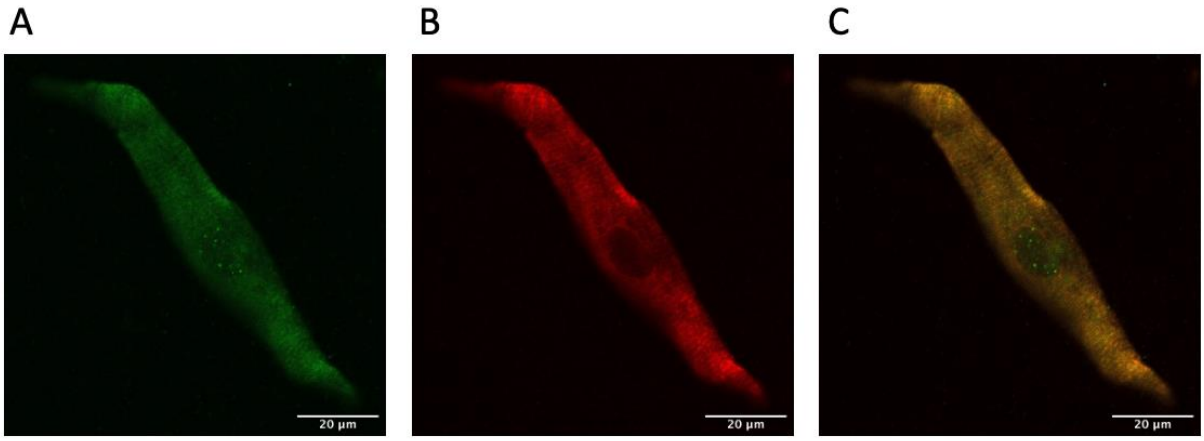

Figure 3.10: Immuno-fluorescent labelling of isolated guinea pig SAN myocytes with LAMP2 and AC1.

Isolated, fixed and stained representative guinea pig SAN myocyte LAMP2 (**A**, green), AC1 (**B**, red) and overlap of both signals in **C**.

Pixel-by-pixel analysis, Pearson's overlap coefficient is R=0.8095 ± 0.04565 (*n*=5). Data are represented as mean ± SEM.

3.6 Discussions

NAADP is the most potent calcium signalling second messenger present in a large range of cell types across species acting by releasing calcium from acidic stores via TPC2 channels. NAADP mediated acidic store calcium signalling has been shown to play a role in cellular physiology.

The observations presented in this chapter confirm NAADP action in atrial cardiomyocytes in response to β-adrenergic stimulation at the intact tissue and single cell level in animal and hiPSC-CMs. Experiments demonstrate for the first time NAADP-mediated calcium release from lysosomes, makes significant contribution to physiological changes of beating rate to the SAN pacemaker and force of contraction in intact left atria tissue. Additionally, to this, FRET experiments show NAADP pathway modulates cytosolic cAMP levels in NRAMs and hiPSC-CMs.

The first part of this chapter investigates the intrinsic activity of NAADP pathway in spontaneously beating right intact atrial preparations. Abolition of lysosomal calcium signalling pharmacologically by bafilomycin A1, and *trans*-Ned-19 led to a rightward shift in EC50 in the presence of bafilomycin A1 and in the presence of *trans*-Ned-19 led to a rightward shift in EC50 and a reduction in maximal response in spontaneous beating rate in intact SAN. Bafilomycin A1 and *trans*-Ned-19 significantly inhibited the contractile response of the intact, paced left atrium to β-adrenergic stimulation with isoprenaline. This inhibition manifests as a reduction in maximal response in all conditions. These data suggest the downstream effects of β-adrenergic signalling is dependent upon NAADP mediated calcium signalling from lysosomes in atrial myocytes and represent a novel finding and avenue for future research. Bafilomycin A1 or *trans*-Ned-19 alone did not have a significant effect on cellular beating rate or force of contraction, this may suggest that lysosomal calcium signalling is not constitutively active in the SAN and in atrial myocytes. These experiments are in alignment with previous published data (Capel et al. 2015; Collins et al. 2011), strengthens the dependence of NAADP in SAN pacemaking β-adrenergic responses and to our knowledge provide first findings demonstrating lysosomal calcium signalling contributing to physiological control of beating rate in intact tissue.

One mechanism that could explain chronotropic and inotropic in responses to β-adrenergic stimulation seen in tissue preparations after inhibition of lysosomal calcium signalling, could be from lysosomal-mediated calcium release activating cytosolic cAMP. Indeed, FRET work

showed a decrease in synthesis of cAMP in response to isoprenaline following addition of the NAADP inhibitor, bafilomycin A1. These results do provide a strong indication that cAMP synthesis is reduced by the NAADP pathway inhibitors, indicating a role for calcium stores in atrial function. In our FRET studies, perturbation of NAADP-mediated calcium signalling led to around a 50 % reduction in cellular cAMP accumulation in response to isoprenaline, whether in normal extracellular solution, 0 calcium conditions or after depletion of SR calcium. Gul and co-workers, also using quiescent myocytes, reported that NAADP pathway inhibition completely abolished the cardiac ventricular myocyte response to isoprenaline (Gul et al. 2016). NAADP mediated calcium release from lysosomes could play a greater role in neonatal or quiescent myocytes, as β-adrenergic stimulation is known to lead to cellular responses independent of NAADP pathway.

Human work presented in this chapter have been collected from 3 different hiPSC-CMs lines (Winbo et al. 2020; Benzoni et al. 2020; Calamaio et al. 2023) to ensure reproducibility, confirm effects of NAADP and further enhance the translational value of this research and provide evidence of the importance of this pathway in humans.

It is important to note, in the FRET experiments presented in this chapter, levels of cAMP were measured as a whole/in bulk in the cytosol. cAMP is a ubiquitous second messenger capable of modulating multiple cellular functions by a complex system of local mechanisms that result in compartmentation (Chao et al. 2019). cAMP signals are found to be dependent on the activity of PDEs, ACs and signal heterogeneity such as having distinct subcellular responses. Another way other than depletion of the SR and 0 calcium conditions to specifically measure cAMP response to lysosomal calcium release would be to measure cAMP levels with a FRET-based reporter fused with a lysosomal membrane protein such as LAMP2. This method would enable us to observe in intact living cells cAMP production in direct response to calcium release from lysosomes in physiological conditions in response to β-adrenergic stimulation. FRET percentage change was measured in direct response to TPC2 activator (TPC2-A1-N), and results are presented in Chapter 5.

The investigation of L-type calcium channels was previously conducted as a possible effector of NAADP response to β-adrenergic stimulation, as increase observed in calcium transient amplitude could be due to the increase in cytosolic calcium from extracellular calcium entering the cells through these channels. However, work confirmed NAADP has no effect on calcium influx through sarcolemma L-type channels in ventricle myocytes measured under voltage

clamp conditions (Macgregor et al. 2007). Collins et al., confirmed this finding by showing that increase in calcium transient amplitude induced by photorelease of "caged" NAADP also occurred in the absence of any change in the L-type calcium current in atrial myocytes (Collins et al. 2011). The change in L-type calcium current amplitude upon β-AR stimulation was also investigated *Tpcn2*$^{-/-}$ mice and found there to be no statistically significant difference in WT mice (Capel et al. 2015). Therefore, responses observed in these papers are not due to an increase in the entry of calcium from outside the cell through this pathway.

FRET experiments in this chapter present perturbations in NAADP calcium signalling led to around a 50% reduction in cellular cAMP levels in response to isoprenaline, whether in normal extracellular solution, 0 calcium solution or after depletion of SR calcium. FRET experiments were carried out on quiescent myocytes. Gul and co-workers, also using quiescent myocytes, reported that NAADP pathway inhibition completely abolished the cardiac ventricular myocyte response to isoprenaline (Gul et al. 2016). It would seem unlikely, however, that the sole gatekeeper to β-adrenergic signalling in the heart is the lysosome. As, β-adrenergic stimulation has been shown to lead to cellular effects known to be independent of the NAADP pathway such as exogenous NAADP has no effect on L-type calcium current (Collins et al. 2011; Macgregor et al. 2007), nor did NAADP pathway inhibition alter the increase in L-type calcium current stimulated by isoprenaline (Capel et al. 2015). FRET work in this chapter and those of Gul et al, support that in the absence of continuous calcium cycling, the proportion of the isoprenaline response attributable to NAADP calcium signalling is relatively high.

Stimulation of AC1 activity by calcium release from the lysosomes could be a possible calcium handling mechanism in response to isoprenaline in this chapter, as it has been reported to be significantly augmented in the presence of Gs activation such as by isoprenaline signalling (Wayman et al. 1994); leaving open the potential that the contribution of this mechanism could be augmented under these physiological conditions. Immunolocalisation studies of AC1 and LAMP2 on isolated SAN guinea pig myocytes, pixel by pixel analysis presented a Pearson's colocalization overlap coefficient of R=0.8095 ± 0.04565 (Figure 3.12), This pattern of expression highlights that calcium release via lysosomes may directly lead to activation of calcium sensitive AC1 in SAN myocytes.

Autophagy is a major intracellular degradation system and lysosomes are a main driver in this process by their degradative abilities. Autophagic flux is activated in atria of patients with persistent AF with significant increase of LAMP2 expression compared to patients with sinus

rhythm and is shown to promote atrial electrical remodelling in AF (Yuan et al. 2018), a known promoter the disease (Iwasaki et al. 2011). Biopsies from AF goat tissue highlighted structural anomalies, such as autophago-vacuole formation (Ayagama et al.). Here, I report that lysosomes are further apart to the SR and larger in diameter in patients with AF than in patient with a sinus rhythm. TPC1 and TPC2 studies have shown to be involved in regulating autophagy and are essential for basal and induced autophagy in cardiomyocytes (García-Rúa et al. 2016). These structural and expression changes reported in rhythm dysfunctions could be the underlying disruption in compartmentation and strict calcium handling and could be playing a major role in initiation and/or maintenance or AF. Even with all this evidence, the position of lysosome has not previously been reported with respect to AF. Further functional studies to investigate the structural-functional remodelling, that could be affecting calcium handling between the SR and lysosomes, observed in human samples are needed. Autophagic flux was assessed whether it was activated or impaired during AF, reports showed that autophagic flux was increased in atria of persistent AF patients and rabbit model of atrial rapid pacing and autophagy-related gene 7 (*atg7*), a key protein for degradation in autophagy, was significantly upregulated in AF patients as well as tachypacing rabbits. Lentivirus-mediated ATG7 knockdown restored the shortened atrial effective refractory period and demonstrated that inhibition of autophagy could attenuate atrial electrical remodelling and reduce AF susceptibility. In contrast, ATG7 overexpression significantly promoted the incidence and persistence of AF and decreased L-type calcium channel along with abbreviated action potential duration and diminished L-type calcium current (Yuan et al. 2018).

3.7 Conclusions

The observations presented in this chapter in rodents and human derived iPSC cardiomyocytes both strengthen the literature on NAADP calcium signalling in the heart and contribute new knowledge in the field. For the first time, a role for NAADP mediated calcium release in pacemaking activity is reported in the SAN and is functionally important for β-adrenergic responses. A contribution of NAADP mediated calcium release in atrial contractile force has been confirmed at the tissue level as contributing to β-adrenergic responses. A novel pathway in cardiomyocytes signalling, in which NAADP mediated calcium release contributes directly to cellular cAMP is put forward and a model of the proposed mechanism is illustrated in Figure 3.11. Further, I have added structural observations in human AF tissue and present the first evidence that structural remodelling in this disease extends to lysosomal positioning. Taken together, data presented in this chapter brings forward the NAADP calcium pathway as a major

calcium handling actor in the heart but the precise mechanism of NAADP pathway and its physiological and pathophysiological importance in the atria warrant further investigation.

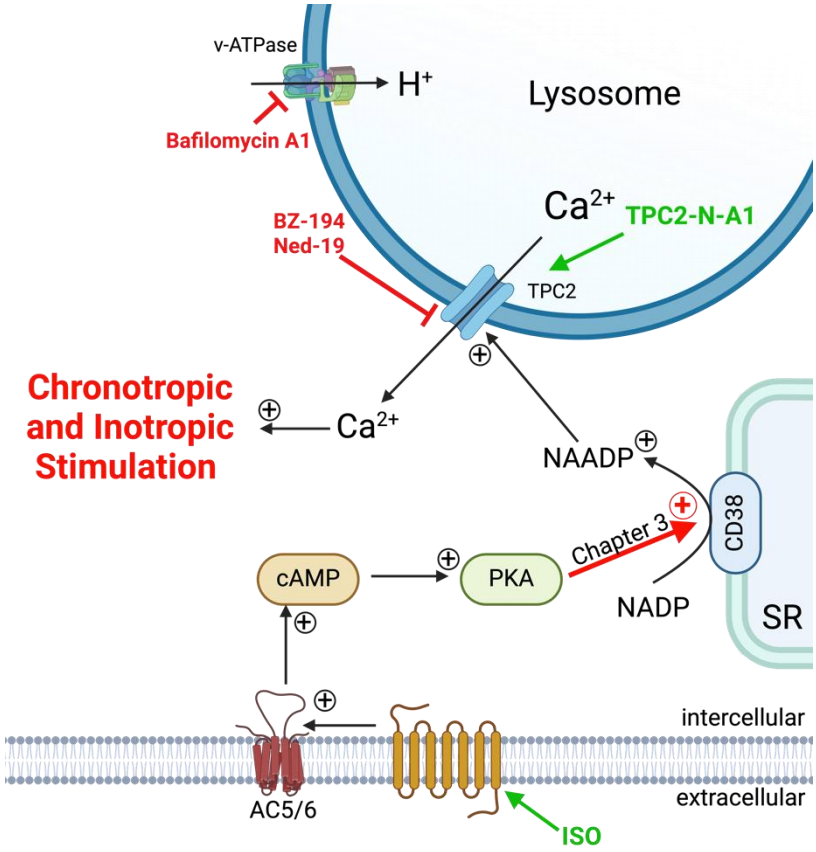

Figure 3.11: Representative scheme of proposed mechanisms from Chapter 3. Activation of β-AR by isoprenaline lead to ACs activation leading to activation of PKA by cAMP and synthesis of NAADP by CD38 enhancing lysosomal calcium release by the action of NAADP on lysosomal TPC2 channels. Ca^{2+}, calcium.

4 Chapter 4: Elucidating the interactions between IP_3-dependent calcium release and calcium-stimulated ACs in controlling atrial function.

4.1 Summary of contribution:

This Chapter presents a paper investigating the lysosomal calcium signalling contribution to the acute α-adrenergic response. I am first author, I carried out experiments, conceptualisation, methodology, and writing of the project. Figures reproduced from the paper were my own work. Additionally, this Chapter contains data that was published in Bose, Read, Akerman et al 2022. Front Pharmacol 2022 Aug 29:13:951897 (Bose et al. 2022).

4.2 Introduction

Intracellular calcium release for intracellular organelles is a driving force for normal cardiac pacemaker cell automaticity (Maltsev, Vinogradova, and Lakatta 2006). In 1983, calcium release induced by IP_3 from the ER was demonstrated in pancreatic acinar cells for the first time (Streb et al. 1983). Since then, this mechanism has been shown in many other cell types (Berridge 2009); as well as in non-excitable cells such as proliferation in lymphocytes (Feske 2007) and excitable cells including cardiac myocyte (Kockskämper, Zima, et al. 2008). IP_3 is a calcium-mobilising second messenger (Berridge 1984) and is synthesised upon stimulation of phospholipase C that acts to open IP_3R located on the SR in cardiac myocytes and leads to calcium release in to the cytosol. This mechanism enhances calcium-induced force oscillations (Zhu and Nosek 1991) but compared to the role played by RyR in CICR, the involvement of IP_3 signalling in cardiac cellular calcium handling is poorly known.

The importance of highly regulated calcium signalling in the heart has been shown to be vital for normal physiological function and rhythm mechanisms. Even if little data is published regarding IP_3 signalling pathway in the atria (compared to RyR), IP_3R expression in atrial tissue has been shown to be of great importance in regulating calcium handling. IP_3R2 is the highest subtype of IP_3R expressed in the atria making it a possible modulator of the heartbeat (Lipp et al. 2000). Evidence has shown IP_3R modulates ECC as exposure to endothelin 1, a Gq protein coupled agonist increases calcium transients in rabbit atrial myocytes and was abolished in the presence of a IP_3R inhibitors, 2-Aminoethyl diphenylborinate (2-APB) and xestospongin C (Kockskämper, Seidlmayer, et al. 2008). Previous work from the lab has shown that direct application of IP_3, by photorelease, in guinea pig isolated atrial myocytes led to an increase in stimulated calcium transient amplitude and this response was abolished in the presence of either AC inhibitor MDL-12,330A or PKA inhibitor H89 (Capel et al. 2021).

Kapoor et al, used atrial specific sodium-calcium exchanger (NCX) KO SAN cells (Kapoor et al. 2015). Calcium flux across the sarcolemma membrane is demolished because of no expression of NCX and insignificant calcium flux through L-type calcium channels due to no depolarisation events but intracellular calcium release still occurs. The results show SAN myocytes to have a chronotropic change in response to stimulation (PE) and inhibition of IP_3R (2-APB) and NCX KO SAN cells were still able to respond to heart rate and calcium waves demonstrating the independent of NCX, demonstrating a crucial role for IP_3R-mediated SR calcium release (Kapoor et al. 2015). Additionally, maximum beating rate in right atrial

preparations on addition of PE was significantly reduced in the presence of these 2 inhibitors compared to control (Capel et al. 2021). Confirming that IP_3-mediated calcium release regulates atrial calcium transients and pacemaker function by stimulation of AC1 and AC8.

Studies in healthy atrial myocytes have shown that stimulation of IP_3 pathway causes arrhythmogenicity. Indeed, single paced atrial myocytes showed generation of spontaneous calcium transients between action potential upon addition of membrane permeant IP_3 (Lipp et al. 2000), highlighting the pro-arrhythmogenic action of IP_3. Inhibition of IP_3R using 2-APB suppressed the arrhythmogenic action of Endothelin 1 and membrane permeant IP_3 in isolated rat atrial myocytes (Mackenzie et al. 2002).

Investigation of IP_3R expression in right atrial myocardium in AF patients and control patient with normal sinus rhythm showed expression levels of non-specific subtypes of IP_3R were greater in AF patients (Yamda et al. 2001), linking IP_3R expression to heart rhythm in humans and it's possible implications in calcium homeostasis. Similar studies on IP_3R2 expression have been conducted in a chronic AF dog model; IP_3R2 expression increased in chronic AF group compared to control while RyR2 expression downregulated (Zhao et al. 2007), highlighting a role for IP_3R in initiation or perpetuation of AF. Although the functional consequences of the increase of IP_3R remain to be investigated. Later, calcium activated AC1 and AC8 are expressed in SAN myocytes and were shown to contribute to the generation of rhythmic action potentials by regulating the L-type calcium current (Younes et al. 2008).

Georget et *al*. (Georget et al. 2002)specifically explored the functional consequences of AC8 expression. In transgenic mouse line AC8TG, mice expressing human AC8 expression, the perfused heart had an increase in contractility and single cells demonstrated an increase in calcium transients with no change in L-type calcium current. It is important to note that this expression of AC8 led to an increase in cAMP that activates specifically calcium handling with the SR but not with the sarcolemma, suggesting a strong compartmentation of the cAMP signal (Georget et al. 2002). Additionally, (Moen et al. 2019) conducted similar work, where overexpression of AC8 in mice increased heart rate *in vivo*. Work form (Mattick et al. 2007) also demonstrated the importance of AC1 and AC8 activity in SAN myocytes by localising then on the plasma membrane of SAN myocytes and by monitoring activation of funny current. Inhibition of AC activity with MDL-12,330A shifted activation the hyperpolarizing direction, adding a role for basal activity of AC in isolated SAN myocytes whereas inhibition of

phosphodiesterases with IBMX shifted the funny current activation in the depolarizing direction in guinea pig SAN myocytes (Mattick et al. 2007).

ACs are enzymes that catalyse the conversion of ATP into cAMP, cAMP in involved in multiple physiological function, it is not a surprise that cardiac function is also controlled by pathways involving production of cAMP (Chao et al. 2019). How cardiac myocytes respond differently to cAMP signals remains to be determined, a suggestion that has been put forward these past years, is the compartmentation of cAMP at the nanoscale level (Zaccolo, Zerio, and Lobo 2021). The possibility of calcium release via IP_3R stimulating AC1 and or AC8 and changing cAMP levels in specific micro/nano domains will be explored in this Chapter.

Previous work by Vinogradova *et al*. (Vinogradova et al. 2006) has shown cAMP production shows greater importance in pacemaking activity in SAN myocytes. High basal cAMP levels in isolated rabbit SAN myocytes are required for subsarcolemmal calcium release (important mechanism in SAN spontaneous beating (Vinogradova et al. 2006). Additionally, as explained above (Younes et al. 2008) show SAN express AC1 and AC8 and high basal AC activity produces a high level of cAMP that is further elevated by phosphodiesterase inhibition. Suggesting that, spontaneous rhythmic subsarcolemmal local calcium releases driven by cAMP are crucial for pacemaker function of SAN myocytes.

Findings highlighted above put forward the involvement of cAMP in IP_3 signalling pathway but the direct effect of IP_3 on cellular cAMP levels has not yet been investigated. The cAMP signalling regulates major heart functions involving chronotropy and inotropy via ECC process (Bers 2002). I have presented previous work demonstrating that IP_3 and calcium-stimulated AC play major role in the normal function of atrial muscle, these pathways have the potential to play a major role in arrhythmias. Understanding and linking the direct interactions with cAMP (and PKA) makes the IP_3 signalling pathway a potential target for the treatment of AF.

4.3 Aim of Chapter 4

This Chapter focuses on elucidating the interactions between IP_3-dependent calcium release and calcium-stimulated ACs specifically AC1 and AC8 in controlling atrial function. The link between the IP_3 mediated calcium release from the SR and downstream activation of calcium stimulated ACs has been relatively understudied. The possible interactions between IP_3 signalling and calcium stimulated ACs and downstream activation of cAMP will be investigated in this Chapter using a double knock-out of AC1 and AC8 (DKO) mouse colony obtained from our collaborators lab Prof. Alana Conti (USA). Understating these key calcium handling mechanisms and downstream activators in the atrium has the potential to provide important insights concerning acute mechanisms for initiation of atrial arrhythmias and may provide a novel atrial specific therapeutic approach for arrhythmias.

4.4 Methods

Methods used in this Chapter are presented in more detail in Chapter 2. Briefly, this Chapter uses immunocytochemistry, atrial preparations, and FRET methods to study the IP_3 signalling pathway in cardiac activity.

Standard immunocytochemical techniques were used to determine the localisation of intracellular IP_3R2 and AC1 in atrial myocytes and SAN myocytes. To compare the localisation of various proteins, secondary antibodies conjugated to different fluorophores were used and pixel by pixel analysis using ImageJ was conducted.

PE was administered to isolated single myocytes and heart tissue, PE stimulates is an α1-AR agonists in myocytes, α1-AR are coupled to the Gq-protein that activates the effector PLC causing the release of IP_3 through IP_3R. PE has been shown to have off target effects at high concentrations. A concentration of 100 µM PE increases the activity of the cAMP-dependent protein kinase, protein kinase A (PKA) through the β-AR (Valks et al. 2002). For this reason, I have run PE dose response curves 0.1 µM up to 30 µM in the presence of 1 µM metoprolol (a non-selective β-adrenergic inhibitor) and conducted single cell FRET experiments at 3 µM PE, a suitable concentration of PE to ensure no confounding effect β-adrenergic activity throughout my experiments (Figure 4.1). This Chapter uses 2 pharmacological agents to inhibit IP_3R activity: 2-APB and xestospongin-C. 2-APB is a IP_3R inhibitor but has been shown to have blocker effects of store-operated calcium entry channel TRP channels (Lievremont, Bird, and Putney 2005), to overcome this we have repeated experiments with an alternative IP_3R inhibitor xestospongin-C. ST034307 (Brust et al. 2017) was administered to inhibit AC1.

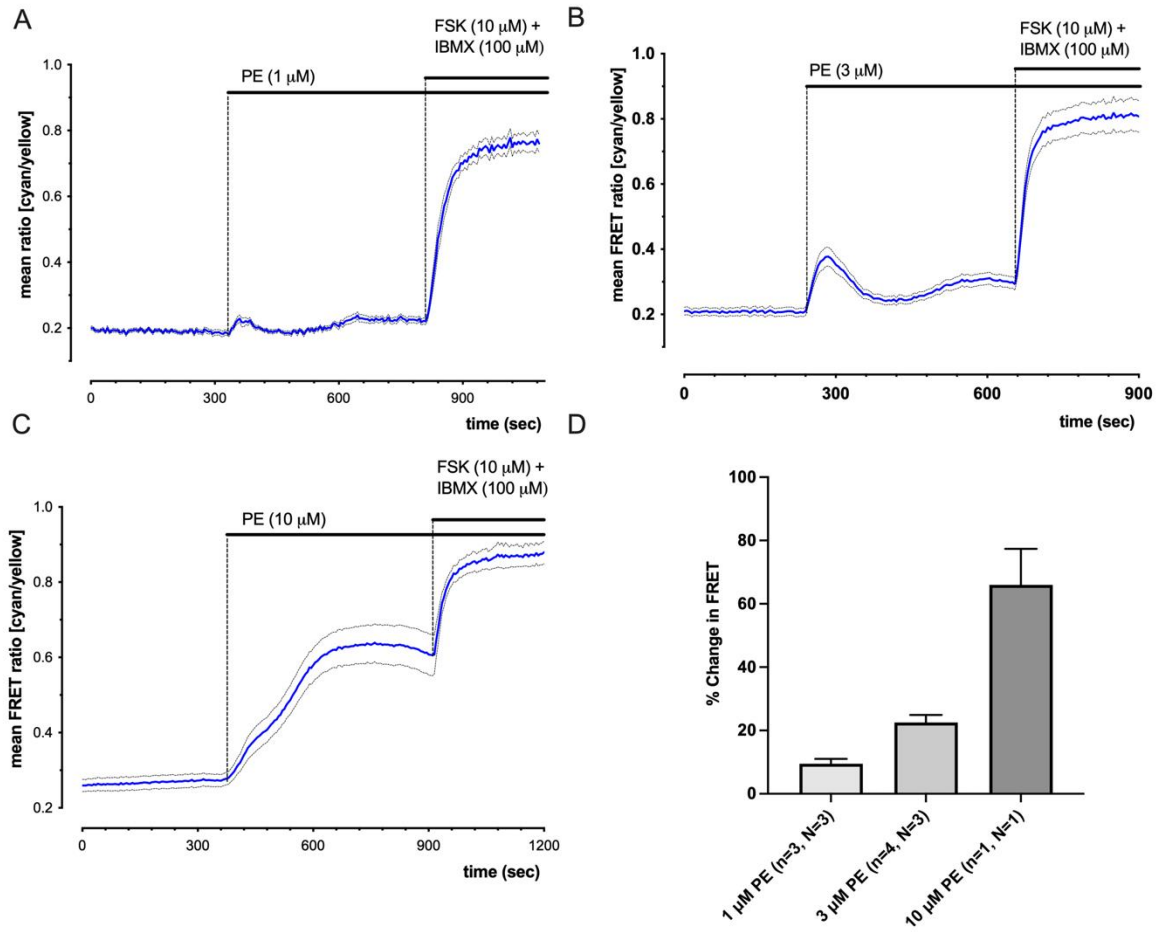

Figure 4.1: PE concentrations (1, 3 and 10 μM) tested for FRET, experiments conducted by Dr Bose (former post-doctoral scientist in the lab).

A: Representative example single well trace of the effect of 1 μM PE on cAMP levels in NRAMs loaded with EPAC-S^{H187}.
B: Representative example single well trace of the effect of 3 μM PE on cAMP levels in NRAMs loaded with EPAC-S^{H187}.
C: Representative example single well trace of the effect of 10 μM PE on cAMP levels in NRAMs loaded with EPAC-S^{H187}.
D: Comparison of the peak response to 1 (n=3, N=3), 3 (n=4, N=3) and 10 (n=1, N=1) μM PE on cAMP levels in NRAMs loaded with EPAC-S^{H187}.

Solid line = mean ratio of all viable cells in well. Dotted line = standard deviation of ratio of all viable cells in well. Data in panel D presented as mean ± SEM.

Conserved sequence homology of intracellular C1 and C2 cytoplasmic loops between ACs family (Cooper 2003) has made it difficult to create specific inhibitors for AC subtypes. To overcome this, I used a DKO of AC1/8 mouse colony (DKO, described in Chapter 2). The phenotype of the heart in DKO mice was first investigated with High Resolution Episcopic Microscopy (HREM) technique. A robust method for processing and visualising organic

materials, by generating stacks of aligned digital images captured from histological sections. Whole hearts of WT and DKO mice were fixed and embedded in methacrylate resin and sectioned on a microtome. Each section of the heart embedded in the block is captured as a digital image to create series of aligned images to allow visualisation of the heart in 3D. Analysis was then carried out to measure volumes of each chamber of the heart using a 3D optical HREM imaging system (Indigo Scientific). HREM data were evaluated using Horos 3.3.6 and Amira for Life & Biomedical Sciences version 2019.4 (Thermo Fisher Scientific).

After investigating the phenotypic differences between WT and DKO hearts, functional studies were conducted such as force transducer experiments in intact paced (5 hertz) left and in spontaneously beating right atria in response to α1-AR, PE. Intact atria were attached to a force transducer in an organ bath at 37°C containing oxygenated physiological saline solution (PSS). After stabilisation, cumulative concentrations of PE were added to the bath (range 0.1–30 μM) in the presence of 1 μM of metoprolol was applied 30 min before PE was added to ensure specificity to α-adrenergic effects. In collaboration with Zaccolo group, the direct effect of DKO upon stimulation of IP_3R via PE on cellular cAMP concentration has been investigated using a FRET cytosolic biosensor EPAC-s^{H187}, expressed in neonatal mouse atrial myocytes (NMAMs) through viral infection 24 h before conducting experiments. This method permitted me to monitor cytosolic cAMP levels in real time in atrial myocytes.

For whole single cell fluorescence calcium transient experiments, cells were incubated with Fluo-5F-AM (3 μM) for 10 min then plated on to a glass cover slip for imaging. Cells were incubated for a further 10 min in the organ bath to allow time for cells to adhere to the glass cover slip before perfusion with Tyrode. Carbon fibre electrodes were used to field-stimulate calcium transients at a rate of 1 hertz. All experiments were carried out at 37°C. To avoid dye bleaching, the cells were not continually exposed to 488 nm light. Instead, a video of 8–10 s of calcium transients was recorded at several timepoints: at baseline levels before addition of 10 μM of PE and immediately after addition of PE, 1 minute and 2 minutes after PE exposure. Normalised calcium transient amplitude is expressed as change in mean cell fluorescence (F-F0)/F0 in the cell where F is the fluorescent value at a given time and F0 is the resting fluorescence value.

Statistical analyses in this Chapter were performed using Prism 10 (Graphpad). Differences were considered statistically significant at values of non-significant (ns)$P>0.05$, *$P<0.05$, **

P<0.01, *** P<0.001, **** P<0.0001. Statistical methods used are given in the legend of each figure.

.

4.5 Results

4.5.1 Inhibition of AC1 using ST034307 reduces chronotropy but not inotropy upon α-adrenergic stimulation in intact atria

Figure 4.2 shows representative confocal images of a right atria (Figure 4.2A) and SAN (Figure 4.2B) isolated adult guinea pig myocytes stained with primary antibodies raised against the IP_3R2 (magenta) and AC1 (cyan) proteins. AC1 puncta are in close proximity to IP_3R2 in both myocytes, suggesting calcium release from IP_3R can contribute to calcium-sensitive AC1 activation. ImageJ intensity analysis revealed, pixel by pixel by line intensity plots (Figure 4.2C-D), levels of colocalisation between AC1 and IP_3R2 in isolated guinea pig SAN myocytes were higher (R=0.82 ± 0.02, *n*=7) than in atrial myocytes (R=0.69 ± 0.02, *n*=11, p<0.001).

As described in Chapter 3 in response to isoprenaline, I measured beating rate and contractile force in atrial preparations of intact right and left tissue in response to PE. Previous work presented in the introduction by (Capel et al. 2021) showed nonspecific inhibition of ACs, using MDL-12.330A, reduces the response of intact right atria to PE stimulation. Figure 4.3 therefore shows the effect of ST034307, a specific AC1 inhibitor, on the positive chronotropic and inotropic response to PE. In the absence of ST034307 but in the presence of 1 μM metoprolol, the spontaneous beating rate of the right atria increased by a maximum of 14.5 (12.2–17.1) % at 30 μM of PE and an EC50 of 0.9 (0.4–2.2) μM (*n*=15, Figure 4.3A). 1 μM ST034307 significantly reduced the response of beating rate to PE at all concentrations tested (*n*=12, *P*<0.0001, Figure 4.3A), with a maximum increase of 8.2 (6.1–12.6) % at 30 μM PE and a significant rightward shift of the EC50 to 3.9 (1.1–17.6) μM. The basal heart rate of right atria after stabilisation and before addition of 1 μM metoprolol was 364 ± 15.5 BPM. No change in the right atrial basal heart rate was observed on addition of either metoprolol (362 ± 16.3 BPM) or metoprolol plus ST034307 (359 ± 16.8 BPM) before addition of PE (Figure 4.4). In left atrial preparations (Figure 4.3B), PE increased the tension generated in response to electrical stimulation at 5 hertz. The maximum increase was 14.2 (11.2–18.5) % (*n*=5) at 30 μM PE, with an EC50 of 4.4 (1.92–18.5) μM (*n*=5). In the presence of ST034307, no difference was observed in the response to PE compared with vehicle control (DMSO). The maximum change in tension generated in the presence of ST034307 was 16.3 (11.7–23.3) % (*n*=7) at 30 μM PE, with a non-significant left shift of EC50 to 0.9 (0.8–10.8) μM (*n*=7).

4.5.2 IP_3 signalling pathway activation using phenylephrine induced cAMP levels in neonatal cardiomyocytes

To determine whether the changes in cytosolic cAMP recorded in response to PE occurs downstream of IP_3R activation, we ran FRET experiments using IP_3R inhibitors 2-APB and xestospongin-C (Figure 4.5) in NRAMs expressing EPAC-S^{H187}. Prior application of any IP_3R inhibitors, the peak change in FRET following addition of 3 µM of PE was 21.20 ± 7.43 % (*n*=9, *N*=4), in the presence of 2.5 µM of 2-APB the peak change decreased to 5.88 ± 5.66 % (*n*=6, *N*=4, $p<0.05$), whilst 0.3 µM of xestospongin-C reduced peak to 8.76 ± 6.43 % (*n*=6, *N*=4, $p<0.01$).

As IP_3R expression has been shown to be greater in atrial myocytes compared to ventricular myocytes (Lipp et al. 2000). We were interested in determining whether cAMP changes in response to α-adrenergic stimulation would differ in NRVMs compared to NRAM (Figure 4.6). A rise in cytosolic cAMP was observed in NRVMs expressing EPAC-S^{H187} in response to PE, with an amplitude of 14.07 ± 0.9 % (*n*=10, *N*=6) and the rise in cAMP observed in response to PE in NRAMs (20.61 ± 2.9 %, *n*=9, *N*=4) did not differ from the peak observed in response to PE in NRVMs (Figure 4.6A).

In addition to PE, experiments using isoprenaline were also performed. The rise in cAMP observed in response to 1 nM isoprenaline was 1.5-fold greater in response to PE. No significant difference in response to isoprenaline was observed in NRAMs (53.97 ± 5.2 %, *n*=8, *N*=3) compared to NRVMs (72.26 ± 3.4 %, *n*=8, *N*=6) (Figure 4.6A). In contrast to NRAMs (Figure 4.5), rises in cAMP in response to PE (14.07 ± 0.9 %, *n*=10, *N*=6) measured in NRVMs were not found to undergo inhibition by neither 2-APB (14.12 ± 1.7 %, *n*=7, *N*=5) or xestospongin-C (13.38 ± 1.7 %, *n*=6, *N*=4, Figure 4.6B). Additionally, same observations were observed in response to isoprenaline (72.26 ± 3.4 %, *n*=8, *N*=6) in NRVMs and showed no inhibition by neither 2-APB (62.49 ± 3.8 %, *n*=8, *N*=) or xestospongin-C (57.8 ± 5.6 %, *n*=7, *N*=Figure 4.6C).

4.5.3 Phenotype of DKO hearts is not altered compared to WT in mice using HREM

AC1/AC8 DKO animals have been previously used to study AC1 and AC8 expression in the brain and role hippocampus dependant in long-term memory (Wong et al. 1999). Phenotype of these mice have not been investigated outside of the brain previously. The lab established this colony in Oxford to study the heart. To ensure differences observed from WT and DKO mice

weren't caused by structural changes in the heart, 3D modelling of WT and DKO heart were conducted. Results showed no significant structural/size changes in right (Figure 4.7A) and left (Figure 4.7B) atria and in both ventricles (Figure 4.7C).

4.5.4 DKO of AC1 and AC8 expression decreases chronotropic effect induced by PE in intact right atria

Previous published work has used pharmacological tools (MDL-12,330A) to inhibit AC activity (Capel et al. 2021) but these methods, are non-specific for ACs subtypes and may have some potential off-target effects. To overcome this, I used a double knockout of AC1 and AC8 (DKO) transgenic mouse line, described in Chapter 2 (Methods, 2.1.1 Mice, page 46). Figure 4.8 shows dose-response curves to PE in the concentration range 0.1–30 μM carried out on spontaneously beating isolated murine right atria in the presence of 1 μM metoprolol to ensure no confounding action of β-AR. In WT mice, the positive chronotropic response to PE fits a standard agonist dose-response curve with an EC50 of 1.5 (0.5–4.2) μM with a maximum rate increase of 17.78 ± 2 % (*n*=8) and DKO mice show an EC50 of 0.3 (0–1.8) μM with a maximum rate increase of 10.13 ± 1.7 % (*n*=14).

Starting baseline beating rates, before addition of PE or metoprolol, of WT and DKO mice were compared; and no significant differences were observed between the two groups (Figure 4.9A). The mean starting heart rate of WT mice was 509.4 ± 21 BPM (*n*=8) while DKO mice had a mean heart rate of 466.5 ± 15 BPM (*n*=14). Rates were also measured after addition of 1 μM of metoprolol (to ensure no β-adrenergic responses during addition of PE) and showed no significant differences between the two groups (Figure 4.9B). The mean baseline heart rate of WT mice was 334.7 ± 12 BPM (*n*=8) while DKO mice had a mean heart rate of 354.3 ± 8 BPM (*n*=14). Percentage decrease rate of atria after addition of 1 μM metoprolol and stabilisation of the preparation of WT and DKO mice were compared; a higher decrease percentage was observed in WT mice compared to DKO mice (Figure 4.10). Even if non-significant, DKO atria had a lower starting beating rate and a higher basal beating rate, explaining the higher decrease percentage observed in WT mice overtime, WT had a mean decrease of 31.95 ± 3.5 % (*n*=8) while DKO mice had a mean decrease of 23.41 ± 2 % (*n*=14). Metoprolol was added at the 40-minute mark of the protocol, after the preparation had stabilised, and the baseline was measured before addition of PE, after the preparation had stabilised from addition of metoprolol. The time period between the mean starting heart rate and mean baseline heart rate

was 70 min. The beating rate of the preparation naturally reduced, and addition of metoprolol reduced the rate further explaining such a reduction.

In the process of backcrossing mice to generate the DKO genotype, 3 groups of animals heterozygous (Het) and homozygous (Hom) for AC1 and AC8 were also generated: [1] Het for both AC1 and AC8 (HetAC1/8), [2] Het for AC1/Hom for AC8 and [3] Hom for AC1/Het for AC8 mice. Rate studies were conducted on these animals to study the impact separately of either AC1 or AC8. Figure 4.11 shows dose-response curves to PE in the concentration range 0.1–30 μM carried out on spontaneously beating isolated murine right atria also in the presence of metoprolol. Data for WT and DKO are the same as presented above in Figure 4.8. Het AC1/8 show an EC50 of 0.8 (0.13–3.47) μM and a maximum rate increase of 16.5 ± 2.8 % (*n*=9), Het AC1/Hom AC8 show an EC50 of 1.7 (0.11–25.65) μM and a maximum rate increase of 16.3 ± 5.2 % (*n*=3) and Hom AC1/Het AC8 show an EC50 of 3.7 (3.2–9.2) μM and a maximum rate increase of 10.9 ± 2.7 % (*n*=5), the only genotype with a significant decrease in maximum rate response to PE compared to WT. Percentage decrease rate of atria after addition of 1 μM metoprolol and stabilisation of the preparation of WT, Het AC1/8, Het AC1/HomAC8, HomAC1/HetAC8 and DKO mice were compared; no significant differences were observed in decrease rate between all Het groups (Figure 4.12C). WT mice had a mean decrease of -31.9 ± 3.5 % (*n*=8), Het AC1/8 mice had a mean decrease of -25.6 ± 3 % (*n*=9), Het AC1/HomAC8 mice had a mean decrease of 37.1 ± 3.1 % (*n*=3), HomAC1/HetAC8 mice had a mean decrease of 27.5 ± 5.1 % (*n*=5) and DKO mice had a mean decrease of 23.4 ± 2 % (*n*=14).

4.5.5 DKO of AC1 and AC8 expression decreases inotropic effect of PE in intact paced left atria

Intact left atria were also dissected in WT and DKO mice to investigate the effect of AC1 and AC8 on the dose-response curve to PE. Contractile force was measured in Figure 4.13 in response to PE in the concentration range of 0.1–30 μM in paced left atria at 5 hertz in the presence of 1 μM metoprolol. In WT mice, the positive inotropic response to PE fits a standard agonist dose-response curve with an EC50 of 6 (1–106.2) μM and a maximum rate increase of 11.94 ± 1.7 % (*n*=8). DKO data show a leftward shift in the EC50 of 1.1 (0.15–8.1) μM with a significant decrease in maximum rate of 5.89 ± 0.8 % (*n*=9). Starting tension of WT and DKO mice were compared; and no significant differences were observed between the two groups (Figure 4.14C). The tension of WT mice was 0.1119 ± 0.02 g (*n*=8) while DKO mice had a mean tension of 0.1047 ± 0.09 g (*n*=9). Baseline tension after addition of metoprolol in WT

and DKO mice were compared; and no significant differences were observed between the two groups (Figure 4.14B). The tension of WT mice was 0.1031 ± 0.01 g (*n*=8) while DKO mice had a mean tension of 0.0957 ± 0.01 g (*n*=9). Percentage decrease in tension of left atria at starting tension and after addition of 1 µM metoprolol and stabilisation of the preparation of wildtype and DKO mice were compared; a higher decrease rate in WT mice was observed between the two groups (P=0.7419, Figure 4.14C). WT mice had a mean decrease of -4.173 ± 5.2 % (*n*=8) while DKO mice had a mean decrease of -6.279 ± 3.7 % (*n*=9). The effect of Het AC1/8 of inotropy was also investigated and showed no significant change in response to PE but had a significant decrease in the presence of 1 µM metoprolol.

4.5.6 DKO of AC1 and AC8 expression reduces amplitude in stimulated calcium transients in atrial myocytes in response to phenylephrine

Adult WT and DKO isolated atrial myocytes were loaded with the cell-permeant calcium sensitive dye Fluo-5F-AM to measure changes in cytosolic calcium in response to PE. When stimulated at 1 hertz in Tyrode at 37°C, atrial myocytes exhibited the classical pattern of calcium transient (Figure 4.16A and B). Basal calcium showed no significant differences between both groups. As shown in Figure 4.17C, DKO of AC1 and AC8 did not alter the basal calcium compared to WT atrial myocytes. Normalised calcium transient amplitude is expressed as change in mean cell fluorescence (F-F0)/F0 in the cell (F is the fluorescent value at a given time and F0 is the resting fluorescence value, Figure 4.17C). Addition of 10 µM of PE to the perfusion solution resulted in a maximum percentage increase in calcium transient amplitude of 26.6 ± 3.9 % in WT atrial myocytes (*n*=10, *N*=3) while DKO atrial cells resulted in an increase of 1.1 ± 4.4 % (*n*=10, *N*=3), a significant decrease in response to PE (Figure 4.18B). I conducted a calcium transient time-control experiment to verify that the baseline calcium handling in the WT atrial cardiomyocyte remains stable over the total time course of the experiment (2 min) without intervention (Figure 4.19). After 1 min, calcium transient amplitude reduced by 20.5 ± 2.8 % and reduced by 18.1 ± 1 % after 2 min, this reduction could be due to photobleaching or signal degradation over time.

4.5.7 DKO of AC1 and AC8 expression reduces cAMP levels in response to phenylephrine in NMAMs

FRET-based sensors enable real-time measurement of intracellular cAMP signalling and can be used to demonstrate compartmentation of cAMP/PKA signalling. Cytosolic sensors (EPAC-

S^{H187}) enable global changes in cytosolic cAMP to be measured from intact cells in real-time using fluorescent imaging. FRET response changes in the background-subtracted 480 nm/545 nm fluorescence emission intensity on excitation at 430 nm (Figure 4.20A) and expressed as R/R_0 where R is the ratio (Figure 4.20B), results are presented as changes measured as percentage change from saturating FSK (10 μM) and IBMX (100 μM).

FRET pipetting time control experiments was conducted and expression of biosensor was stable throughout the duration of the protocol and pipetting E1 buffer did not affect results (Figure 4.21). Extracellular application of 3 μM PE to NMAMs expressing EPAC-S^{H187} resulted in an increase in the mean ratio (cyan/yellow) in all conditions (Figure 4.22). In WT NMAMs, in solvent control conditions, in the presence of 0.1 % DMSO, FRET change in response to PE represented 13.05 ± 1.5 % of the saturating FSK/IBMX response (Figure 4.22A). The addition of ST034307 to the cells did not cause a significant reduction in response to 3 μM PE (11.32 ± 2.4 %, Figure 4.22A). Activation of α-ARs using PE resulted in a FRET change of 7.65 ± 0.3 % in DKO NMAMs, a significant decrease compared to WT NMAMs (Figure 4.22B).

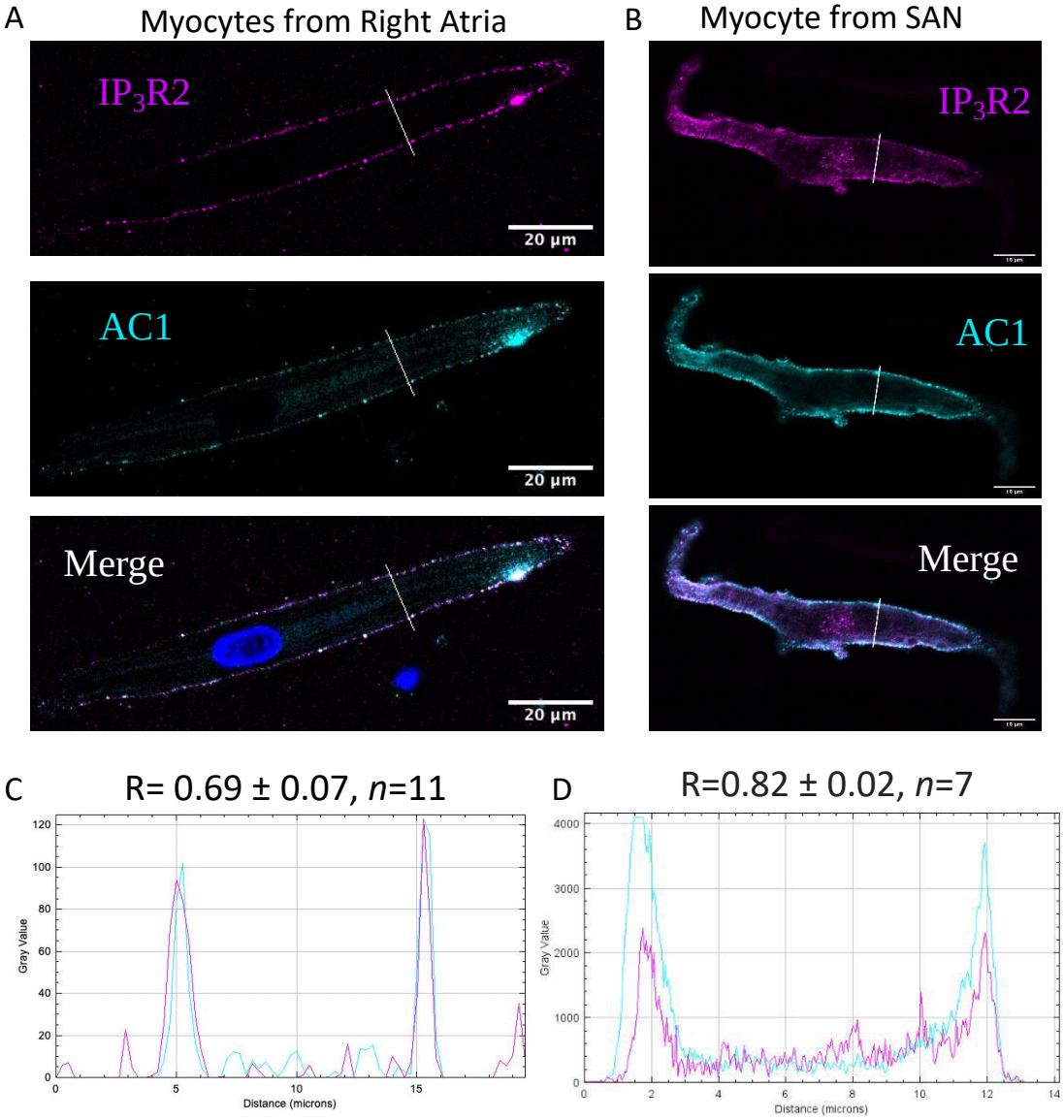

Figure 4.2: Immunohistochemistry show higher colocalisation of IP$_3$R2 and AC1 in isolated adult guinea pig SAN myocytes.

A: Representative confocal image of a fixed, isolated guinea pig atrial myocyte immunolabelled for IP$_3$R2 (magenta), AC1 (cyan) and merge.
B: Representative confocal image of a fixed, isolated guinea pig SAN myocyte immunolabelled for IP$_3$R2 (magenta), AC1 (cyan) and merge.
C: Intensity plot to show staining intensity along the line shown in A.
D: Intensity plot to show staining intensity along the line shown in B.
R=Pearson's overlap coefficient, scale bar represents 20 µM.

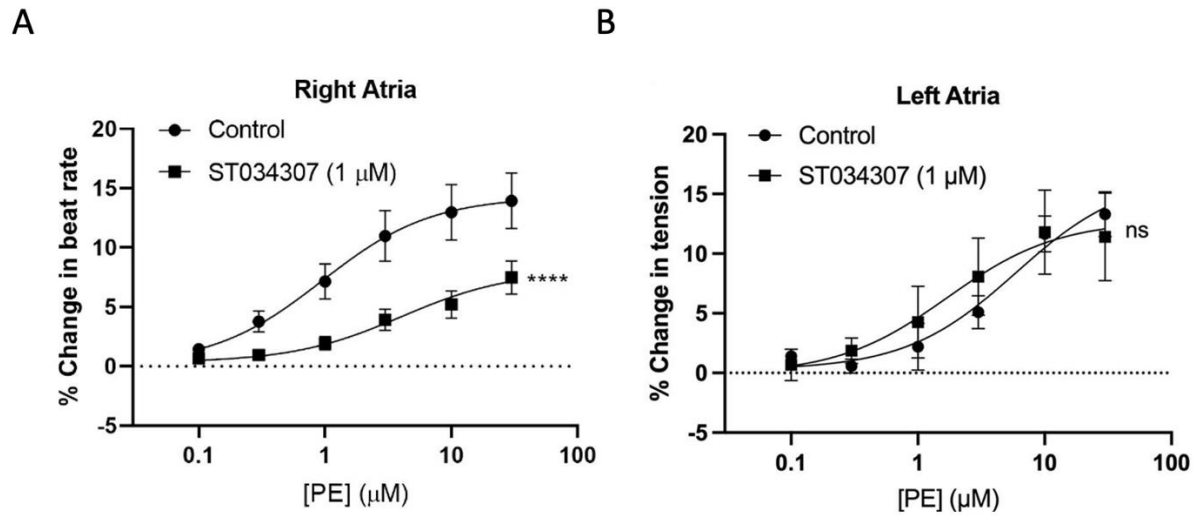

Figure 4.3: Inhibition of AC1 by ST034307 reduces the positive chronotropic effect of PE in the intact sino-atrial node.

A, Dose response curves to show the change in beating rate on cumulative addition of PE to spontaneously beating mouse right atria preparations under control conditions (*n*=15) and in the presence of 1 μM ST034307 (*n*=12).
B, Dose response curves to show the change in tension on cumulative addition of PE to spontaneously beating mouse right atria preparations under control conditions (*n*=5) and in the presence of 1 μM ST034307 (*n*=7).

Asterisks indicate significance level for effect of ST034307 compared to control at individual concentrations as determined using 2-way repeated measures ANOVA followed by Šídák's multiple comparisons test. ****P<0.0001. Data are represented as mean ± SEM.

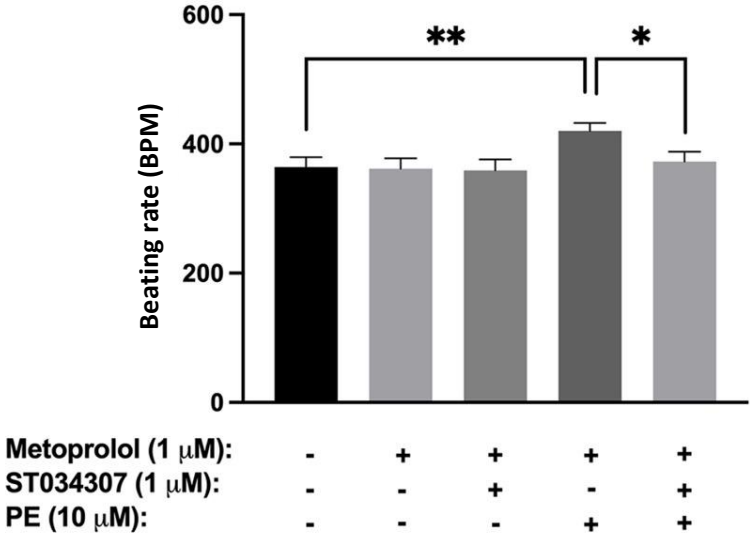

Figure 4.4: No change in beating rate before addition of PE.

Effect of different combinations of metoprolol (1 μM), ST034307 (1 μM) and PE (10 μM) on mouse right atrial beating rate.

Bars represent mean heart rate (BPM) under different conditions as indicated below the x-axis.) (*n*=11–14). *P<0.05; **P<0.01. Data are represented as mean ± SEM.

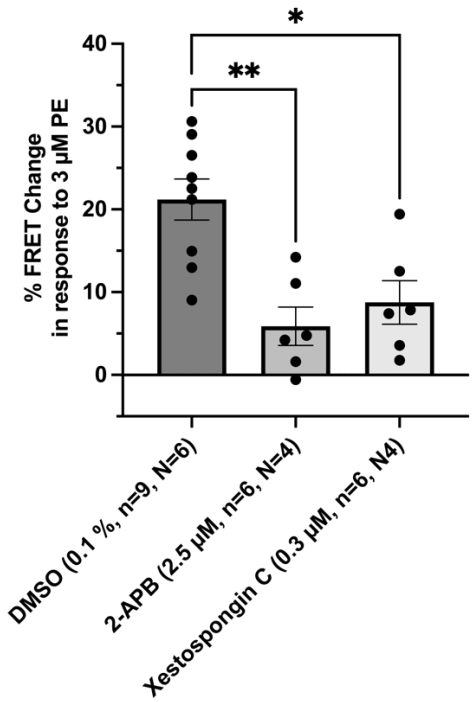

Figure 4.5: IP$_3$R inhibitors reduce FRET change in response to 3 µM PE.

Quantification of peak for PE (3 µM; *n*=9, *N*=4) alone, or in the presence of 2.5 µM 2-APB (*n*=6, *N*=4) or 0.3 µM xestospongin-C (*n*=6, *N*=4), expressed as a fraction of the saturating response in the presence of 10 µM FSK + 100 µM IBMX.

Data represented as mean ± SEM. Asterisks indicate significance level compared to control using Kruskal-Wallis followed by Dunn's multiple comparison test. *P<0.05; **P<0.01.

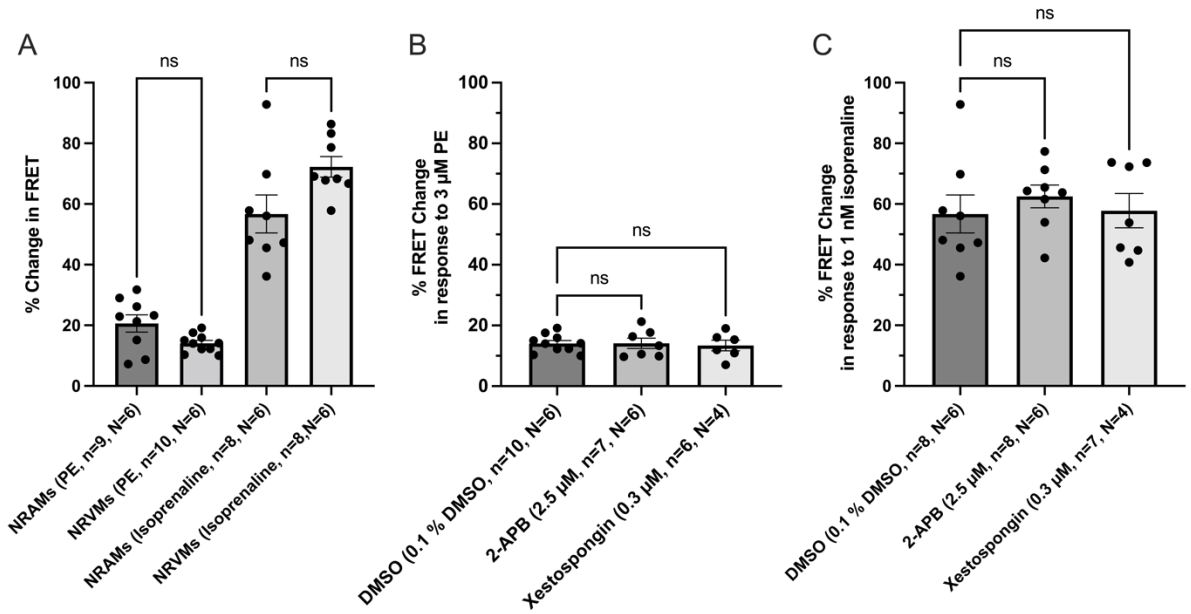

Figure 4.6: PE and isoprenaline stimulation on cytosolic cAMP levels recorded in ventricular myocytes show that responses are not affected by IP$_3$R inhibition.

A, Comparison of peak response to 3 µM PE or 1 nM isoprenaline in NRAMs and NRVMs (*n*=8-10, *N*=6), shown as % FRET change from baseline as normalised to saturating FSK/IBMX.
B, Quantification of the peak FRET change in response to 3 µM PE in NRVMs in the presence of 1 µl/ml DMSO, 2.5 µM 2-APB or 0.3 µM xestospongin-C in NRVMs (*n*=6-10, *N*=4-6).
C, Quantification of the peak FRET change in response to 1 nM isoprenaline in NRVMs in the presence of 1 µl/ml DMSO, 2.5 µM 2-APB or 0.3 µM xestospongin-C in NRVMs (*n*=7-8, *N*=4-6).

Data shown as mean ± SEM, Asterisks indicate significance level using Kruskal Wallis followed by Dunn's multiple comparison, non-significant (ns)=P>0.05.

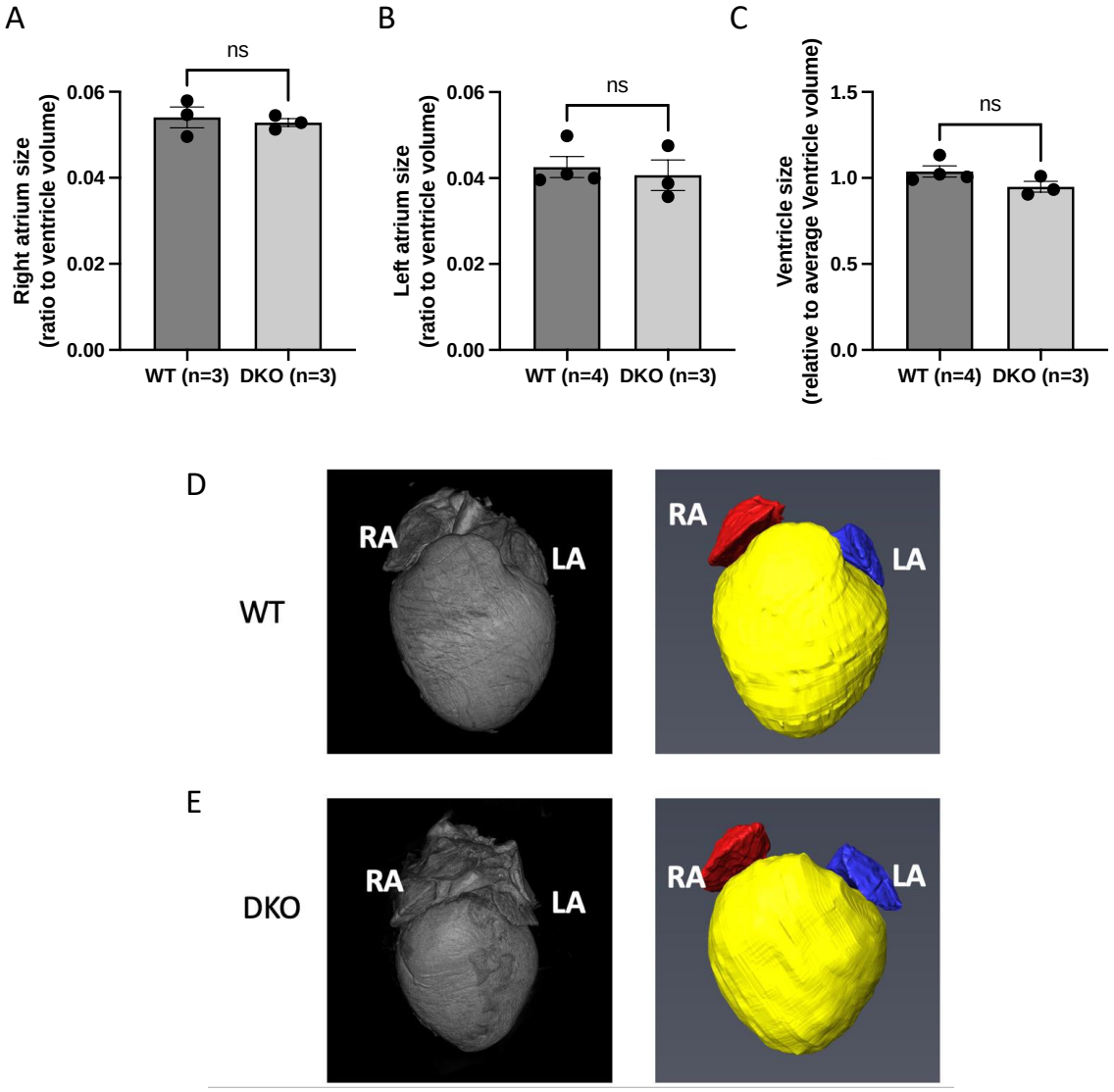

Figure 4.7: 3D modeling using HREM of WT and DKO whole hearts show no significant differences.

A, Comparison of right atrium size relative to average ventricle volume in WT (*n*=3) and DKO (*n*=3) mice hearts.
B, Comparison of left atrium size relative to average ventricle volume in WT(*n*=4) and DKO (*n*=3) mice hearts.
C, Comparison of ventricle size relative to average ventricle volume in WT (*n*=4) and DKO (*n*=3) mice hearts.
D, Representative image of WT heart
E, Representative image of DKO heart

Data are represented as mean ± SEM and were analysed using paired t-test; non-significant (ns)=P>0.05.

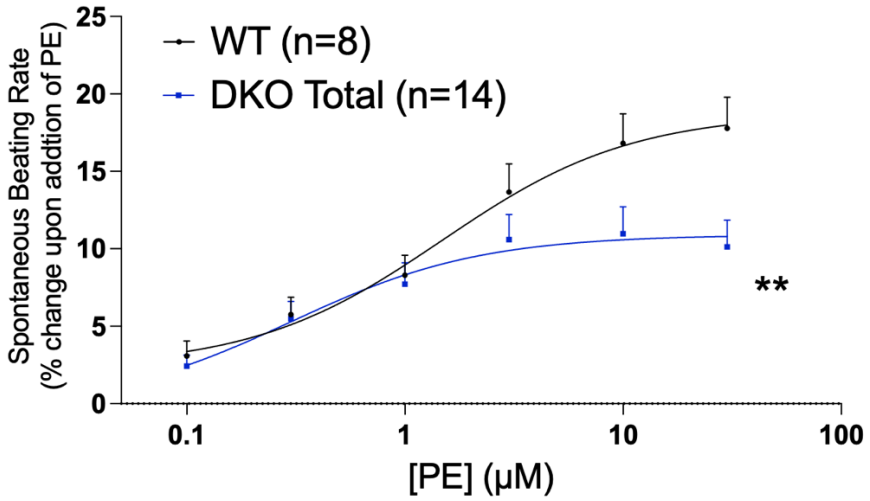

Figure 4.8: Knockout of AC1 and AC8 reduces the positive chronotropic effect of PE in the intact sino-atrial node of DKO mice.

Dose response curves to show the change in beating rate on cumulative addition of PE (0.1 μM - 30 μM) to spontaneously beating mouse right atria preparations in WT mice (black, *n*=8) and DKO mice (blue, *n*=14).

Data are represented as mean ± SEM. Asterisks indicate significance level for effect of DKO compared to WT at individual concentrations as determined using 2-way repeated measures ANOVA followed by Šídák's multiple comparisons test; **P<0.01.

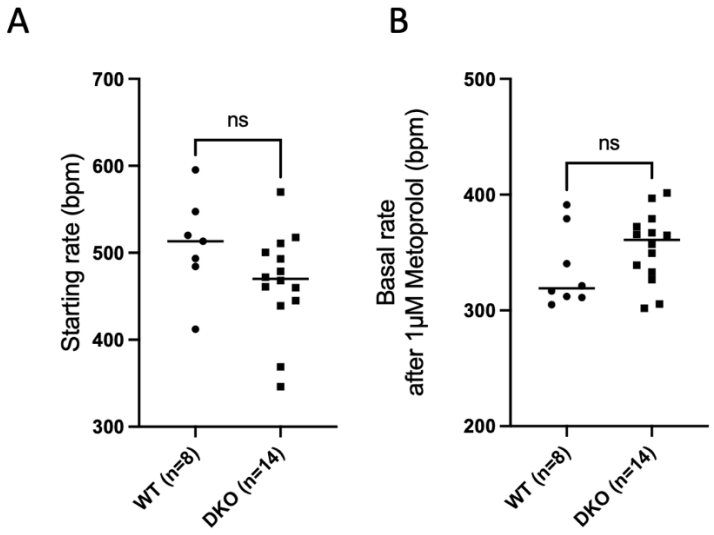

Figure 4.9: No significant changes in beating rate before addition of PE in WT and DKO mice.

A, Comparison of spontaneously starting beating rate of WT (*n*=8) and DKO (*n*=14) C57s murine right atrial preparations in PSS prior to addition of drug or stimulation with PE.
B, Comparison of spontaneously baseline beating rate of WT(*n*=8) and DKO (*n*=14) C57s murine right atrial preparations in PSS after addition of 1 µM metoprolol.

Data are represented as mean and were analysed using paired t-test; non-significant (ns)=P>0.05.

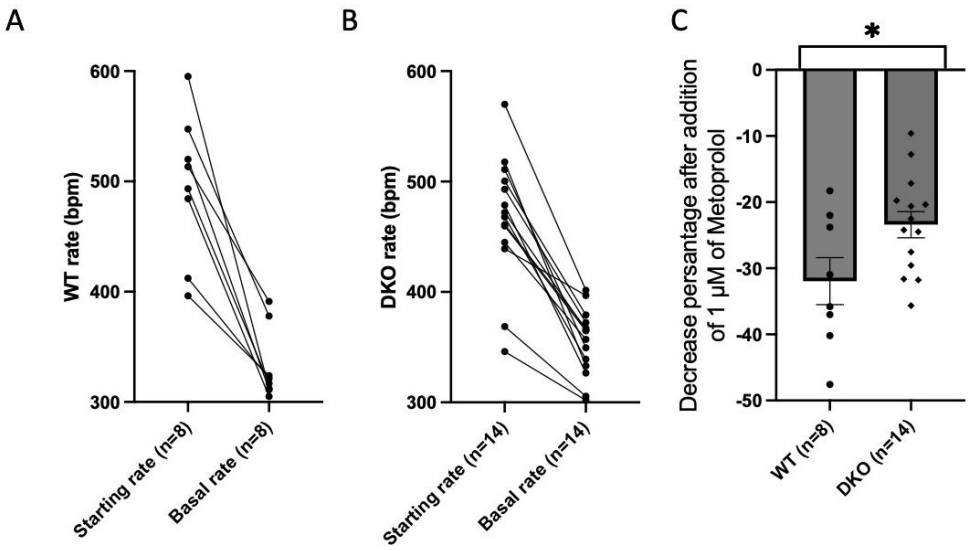

Figure 4.10: DKO showed less beating rate reduction after metoprolol.

A, Comparison of spontaneously starting and basal beating rate of WT (*n*=8) C57s murine right atrial preparations in PSS.
B, Comparison of spontaneously starting and basal beating rate of DKO (*n*=14) C57s murine right atrial preparations in PSS.
C, Comparison of percentage decrease rate between starting rate and basal rate of WT (*n*=8) and DKO (*n*=14) C57s murine right atrial preparations.

Data in panel C are represented as mean ± SEM and were analysed using paired t-test; *P<0.05.

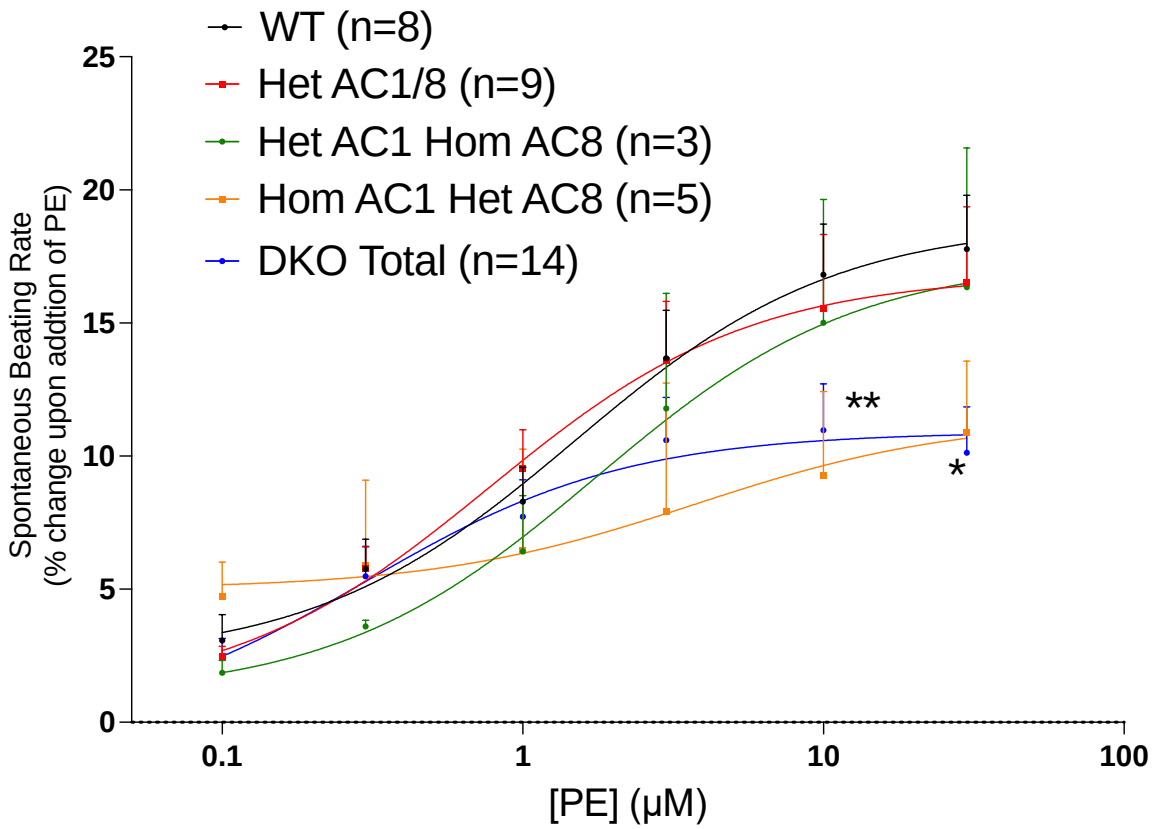

Figure 4.11: HomAC1/HetAC8 shows reduced rate response to PE similar to DKO.

Rate responses to PE (0.1 μM - 30 μM) in spontaneously beating murine right atrial preparations in WT (*n*=8, black), Het AC1/8 (*n*=5, red), Het AC1/HomAC8 (*n*=3, green), HomAC1/HetAC8 (*n*=6, orange) and DKO AC1/8 (*n*=14, blue).

Data are represented as mean ± SEM. Asterisks indicate significance level for effect of Het AC1/8, Het AC1/HomAC8, HomAC1/HetAC8 and DKO compared to WT at individual concentrations as determined using 2-way repeated measures ANOVA followed by Šídák's multiple comparisons test; *P<0.05; **P<0.01.

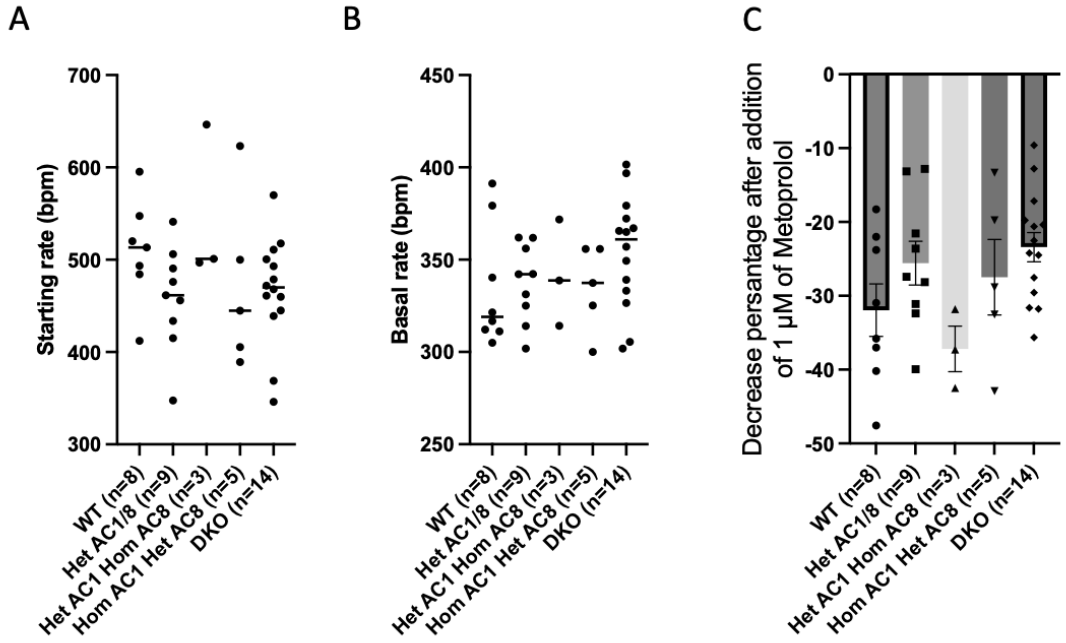

Figure 4.12: Baseline rate comparison shows no significant difference in WT, Het AC1/8, Het AC1/HomAC8, HomAC1/HetAC8 and DKO before addition of PE.

A, Comparison of spontaneously starting beating rate of WT (*n*=8), Het AC1/8 (*n*=5), Het AC1/HomAC8 (*n*=3) and HomAC1/HetAC8 (*n*=5) and DKO AC1/8 (*n*=14) C57s murine right atrial preparations in PSS prior to addition of drug or stimulation with PE.
B, Comparison of spontaneously baseline tension WT (*n*=8), Het AC1/8 (*n*=9), Het AC1/HomAC8 (*n*=3) and HomAC1/HetAC8 (*n*=5) and DKO AC1/8 (*n*=14) C57s murine right atrial preparations in PSS after addition of 1 µM metoprolol.
C, Comparison of percentage decrease rate between starting rate and basal rate of WT (*n*=8), Het AC1/8 (*n*=9), Het AC1/HomAC8 (*n*=3) and HomAC1/HetAC8 (*n*=5) and DKO AC1/8 (*n*=14) C57s murine right atrial preparations.

No significance for effect of Het AC1/8, Het AC1/HomAC8, HomAC1/HetAC8 and DKO compared to control at individual concentrations was observed, determined using 2-way repeated measures ANOVA followed by Dunnett's multiple comparisons test. Data are represented as mean ± SEM.

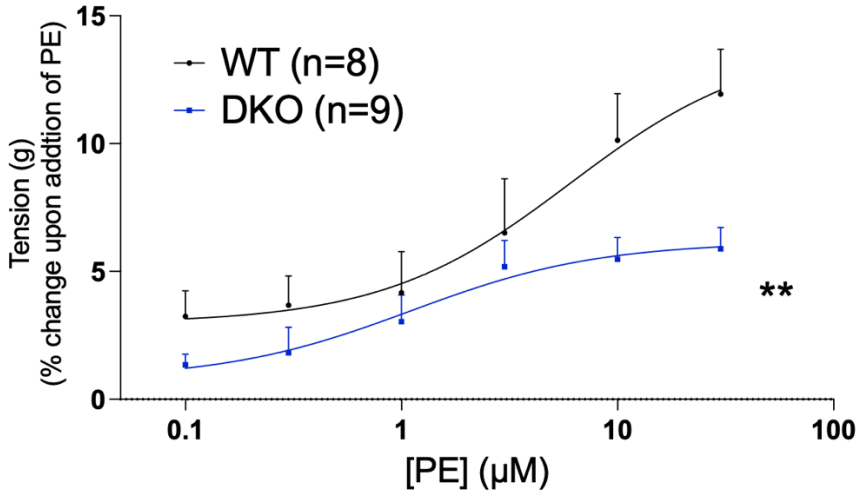

Figure 4.13: Knockout of AC1 and AC8 reduces tension change to PE in stimulated beating murine left atrial preparations in DKO mice.

Dose response curves to show the force of contraction on cumulative addition of PE (0.1 μM - 30 μM) to spontaneously beating mouse right atria preparations in WT mice (black, *n*=8) and DKO mice (blue, *n*=9).

Asterisks indicate significance level for effect of DKO compared to WT at individual concentrations as determined using 2-way repeated measures ANOVA followed by Šídák's multiple comparisons test; **P<0.01. Data are represented as mean ± SEM.

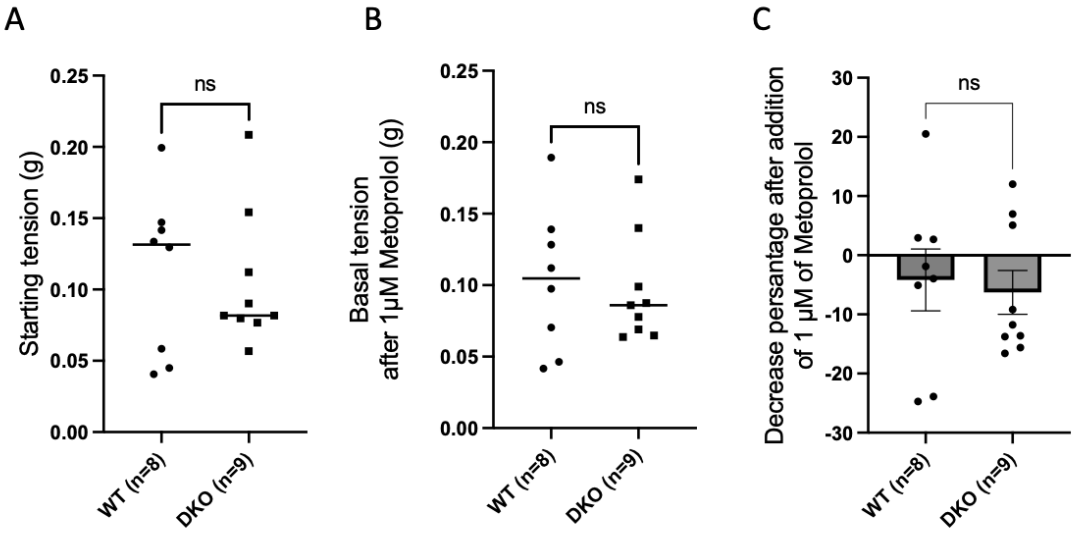

Figure 4.14: No significant changes observed in baseline tension between WT and DKO left atrial preparation before addition of PE.

A, Comparison of starting tension of WT (*n*=8) and DKO (*n*=10) C57s murine right atrial preparations in PSS prior to addition of drug or stimulation with PE.
B, Comparison of baseline tension of WT (*n*=8) and DKO (*n*=10) C57s murine right atrial preparations in PSS after addition of 1 µM metoprolol.
C, Comparison of percentage decrease rate between starting rate and basal rate of WT (*n*=8) and DKO (*n*=9) C57s murine right atrial preparations.

Data are represented as mean ± SEM and were analysed using paired t-test; non-significant (ns)=P>0.05.

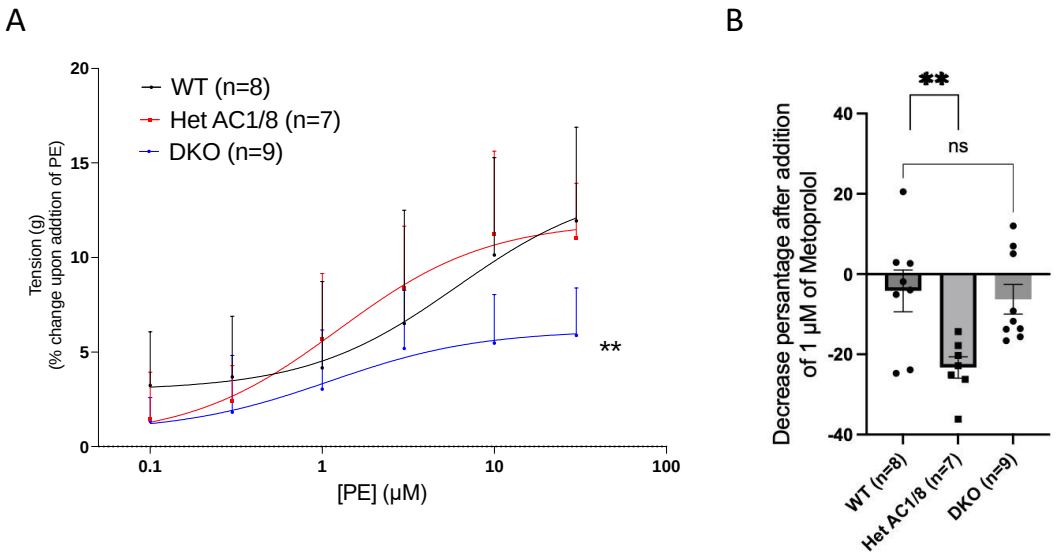

Figure 4.15: Tension change show no change in Het AC1/8 upon PE stimulated on stimulated left atria.

A, Tension change to PE (0.1μM - 30 μM) in stimulated beating murine left atrial preparations in WT (*n*=8), HetAC1/8 (*n*=10) and DKO AC1/8 (*n*=9)**.**
B, Comparison of percentage decrease contractile force between starting rate and basal rate of WT (*n*=8) Het AC1/8 (*n*=7) and DKO (*n*=9) C57s murine right atrial preparations.

Asterisks indicate significance level for effect of Het AC1/8 and DKO compared to WT at individual concentrations as determined using 2-way repeated measures ANOVA followed by Šídák's multiple comparisons test in panel A. Data are represented as mean ± SEM, using 2-way repeated measures ANOVA followed by Dunnett's multiple comparisons test in panel B; non-significant (ns)=P>0.05; **P<0.01.

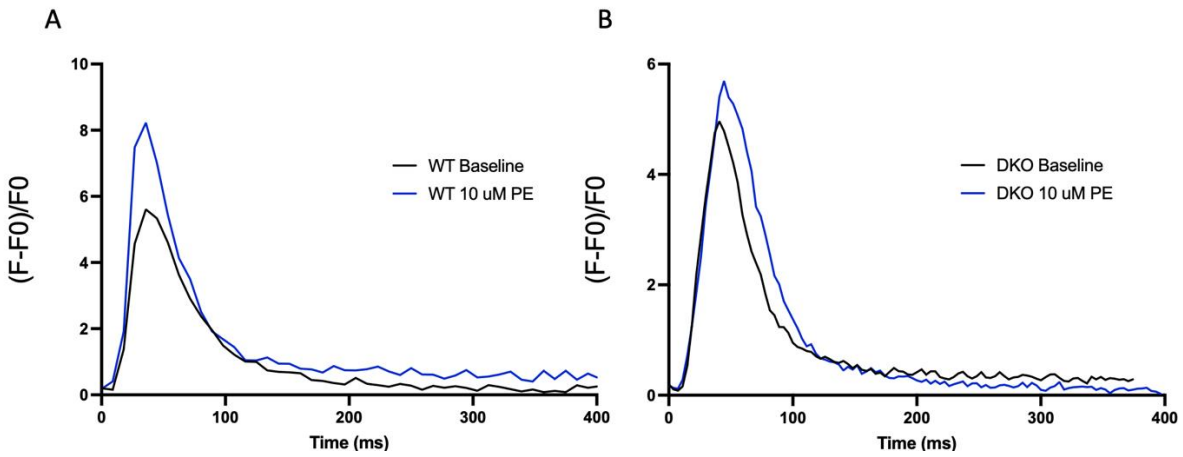

Figure 4.16: Representative calcium transient traces in response to PE in WT and DKO isolated atrial myocytes.

A, Representative traces to show spontaneously generated calcium transients in isolated atrial myocytes WT C57s in control condition (black) and after exposure to 10 μM PE (blue).
B, Representative traces to show spontaneously generated calcium transients in isolated atrial myocytes DKO C57s in control condition (black) and after exposure to 10 μM PE (blue).

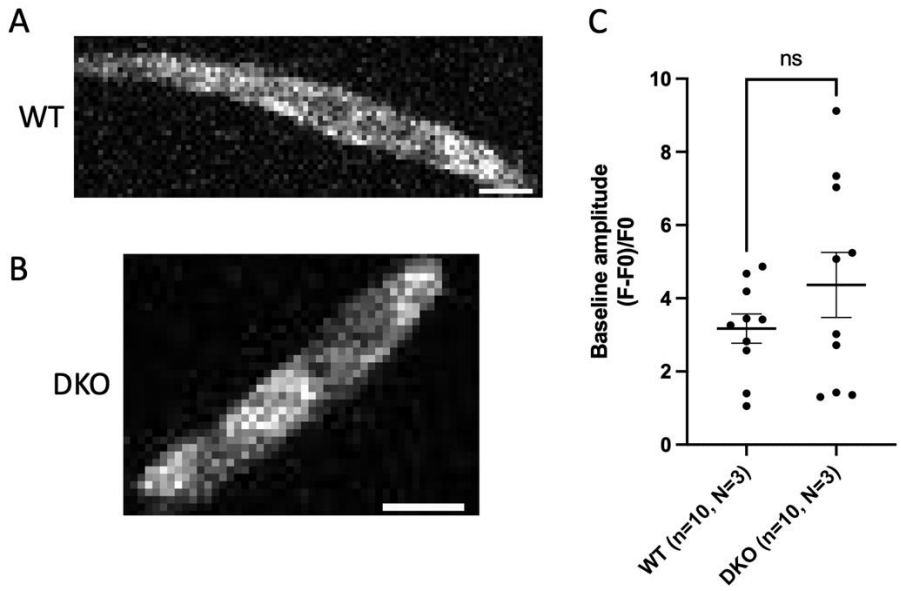

Figure 4.17: Baseline measures show no change in atrial myocytes loaded with 3 µM Fluo-5F.

A, Representative image of a WT atrial myocyte loaded with 3 µM Fluo-5F.
B, Representative image of a DKO atrial myocyte loaded with 3 µM Fluo-5F.
C, Baseline calcium transient amplitude in isolated WT (*n*=10, *N*=3) and DKO (*n*=10, *N*=3) C57s atrial myocytes in control conditions in Tyrode.

Scale bar represents 20 µm in panel A and B. Data are represented as mean ± SEM and were analysed using paired t-test in panel C. *n*=experiments; *N*=animals; non-significant (ns)=P>0.05.

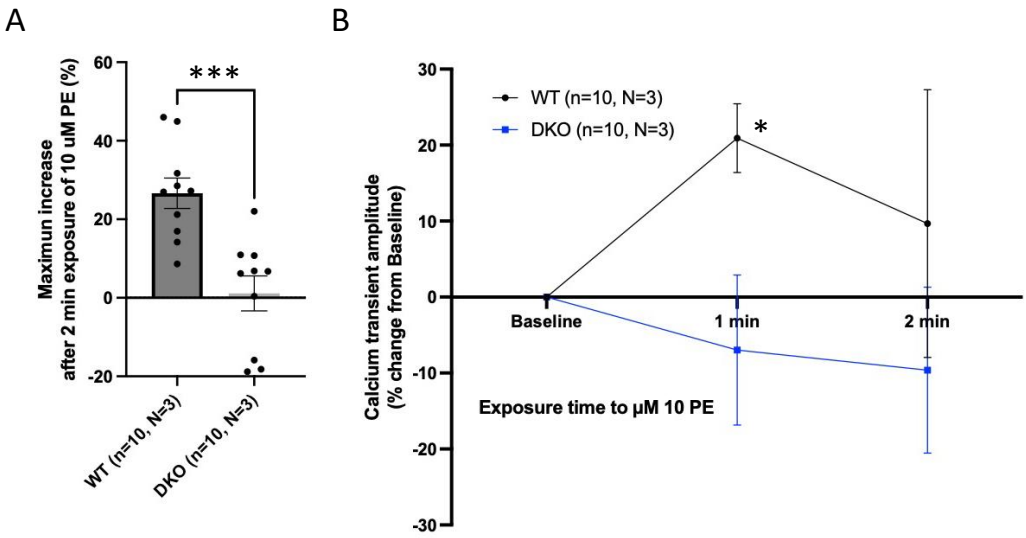

Figure 4.18: Knockout of AC1 and AC8 reduces calcium transient amplitude response to PE in DKO isolated atrial myocyte.

A, Maximum increase (in %) recorded over 2 minutes of exposure to 10 µM PE in isolated WT (*n*=10, *N*=3) and DKO (*n*=10, *N*=3) C57s murine atrial myocytes.
B, Calcium transient amplitude response (in %) in isolated WT (*n*=10, *N*=3) and DKO (*n*=10, *N*=3) C57s murine atrial myocytes after exposure of 10 µM PE over 2 minutes.

Data are represented as mean ± SEM and were analysed using paired t-test in panel A and using 2-way repeated measures ANOVA followed by Šídák's multiple comparisons test in panel B. *n*=experiments; *N*=animals; **P<0.01, ***P<0.001

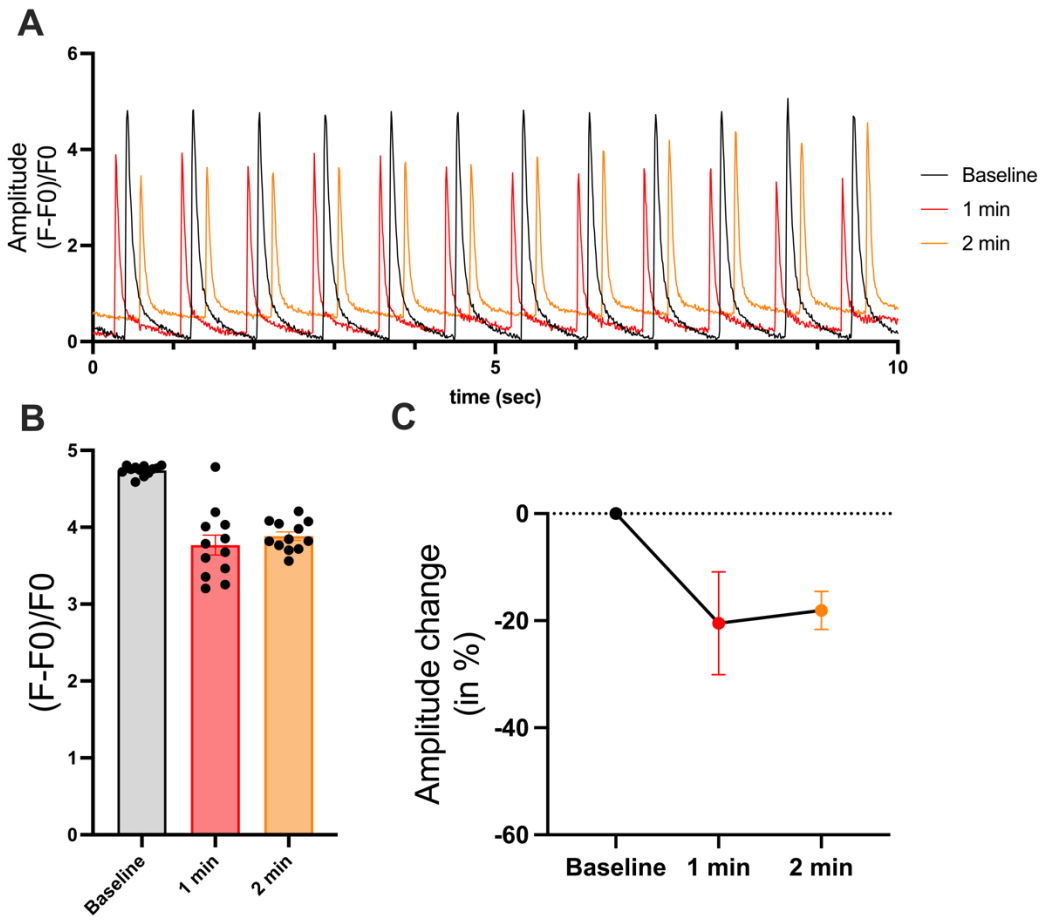

Figure 4.19: Time control in isolated WT atrial myocytes.

A, Representative 10 second trace to show amplitude of stimulated (1 hertz) calcium transients in WT C57s over at 0 second (black), 1 minute (red) and 2 minutes (orange).
B, Calcium transient amplitude at 0 second (baseline, grey), at 1 minute (red) and at 2 minutes (orange).
C, Calcium transient amplitude at 0 second (baseline), at 1 min and at 2 mins as a percentage change compared to baseline.

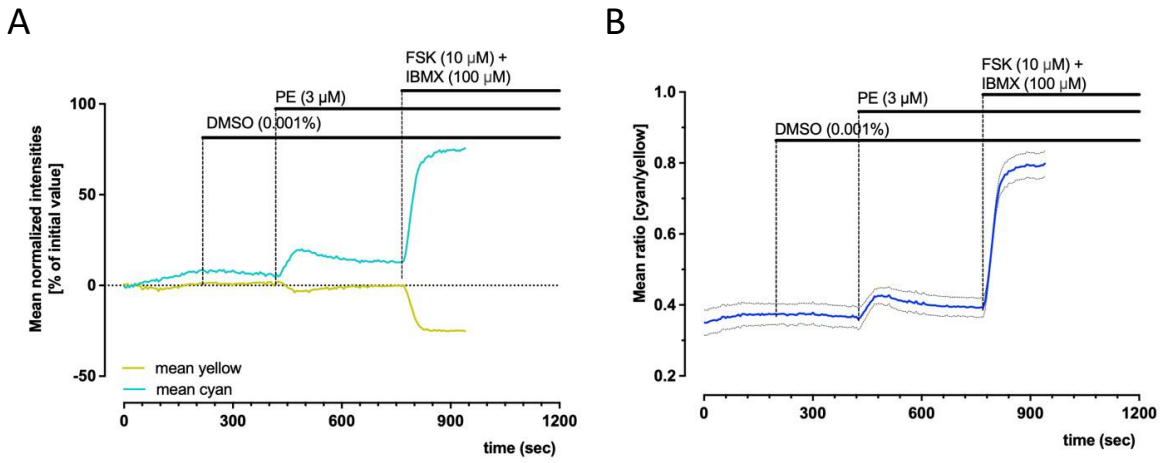

Figure 4.20: Protocol for FRET experiments.

A, CFP/YFP changes in FRET signal in response to 3 µM PE in the presence of DMSO in NMAMs.

B, Representative example single well trace of the effect of 1 µM PE on cAMP levels in NMAMs loaded with EPAC-S^{H187}.

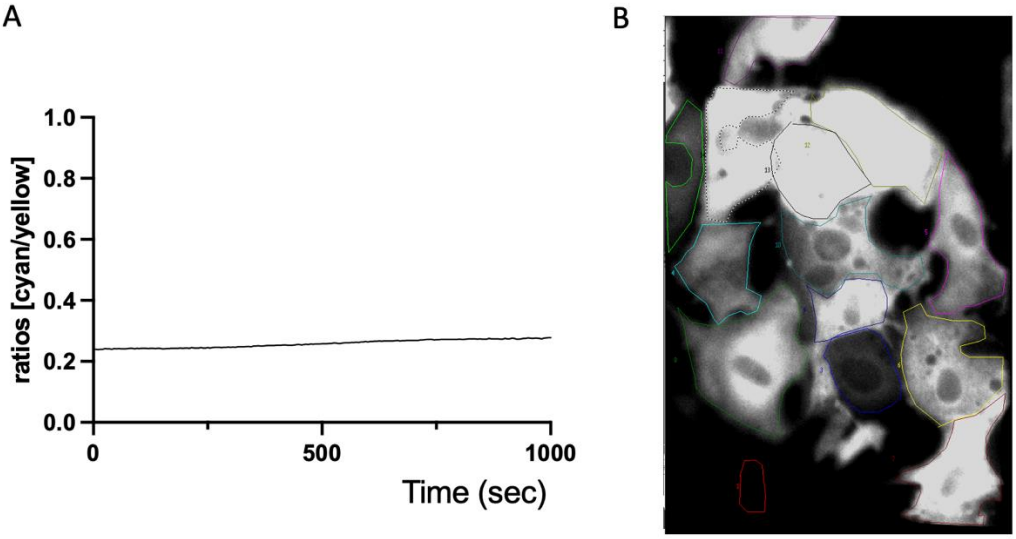

Figure 4.21: FRET pipetting control and expression of biosensor.

A, Trace showing FRET change of DKO NMAM over time course of protocol.
B, Representative image of NMAMs expressing EPAC-S^{H187}.

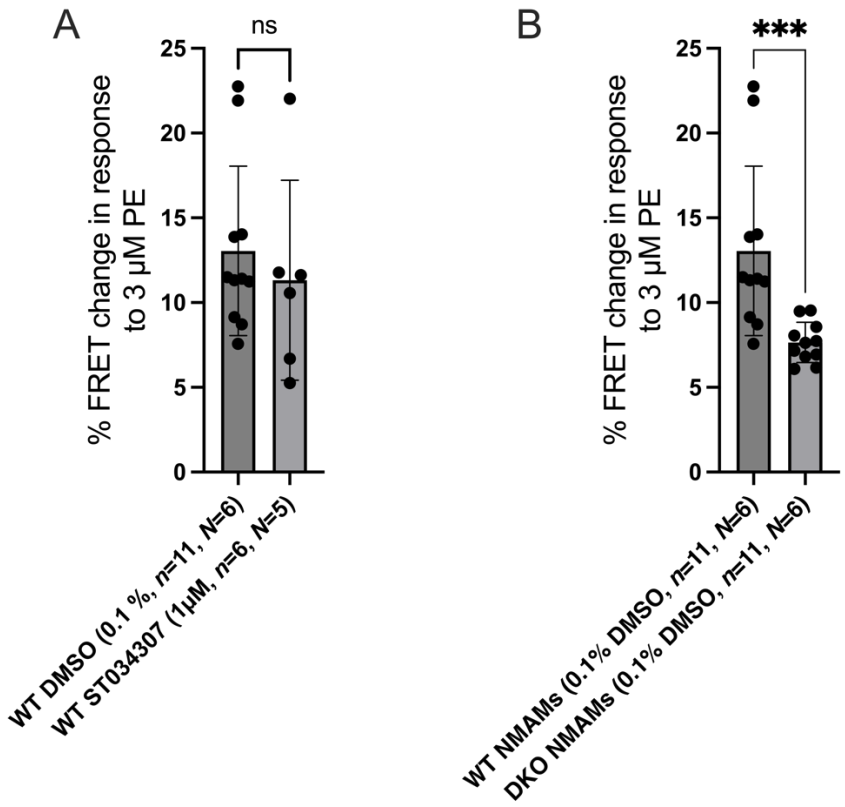

Figure 4.22: FRET response comparison in WT and DKO in response to PE in WT NMAMs.

A, Comparison of peak response to 3 µM PE in single WT NMAMs expressing EPAC-S^{H187}, normalised to maximum response under control conditions (*n*=11, *N*=6) and following addition of 30 µM ST034307 (*n*=6, *N*=5).
B, Comparison of control condition between WT (*n*=11, *N*=6) and DKO (*n*=11, *N*=6) in NMAMs.

Data are represented as mean ± SEM and were analysed using non-parametric Mann-Whitney U test; non-significant (ns)=P>0.05, ***P<0.001.

4.6 Discussions

The IP_3/calcium signalling pathway is very versatile, highlighting it's adaptiveness to control diverse processes in many organisms (Berridge 2009). The first part of this Chapter demonstrates that activation of the IP_3 pathway using PE, an α1-AR agonist, leads in NRAMs to a downstream increase in cAMP as shown using lice imaging FRET technique. These changes were inhibited using pharmacological inhibition of IP_3R2. In contrast, the cAMP rise observed in ventricular neonatal myocytes was not inhibited by the presence of either 2-APB or xestospongin-C, indicating that this cAMP rise in ventricular myocytes is independent of IP_3R calcium release in NRVMs. The second part investigates knockout of AC1 and AC8 in mice as a possible explanation to these observations. DKO showed a decrease in positive chronotropic and inotropic observed in response to PE in intact atrial tissue, inhibited amplitude of calcium transient in response to PE in adult isolated atrial myocytes and presented a decreased response to cAMP levels in response to PE in neonatal atrial myocytes.

The increased cAMP levels seen in response to PE saw a decrease with inhibition of IP_3R with 2-APB or xestospongin-C, one mechanism to explain this could be calcium released via IP_3R upon α-adrenergic stimulation may directly lead to the activation of calcium-sensitive ACs: AC1 and/or AC8 in cardiac cells. This hypothesis will be discussed below.

Addition of 1 μM ST034307 resulted in a significant inhibition of the increase in spontaneous beating rate of intact right atrial preparations but did not have a significant effect on the positive inotropic response to PE in paced murine left atria. Immunocytochemistry work in SAN myocytes suggests that AC1 and IP_3R2 are located within close proximity with higher colocalisation index than in atrial myocytes. The simplest explanation for this observation could be that AC1 is not involved or minimally contributes to the downstream effect of IP_3 signalling in non-SAN atrial myocytes in basal activity and is activated upon α-stimulation. However, AC1 could play a more dominant role in the regulation of SAN pacemaker cells in baseline activity (Bose et al. 2022). Data presented in this chapter are consistent with previous work by (Mattick et al. 2007), confocal microscopy also showed AC1 to be present in SAN myocytes but no in ventricular muscle and is able to regulated of funny current. ST034307 data presented from this study is published in (Bose et al. 2022).

Evidence presented in the first part of this chapter raises the possibility that calcium released via IP_3R2 may influence the activity of AC1 in the SAN. Activation of the IP_3 signalling

pathway in atrial cells leads to the downstream activation of membrane bound calcium sensitive AC1 and AC8.

Pacemaker activity in mouse SAN myocytes have been previously studied by looking at IP_3 signalling (Ju et al. 2011). SAN function undergoes modulation by IP_3 agonists and antagonists, and these changes are abolished in IP_3R2 KO mice. Investigation of the requirement of AC1 and AC8 expression for downstream actions of IP_3R in atrial myocytes was next described in this Chapter. Further chronotropic and inotropic work conducted on DKO mice revealed that AC1 and AC8 play an important role in α-adrenergic stimulation with PE. Pacemaker activity was measured in spontaneously beating right atrial preparations and showed that KO of AC1 and AC8 impaired the SAN to respond to PE contributing additional evidence of the functional interaction of IP_3R and cAMP signalling via AC1/8.

Specific inhibition of AC1 was investigated via pharmacological tools with ST034307 or genetically with Hom AC1 and Het AC8 mice. Hom AC1 and Het AC8 mice showed a greater decrease compared to Het AC1/8 and Het AC1 and Hom AC8, suggesting AC1 could be playing a greater role. The lack of pharmacological inhibitors to target AC8 subtypes hindered our research in specific implications of AC8 but studies of AC8 have shown that overexpression of AC8 increased heart rate and decreases heart rate variability (Moen et al. 2019). Given expression levels of AC1 and AC8 in the SAN (Mattick et al. 2007; Moen et al. 2019) and both are shown to be implicated Pacemaker physiology, both are likely to play crucial roles in heart function and rhythm control.

This was the first time investigating the cardiovascular system in the DKO mouse colony. KO of AC1 and AC8 were only previously used to study long term memory in the brain (Moulder et al. 2008). HREM is a highly robust microscopic imaging method for visualising whole tissue or organs (Kalisch-Smith et al. 2021). I used this method for visualisation of DKO hearts and compared them to WT to perform an analysis on tissue architecture and morphology of the hearts. No structural changes were observed in any chambers of the WT and DKO hearts as potential compensatory mechanisms.

No significant changes were observed in beating rate or contractile force in basal conditions either before or after metoprolol (1 μM) but the difference in decrease after addition of metoprolol in WT and DKO did show a significant difference, with WT right atria resulting in a larger decrease compared to DKO, 31.9 ± 3.5 % (n=8) in WT and 23.41 ± 2 % (n=14) in

DKO (Figure 4.10C and 4.11). These findings raise questions on how compensatory mechanisms adapted to AC1/AC8 DKO, as DKO results in a smaller response to non-specific β-blocker (metoprolol). This could indicate altered signalling calcium pathways that affect downstream responses, resulting reduced functionality despite the presence of the drug. Alternatively, compensatory mechanisms might be activated, such as modulation of calcium signalling within the cell through regulation of SR channels expression (IP_3R or RyR). Reducing reliance on β-adrenergic signalling by either reduced β1-adrenergic receptor expression or increases β2-adrenergic receptor expression leading to diminished responsiveness to the blocker. Changes in catecholamine levels such as adrenaline and noradrenaline could also influence the effectiveness of β-blockade. 3D modelling did not show structural changes to the atria but fibroses or conductivity have not been investigated so far.

Whole tissue experiments offer several benefits in research such as physiological relevance, they allow to study functional work in a physiological environment while keeping complex interactions at a whole organ level and spatial organisations: providing a comprehensive view of tissue function, interactions, and responses. But in this case, it can also make it quite difficult to tease out what compensation mechanisms might be involved to the DKO. The next experiments described in this Chapter were experiments conducted on single cells to study calcium transients and cAMP through FRET on atrial myocytes to investigate, at an intracellular level, mechanisms involved in the interaction between calcium released via IP_3R2 and activity of AC1/AC8.

Calcium transient experiments were next investigated to monitor changes in intracellular calcium in isolated adult atrial myocytes of WT and DKO mice. Stimulation of IP_3R2 with 10 μM of PE caused an increase in amplitude in WT myocytes and this increase was abolished in KO of AC1 and AC8 myocytes from DKO mice. In contrast, previous calcium transient work (Bose et al. 2022) with inhibition of only AC1 with ST034307 did not have a significant decrease on the positive inotropic response to PE in paced murine atria (Figure 4.2B). In contrast, ST034307 did inhibit beating rate in isolated SAN myocytes without causing an inhibition of amplitude in calcium transients (Bose et al. 2022). This result could suggest possible compensation mechanisms of AC8 in atrial cells and/or AC1 activation by IP_3R calcium release may be enhanced or specific in SAN by funny current and modulate both basal and stimulated pacemaker mechanisms. These calcium transient experiments provide support that activation of AC1 and AC8 from IP_3R mediated calcium release are valuable in regulation

of heart rate and calcium signalling. In SAN myocytes, cAMP has been shown to activate funny current by shifting it's activation curve to more positive voltage (DiFrancesco and Tortora 1991). In parallel, cAMP levels were also measured in response to PE and caused an increase in % change of FRET, which was non significantly inhibited by ST034307 in both WT NMAMs (Figure 4.20A) but caused a significant decrease in cAMP level in DKO (7.65 ± 0.3 %, *n*=11, *N*=6) compared to WT (13.05 ± 1.5 %, *n*=11, *N*=6, Figure 4.20B) in NMAMs, suggesting a possible compensation mechanism by AC8. Expression of *Adcy8* could by higher in atrial cells and/or quiescent neonatal cells, causing a stronger effect.

As well as structural and expression differences observed in atrial and SAN myocytes discussed above, differences in atrial and ventricular myocytes also have been reported (Blatter 2017). As the atrial and ventricular chambers of the heart serve different functions, they also present different morphology and markers expression to respond to different needs in ECC and in calcium handling by different intracellular compartment. IP_3R are found in significantly higher density in atrial cells compared with ventricular myocytes (Lipp et al. 2000). FRET experiments in this Chapter presented no inhibition of IP_3 signalling in the presence of IP_3R inhibitors in NRVMs compared to NRAMs (Figure 4.5 and Figure 4.6B). Opening an avenue of research into tissue specific treatment options for arrhythmias.

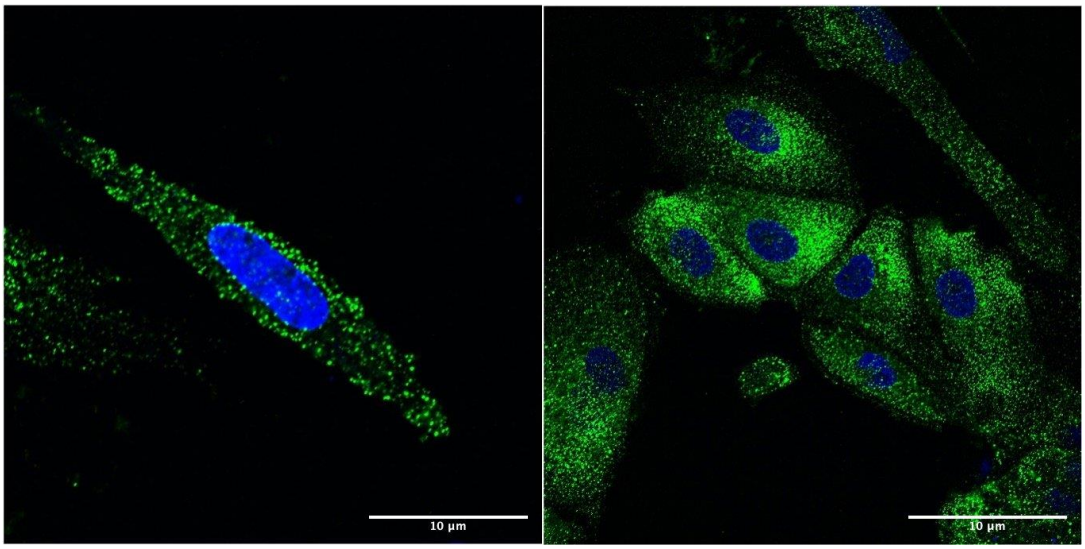

Figure 4.23: Immunohistochemistry of hiPSC-aCMs show IPR3R2 expression.

Representative confocal image of a fixed, hiPSC-aCMs stained with DAPI (blue) immunolabelled for IP_3R2 (Chandler et al.).

IP_3R (Berridge 2009) and AC1 and AC8 (Mattick et al. 2007) being linked to pacemaking and unravelling the interaction between IP_3R pathways and ACs in this Chapter provides important insights mechanisms for initiation of atrial arrhythmias, Figure 4.23 shows expression of IP_3R2

expression in atrial cardiomyocytes derived from human-induced pluripotent stem cells (hiPSC-aCMs, fixed and stained with IP_3R2 antibody), highlighting functional relevance of this pathway in hiPSC-aCMs. Abnormal calcium signalling leads to pathological conditions especially rhythm disorders and we currently have limited medication and treatment for rhythm disorders. Using human cell models such as hiPSC-CMs will help investigate IP_3 signalling pathway and possibly link this pathway to rhythm disorders and AF (Brown et al. 2024).

A possible mechanism explaining cAMP production in response to IP_3R stimulation could be from another calcium intracellular store. Experiments from (Kockskämper, Seidlmayer, et al. 2008) showed activation of IP_3R induced calcium transient amplitude increase with an unchanged SR load. Could Lysosomes be contributing as a calcium store to this mechanism? Work has shown lysosomes to influence cardiac calcium handling (Capel et al. 2015; Collins et al. 2011). In addition, very recent work has shown crosstalk between IP_3-NAADP (Capel et al. 2024). This will be discussed in next Chapter.

4.7 Conclusions

Findings in this Chapter link direct cellular stimulation with IP_3 in atrial myocytes to downstream actions via the generation of cAMP, illustrated in Figure 4.24. Overall, the results presented in this Chapter provide support for the hypothesis that atrial myocytes express IP_3R and that IP_3 has a signalling role in the atrium. The results also provide novel insights on downstream cAMP levels in response to activation of IP_3R. Using a transgenic mouse line, I have demonstrated AC1 and AC8 to be key modulators in the response to α-adrenergic stimulation in pacemaking in the SAN and in inotropy, these observations strengthen previous work that a functional interaction between IP_3 and cAMP signalling involving calcium stimulation of ACs in the SAN pacemaker and provides precious insight concerning potential mechanisms for initiation of AF and a target treatment. Higher resolution imaging studies would be required to pinpoint affecters in these microdomains.

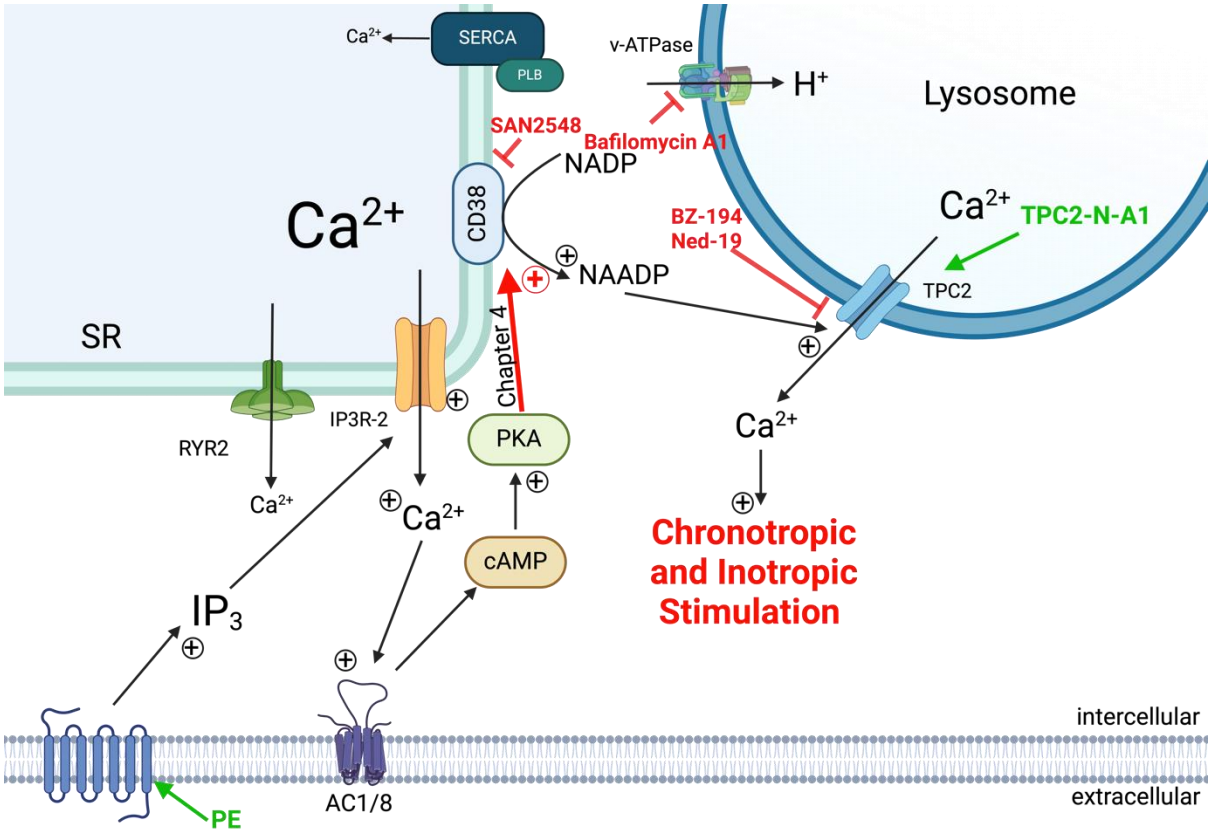

Figure 4.24: Representative scheme of proposed mechanisms from Chapter 4. Activation of α1-AR by PE lead to increased atrial cytoplasmic calcium transients and cAMP production. Activation of α1-AR leads to elevated IP_3 resulting from cleavage of PIP_2 to DAG and IP_3 by PLC. IP_3 activation of IP_3R2 results in release of calcium from the SR, which subsequently leads to activation of AC8 or AC1, activation of PKA by cAMP. Ca^{2+}, calcium.

5 Chapter 5: Crosstalk between IP_3-dependent calcium release from the SR and lysosomal NAADP signalling in response to α-adrenergic stimulation in atrial function.

5.1 Summary of contribution:

This Chapter presents a paper into investigating lysosomal calcium signalling contribution to the acute α-adrenergic response. I am first author, I carried out experiments, conceptualisation, methodology, and writing of the project. Figures reproduced from the paper were my own work. Additionally, this Chapter contains FRET data and immunostaining that was published in (Capel et al. 2024).

5.2 Introduction

As described in previous Chapters, NAADP is a highly potent calcium releasing second messenger and acts by releasing calcium from acidic calcium stores such as lysosomes (Churchill et al. 2002; Zhang et al. 2006). These studies provided evidence that these acidic stores, are lysosomal organelles that function as calcium stores to mobilise calcium in response to NAADP. NAADP signalling regulates a large range of cell types across species and a broad range of cellular signalling processes from osteoclastogenesis in osteoclasts to neurotransmitter release and neurosecretion in neuroses (Galione 2015). Mutations in genes encoding for lysosomal enzymes can lead to a wide range of disease associated lysosomal dysfunctions (Galione et al. 2009). Niemann-Pick disease type 1, is a genetic disorder characterised by the accumulation of sphingomyelin in cells due to a deficiency in the enzyme acid sphingomyelinase and is associated with abolition of NAADP-induced calcium release (Lloyd-Evans et al. 2008). It leads to severe neurological impairment and has secondary complications, including cardiomyopathy due to lipid accumulation and heart failure as the disease progresses. Anderson-Fabry disease is a genetic disorder caused by the deficiency of the enzyme alpha-galactosidase A, leading to the accumulation of glycosphingolipids (Bernardes, Foresto, and Kirsztajn 2020).. Anderson-Fabry disease can lead to hypertrophic cardiomyopathy, arrhythmias, and heart failure due to the deposition of lipids in the heart tissue (Azevedo et al. 2021).

NAADP receptors were reported to been present and functionally active in the heart (Bak et al. 2001). NAADP mediated calcium release was abolished in TPC-deficient mouse embryonic fibroblasts compared to WT. (Ruas et al. 2015). Inhibition of NAADP signalling on reperfusion protects the heart by preventing lethal calcium oscillations via TPC1 (Davidson et al. 2015). TPC2 demonstrates a key role in contractile responses, TPC2 is necessary for β-adrenergic stimulation to induce NAADP-evoked calcium across endo-lysosomal membranes and this action depends on lysosomal voltage-gated calcium-permeable TPC2 (Calcraft et al. 2009) and are located on vacuolar or lysosomal membranes (Patel 2015).

Research groups have demonstrated lysosomes to participate in calcium homeostasis, acting as calcium stores (Burgoyne, Patel, and Eden 2015; Ogunbayo et al. 2018). NAADP is synthesised in the heart in response to β-adrenergic stimulation, through the ADP ribosyl cyclase enzyme CD38 (Aarhus et al. 1995). Stimulation of β-adrenergic pathway has been shown to increase NAADP levels in cardiac muscles, and direct addition of NAADP by photorelease has been

showed to increases calcium transient amplitude in atrial myocytes (Collins et al. 2011) and in ventricular myocytes (Macgregor et al. 2007). Evidence later showed that Tpcn2$^{-/-}$ cardiac myocytes show a reduced response to β-AR stimulation and chronically reduced cardiac hypertrophy and arrhythmogenesis compared to WT (Capel et al. 2015); demonstrating a role for NAADP/TPC2 signalling in ECC process and response to cardiac β-AR stimulation. NAADP is synthesised in the heart in response to β-adrenergic stimulation, it is hypothesised that enzyme CD38 is responsible for the production by catalysing NAADP *in vitro*. CD38$^{-/-}$ myocytes showed a decrease in isoproterenol-induced calcium transients compared to WT (Lin et al. 2017), targeting SAN4824, an ADP-ribosyl cyclase inhibitor that reduces NAADP synthesis as a potential therapeutic target (Kannt et al. 2012). High resolution structural studies presented lysosomes forming contact sites with the SR in ventricular myocytes possibly enhancing calcium release from the SR (Aston et al. 2017).

Work presented in the previous Chapter showed IP_3-dependent calcium release to activate calcium-stimulated ACs and play a major role in response to α-adrenergic stimulation and in controlling atrial physiology. There is a large body of evidence that supports the hypothesis that NAADP mobilises calcium from an acidic organelle in response to β-adrenergic stimulation (Capel et al. 2015; Collins et al. 2011) but no work has been conducted or described in response to α-adrenergic stimulation. Moreover, work has shown that lysosomes associate with ER by staying located at regions populated by IP_3R clusters in Human Embryonic Kidney (HEK) cells and lysosomes sequester the calcium released by IP_3R in HeLa cells (Atakpa et al. 2018). More recently, a study in HeLa and HEK cells revealed TPC2 opening and signals to be coupled to IP_3R and calcium signals evoked NAADP-sensitive channels on lysosomes comprise exhibit a major dependence on ER calcium despite their lysosomal origin (Yuan et al. 2024). A novel mouse ventricular cardiomyocyte mathematical model including a lysosomal calcium pool presented lysosomal calcium handling to directly influences RyR spontaneous release by regulating RyR open probability (Meng et al. 2023). Taken together, these results open the possibility of involvement of IP_3 in a crosstalk in regulating calcium exchange between the SR and lysosomes in the heart. First evidence of a novel interaction opening new regulation mechanism and adding to the complexity of calcium signalling in the heart

The interaction between IP_3 and ACs investigated in Chapter 4 represents a novel mechanism and explains how IP_3 influences calcium signals and present downstream signalling through cAMP, here, I sought out to investigate the cytosolic cAMP levels in response to TPC2

stimulation, to discover how NAADP signalling can modulate calcium handling in regard to the SR.

5.3 Aim of Chapter 5

Evidence relating to the involvement of NAADP signalling in the heart have mainly been related to β-adrenergic responses. The role of α-adrenergic signalling in the atria is not only less studied but involvement of NAADP pathway in α-adrenergic response has not been investigated so far. In the first part of this Chapter I investigate the physiological role of NAADP specifically in response to α-adrenergic stimulation. In the second part of this Chapter investigates the downstream effects lysosomal calcium release into the cytosol in α-adrenergic signalling in atrial function. I will investigate how acidic calcium stores trigger signalling cascades in the atria by running FRET experiments in DKO and WT neonatal murine myocytes. This Chapter will focus on investigating the physiological role of the NAADP pathway in myocytes to bring insight on a novel mechanism of NAADP signalling pathway impacting α-adrenergic response that influence calcium dynamics in the atria.

5.4 Methods

I have used multiple pharmacological agents that inhibit the NAADP pathway at different steps, as seen below in Figure 5.1, is a schematic of the different agents and cites of action.

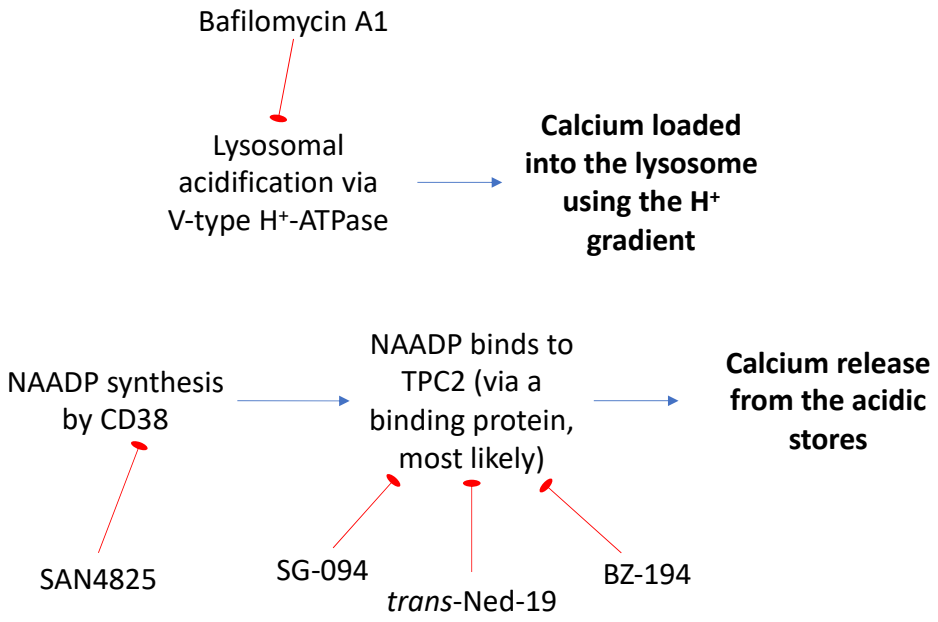

Figure 5.1: Illustration of pharmacological agents used in the Chapter 5 to study α-adrenergic stimulation of the NAADP pathway. Image creating using Biorender.

Inhibitors presented are 100 nM bafilomycin A1, used in previous Chapters that acts as a vacuolar H^+-ATPase inhibitor, 1 µM *trans*-Ned-19, a TPC blocker and inhibits the calcium signal, 10 µM SG-094, a specific TPC2 blocker to inhibits the calcium release, 10 µM SAN4825 an ADP-ribosyl cyclase inhibitor that reduces NAADP synthesis and 500 µM BZ-194 a small molecule that inhibits NAADP-mediated calcium signalling. SAN4825 (1:1000; vehicle) was added under control conditions to replicate addition of drugs that are diluted in SAN4825.

Left and right atrial force transducer experiments were conducted in mice in response to PE in the presence of NAADP inhibitors to access chronotropic and inotropic effect of NAADP pathway in α-adrenergic signalling in the atria. These experiments were conducted in the presence of 1 µM metoprolol to ensure no confounding β-adrenergic responses. The effects of PE were investigated over a cumulatively increasing concentration range of 0.1 µM to 30 µM added every 4 minutes to ensure maximum response was achieved and stable between increasing dosage. Inhibitors were administered 30 minutes prior to the first dose of PE,

allowing sufficient time for these pharmacological agents to penetrate the multicellular preparations.

Neonatal rat atrial myocytes (NRAMs), Neonatal rat ventricular myocytes (NRVMs) and Neonatal mouse atrial myocytes (NMAMs) isolations were used in FRET experiments, details of each protocol are presented in Chapter 2 (2.5 Neonatal isolations, page 50). Pups (P3-P5) were culled, and neonatal myocytes underwent 2 separate enzymatic digestions in trypsin (1 mg/mL) followed by collagenase type IV (1 mg/mL). Myocytes were then centrifuged and strained to wash out digestive enzymes and separate myocytes. Myocytes were then counted and plated at 30,000 per 24 mm laminin coated glass coverslips in 35 mm 6-well plates and cultured for 4 days before FRET experiments or confocal imaging.

FRET experiments were conducted 24 h after infection with adenovirus carrying EPAC-S^{H187}, a cytosolic biosensor in NRAMs, NRVMs and NMAMs to measure cAMP levels in response to 3 μM PE and 10 μM TPC2-A1-N (Gerndt et al. 2020). During experiments, cells were maintained at room temperature in a modified Ringer solution. Data from individual cells were averaged per plate to give *n*=1 and data are represented as *n*=number of biological replicates and *N*=number of litters used for neonatal isolations (10-14 pups per litter).

Calcium transients were conducted in response to TPC2-A1-N in WT and DKO AC1 and AC8 (details of mouse line described in Chapter 2, 2.1.1 Mice, page 46) murine atrial myocytes. Single cells were incubated with 3 μM Fluo-5F-AM in SAN KB (Chapter 2, 2.11 Recipe for solutions, page 59) for 10 min at 37ºC in the dark. Cells were then plated to a glass coverslip for an additional 10 mins to adhere to the coverslip before imaging with flow-through. Carbon fibre electrodes were used to field-stimulate calcium transients at 1 hertz. All recordings were made at 37ºC under gravity-fed superfusion of Tyrode (Chapter 2, 2.11 Recipe for solutions, page 59).

Standard immunocytochemical techniques and LysoTracker™ probes were used to determine the localisation of intracellular calcium channels and lysosomes. To compare the localisation of various proteins, secondary antibodies conjugated to different fluorophores were used. LysoTracker™ probes are fluorescent acidotrophic probes for labelling and tracking acidic organelles in live cells, they label sub-cellular compartments.

FRET experiments were conducted in healthy hiPSC-CMs to investigate NAADP pathway in humans. To enhance reliability and ensure translation value, all FRET experiments were

conducted using 3 different hiPSC-CMs derived lines described in detail in Chapter 2, 2.8 Human IPSC culture, from page 55.

Statistical analyses in this Chapter were performed using Prism 10 (Graphpad). Differences were considered statistically significant at values of non-significant (ns)$P>0.05$, *$P<0.05$, ** $P<0.01$, *** $P<0.001$, **** $P<0.0001$. Statistical methods used are given in the legend of each figure.

5.5 Results

5.5.1 Inhibition of lysosomal calcium reduces chronotropic effect of phenylephrine in intact right atria

To evaluate the impact of NAADP pathway in atrial function I recorded intact, spontaneously beating right atrial preparations to measure SAN activity through the measurement of beating rate. Figure 5.2 shows dose response curves for spontaneous beating rate in the right atria were generated in response to 0.1 to 30 μM PE to measure effect of NAADP in α-stimulation. Under control conditions, in the presence of vehicle (SAN4825), the spontaneous beating rate of right atria increased by a maximum of 23.69 (18.97-30.13) % at 30 μM PE, with an EC50 of 1.4 (0.3-5.8) μM (n=7). NAADP inhibitors and bafilomycin A1 reduced the response of beating rate to PE at all concentrations tested and caused a significant rightward shift in the EC50 (Figure 5.2). The presence of 500 μM of BZ-194, a small molecule that inhibits NAADP-mediated calcium signalling, significantly reduced the response at all concentration of PE (P=0.037), with a maximum increase of 11.01 (8.6-15.6) % at 30 μM (P<0.0001) of PE with an EC50 of 3 (0.7-14.4) μM (n=4, P<0.001, Figure 5.2). In agreement, the presence of 10 μM of SAN4825, an ADP-ribosyl cyclase inhibitor that reduces NAADP synthesis, also significantly reduced the response of beating rate at all concentration of PE (P<0.0001), with an increase of 7.02 (4.8-12) % at 30 μM PE (P<0.0001) with an EC50 of 2.9 (0.4-24.4) μM (n=6, P<0.0001, Figure 5.2). Incubation with 100 nM bafilomycin A1 caused an increase of 9.42 (6.4-22.7) % at 30 μM PE (P<0.0001), a significant decrease compared to control, with a rightward shift of EC50 to 3.1 (0.4-50.5) μM (n=5, P<0.0002, Figure 5.2).

No significant differences were seen in beating rate before addition of PE (Figure 5.3). Beating rate at the start of the experiment and after stabilisation of addition of inhibitor was measured and showed a non-significant de change in decrease percentage (figure 5.3A), stabilisation took around 40 minutes in all conditions. Control (-7.7 ± 3.2 %, n=7), incubation with BZ-194 (-8.6 ± 0.8 %, n=7) and SAN4825 (-3.2 ± 2.5 %, n=6) showed a decrease and bafilomycin A1 had a small increase of 0.7± 3.6 % (n=5) (Figure 5.3A). Metoprolol was added to each condition to ensure no confounding effects of β-adrenergic response during PE cumulative doses. Beating rate stabilisation after addition of inhibitors and stabilisation after metoprolol was compared and also showed a non-significant decrease in beating rate percentage (Figure 5.3B), stabilisation took around 30 minutes in all conditions, control (-4.3 ± 1.1 %, n=7), incubation with BZ-194 (-6 ± 1.9 %, n=7), SAN4825 (-3.3 ± 1.8 %, n=6) and bafilomycin A1 (-4.7 ± 2.3 %, n=5) (Figure 5.3B). Beating baseline was measured before first 0.1 μM PE was added to

the bath, baseline beating rate showed no significant changes in BZ-194 (340 ± 9 BPM, *n*=7), SAN4825 (350 ± 15 BPM, *n*=6) and bafilomycin A1 (343 ± 5 BPM, *n*=5) compared to control condition (342 ± 8 BPM, *n*=7) (Figure 5.3C).

5.5.2 Inhibition of lysosomal calcium reduces inotropic effect of phenylephrine in intact left atria

Intact left atria were used to record changes in contractile force generated when stimulated at a constant rate and voltage in response to PE to see whether NAADP pathway had inotropic effects with NAADP inhibitors and bafilomycin A1 (V-ATPase inhibitor, to disrupt lysosomal signalling) (Figure 5.4). Under control conditions, in the presence of SAN4825, the maximum change in tension of left atria increased was 19.05 (14.9-25.5) % at 30 μM PE, with an EC50 of 2 (0.3-10.5) μM (*n*=6). Bafilomycin A1 reduced the maximum tension generated by PE at all concentrations tested. The presence of 500 μM of BZ-194 (inhibits NAADP-mediated calcium signalling) significantly reduced the response to PE in the last 3 concentrations added, with a maximum increase of 8.8 (6.6-13.3) % at 30 μM of PE ($P<0.01$) with a non-significant change of EC50 (2.3 (0.2-14) μM (*n*=4) Figure 5.4). Incubation of SAN4824 (reduces NAADP synthesis) or bafilomycin A1 showed a trend to decrease PE responses compared to control and only showed a significant decrease at 10 μM PE ($P<0.05$). 10 μM of SAN4825, had a maximum increase of 10.91 (8.1-14.6) % at 30 μM PE with an EC50 of (1.1 (0.2-5.5) μM (*n*=5)). Incubation with 100 nM bafilomycin A1 caused a maximum increase of 11.75 (8.3-16.9) % at 30 μM PE, with an EC50 of 0.6 (0-9.1) μM (*n*=5, Figure 5.4).

No significant differences were seen in the maximum force of contraction generated before addition of PE (Figure 5.5) in left atrial preparations. Tension at the start of the experiment and after stabilisation with addition of inhibitor was measured and showed a non-significant change in beating percentage (Figure 5.3A), stabilisation took around 40 minutes in all conditions. Control (-5.5 ± 1.2 %, *n*=6), incubation with SAN4825 (-16.3 ± 5.7 %, *n*=5) and bafilomycin A1 (-11.6 ± 4 %, *n*=4) showed a decrease and BZ-194 had a small increase of 2.9 ± 3.1 % (*n*=4) (Figure 5.5A). Similar to right atrial preparations, 1 μM metoprolol was added to the bath of each condition. Tension after stabilisation following addition of inhibitor and stabilisation after metoprolol was compared and also showed a non-significant decrease in tension percentage in all conditions compared to control (Figure 5.5B), stabilisation took around 30 minutes in all conditions; Control (-20.8 ± 7.3 %, *n*=6), incubation with BZ-194 (-613.8 ± 4.3 %, *n*=4), SAN4825 (-5.9 ± 7.8 %, *n*=5) and bafilomycin A1 (-17.14 ± 4.6 %, *n*=4) (Figure 5.5B). Tension

(in g) baseline was measured before first addition of 0.1 µM PE to the bath. Baseline tension only showed a significant increase with bafilomycin A1 (0.1 ± 0.02 g, *n*=5), not with BZ-194 (0.08 ± 0.01 g, *n*=4) or SAN4825 (0.05 ± 0.02 g, *n*=5) compared to control condition (0.06 ± 0.01 g, *n*=6) (Figure 5.5C).

5.5.3 Lysosomal signalling contributes to the increase in cellular cAMP in response to phenylephrine in NRAMs

Chapter 4 describes novel observations that activation of IP_3R in atrial cardiomyocytes leads to generation of cytosolic cAMP. This section of the chapter aims to determine the dynamic interactions between α-adrenergic signalling and NAADP signalling in cAMP production. cAMP-sensitive FRET experiments in the presence of PE and NAADP inhibitors were conducted in NRAMs (Figure 5.6). Figure 5.7 shows representative FRET traces of 3 µM PE under control conditions and in the presence of 10 µM SAN4825, 100 nM bafilomycin A1, 1 µM *trans*-Ned-19, 10 µM SG-094 and 500 µM BZ-194 in NRAMs. Results are percentage FRET change of peak-like response of the saturation response with 10 µM FSK and 100 µM IBMX (Figure 5.7). Control conditions (SAN4825) resulted in a FRET change response 27.07 ± 2.8 % (*n*=9, *N*=6) in response to 3 µM PE (Figure 5.8). Addition of PE (3 µM) in the presence of inhibitors caused a significant decrease in all conditions compared to control, I see an increase of 14.86 ± 2.2 % in the presence of SAN4825 (*n*=8, *N*=3, *P*<0.001), an increase of 12.17 ± 2.4 % in the presence of bafilomycin A1 (*n*=6, *N*=4, *P*<0.001), an increase of 10.7 ± 1.5 % in the presence of *trans*-Ned-19 (*n*=9, *N*=3, *P*<0.0001) and an increase of 10.01 ± 0.8 % in the presence of SG-094 (*n*=3, *N*=1, *P*<0.001) (Figure 5.8). Figure 5.9 shows representative confocal microscopy of NRAMs stained with LAMP2 on lysosomes and confirm the presence of lysosomes in the neonatal atrial myocytes.

Previous data in Chapter 3 and published work has put forward the specificity of this pathway in atrial myocytes, these experiments were repeated in NRVMs to investigate the specificity of cAMP response to NAADP pathway in response to PE. NRVMs representative FRET traces of 3 µM PE in control conditions and in the presence of 100 nM bafilomycin A1, 10 µM *trans*-Ned-19, 500 µM BZ-194 and 10 µM SAN4825 are presented in Figure 5.10. In contrast to NRAMs, addition of these inhibitors showed no significant changes compared to control in NRVMs. Control conditions resulted in a FRET change response 12.62 ± 0.8 % (*n*=9, *N*=4) (Figure 5.11A), significantly lower than control responses observed in NRAMs (*P*<0.001, Figure 5.11B). Addition of bafilomycin A1 caused an increase of 9.64 ± 1.9 % (*n*=3, *N*=1,

P=2852), *trans*-Ned-19 caused an increase of 7.55 ± 0.2 % (*n*=2, *N*=1, *P*=0.0686), BZ-194 caused an increase of 8.8 ± 1.1 % (*n*=3, *N*=1, *P*=0.1285) and SAN4825 resulted in an increase of 9.55 ± 2.2 % (*n*=2, *N*=1, *P*=0.3953), (Figure 5.11A).

5.5.4 Combined *Adcy1* and *Adcy8* gene knock out resulted in reduced calcium transient amplitude in response to TPC2 stimulation in atrial myocytes

Investigations were next carried on NAADP pathway activation in WT and DKO mice (DKO colony described in Chapter 4. Adult WT and DKO isolated right atrial myocytes were loaded with a cell-permeant calcium sensitive dye Fluo-5F-AM (3 µM) to measure changes in cytosolic calcium in response to TPC2-A1-N, a TPC2 activator (Gerndt et al. 2020). When stimulated at 1 hertz in Tyrode at 37°C, atrial myocytes exhibited the classical pattern of calcium transient as observed in Chapter 4 (Figure 4.16A-B and Figure 5.12A-B). As shown in Figure 5.13A-B, DKO of AC1 and AC8 (2.21 ± 0.8, *n*=13, *N*=4) did not alter the basal calcium compared to WT (3.68 ± 0.6, *n*=11, *N*=3) atrial myocytes, Statistical measurements of basal calcium showed no significant differences between both groups (Figure 5.13C), expressed as change in mean cell fluorescence (F-F0)/F0 in the cell. Addition of 10 µM of TPC2-A1-N to the perfusion solution resulted in an increase in calcium transients in WT and not in DKO (Figure 5.14). Maximum percentage increase in calcium transient amplitude was measured over 1 min exposure of TPC2-A1-N with WT presenting an increase in amplitude over the first 30 s then decreased to 1 minute as DKO amplitude decrease over 1 min of exposure (Figure 5.14B). WT resulted in a maximum increase of 22.71 ± 4.4 % (*n*=11, *N*=3) while DKO atrial cells resulted in a decrease of 11.69 ± 6.8 % (*n*=13, *N*=4), representing a significant change in response to TPC2-A1-N (*P*<0.001, Figure 5.14A-B). A Calcium transient time-control experiment was conducted in Figure 4.19, a 20 % reduction is observed over 1 min and could explain such a decrease overserved in these cells.

5.5.5 cAMP levels do not increase in DKO AC1/AC8 neonatal mouse atrial myocytes upon α-adrenergic stimulation

Differences in cAMP levels in the presence of NAADP pathway inhibitors in response to PE were next compared in WT and DKO mice during FRET experiments. In WT NMAMs, in the presence of 0.1 % SAN4825 (solvent control), FRET change in response to PE represented 13.05 ± 1.5 % (*n*=11, *N*=6) peak of the saturating 10 µM FSK and 100 µM IBMX response (Figure 4.20A). The addition of ST034307, an AC1 inhibitor, did not cause a significant reduction in response to 3 µM PE (11.32 ± 2.4 %, *P*=0.8583, Figure 4.20A). Addition of

NAADP pathway inhibitors caused a decrease in all conditions compared to control. Bafilomycin A1 caused an increase of 4.58 ± 0.8 % (n=7, N=4, P<0.001) and SG-094 caused an significant increase of 5.08 ± 0.8 % (n=4, N=3, P<0.05), whereas *trans*-Ned-19 caused an increase of 7.29 ± 1.2 % (n=6, N=5) but represented a non-significant decrease in FRET change when compared to control condition (Figure 5.15)

In contrast, activation of α-ARs using PE resulted in a FRET change of 13.05 ± 1.5 % (n=11, N=6) in WT and of 7.65 ± 0.3 % (n=11, N=6) in DKO NMAMs, a significant decrease compared to WT NMAMs (P<0.01, Figure 5.16A). Addition of bafilomycin A1 or *trans*-Ned-19 to DKO NMAMs did not cause small non-significant reduction in response to 3 µM PE. Addition of 100 nM bafilomycin A1 resulted in a peak of 6.7 ± 1.2 % (n=6, N=3, P=0.6813) and addition of *trans*-Ned-19 resulted in a FRET change of 6.2 ± 1.6 % (n=3, N=3, P=0.5815) in response to 3 µM of PE. Inhibition of TPC2 by 10 µM SG-094 prior to addition of PE caused a reduction of peak resulting in an increase of only 4.5 ± 0.5 % (n=8, N=4, P<0.01) (Figure 5.16B).

5.5.6 Inhibition of AC1 and CaMKII reduces cAMP levels in response to TPC2 stimulation in neonatal rat atrial myocytes

Direct stimulation of NAADP dependent lysosomal calcium release by 10 µM TPC2-A1-N resulted in a FRET change of 26.28 ± 2.7 % (n=7, N=5). The protocol was repeated in 0 calcium condition and after a 45 min incubation with ryanodine and thapsigargin (both 2 µM) to empty SR stores and a FRET change of 19.85 ± 1.9 % (P=0.1662, Figure 5.17) was observed. The presence of 100 nM bafilomycin A1 resulted in a peak of 13.64 ± 2.1 % (n=6, N=6, P<0.05) and the presence of *trans*-Ned-19 resulted in a FRET change of 10.83 ± 1.4 % (n=6, N=4, P<0.01, Figure 5.17), both addition of bafilomycin A1 or *trans*-Ned-19 caused a significant reduction in response to 10 µM TPC2-A1-N. ST034307 (1 µM), an AC1 inhibitor, resulted in a peak of 13.18 ± 2.7 % (n=4, N=4) and caused a significant FRET change compared to SAN4825 control (26.28 ± 2.7 %, P<0.01, Figure 5.18). KN-93, a CaMKII inhibitor, was also tested as CaMKII has been reported to be required for ventricular cardiomyocyte responses to NAADP (Capel et al. 2015) and the presence of KN-93 resulted in a FRET change of 11.57 ± 2.7 % (n=4, N=4) also a significant reduction compared to control (26.28 ± 2.7 %, P<0.01), dataset reported in Figure 5.18.

5.5.7 NAADP signalling in hiPSC-CMs and hiPSC-aCMs

FRET experiments were carried out on hiPSC-aCM to build on the FRET data collected in Figure 5.8 on NRAMs and to demonstrate the relevance of NAADP pathway in human myocytes. Figure 5.19A presents cAMP levels in response to 10 µM TPC2-A1-N in the presence or absence of 10 µM SG-096. Peak in cAMP levels were significantly lower in the presence of SG-096 with a FRET change of 22.59 ± 6.2 % (n=6, N=3) in response to 10 µM TPC2-A1-N compared to the control condition (34.5 ± 4.1 %, n=4, N=3, P<0.05, Figure. 5.19A). Live cell imaging with Lysotracker™ was conducted to confirm presence of lysosomes in hiPSC-CMs (Figure. 5.19B).

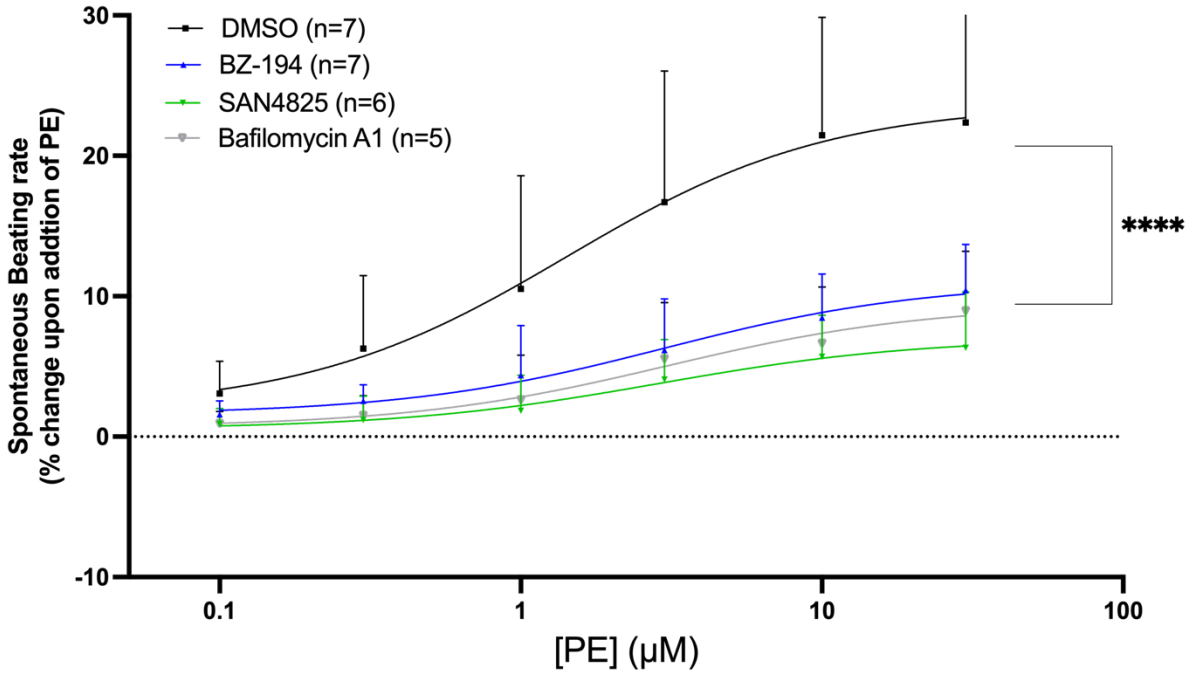

Figure 5.2: Rate responses are reduced in the presence of NAADP inhibitors in response to PE in spontaneously beating murine right atrial preparations.

Rate responses to PE (0.1 μM – 30 μM) in spontaneously beating murine atrial preparations under control conditions (*n*=7, black) and in the presence of 500 μM BZ-194 (*n*=7, blue), 10 μM SAN4825 (*n*=6, green) and 100 nM of bafilomycin A1 (*n*=4, grey).

Dose-response curves were fitted using log(agonist) vs. response (three-parameter model). Asterisks indicate significance level for effect of BZ-194, SAN4825 and bafilomycin A1 compared to control at individual concentrations, determined using 2-way repeated measures ANOVA followed by Dunnett's multiple comparisons test. Data on graph are represented as mean ± SEM; ****p<0.0001.

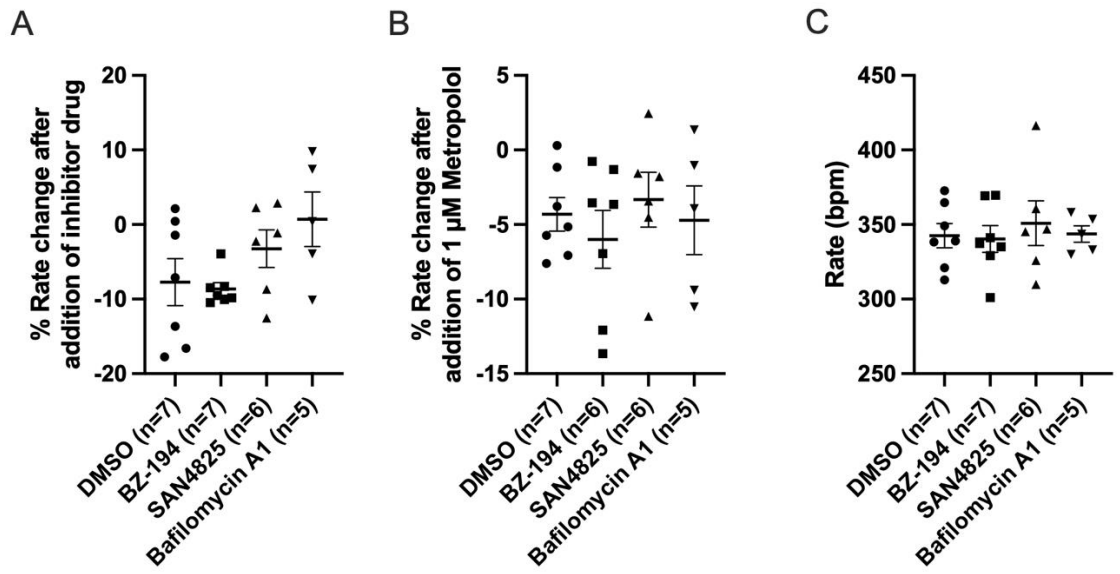

Figure 5.3: Baseline beating rates comparison show no significant differences in right atrial preparations.

A, Comparison of percentage decrease rate after addition of 0.001 % DMSO (*n*=7), 500 µM BZ-194 (*n*=7), 10 µM SAN4825 (*n*=6) or 100 nM bafilomycin A1 (*n*=5).
B, Comparison of percentage decrease rate after addition of 1 µM metoprolol, under control conditions (0.001 % DMSO, *n*=7) or in the presence of 500 µM BZ-194 (*n*=7), 10 µM SAN4825 (*n*=6) and 100 nM bafilomycin A1 (*n*=5).
C, Baseline beating rate after 1 µM metoprolol before cumulative addition of PE under control conditions (0.001 % DMSO, *n*=7) or in the presence of 500 µM BZ-194 (*n*=7), 10 µM SAN4825 (*n*=6) and 100 nM bafilomycin A1 (*n*=5).

No significance for effect of BZ-194, SAN4825 and bafilomycin A1 compared to control at individual concentrations was observed, determined using 2-way repeated measures ANOVA followed by Dunnett's multiple comparisons test. Data are represented as mean ± SEM.

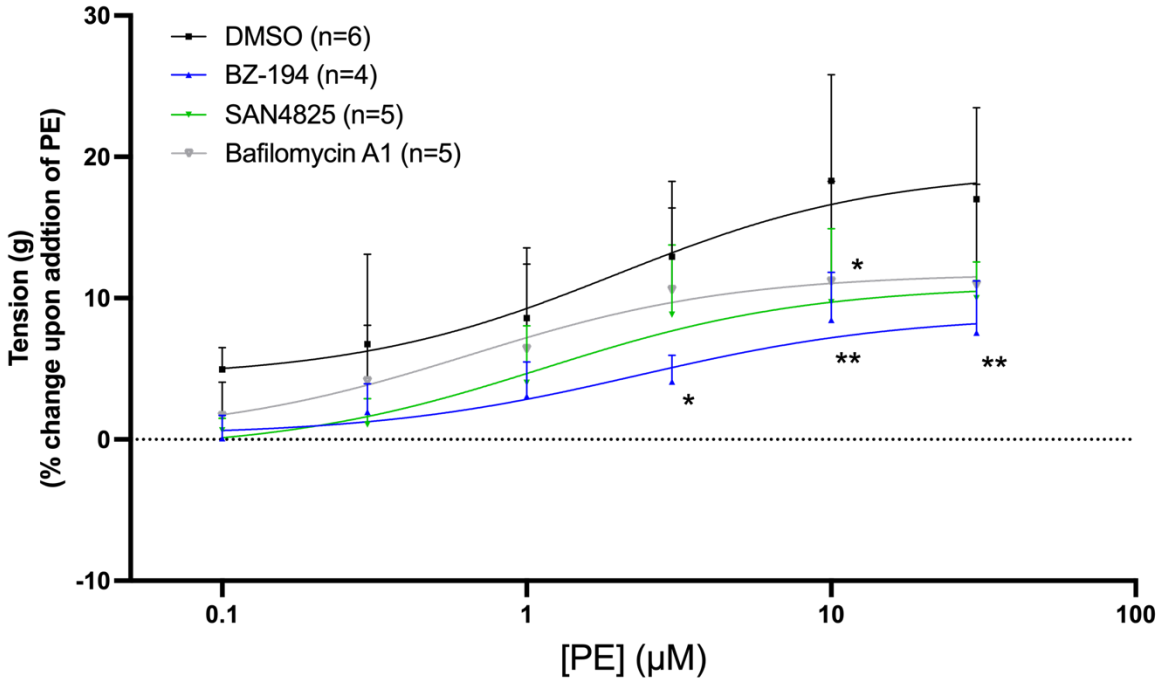

Figure 5.4: Tension reduces in the presence of NAADP inhibitors in response to PE in stimulated beating murine left atrial preparations.

Force of contraction responses to PE (0.1 μM – 30 μM) in paced (5 hertz) left murine atrial preparations under control conditions (*n*=5, black) and in the presence of 500 μM BZ-194 (*n*=3, blue), 10 μM SAN4825 (*n*=5, green) and 100 nM of bafilomycin A1 (*n*=4, grey).

Dose-response curves were fitted using log(agonist) vs. response (three-parameter model). Asterisks indicate significance level for effect of BZ-194, SAN4825 and bafilomycin A1 compared to control at individual concentrations, determined using 2-way repeated measures ANOVA followed by Dunnett's multiple comparisons test. Data on graph are represented as mean ± SEM; *p<0.05; **p<0.01.

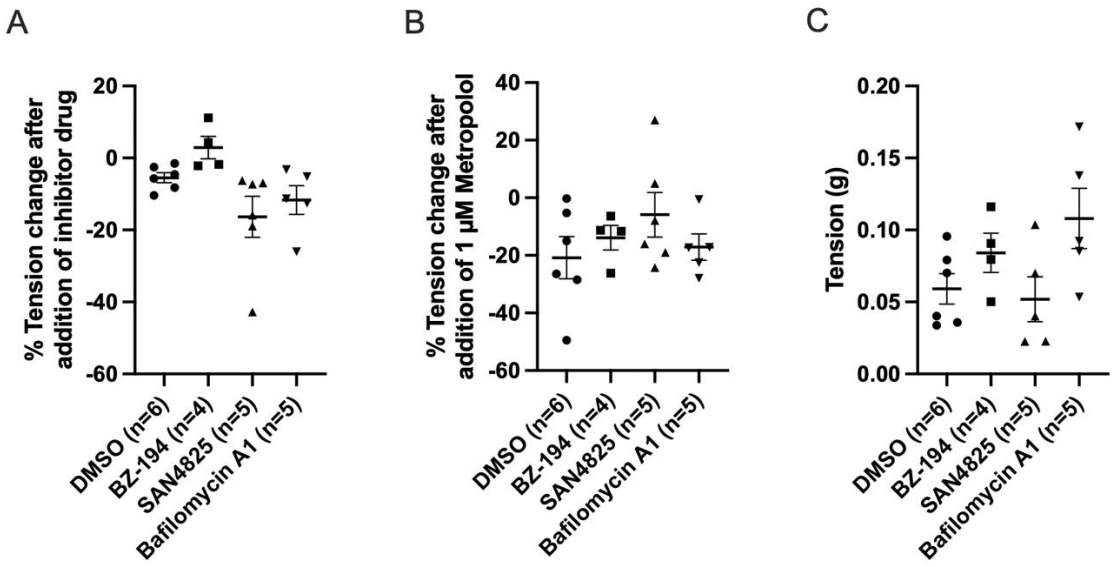

Figure 5.5: Baseline tensions comparison show no significant change in left atrial preparations.

A, Comparison of percentage decrease in tension after addition of 0.001 % DMSO (*n*=6), 500 µM BZ-194 (*n*=4), 10 µM SAN4825 (*n*=5) or 100 nM bafilomycin A1 (*n*=5).
B, Comparison of percentage decrease in tension after addition of 1 µM metoprolol, under control conditions (0.001 % DMSO, *n*=6) or in the presence of 500 µM BZ-194 (*n*=4), 10 µM SAN4825 (*n*=5) and 100 nM bafilomycin A1 (*n*=5).
C, Baseline tension after 1µM metoprolol before cumulative addition of PE, under control conditions (0.001 % DMSO, *n*=6) or in the presence of 500 µM BZ-194 (*n*=4), 10 µM SAN4825 (*n*=5) and 100 nM bafilomycin A1 (*n*=5).

No significance for effect of BZ-194, SAN4825 and bafilomycin A1 compared to control at individual concentrations was observed, determined using 2-way repeated measures ANOVA followed by Dunnett's multiple comparisons test. Data are represented as mean ± SEM.

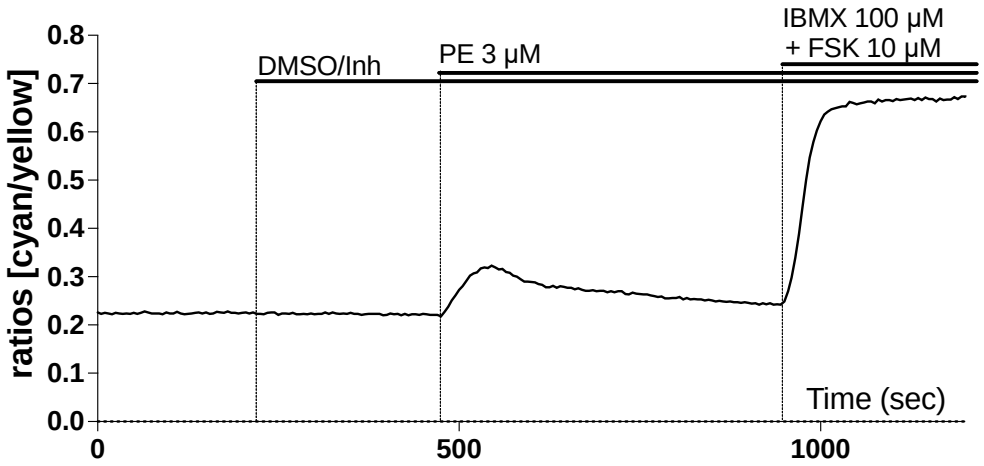

Figure 5.6: FRET Protocol in neonatal myocytes.

After 240s of baseline 0.1 % DMSO, 10 µM SAN4825, 100 nM bafilomycin A1, 10 µM *trans*-Ned-19, 10 µM SG-094 and 500 µM BZ-194.were added. At 480s 3 µM PE and at 980s saturation response with 10 µM FSK and 100 µM IBMX.

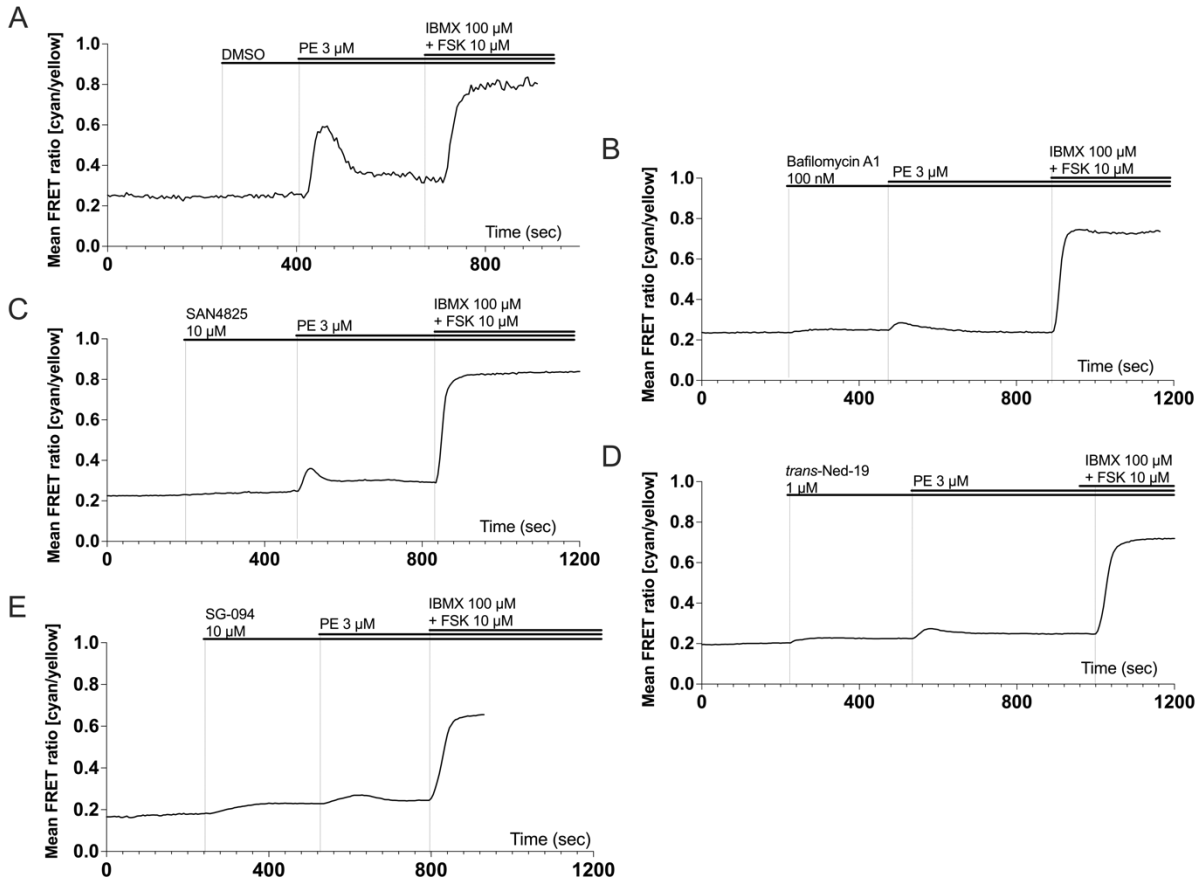

Figure 5.7: NRAMs Representative FRET traces in response to PE in the presence of NAADP inhibitors.

Representative traces showing FRET change in single NRAMs expressing EPAC-S^{H187} in response to 3 µM PE under control conditions and following addition of 0.1 % DMSO (**A**), 100 nM bafilomycin A1 (**B**), 10 µM SAN4825 (**C**), 10 µM *trans*-Ned-19 (**D**) and 10 µM SG-094 (**E**).

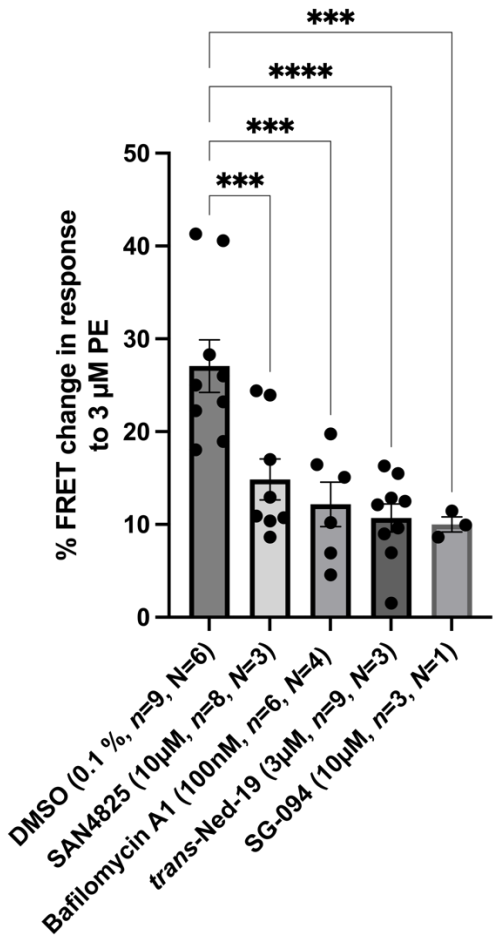

Figure 5.8: cAMP levels are reduced in the presence of NAADP inhibitors and bafilomycin A1 in NRAMs FRET experiments.

Comparison of peak response to PE, in FRET change (normalised to maximum response) in single NRAMs expressing EPAC-S^{H187} in response to 3 µM PE under control conditions (*n*=9, *N*=6) and following addition of 10 µM SAN4825 (*n*=8, *N*=3), 100 nM bafilomycin A1 (*n*=6, *N*=4), 10 µM *trans*-Ned-19 (*n*=9, *N*=3) and 10 µM SG-094 (*n*=3, *N*=1).

Data are represented as mean ± SEM. Normality was assessed using the Shapiro-Wilk test. Data were analysed using 2-way repeated measures ANOVA followed by Dunnett's multiple comparisons test; n=experiments; N=isolations; ***P<0.001, ****P<0.0001.

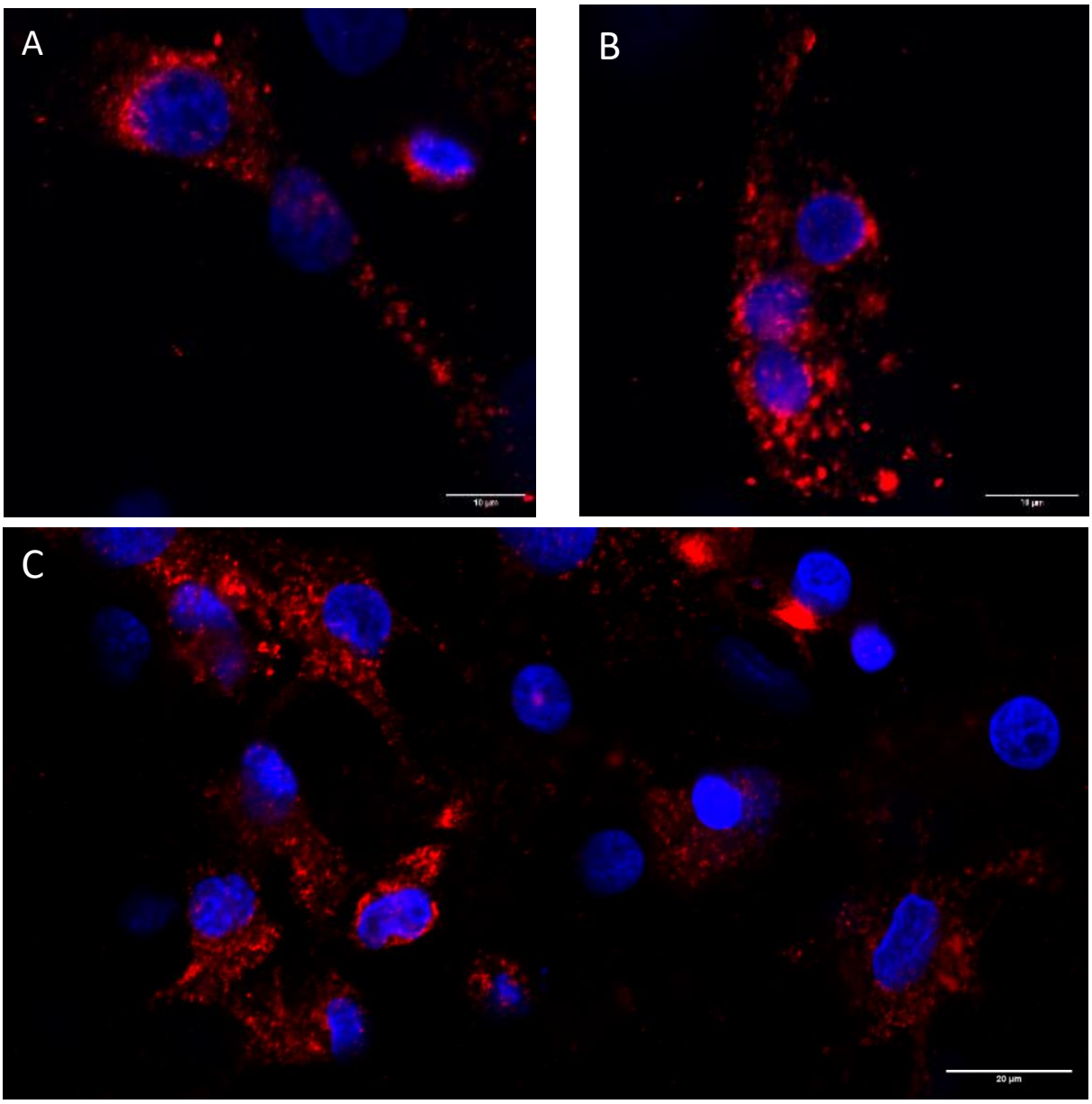

Figure 5.9: Representative confocal images of lysosomes in NRAMs.

Representative confocal images of fixed cultured NRAMs stained with DAPI (blue) for the nucleus and immunolabelled with LAMP2 (red).

Scale bar in A and B represents 10 µM and scale bar in C represents 20 µM.

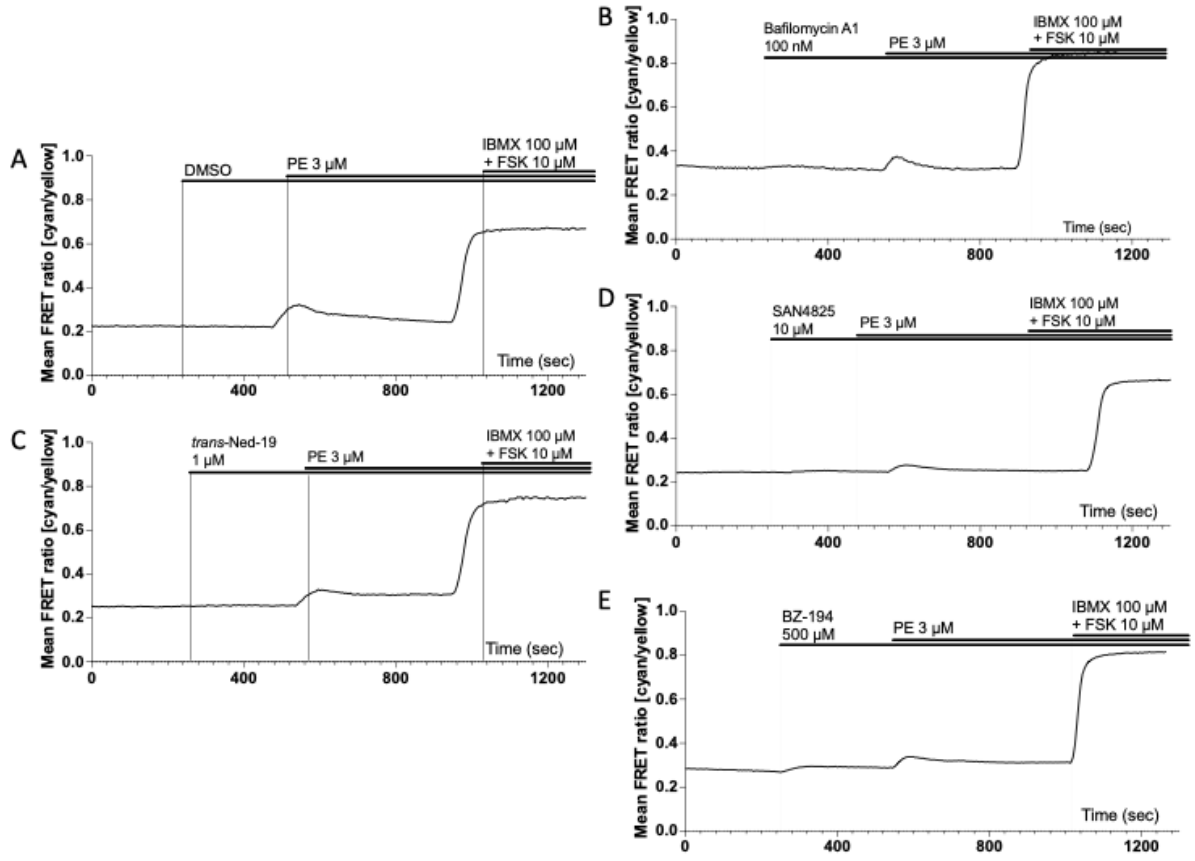

Figure 5.10: NRVMs Representative FRET traces in response to PE in the presence of NAADP inhibitors.

Representative traces showing FRET change in single NRVMs expressing EPAC-S^{H187} in response to 3 µM PE under control conditions (**A**) and following addition of 100 nM bafilomycin A1 (**B**), 1 µM *trans*-Ned-19 (**C**), 10 µM SAN4825 (**D**) and 500 µM BZ-194 (**E**).

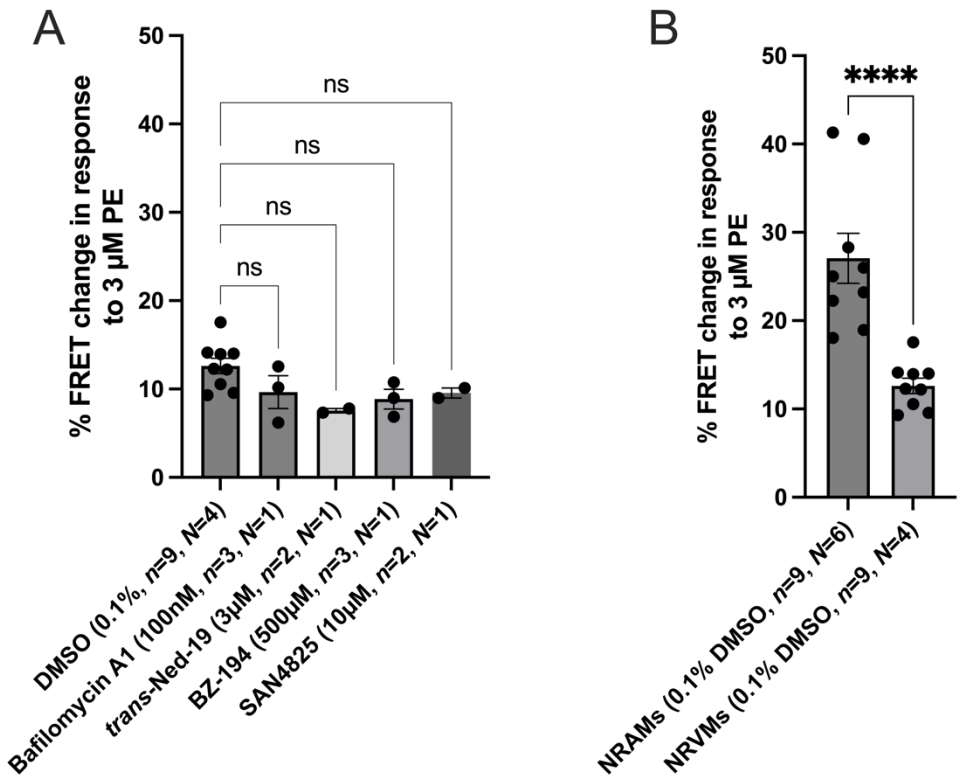

Figure 5.11: NAADP inhibitors prevented FRET change in response to PE in NRVMs.

A: Comparison of peak response to PE, in FRET change (normalised to maximum response) in single NRVMs expressing EPAC-S^{H187} in response to 3 µM PE under control conditions (*n*=9, *N*=4) and following addition of 100 nM bafilomycin A1 (*n*=3, *N*=1), 1 µM *trans*-Ned-19 (*n*=2, *N*=1), 500 µM BZ-194 (*n*=3, *N*=1), 10 µM SAN4825 (*n*=2, *N*=1).
B: Comparison of peak response to PE, in FRET change (normalised to maximum response) in single NRAMs (*n*=9, *N*=6) and in NRVMs (*n*=9, *N*=4) expressing EPAC-S^{H187} in response to 3 µM PE under control conditions.

Data are represented as mean ± SEM and were analysed using Kruskal Wallis followed by Dunn's multiple comparison in panel A and non-parametric Mann-Whitney U test in panel B. *n*=experiments; *N*=neonatal isolations. Non-significant (ns), ****P<0.0001.

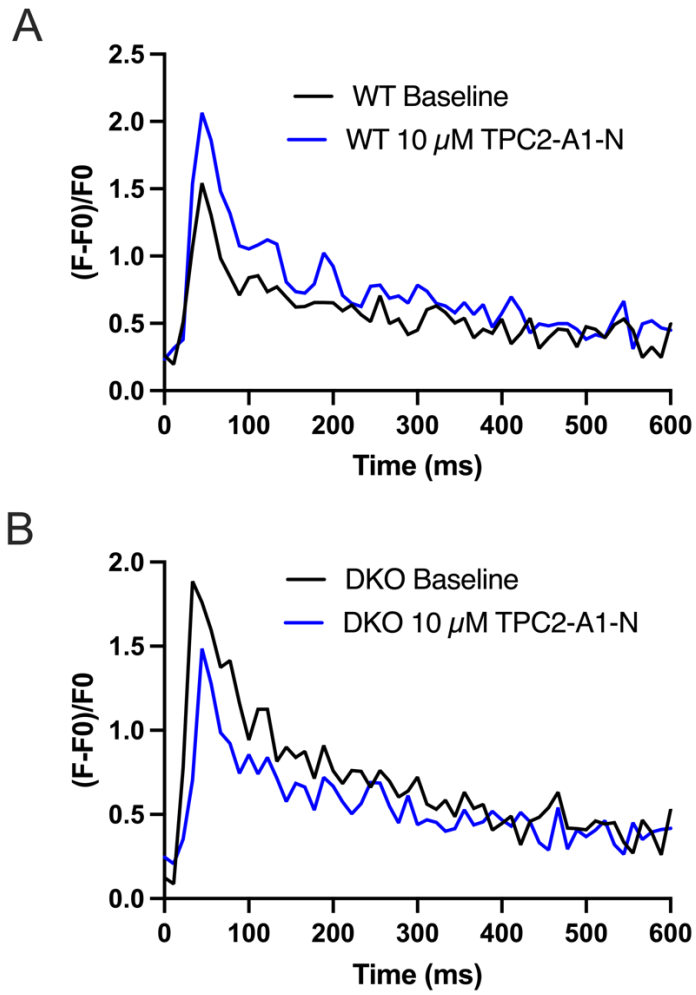

Figure 5.12: Representative calcium transient in response to TPC2-A1-N in WT and DKO atrial myocytes.

A, Representative traces to show spontaneously generated calcium transients in isolated atrial myocyte WT C57s in control condition (black) and after exposure to 10 μM TPC2-A1-N (blue). **B**, Representative traces to show spontaneously generated calcium transients in isolated atrial myocyte DKO C57s in control condition (black) and after exposure to 10 μM TPC2-A1-N (blue).

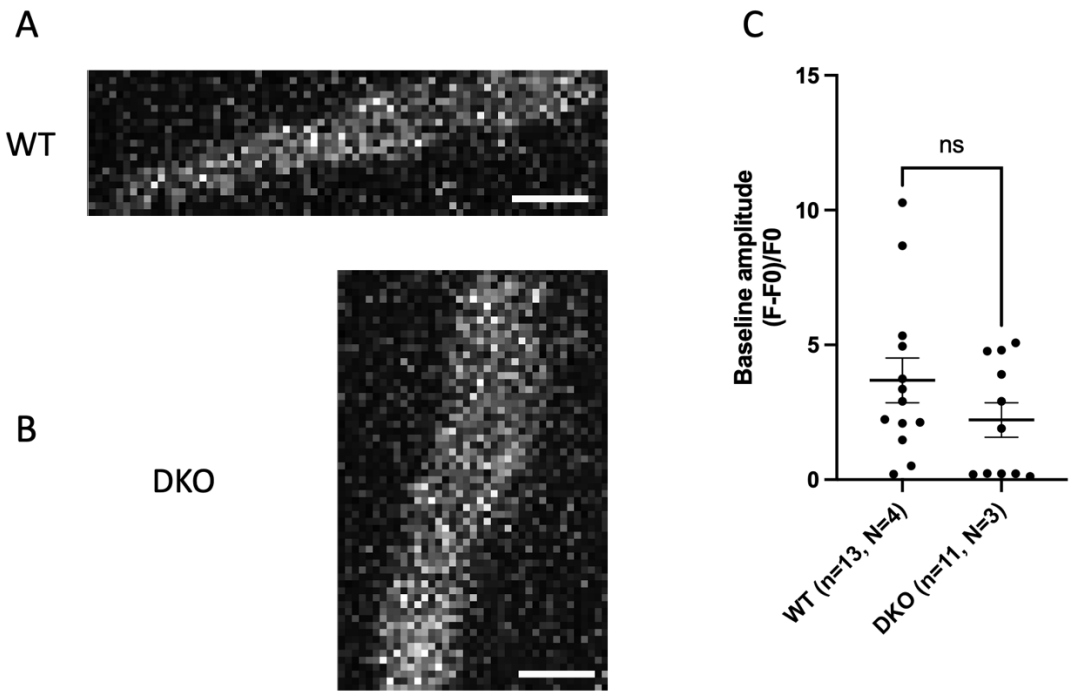

Figure 5.13: Baseline calcium transient amplitude show no differences between WT and DKO cells.

A, Representative image of a WT atrial myocyte loaded with 3 µM Fluo-5F.
B, Representative image of a DKO atrial myocyte loaded with 3 µM Fluo-5F.
C, Baseline calcium transient amplitude in isolated WT (*n*=10, *N*=3) and DKO (*n*=10, *N*=3) C57s atrial myocytes in control conditions in Tyrode.

Scale bar represents 20 µm in panel A and B. Data are represented as mean ± SEM and were analysed using paired t-test in panel C. *n*=experiments; *N*=animals; non-significant (ns)=P>0.05.

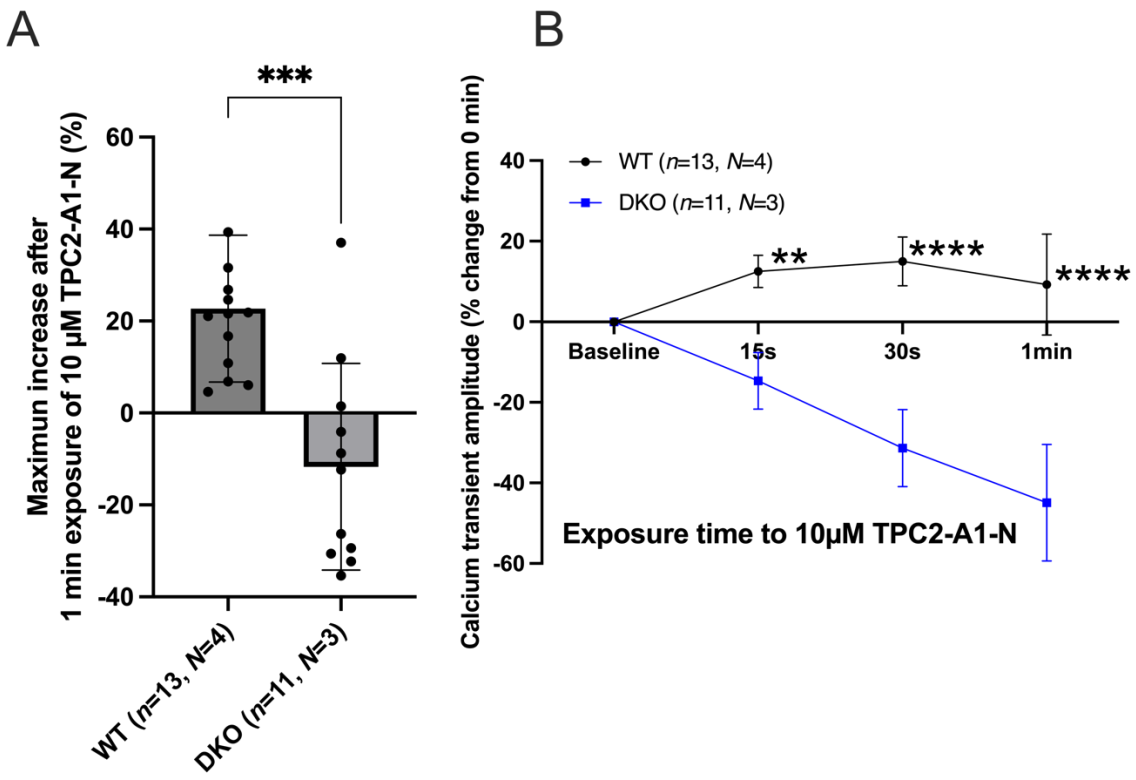

Figure 5.14: Reduction of calcium transient in response to TPC2-A1-N in isolated DKO atrial myocytes.

A, Maximum increase (in %) recorded over 2 minutes of exposure to 10 µM TPC2-A1-N in isolated WT (*n*=10, *N*=3) and DKO (*n*=10, *N*=3) C57s murine atrial myocytes.
B, Calcium transient amplitude response (in %) in isolated WT (*n*=10, *N*=3) and DKO (*n*=10, *N*=3) C57s murine atrial myocytes after exposure of 10 µM TPC2-A1-N over 1 minute.

Data are represented as mean ± SEM and were analysed using paired t-test in panel A and using 2-way repeated measures ANOVA followed by Šídák's multiple comparisons test in panel B; *n*=experiments; *N*=animals; **P<0.01, ***P<0.001, ****P<0.0001.

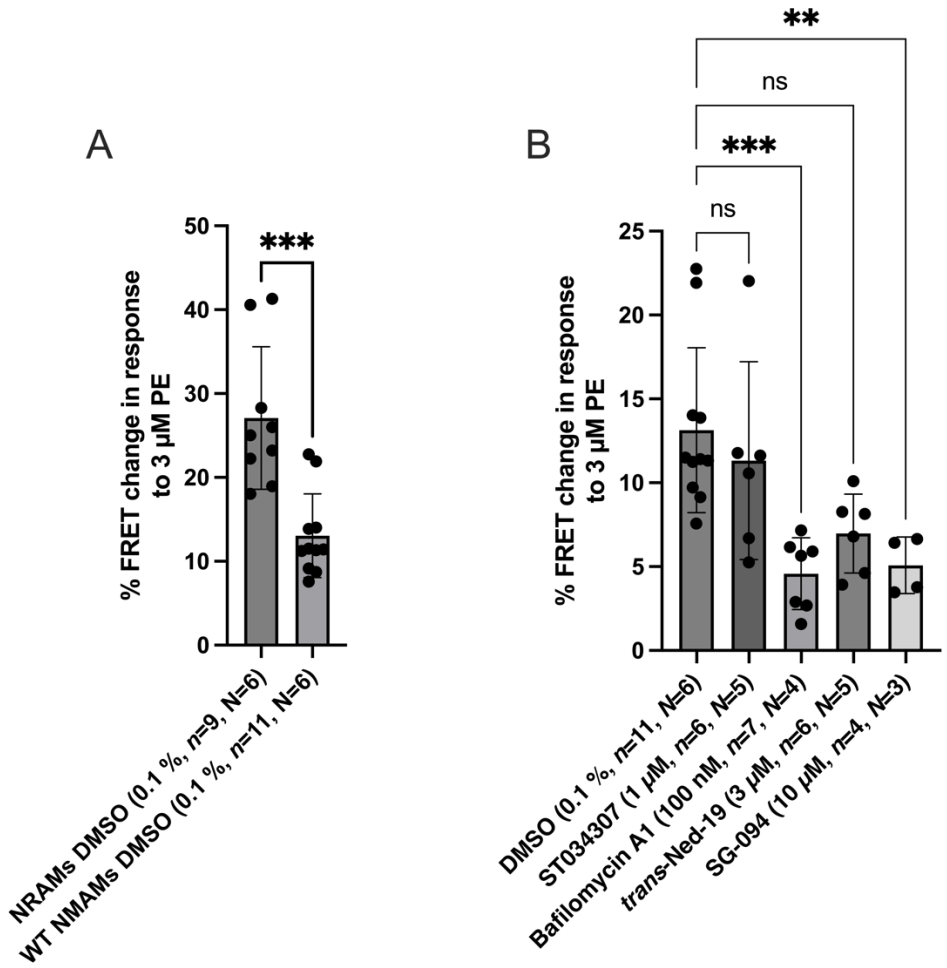

Figure 5.15: NAADP inhibitors and bafilomycin A1 reduces cAMP levels in WT NMAMs in response to PE.

A, Quantification of the peak FRET change in response to 3 µM PE in NRAMs in the presence of DMSO (*n*=9, *N*=6) and in WT NMAMs in the presence of DMSO (*n*=11, *N*=6) in E1 buffer. **B**, Quantification of the peak FRET change in response to 3 µM PE in WT NMAMs in the presence of either 0.1 % DMSO (*n*=11, *N*=6), 1 µM ST034307 (*n*=6, *N*=5), 100 nM bafilomycin A1 (*n*=7, *N*=4), 1 µM *trans*-Ned-19 (*n*=6, *N*=5) or 10 µM SG-096 (*n*=4, *N*=3) in E1 buffer.

Data are represented as mean ± SEM and were analysed using non-parametric Mann-Whitney U test in panel A and Kruskal Wallis followed by Dunn's multiple comparison in panel B; *n*=experiments; *N*=isolations; non-significant (ns)=P>0.05, *P<0.05, **P<0.01, ***P<0.001.

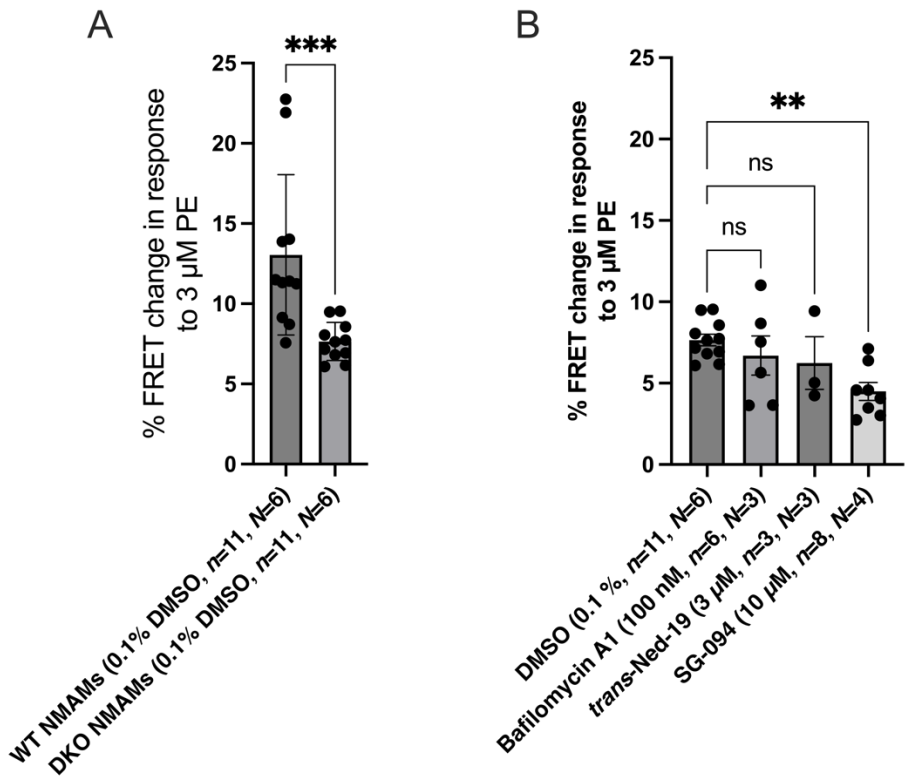

Figure 5.16: Knockout of AC1 and AC8 shows little to no reduction in cAMP in response to PE in DKO NMAM.

A, Quantification of the peak FRET change in response to 3 µM PE in WT NMAMs in the presence of DMSO (*n*=11, N=6) and in DKO NMAMs in the presence of DMSO (*n*=11, N=6) in E1 buffer.
B, Quantification of the peak FRET change in response to 3 µM PE in DKO NMAMs in the presence of either 0.1 % DMSO (*n*=11, N=6), 100 nM bafilomycin A1 (*n*=6, N=3), 1 µM *trans*-Ned-19 (*n*=3, N=3) or 10 µM SG-096 (*n*=8, N=4) in E1 buffer.

Data are represented as mean ± SEM and were analysed using non-parametric Mann-Whitney U test in panel A and Kruskal Wallis followed by Dunn's multiple comparison in panel B; n=experiments; N=isolations; non-significant (ns)=P>0.05, **P<0.01, ***P<0.01.

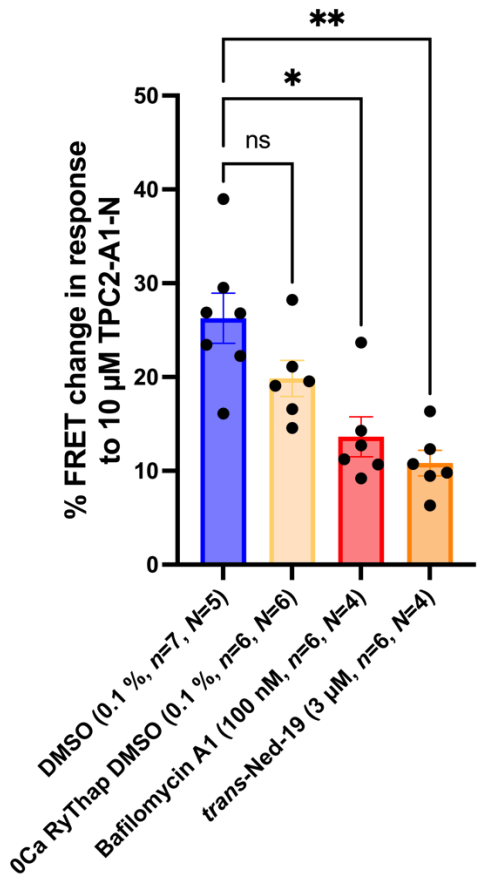

Figure 5.17: NAADP inhibitor (*trans*-Ned-19) and bafilomycin A1 reduces cAMP levels in response to TPC2-A1-N in NRAM.

Quantification of the peak FRET change in response to 10 µM TPC2-A1-N in NRAMs in the presence of either DMSO in E1 (*n*=7, *N*=5, blue) or in NRAMs myocytes pre-incubated for 45 minutes with 2 µM ryanodine (Ry) and 2 µM thapsigargin (Thap) in 0 calcium (0Ca) E1 buffer (*n*=5, *N*=5, off-white), 100 nM bafilomycin A1 (*n*=6, *N*=4, red) and *trans*-Ned-19 (*n*=6, *N*=4, orange) in E1 buffer.

Data are represented as mean ± SEM and were analysed using Kruskal Wallis followed by Dunn's multiple comparison; *n*=experiments; *N*=isolations; non-significant (ns)=P>0.05, *P<0.05, **P<0.01.

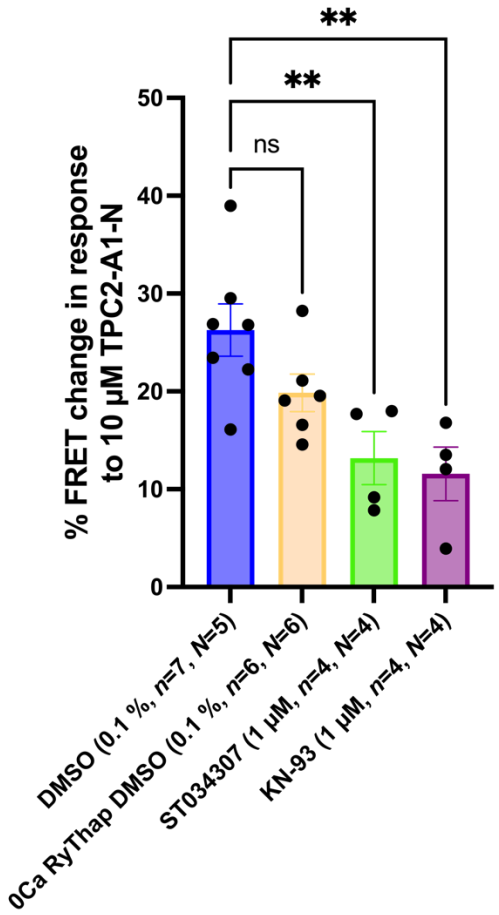

Figure 5.18: AC1 (ST034307) and CaMKII (KN-93) inhibitors reduces cAMP levels in response to TPC2-A1-N in NRAM.

Quantification of the peak FRET change in response to 10 µM TPC2-A1-N in NRAMs in the presence of either DMSO in E1 (*n*=7, *N*=5, blue) or in NRAMs myocytes pre-incubated for 45 minutes with 2 µM thapsigargin and 2 µM ryanodine in 0 calcium E1 buffer (*n*=5, *N*=5, off-white), 30 µM ST034307 (*n*=4, *N*=4, green) or KN-93 (*n*=4, *N*=4, purple) in E1 buffer.

Data are represented as mean ± SEM and were analysed using Kruskal Wallis followed by Dunn's multiple comparison; *n*=experiments; *N*=isolations; non-significant (ns)=P>0.05, ** P<0.01.

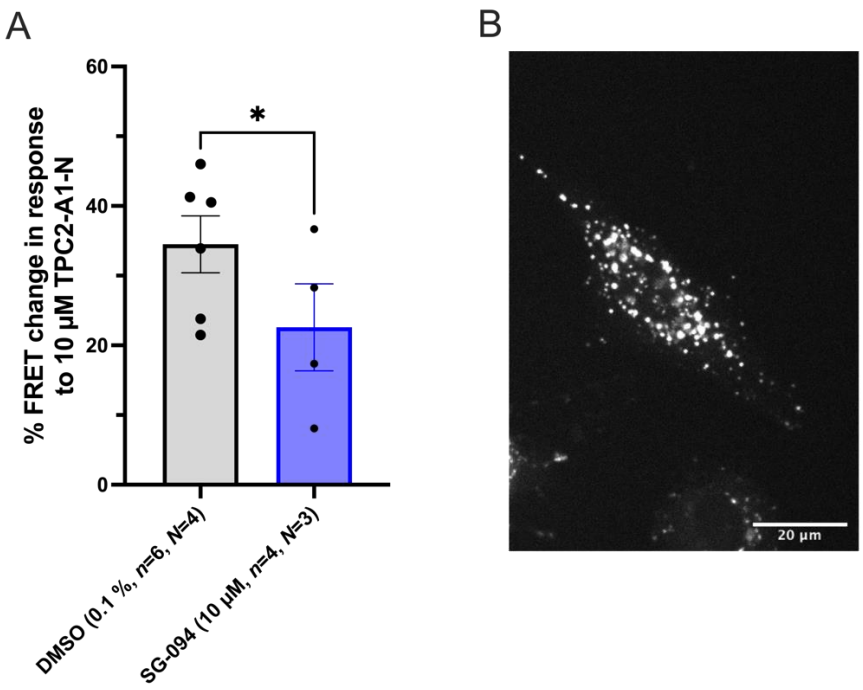

Figure 5.19: TPC2 inhibitor SG-094 reduces cAMP levels in response to TPC2-A1-N in hiPSC-aCMs.

A, Representative live image of hiPSC-aCMs loaded with Lysotracker™.
B, Quantification of the peak FRET change in response to 10 µM TPC2-A1-N in hiPSC-aCMs in the presence of either DMSO in E1 (*n*=6, *N*=3, grey) or 10 µM SG-094 (*n*=4, *N*=3, blue) in E1 buffer.

Data are represented as mean ± SEM and were analysed using paired t-test comparison. To assess normality, I performed the Shapiro-Wilk test on the dataset. The test indicated that the data followed a normal distribution ($p > 0.05$), justifying the use of parametric analyses. *n*=experiments; *N*=isolations; * $P<0.05$.

5.6 Discussions

This chapter focusses on NAADP signalling in response to α-adrenergic stimulation and presents evidence for novel crosstalk between NAADP-mediated calcium release and IP_3 mediated calcium release. As summarised previously, NAADP is known to be synthesised in the heart in response to β-adrenergic stimulation through the ADP ribosyl cyclase enzyme CD38. Acidic stores and the NAADP pathway have been shown to contribute the positive inotropic effects of β-adrenergic stimulation in the heart. Here, I present the involvement of NAADP signalling in response to α-adrenergic stimulation using PE.

Pharmacological inhibition of the NAADP pathway reduces contractile response to PE in intact atrial tissue. The functional work showed that inhibition of NAADP signalling by addition of 500 μM BZ- 194, 1 μM *trans*-Ned-19 or 100 nM bafilomycin A1 significantly reduced the positive chronotropic and inotropic effect of PE (Figure 5.2 and 5.4). These datasets provide evidence that the downstream effects of α-adrenergic signalling are dependent upon NAADP mediated calcium signalling from lysosomes in chronotropy and inotropy atrial myocytes. As far as I am aware, this represents a novel finding and avenue for future research. Furthermore, FRET work shows a decrease in synthesis of cAMP in response to 3 μM PE following addition of several NAADP inhibitors. These results do provide strong indications that cAMP synthesis is reduced by the NAADP pathway inhibitors, indicating a role for calcium stores in atrial function. Lysosomal signalling is seen to present a significant contribution to cellular cAMP level in response to α-adrenergic signalling in neonatal atrial myocytes but not in neonatal ventricular myocytes. NRVMs did not show inhibition in the presence of NAADP pathway inhibitors and presented a much lower decrease in NRVMs compared to NRAMs, previous work has shown IP_3R expression to be greater in atrial cells compared to ventricular cells (Lipp et al. 2000), indicating IP_3R dependent pathway and NAADP pathway crosstalk of cAMP activation is present in atrial myocytes but less important or reduced in ventricular myocytes.

Calcium transient investigations using direct stimulation of TPC2 channel opening (ligand biased towards TPC2 calcium flux, 10 μM TPC2-A1-N caused a calcium transient amplitude increase in WT atrial myocytes, similar to previous work by Collins et al, using caged NAADP (Collins et al. 2011). Experiments repeated in DKO atrial myocytes did not respond to 10 μM TPC2-A1-N and showed a decrease over the exposure time. Calcium transient work presented in this Chapter present a first link that lysosomal calcium release could be directly stimulating AC1 and or AC8, highlighting such a mechanism. Calcium plays a pivotal role in regulating

cardiac muscle contraction and relaxation. The stimulation of the NAADP pathway in DKO completely abolished the increase in calcium transient and even presented a decrease of amplitude for the total duration of the protocol, underlining a crucial role for NAADP signalling.

PE caused a significant increase in cellular cAMP. This increase was drastically reduced when NAADP agonists (*trans*-Ned-19 and SG096) and bafilomycin A1 were applied to NMAMs as observed in NRAMs with NMAMs. In contrast, DKO NMAMs showed no FRET change in the presence of 100 nM bafilomycin A1 or 1 μM *trans*-Ned-19 but showed a small but significant decrease with 10 μM SG-094. SG-094 is a specific TPC2 inhibitor (Du, Guan, and Yan 2022) and TPC2 are the main channels for lysosomal calcium via NAADP pathway in response to β-adrenergic stimulation (Capel et al. 2015; Calcraft et al. 2009; Patel 2015). Taken together, results confirm activation of AC1 and or AC8 in response to calcium release via NAADP in lysosomes. Using ST034307 (Brust et al. 2017), a specific AC1 inhibitor pharmacological agent, made possible to investigate whether AC1 or AC8 where crucial cAMP response to TPC2-A1-N, dataset presented in Figure 5.18 showed prior addition of ST034307 cut the FRET change into half, suggesting AC1 and AC8 to be both equally responsible to cAMP production to TPC2-A1-N. A possible explanation to this would be the location of AC1 and AC8 to the lysosomes (distance between them) and more importantly to TPC2, further research in exploration of intracellular locations of AC1, AC8 and TPC2 are lacking in cAMP compartmentation. KN-93, a CaMKII inhibitor, shows a significant decrease in FRET change to 11.57 ± 2.7 % in response to TPC2-A1-N when incubated with 1 μM KN-93 compared to control (26.28 ± 2.7 %). Given these results, it is not implausible that calcium release from lysosomes could also lead to CaMKII activation via Calcium/CaM and enhance cAMP through a yet to be identified interaction leading either to stimulation of an AC or inhibition of a PDE.

The observations presented in this Chapter confirm a role for NAADP signalling in response to α-adrenergic stimulation (using PE) in the study of chronotropy and inotropy and for cAMP production in FRET experiments. Abolition of lysosomal calcium signalling at multiple stages of the NAADP signalling pathway was studied in this Chapter enhancing robustness of these datasets. Measurements of calcium concentration in acidic organelles such as lysosomes are not trivial. One way around was an indirect measurement through FRET studies, and my FRET-based study measured total intracellular cAMP. Developing a FRET biosensor that targets

cAMP production around the lysosomes would be of great interest in order to directly visualise in real time cAMP synthesis directly from calcium release from lysosomes.

Autophagy is an evolutionarily conserved mechanism across species of plants and animals. It is the primary pathway for degradation and recycling of obsolete and potentially harmful cytoplasmic materials, including proteins, lipids and entire organelles through lysosomes. NAADP, TPCs and CD38 have been implicated in the regulation of autophagy, and autophagy-related genes were upregulated in atria of patients with persistent AF and that autophagy induced atrial electrical remodelling (Yuan et al. 2018). Could autophagy be a main driver for positioning lysosomes near calcium-sensitive AC1 and AC8 and contributing to physio-pathologies in the heart? The functional consequences of these structural changes in terms of lysosomal calcium signalling in AF will be important to determine in future work.

FRET work on hiPSC-CMs in Figure 5.19, confirmed presence and provided firm evidence of the importance NAADP pathway. Given the influence of NAADP pathway on calcium handling presented in this Chapter in small mammals and human myocytes, an investigation of NAADP signalling in atrial physiopathology is warranted and may shed light on the underlying mechanisms of AF.

5.7 Conclusions

In summary, this Chapter brings together two major aspects of calcium handling, IP_3-mediated calcium release from the SR and calcium release from lysosomes via NAADP signalling, illustration of proposed model is presented in Figure 5.20. I have demonstrated that NAADP pathway is involved in the α-adrenergic response, highlighting that lysosomal calcium is an important component of α-adrenergic stimulation in the cardiac atria. Lysosomal calcium signalling contributes to cellular cAMP generation in the cardiac atria and presents an important pathway for the control of SAN activity and atrial inotropy and may contribute to cardiac pathologies. The observations I present in this study strengthens the relevancy of these mechanisms in human physiology.

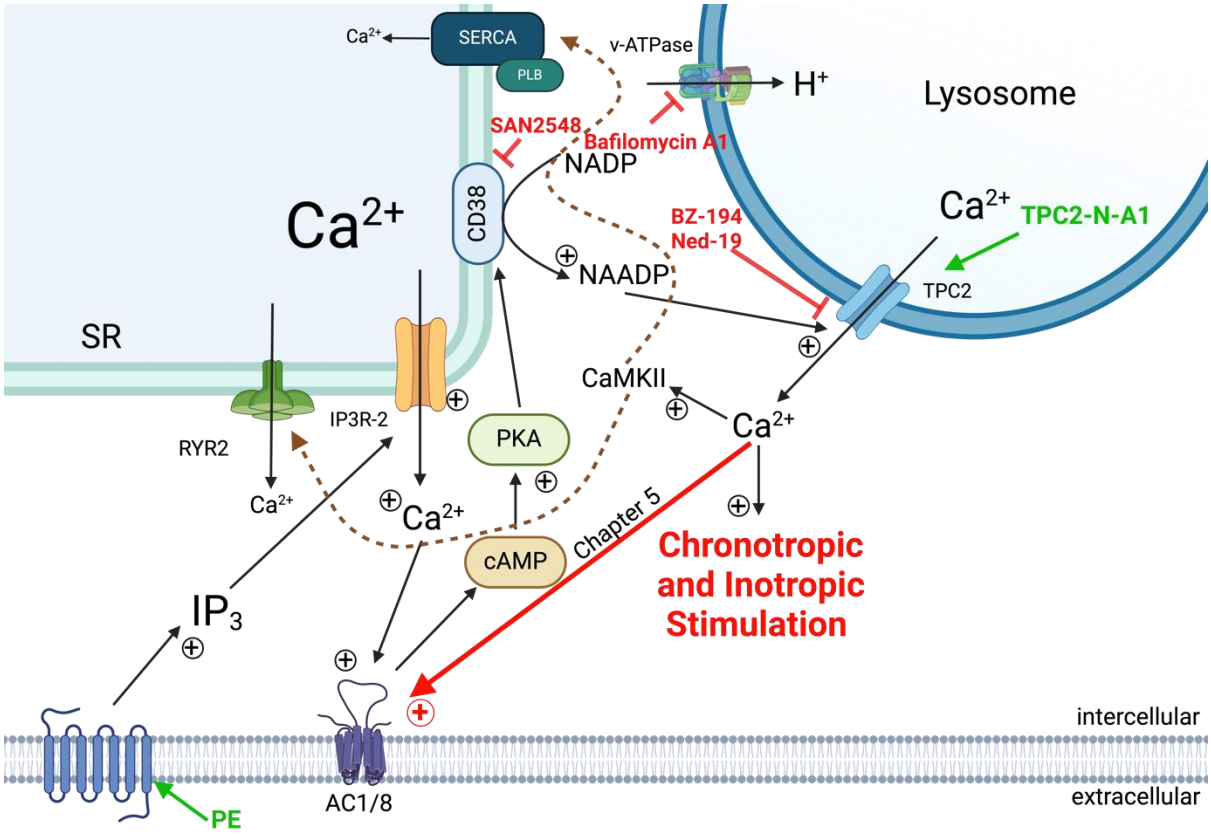

Figure 5.20: Representative scheme of proposed mechanisms from Chapter 5. The release of calcium from lysosomes leads to activation of AC1 or AC8. The mechanism demonstrates the importance of lysosomal calcium in the α-adrenergic response.

6 Chapter 6: Discussions and conclusions

6.1 Summary

Calcium homeostasis is a vital signalling mechanism in the heart and alterations in the intracellular concentration of calcium lead to cardiovascular related diseases (Nattel et al. 2014). The release of calcium from intracellular stores is a major component of this signalling cascade (Berridge, Lipp, and Bootman 2000). I investigated calcium handling pathways in the atria through adrenoceptor stimulation triggers, using isoprenaline for β-adrenergic stimulation and PE for α-adrenergic stimulation. The work presented here brings together two major aspect of calcium handling: NAADP signalling and IP_3 signalling and for the first-time studies these pathways in human cells. The experiments conducted in this thesis were designed to investigate how IP_3 mediated calcium release from the SR and NAADP mediated calcium release from the lysosomes impacted atrial function. In addition, calcium stimulated isoforms of ACs, AC1 and AC8, the enzymes that catalyse the synthesis of ATP into cAMP, were identified in the atria and their role in regulating pacemaking and force of contraction was explored.

The experiments presented in Chapter 3 investigate the very potent lysosomal calcium releasing molecule NAADP in response to isoprenaline. I present, to my knowledge, the first evidence that lysosomal calcium, acting through NAADP-mediated stimulation of TPC2 channels, makes a significant contribution to physiological modulation of heart rate at the SAN pacemaker by monitoring changes in spontaneous beating rate during cumulative dose-response additions of isoprenaline. I also conducted on intact left atrial studies to investigate the change in contractile force (inotropy) in response to isoprenaline. This data provided further evidence that abrogation of lysosomal calcium signalling reduces atrial response to β-adrenergic stimulation. I introduce a previously unknown contribution to cardiac cellular signalling in which lysosomal calcium release directly modulates cAMP independently of the previously reported effects of SR calcium content in NRAMs and in hiPSC-CMs. Therefore, reporting the relevance of this mechanism in an *in vitro* human cardiomyocyte model, strengthening the relevancy of this pathway in humans. The involvement of lysosomal calcium in the response to isoprenaline in atrial myocytes provides evidence for a physiological role for NAADP dependent calcium signalling.

Chapter 4 first investigated the involvement of calcium-sensitive AC1 in the response of intact mouse atrial tissue to the α-adrenoceptor agonist PE using the selective AC1 inhibitor ST034307. The maximum rate change of spontaneously beating mouse right atrial tissue

exposed to PE was reduced from in the presence of 1 μM ST034307 (AC1 inhibitor), from 14.5 (12.2–17.1) % to 8.2 (6.1–12.6) %. I next presented, for the first time, using a FRET-based sensor (EPAC-S^{H187}), that cytosolic cAMP levels are increased in atrial myocytes following α-adrenergic stimulation. This cAMP increase in response to PE was inhibited by pharmacological inhibition of IP_3R using 2-APB (2.5 μM) or xestospongin-C (0.3 μM). Prior application of any IP_3R inhibitors, the peak change in FRET following addition of 3 μM of PE was 21.20 ± 7.43 %, in the presence of 2-APB the peak change decreased to 5.88 ± 5.66 %, whilst 0.3 μM of xestospongin-C reduced peak to 8.76 ± 6.43 % (Figure 4.5). This experiment was repeated on NRVMs, and cAMP rise observed in NRVMs was not inhibited by the presence of either 2-APB or xestospongin-C in response to either PE or isoprenaline (Figure 4.6), indicating that this cAMP rise in ventricular myocytes is independent of IP_3R calcium release, unlike in NRAMs, revealing the specificity of this response in neonatal atrial myocytes. The second part of this Chapter investigates implication of knocking out calcium-sensitive *Adcy1* and *Adcy8* genes to α-adrenergic response the atria. I used a double knockout AC1 and AC8 (DKO) transgenic mouse line for these experiments. The sub-sarcolemmal localisation of IP_3R2 means that they are ideally placed to influence the activity of calcium stimulated AC1 and 8. DKO mice showed a decrease in positive chronotropic and inotropic response observed to cumulative concentrations to PE in intact right and left atria, inhibited amplitude of calcium transient in response to PE in adult isolated atrial myocytes and presented a smaller cAMP level in response to PE in NMAMs compared to WT mice.

Chapter 5 focusses on NAADP signalling in response to α-adrenergic stimulation. Back in 2013, Nebel et al (Nebel et al. 2013) showed first evidence for involvement of NAADP in cardiac arrhythmias evoked by β-adrenergic stimulation. I conducted experiments presenting the involvement of NAADP signalling in response to α-adrenergic stimulation using PE. Ectopic application of PE was shown to increase chronotropy to 23.69 (18.97-30.13) % and inotropy to 19.05 (14.9-25.5) % at 30 μM PE and this response was reduced in the presence of NAADP pathway inhibitors (BZ-194 and SAN4825) and bafilomycin A1 (abrogates acidic calcium store loading by inhibition of V-ATPase proton pump). Cytosolic cAMP levels were also increased in NRAMs following α-adrenergic stimulation using PE in NRAMs. This response was also inhibited using pharmacological agents to inhibit the NAADP pathway (BZ-194, *trans*-Ned-19, SG-094 and SAN4825) and bafilomycin A1. I revealed the specificity of this response to atrial myocytes as the cAMP rise observed in NRVMs was lower (12.62 ± 0.8 %) than in NRAMs (27.07 ± 2.8 %) and was not inhibited by these inhibitors (Figure 5.11).

The results presented here provide the first evidence for a role for NAADP in regulating calcium signalling in response to α-adrenergic stimulation. I also present a novel mechanism highlighting the activation of AC1 and AC8 in response to NAADP-mediated calcium release stimulation from lysosomes. In DKO atrial myocytes, cAMP production and calcium transient amplitude is impaired/reduced in response to NAADP mediated calcium release stimulation from lysosomes. This mechanism maybe specific to atrial myocytes and could be a target for treating AF with minimal off targets to the ventricular myocytes, bypassing a major problem in treating AF patients.

6.2 Limitations of techniques

6.2.1 FRET work

My FRET experiments were all conducted on neonatal mice or rat cardiomyocytes. Neonatal cardiomyocytes from animals are a valuable tool in cardiovascular research, they provide a reproducible *in vitro* culture model able to undergo infection with FRET adenovirus biosensor. However, neonatal cells are considered immature and significant differences (structural and in ECC) between neonatal cardiomyocytes and adult cardiomyocytes have been observed (Delcarpio, Claycomb, and Moses 1989). A study from (Korhonen, Hänninen, and Tavi 2009) have shown neonatal cardiomyocytes to have significantly longer repolarization phases in AP, a more heterogeneous cytosolic calcium signals with changes in calcium diffusion and SR calcium release, having a weaker SR calcium handling, and stronger sarcolemmal calcium handling by the sodium/calcium exchanger (Korhonen, Hänninen, and Tavi 2009).

As well as using immature cardiomyocytes, these were also quiescent cardiomyocytes which have a few limitations. These cells did not beat or contract and limits insights into how these cells might behave when naturally beating. The physiology of quiescent cardiomyocytes differs from actively contracting cardiomyocytes as ion channel activity and calcium handling can vary significantly. As discussed throughout this manuscript, calcium handling is central to cardiac muscle contraction and heart function, but in quiescent cardiomyocytes, the physiological calcium fluxes are altered. Alternatives like spontaneously beating cardiomyocytes such as hiPSC-aCMs have been used in this project not only to overcome these limitations but provide a closer approximation to physiological heart function and response in a human cell model.

A major mechanism for the regulation of cardiac chronotropy and inotropy is the phosphorylation of key proteins that are involved in cardiac ECC (Bers 2002). PKA is activated by the second messenger cAMP and is an essential component of the adrenergic signalling cascade in the heart (Steinberg 1999). To measure live cAMP levels in atrial myocytes, I ran FRET experiments in neonatal mice or rat cardiomyocytes expressing EPAC-S^{H187}, a cytosolic biosensor designed to detect and monitor in real time EPAC (exchange protein activated by cAMP) within the cytosol of a myocyte, EPAC proteins are activated by the binding of the signalling molecule cAMP. I measured global FRET ratio changes in the cytosol which translates to global/cytosolic cAMP levels in the cell. Experiments on NRAMs expressing AKAP79-CUTie were conducted by Dr Sam Bose (postdoc in the lab), a FRET-based cAMP sensor that targets the intracellular surface of the plasmalemma, AKAP79-CUTie (Musheshe et al. 2018). A-kinase anchor proteins (AKAPs) act by forming small signalling complexes in cells and bind to PKA. We wanted to test if cytosolic cAMP dependent response to IP_3R activation in atrial cells were also observed at the plasma membrane, which could imply the involvement of membrane bound calcium-sensitive AC1 and/or AC8 (Capel et al. 2021). In Figure 6.1, NRAMs in response to PE led to FRET change corresponding to an increase in cAMP that was inhibited by 2-APB and xestospongin C. Figure 6.1A shows representative images comparing the distribution of cAMP signal of the cytosolic EPAC-S^{H187} FRET sensor and AKAP79-CUTie. NRAMs expressing AKAP79-CUTie showed a 14.64 ± 2.41% increase in global FRET signal on addition of PE ($P<0.05$, $n=13$, $N=5$, Figure 6.1B), indicating a rise in cAMP at the location of AKAP79/β-AR/AC/LTCC complex. 2-APB was found to cause a significant reduction in the change in FRET signal corresponding to 2.88 ± 15.2% ($n=5$, $N=3$) and xestospongin-C resulted in a reduction in the change of FRET corresponding to 7.31 ± 3.24% ($n=6$, $N=3$) in response to PE, a significant reduction was still observed ($P<0.05$, Figure 6.1B). Highlighting the possibility membrane bound calcium sensitive AC1 or AC8 implicated in this response.

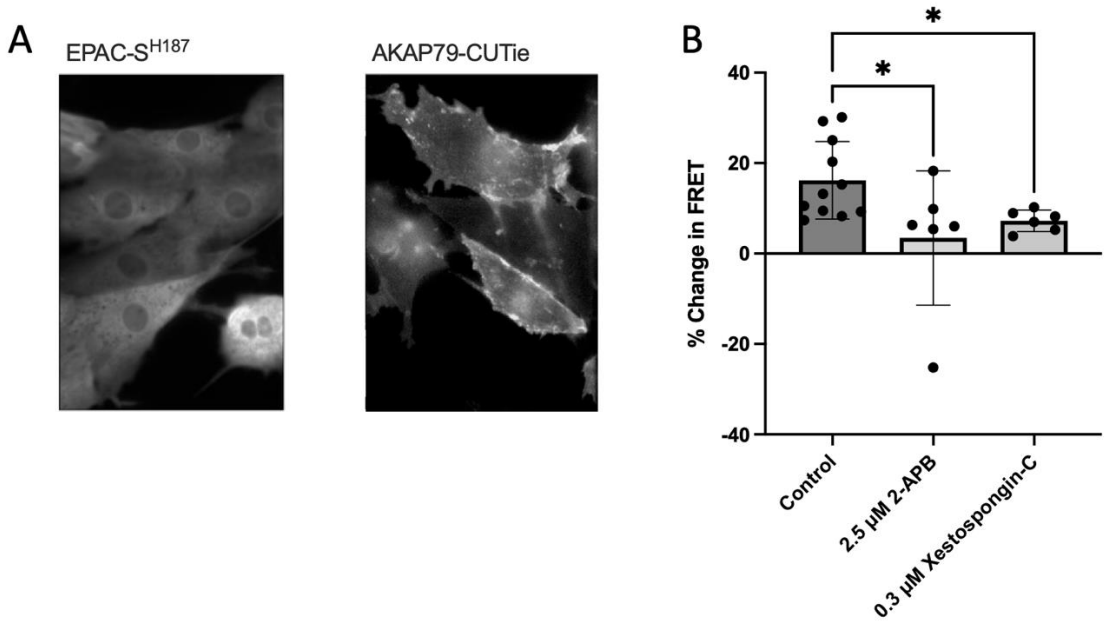

Figure 6.1: FRET experiments conducted by Dr Sam Bose.

A: Representative images comparing the distribution of cAMP signal of the cytosolic EPAC-S^{H187} FRET sensor and AKAP79-CUTie.
B: Quantification of peak response to PE (3 µM; *n*=13, *N*=5) alone, or in the presence of 2.5 µM 2-APB (*n*=5, *N*=3) or 0.3 µM Xestospongin-C (*n*=6, *N*=3).

I was present but did not conduct these experiments.

6.2.2 Study of CaMKII

The LTCC current has been shown to be regulated by cytosolic calcium in both atrial and ventricular myocytes (Collins and Terrar 2012). In ventricular myocytes, this regulation may be predominantly modulated via CaMKII, as the inhibition of LTCC current was observed in the presence of KN-93, a CAMKII inhibitor (Collins and Terrar 2012). However in atrial myocytes, the addition of the calcium selective chelator BAPTA, following KN-93, resulted in a further inhibition of LTCC current which was not observed in ventricular myocytes, suggesting the presence of a CaMKII-independent mechanism of calcium regulation in atrial myocytes (Collins and Terrar 2012). A group, (Mizunami et al. 2014) have also proposed that CaMKII serves as a key molecule for interplay between calcium signalling and cAMP signalling for long-term memory formation in crickets, by being upstream of cAMP accumulation and interacting with ACs. In regard to these findings, I sought out to investigate cAMP levels in response to TPC2-A1-N in the presence of KN-93 (CaMKII inhibitor). I observed in Figure 5.18 significant decrease in FRET change to 11.57 ± 2.7 % in response to TPC2-A1-N when incubated with 1 µM KN-93 as compared to control (26.28 ± 2.7 %).

However, pilot FRET experiments on DKO NMAMs, a dataset completed over 1 neonatal isolation, shows no inhibition in the presence of 10 μM SG-096 (TPC2 inhibitor) or 1 μM KN-93 in response to 10 μM TPC2-A1-N (Figure 6.2), unlike observations made in NRAMs in Figure 5.18. This could be from the activation of calcium sensitive ACs, AC1 and AC8, downstream of IP_3R calcium release (Capel et al. 2021; Collins and Terrar 2012). AC1 and AC8 both show expression in cardiomyocytes, including atrial cells and the SAN (Capel et al. 2021; Collins et al. 2011; Mattick et al. 2007), Figure 4.1. CaMKII has not been fully studied during my thesis and further evidence is needed to confirm CaMKII as a downstream mediator of the NAADP pathway. I also ran FRET experiments in the presence of 3 μM of the AC1 inhibitor ST034307 and observed a significantly smaller increase in cAMP levels in response to TPC2-A1-N (13.18±2.7%) compared to control (26.28±2.7%), as shown in Figure 5.18, raising the possibility that the contribution of this mechanism could be augmented under physiological conditions. Additionally, KN-92 is primarily used in research as a control compound for studying CaMKII inhibition. It is an inactive derivative of KN-93, which is the selective inhibitor of CaMKII, I used in this study to conduct pilot studies of implication of CaMKII in lysosomal calcium and NAADP pathway. While KN-93 actively blocks the binding of calcium/calmodulin to the kinase, KN-92 does not possess this inhibitory effect and serves as a negative control in experiments designed to explore the physiological and biochemical roles of CaMKII, KN-92 will be added as a negative control to complete the datasets presented in this manuscript.

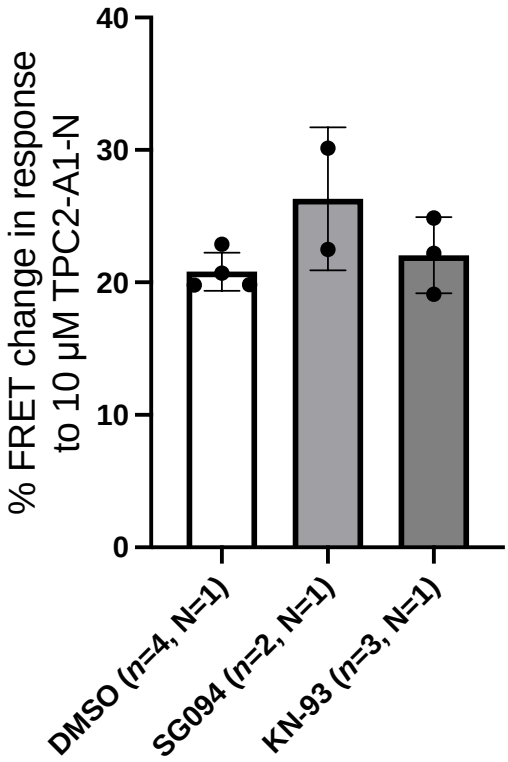

Figure 6.2: Comparison of peak FRET response to 10 µM TPC2-A1-N and isoprenaline in DKO NMAM to NAADP inhibitors.

Quantification of the peak FRET change in response to 10 µM TPC2-A1-N in NRAMs in the presence of either DMSO in E1 (*n*=4, *N*=1), 10 µM SG-094 (*n*=2, *N*=1) or KN-93 (*n*=3, *N*=1) in E1 buffer. Uncompleted datasets in DKO.

6.2.3 Monitoring calcium signals

The results from Chapter 4 show calcium stimulated ACs to be activated by α-adrenergic stimulation using PE and influences calcium transient amplitude (Figure 4.18). The close positioning between calcium stimulated ACs and the sub-sarcolemmal IP_3R means that AC1 and AC8 should be exposed to high levels of calcium release from the SR that will occur in the microdomain around IP_3R2 opening. Lysosomes have been identified to be located in close proximity to the SR in guinea pig atrial myocytes (Figure 3.10) and in rabbit ventricular myocytes (Aston et al. 2017). Chapter 5 present data to support the hypothesis that calcium released from the lysosomes via TPC2 receptors, stimulates AC1 and AC8 and affects atrial function. In addition, these observations also explain how relatively few IP_3R, by high colocalisation with AC1 and/or AC8 and proximity to lysosomes, can influence calcium signalling in the atria at a whole tissue level. Additionally, photorelease of NAADP on adult cardiomyocytes, shown in previous studies, had no effect on LTCC current (Collins et al. 2011) and FRET experiments conducted in a 0 calcium environment with depletion of SR calcium

presented an increase cAMP in response to TPC2 stimulation. Therefore, it can be concluded that the increase in calcium transient amplitude and cAMP are not due to an increase in the entry of calcium from outside the cell. As relaxation occurs in atrial myocytes, lysosomal calcium releases into the cytosol must be either pumped back into the organelles or out of the cell, this process is dependent on spatial organisation of the myocytes but has not been investigated in this project. Pumps involved in calcium uptake by lysosomes are unknown but this process could be dependent on the pH gradient established by VATP-as (Morgan et al. 2011) and TPC2 could be located close to regions of the SR that express more SERCA2.

It is widely known that pulmonary veins are surrounded by an external sleeve of cardiomyocytes that are widely recognised to play an important role in AF. Investigation of calcium signalling in an intact section of the rat pulmonary vein were conducted in these myocytes (Logantha et al. 2010). Under resting conditions cardiomyocytes displayed spontaneous calcium transients, removing extracellular calcium produced a slight reduction in the amplitude and frequency. However, ryanodine had a much greater effect on the amplitude and reduced the frequency and blocking IP_3R also reduced the amplitude and frequency of the spontaneous calcium transients, indicating the importance of calcium release from the SR (Logantha et al. 2010). The pulmonary veins are known to act as a trigger of AF and has not been investigated throughout my work.

6.2.4 Developing an *in vitro* model

Over the past decades many pathophysiological mechanisms have been described to contribute to the initiation of AF such as focal ectopic/triggered activity and re-entry (Heijman et al. 2014). There is a growing interest in generating *in vitro* models reflecting the properties of this disease (van Gorp et al. 2020). An ideal cell culture model of AF (animal or human) remains to be developed to study the fundamental mechanisms that underlie normal and pathological electrophysiology at tissue level. During my project, I have learned and established a cultured cardiac-monolayer and observed beating foci of myocytes. However, developing *in vitro* cultures can be challenging for several reasons such as the complexity of the cellular environment, purity of cells, reproducibility and standardisation. An *in vitro* atria arrhythmic model to test the role of NAADP and IP_3 pathway would allow us to investigate the impact of these changes further, in either culturing primary atrial myocardial cells or culturing hiPSC-CMs from healthy and diseased AF patients. Our aim would be to study IP_3-mediated calcium release from the SR and calcium uptake and release from lysosomes. Figure 6.3 shows

recordings of beating monolayers of NRAMs loaded with FluoVolt™ dye to image membrane potential activity. So far, we have been able to locate spontaneously beating foci (Fig.4 Ai and B) and observe changes by stimulating them. In Figure 6.3A, the cells are able to respond to external stimuli at 1 (Fig.4 A.ii) and 2 hertz (Fig.4 A.iii) but lose rhythm at 4 hertz (Fig.4 A.iv) and stops rhythmic beating at 8 hertz (Fig.4 A.v). Preliminary results showed that monolayers of NRAMs were able to form spontaneously beating foci and that we were able to induce a change in atrial beating through external stimuli by pacing. The results presented are from preliminary findings and more experiments are planned with directions towards establishing an *in vitro* model to study NAADP and IP_3 signalling in atria arrhythmias.

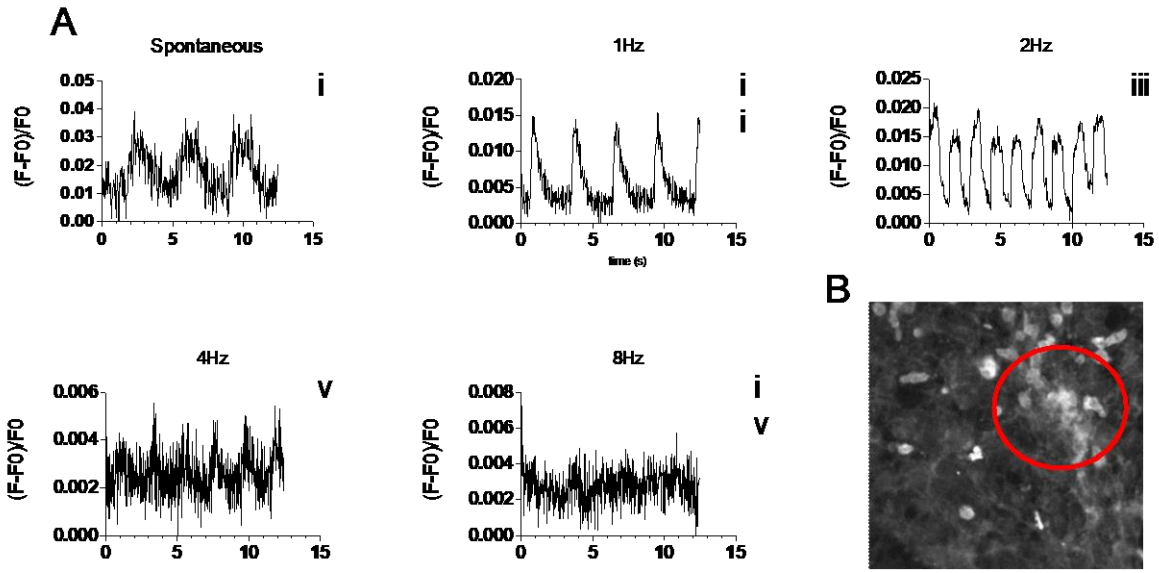

Figure 6.3: Monolayers of NRAMs as a potential for AF model.

A: Recording of dynamic activity of membrane potential in cultured neonatal rat atrial myocytes on day 5 of culture, spontaneously beating foci was located and recorded (i) and was then stimulated at 1 hertz (ii), 2 hertz (iii), 4 hertz (iv) and 8 hertz (v) *n*=1.
B: Monolayer of NRAMs load with FluoVolt™ dye observed at 20X.

The activation of the IP_3 pathway in atrial myocytes by administering increasing concentration of PE into the organ bath has led to positive chronotropy, inotropy and an increase in cAMP levels. These changes can be pharmacologically inhibited using IP_3R inhibitors and NAADP inhibitors in NRAMs, but these observations were not seen in ventricular myocytes. Quantitative reverse transcription polymerase chain reaction (RT-PCR) was conducted in Figure 6.4 on NRAMs and NRVMs, this dataset is not complete, and analysis could not be run but result show lower expression of AC8 in NRVMs while AC1, AC6 and IP_3R2 seem to show similar expression. RT-PCR showing *Adcy1* to be expressed at a higher level to *Adcy8*

expression, a possible explanation to this would be the location of AC1 and AC8 to the lysosomes (distance between them) and more importantly to TPC2. These findings support further investigation into the pro-arrhythmic nature of IP_3-induced cAMP signalling.

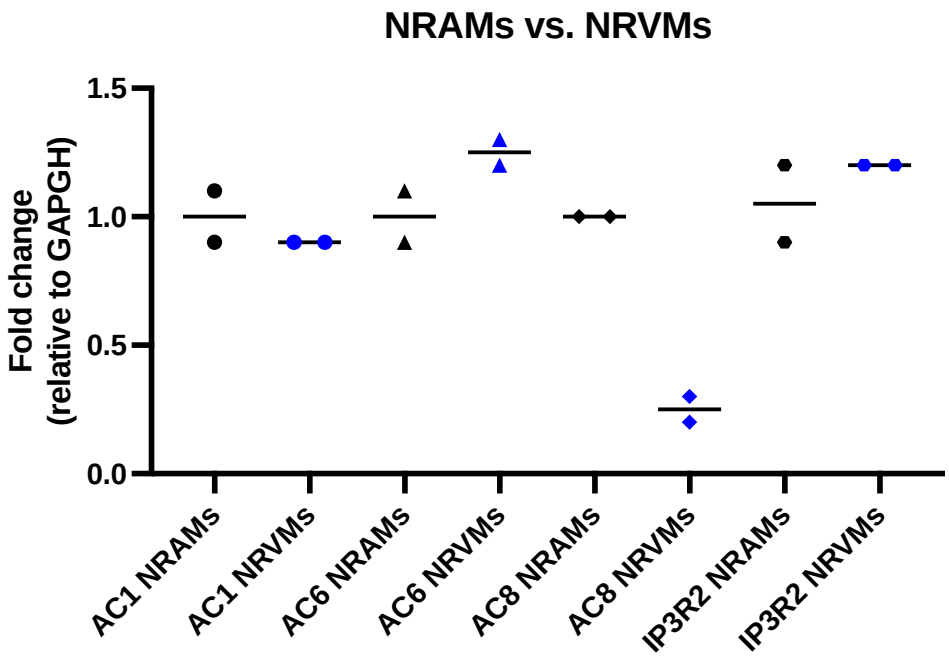

Figure 6.4: Comparison of expression AC1, AC6, AC8 and IP_3R2 in NRAMs and NRVMs using RT-qPCR (*n*=2, uncompleted dataset)**.**

6.2.5 hiPSC-CMs

Development of differentiation of hiPSCs towards specific atrial or ventricular cardiomyocytes holds promise into studying the NAADP pathway within human cardiac physiology and pathology (Benzoni et al. 2020). FRET experiments in this thesis confirmed the activation of NAADP pathway in humans by decrease in cAMP upon β-adrenergic response with isoprenaline in the presence of bafilomycin A1 and cAMP increase in response to TPC2 stimulation. This pathway was investigated under physiological conditions with healthy hiPSC-CMs and hiPSC-aCMs in Figures 3.6 and 5.19 (FRET experiments) and in Figure 3.7 (calcium transient experiments). These hiPSC-CMs experiments were an important inclusion in my thesis as they demonstrate the translational relevance of this research in human cardiac models. All previous work I conducted in my Chapters or previous published work from the lab have shown the presence of the signalling pathways of IP_3 and NAADP in intact mouse atria, isolated guinea pig atrial myocytes (Capel et al. 2021; Bose et al. 2022), neonatal mouse and rat myocytes but has not been previously demonstrated of the relevance of these data in human

cells. Pacing with electric fields have been employed to establish an *in vitro* rapid pacing model (Ji et al. 2013) to study the early electrical remodelling in AF. However, hiPSC-CMs used as a tool to create *in vitro* models to study AF lacks in the field and is likely due to the many drawbacks or difficulties encountered in culturing these cells. Differentiation protocols for hiPSCs can result in heterogeneous cell populations, with variability in cell maturity which can in turn complicate experimental interpretation and standardisation, as well as introduce variability between hiPSC lines between differentiation batches. Differentiated cell types derived from hiPSCs may exhibit immature phenotypes resembling foetal or embryonic stages rather than adult tissues. To overcome this and ensure reproducibility of my experiments, I have conducted experiments using >3 differentiations with different cardiomyocytes differentiation kits and purchased commercialised cell lines and grown the cell to 30 days. I have not been able to successfully culture conduct experiments in AF hiPSC-aCMs to investigate the NAADP and IP_3 signalling. Additionally, I tried to isolate human cells on a few occasions at the University of Leicester with Prof Ng, but these experiments failed, and the logistics were very complicated.

6.3 Atrial fibrillation as a disease of interest

6.3.1 Atrial fibrillation and treatment drawbacks

Atrial fibrillation (AF) is a heart rhythm disturbance (arrhythmia) and is defined by a rapid and irregular electrical activation of the atria, leading to chaotic and uncoordinated atrial contraction. AF is the most frequent cardiac arrhythmia worldwide, with 37.6 million cases worldwide. The pathophysiology of AF is still incompletely understood and therefore has major mortality rate with an attributable 287,200 deaths worldwide ('Global, regional, and national age-sex-specific mortality for 282 causes of death in 195 countries and territories, 1980-2017: a systematic analysis for the Global Burden of Disease Study 2017' 2018). Knowledge about initiation and maintenance of AF has evolved significantly over the past years, however, major calcium and molecular mechanisms underlying the disease are lacking in order to treat patients effectively (Nattel et al. 2020). Current treatments for AF are for rhythm, rate control and anticoagulation medication or catheter ablation to reduce the risk of stroke and restore normal heart rhythm (Verma and Wong 2019), but often have undesirable effects on the ventricles, underlining the need for atrial specific targets for AF therapy, making this disease a global epidemic and major public health issue. The initiation and progression of AF are highly complex and highlight the multifactorial nature of the disease progression where several factors

are involved (Nattel et al. 2014). The current therapeutic arsenal aimed at controlling the rhythm of patients in cases of AF has substantial limitations, not allowing the cure of the atrial disease. Recurrences of AF are frequent and the evolution from a paroxysmal form to a persistent form is unfortunately every hard to slow down, leading to modifications in the atrial tissue, atrial remodelling. The treatment of AF remains suboptimal mainly due to an uncertainty as to its precise pathophysiological mechanisms as exact reasons for why age and certain medical disorders increase the risk of AF are not yet fully understood (Schotten et al. 2011). The rate control treatments mainly consist of calcium-channel blockers and β-blockers. Rate control approach is the first-line treatment for AF (Alobaida and Alrumayh 2021). Rhythm control involves the use of electrical or pharmacological cardioversion with the aim to convert the arrhythmia associated with AF to normal sinus rhythm. However, patients who have been successfully cardioverted are generally given antiarrhythmic drugs for long term to help prevent the recurrence of AF (Sulke, Sayers, and Lip 2007). Different ablative techniques have significant limitations, it is an invasive strategy which has significant short and long-term non-desirable effects and can require re-ablations (Kottkamp, Bender, and Berg 2015). The progressive nature of the disease creates a major problem in treatment and limits the long-term success of both pharmacological and ablation therapies (Nattel et al. 2014).

6.3.2 Lysosomal function and contribution to atrial fibrillation

Emerging research suggests that specific genetic variations related to lysosomal function and may contribute to AF pathology. Lysosomal storage diseases are not associated directly with AF. However certain genes linked to lysosomal function are beginning to show relevance, studies have implicated GLA (encoding α-galactosidase A), a gene involved in Fabry disease, a lysosomal storage disorder (Michaud et al. 2021; Ter Huurne et al. 2023). Fabry disease is associated with cardiac hypertrophy and arrhythmias, including AF, due to the build-up of glycolipids in the heart, which can disrupt electrical conduction and cellular function (Roy et al. 2024; Shah et al. 2005). Niemann-Pick type C disease and AF don’t have a direct causal link, but genome-Wide Association Studies might provide insight into why NPC disease could influence AF susceptibility. NPC disease is a rare genetic disorder caused by mutations in NPC1 or NPC2 genes, leading to abnormal cholesterol and lipid accumulation in lysosomes, primarily affecting the nervous system and liver (Lloyd-Evans et al. 2008). However, disruption of lysosomal storage impairs calcium channels and disrupts the balance of calcium within the cells, potentially affecting cardiac muscle cells excitability and increasing arrhythmogenic risk (Lloyd-Evans and Platt 2011).

Our lab recently published an omics study focused on endolysosomal organelle proteins that highlights possible changes in lysosome function in AF Results showed increased cellular stress, increased vesicle trafficking, changes in ATP demands, accumulation of glycogen, inflammation, and stimulation of cell death (Ayagama et al. 2024). We also to performed data-independent acquisition parallel accumulation-serial fragmentation (DIA-PASEF) on human right atrial appendage tissue samples with label free protein quantification, proteins with roles in lysosomal function and membrane trafficking were significantly affected in AF patients (Capel et al. 2024). Direct links between lysosomal proteins, cAMP signalling genes, and AF markers are currently being investigated, genetic studies suggest that mutations affecting lysosomal function and cAMP signalling may influence AF onset and maintenance. Further research on how lysosomal dysfunction (via NAADP pathway) and altered cAMP pathways are linked with cardiac pacemaking is likely to provide new pathways on treating AF.

6.3.3 NAADP and IP_3 signalling as potential targets for atrial fibrillation

Abnormal intracellular calcium homeostasis occurs in chronic AF (Nattel and Dobrev 2012). AF can be initiated and maintained by rapid focal ectopic activity or by re-entry, and calcium-handling abnormalities have been reported to play a major role in this pathological mechanism (Iwasaki et al. 2011; Heijman et al. 2014). Data presented throughout this manuscript provide evidence that dysregulation of lysosomal calcium signalling affects atria function (chronotropy and inotropy) at a whole tissue level and affects downstream IP_3 signalling and cAMP levels at intracellular level, an intracellular mechanism specific to the atria. This suggest that lysosomal-mediated calcium signalling cascade and may be arrhythmogenic. Data support the proposal that IP_3 signalling in cardiac atria and sinoatrial node involves stimulation of calcium-activated AC1 and AC8 by IP_3-evoked calcium release from the SR and lysosomes and AC1/IP_3R and AC1/LAMP2 are shown to be located close together. Additionally, Chapter 4 provides novel findings on the signalling pathways responsible for IP_3 pathway responses, demonstrating a crucial requirement for cAMP and PKA acting via calcium sensitive AC1 and AC8. adding levels of complexity to calcium modulation in the atria and SAN and raise questions concerning the importance of these interacting signalling pathways in atrial fibrillation and potentially other cardiac pathologies. NAADP and IP_3 signalling in the SAN can be targeted acting on automaticity and rhythm. Lysosome-SR distance change and size of lysosomes in AF patients warrants future investigations as dysregulation of signalling microdomains and alternation in the SR channels, open a new avenue of questions to be answered relating to whether lysosomes contribute to abnormal calcium handling and therefore

a role in AF maintenance. Further investigation of cAMP production in relation to NAADP and IP_3 signalling pathways in cardiac atria may identify novel targets to manage pacemaker activity and bring light on initiation and maintenance of atrial arrhythmias such as AF.

6.4 Future work

6.4.1 Studying NAADP pathway in the context of atrial fibrillation

There is a large body of evidence presented here that supports the hypothesis that NAADP mediated calcium release from lysosomes plays a major role in atria function and pacemaking. Further dissection of NAADP signalling and its pathophysiological importance in the atria warrants investigation. Research in disease hiPSC lines to investigate the upregulation of downregulation of the NAADP and IP_3 pathways will be of great interest. A patient-specific disease model for AF has been previously reported (Benzoni et al. 2020), the study focused the clinical case of three siblings with untreatable persistent AF whose whole-exome sequence analysis revealed several mutated genes. They generated iPSC clones from these patients and differentiated these cells towards the cardiac lineage. The genetic background of the patients induced functional alterations of I_f and LTCC currents leading to a cardiac substrate more prone to develop arrhythmias. Conducting experiments on human iPSC models of a familial form of AF to study the activation of NAADP or IP_3 would be of great interest as potential specific targets for considering alternative therapies for AF. The usage of hiPSC-based disease models will allow for the study of onset and progress by studying the mechanisms that trigger rapid ectopic firing and re-entries to maintain the AF to provide insights into disease mechanisms and potential therapeutic targets.

All previous basic physiology work on IP_3-mediated calcium release and calcium release from the lysosomes via NAADP pathways has been done on healthy myocytes. Whilst IP_3R and calcium stimulated ACs are significantly upregulated in AF, NAADP downstream pathways have not been studied in AF settings. NAADP and its potential physiological and pathological importance in the atria warrant further investigations as it may represent an important pathway for the control of atrial tissue and contribute to cardiac pathologies. An *in vitro* AF model to test the role of these pathways would allow us to investigate the impacts of these changes further. Further studies will be aimed to explore the method of culturing primary atrial myocardial cells *in vitro* as well as to establish an *in vitro* model of rapid electrical pacing in cultured atrial myocardial cells and hiPSCs from AF patients (Benzoni et al. 2020).

Similar FRET experiments could be conducted to study the calcium release from lysosomes. Designing a FRET biosensor targeted to the membrane of lysosomes, such as Lysosomal-associated membrane protein (LAMP2), would be of great interests to link cAMP production to direct calcium release from lysosomes by stimulation of TPC2 receptors. Whole tissue experiments were conducted throughout this project, such as dose-response curves to PE and isoprenaline in intact right and left atria to study chronotropy and inotropy respectively. These experiments allow to investigate the relevance of NAADP signalling and IP_3 signalling in *in vivo* physiology to provide insight of the effect of these pathways at an organ function level.

Chapter 3 presented EM that reported the spatial relationship between lysosomes and the SR to be altered in human atrial tissue from an AF patient. Lysosomes are involved in the autophagic process, autophagy is the cellular survival mechanism that leads a self-degradative pathway. As lysosomes are a driving force in cellular trafficking pathways as they are involved in the final step of degradation. Findings have suggested that atrial autophagic flux is activated in patients with AF and autophagy induces atrial electrical remodelling (Yuan et al. 2018), a marker or mechanism has not been proposed to explain this so far. Autophagy has not been investigated in this manuscript, but work published from other groups suggest dysregulation of this mechanism in AF (Yuan et al. 2018; García-Rúa et al. 2016). Whether autophagy is a cause for AF or AF induces autophagy has not been established. Functional studies to ascertain lysosomal calcium signalling in AF and how it impacts molecular changes in the atria are likely to add translational value in future studies.

6.4.2 Furthering knowledge on Lysosome-IP_3R2 positioning

We have conducted confocal staining studies of AC1 and LAMP2 on isolated SAN guinea-pig myocytes showing colocalisation (Figure 3.10), illustrating that calcium release via lysosomes directly leads to activation of calcium-sensitive AC1 in SAN myocytes. Although, the proportion of acidic stores contributing to a given signal and the time course of this contribution is unknown. I prepared samples to performed super resolution imaging on NRAMs cells labelled with LAMP2 to identify individual lysosomes (performed by Dr Jingyu Wang from The Department of Engineering Science, University of Oxford, Oxford, UK). This was done based on spot quality (a function of both absolute value and local contrast). Analysis was performed by Dr Alexander Corbett (from The Department of Physics and Astronomy, University of Exeter, Exeter, UK) 342 lysosomes were identified within an individual cell (Figure 6.5A). Of these, 296 (87%) were found to be located within 500 nm of their nearest

neighbour (yellow spheres, Figure 6.5B). A size distribution of the lysosomes was also acquired (Figure 6.5C). The stochastic nature of single molecule switching (SMS, in which fluorophores spend the majority of time in a dark state) and the fact that large regions of the cell were obscured by drift correction beads, the absolute value of the lysosome volume measured from the SMS data should be considered an underestimate of the true volume. Based on these limitations and using an estimate of the neonatal cell volume of 1000 μm^3 from my co-supervisor's lab (Koschinski and Zaccolo 2017) a lower limit on the volume fraction of the lysosomes can be estimated as 0.3 μm^3/1000 μm^3 (0.3 %).

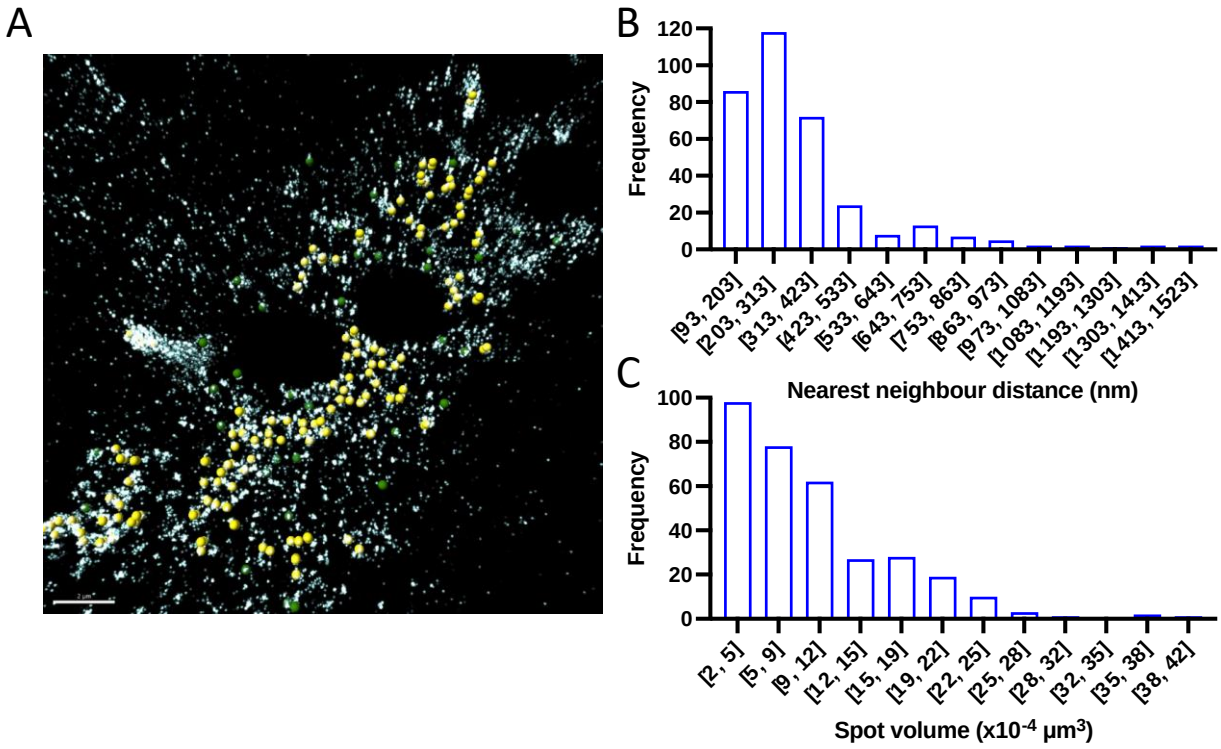

Figure 6.5: 4Pi-SMS super-resolution microscopy analysis.

A: Visualisation Z-projection of the 4Pi SMS image data indicating lysosomes (spheres) which are less than (yellow) or more than (Chandler et al.) 500 nm of their nearest neighbour. Scale bar 2 µm.

B: Distribution of nearest neighbour distances, n=342 lysosomes.

C: Spectrum of measured lysosome volumes, n=342 lysosomes.

Structural studies using immunocytochemistry techniques have been used throughout my project to look at structural and anatomical characteristics on healthy atrial myocytes to study the distribution of IP_3R2, AC1 and LAMP2 with confocal microscopy. This was a first step to visualise lysosomes at a high resolution and the next step would be to study lysosome-SR and lysosome-mitochondria distance, it would be of great interest to images cardiomyocytes at a higher resolution to determine with nanometres resolution, how closely ACs, IP_3R and lysosomes are located in healthy and diseased atrial myocytes. Lysosomes are in close proximity to the SR (Aston et al. 2017) and I performed measurements on EM images on left human tissue samples with AF and sinus rhythm were conducted on an n=1 for each condition. Results showed that lysosomal size and positioning undergo remodelling by increasing in size

and moving further away from the SR (Figure 6.6). This is not an appropriate number to draw any conclusions as the population measured on is too small and results in size and distance between SR and lysosomes can vary from patient and from type of AF. Samples from a larger number of patients need to be analyses to draw any conclusions but first pilot data is promising to continue analysis. Other organelles capable of storing calcium such as mitochondria have been shown to form close associations with lysosomes (Aston et al. 2017). Mitochondria have been shown to carry cargo to the lysosomes (Soubannier et al. 2012), this association between lysosomes and mitochondria could have functional significance in cardiomyocytes. The lab has shown lysosomes to move further away from the SR and closer to mitochondria in goat model of AF (Capel et al. 2024) having a potential functional importance.

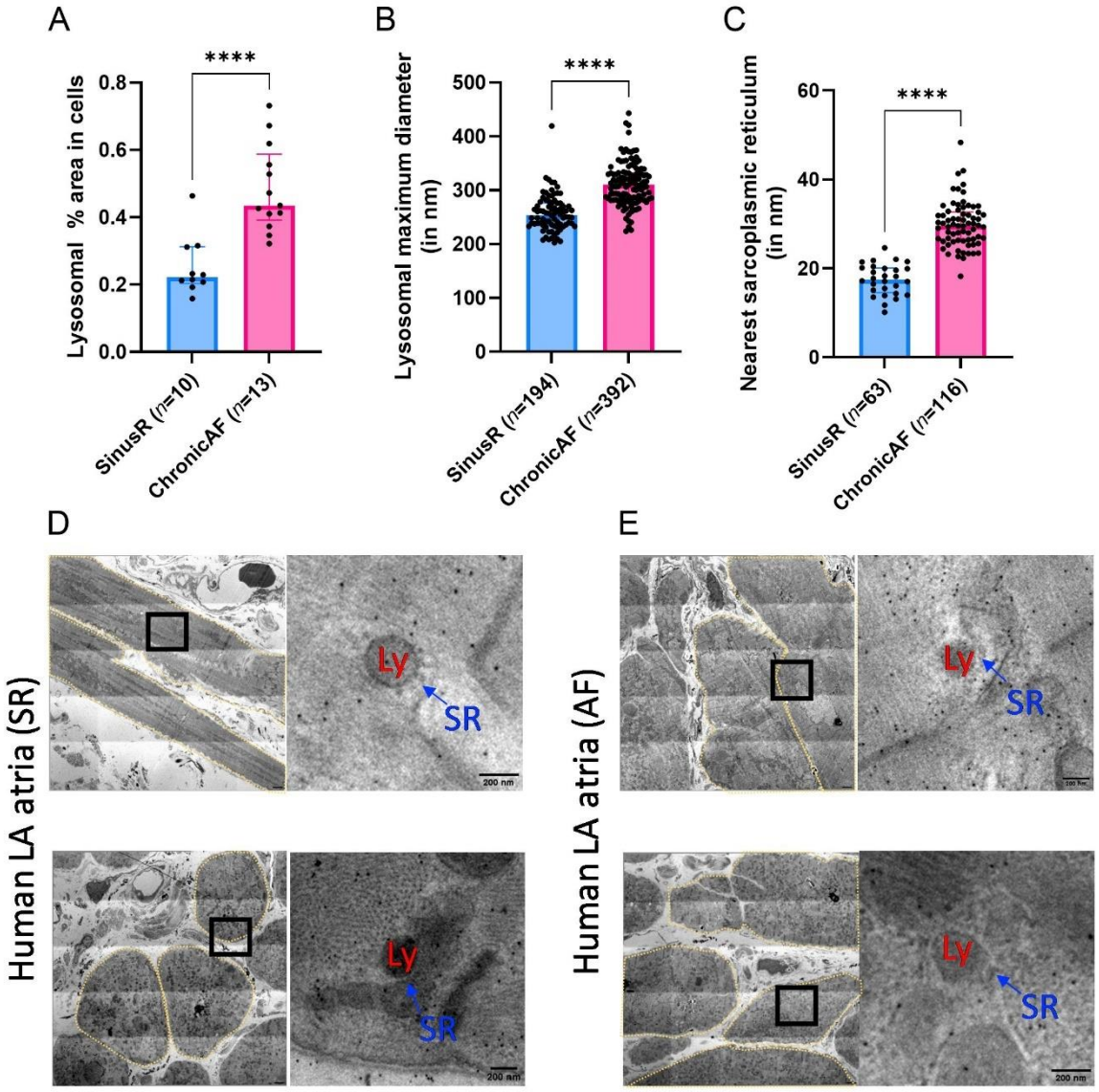

Figure 6.6: Qualitative measurements of EM images of lysosomal positioning in human left atrial tissue samples.

A, Partial cell area occupied by lysosomes in sinus rhythm patient (*N*=1 patient, *n*=10 cells) and in AF patient (*N*=1 patient, *n*=13 cells) atrial myocytes.
B, Lysosomal maximal diameter in sinus rhythm patient (*N*=1 patient, *n*=194 lysosomes) and in AF patient (*N*=1 patient, *n*=392 lysosomes).
C, Distance between lysosomes and SR in sinus rhythm patient (*N*=1 patient, *n*=63 measurement) and in AF patient (*N*=1 patient, *n*=129 measurements).
D, Representative EM image and zoom in of lysosomes and SR in samples from patient in sinus rhythm.
E, Representative EM image and zoom in of lysosomes and SR in samples from patient in atrial fibrillation.

Data are represented as mean ± SEM and were analysed using non-parametric Mann-Whitney U test. Scale bar represents 2 µm.

6.5 Closing remarks

In conclusion, my thesis has provided evidence that the calcium second messengers IP_3 and NAADP regulates the release of calcium from intracellular stores in atrial myocytes, acting through AC1 and AC8, influences cardiac function and pacemaking. I have studied two major aspects of calcium handling, IP_3-mediated calcium release from the SR and calcium release from lysosomes via NAADP signalling and their interactions in controlling cytosolic calcium movement in atrial myocytes. I studied these signalling pathways using different models including from single cells to whole in-tact tissue (using relevant small animal models including genetically altered mice) and tissue cultures to then progress to a hiPSC-CMs model to better understand and describe these pathways, a model of proposed mechanisms is presented in Figure 6.7. In addition, calcium stimulated isoforms of ACs, AC1 and AC8, in the atria were shown to regulate essential atrial function by being linked to IP_3 and NAADP calcium release. The precise mechanism of action of NAADP and its potential physiological importance in the atria warrants further investigation as it represents an important pathway for the control of atrial chronotropy and inotropy and may contribute to cardiac pathologies. The potential interaction between IP_3 and cAMP represents a novel mechanism that could explain how relatively few IP_3 receptors are able to influence calcium signals.

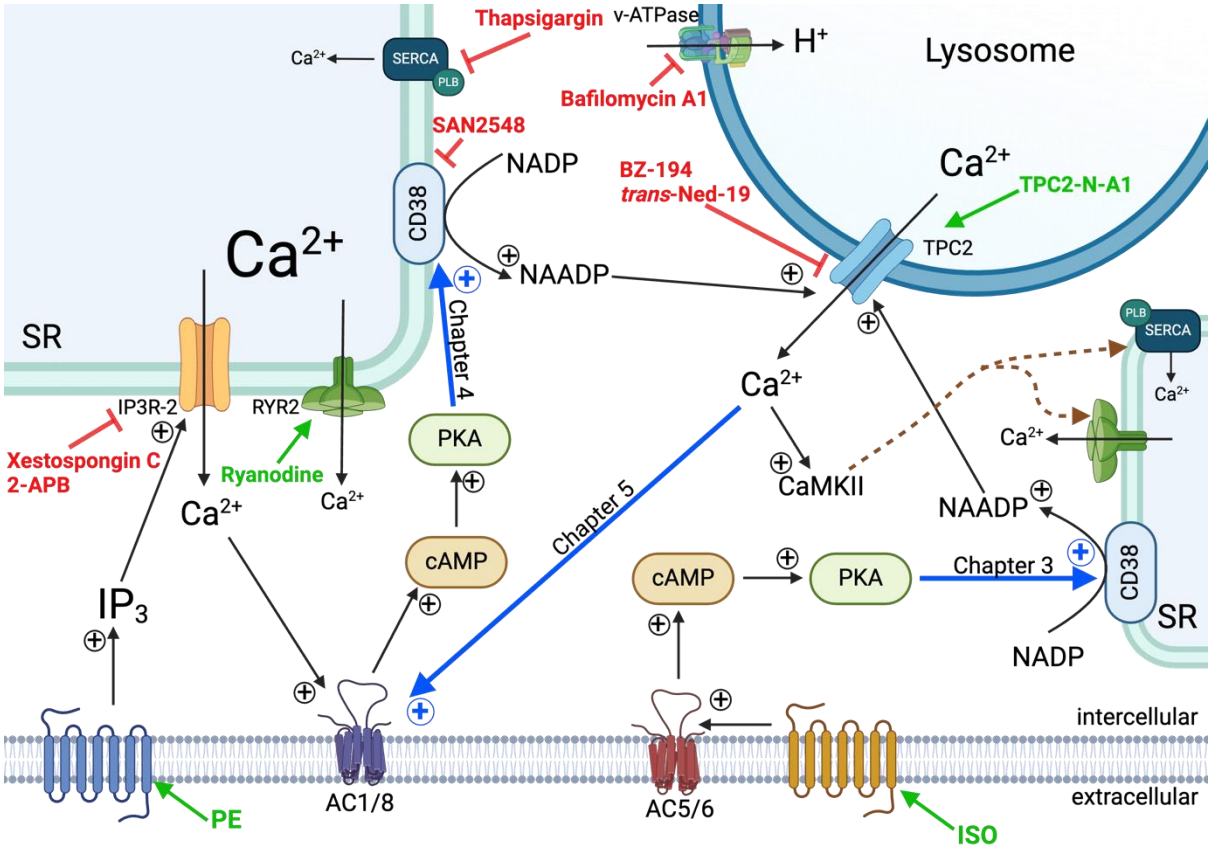

Figure 6.7: Scheme indicating potential mechanisms by which IP_3 and NAADP regulate the release of calcium from intracellular stores atrial myocytes and influence cardiac function and pacemaking. Representative scheme of proposed mechanisms by which activation of β-AR by isoprenaline lead to ACs activation leading to activation of PKA by cAMP and synthesis of NAADP by CD38 enhancing lysosomal calcium release by the action of NAADP on lysosomal TPC2 channels (Chapter 3). In parallel, activation of α1-AR by PE lead to increased atrial cytoplasmic calcium transients and cAMP production. Activation of α1-AR leads to elevated IP_3 resulting from cleavage of PIP_2 to DAG and IP_3 by PLC. IP_3 activation of IP_3R2 results in release of calcium from the SR, which subsequently leads to activation of AC8 or AC1, activation of PKA by cAMP (Chapter 4) and synthesis of NAADP by CD38 leading to the release of calcium from lysosomes also leading to activation of AC8 or AC1 (Chapter 5). The mechanism demonstrates the importance of lysosomal calcium in the α and β-adrenergic response. Calcium release from lysosomes could lead to CaMKII activation and increase cAMP production leading either to stimulation of an ACs or inhibition of a phosphodiesterase, as discussed above in 6.2.2. Study of CaMKII. Ca^{2+}, calcium.

7 References

Aarhus, R., R. M. Graeff, D. M. Dickey, T. F. Walseth, and H. C. Lee. 1995. 'ADP-ribosyl cyclase and CD38 catalyze the synthesis of a calcium-mobilizing metabolite from NADP', *J Biol Chem*, 270: 30327-33.

Alcalay, Y., E. Hochhauser, V. Kliminski, J. Dick, M. A. Zahalka, D. Parnes, H. Schlesinger, Z. Abassi, A. Shainberg, R. F. Schindler, T. Brand, and G. Kessler-Icekson. 2013. 'Popeye domain containing 1 (Popdc1/Bves) is a caveolae-associated protein involved in ischemia tolerance', *PLoS One*, 8: e71100.

Alexander, D. B., and G. S. Goldberg. 2003. 'Transfer of biologically important molecules between cells through gap junction channels', *Curr Med Chem*, 10: 2045-58.

Alobaida, M., and A. Alrumayh. 2021. 'Rate control strategies for atrial fibrillation', *Ann Med*, 53: 682-92.

Anderson, Robert H, Diane E Spicer, Anthony M Hlavacek, Andrew C Cook, and Carl L Backer. 2013. *Wilcox's surgical anatomy of the heart* (Cambridge University Press).

Aston, D., R. A. Capel, K. L. Ford, H. C. Christian, G. R. Mirams, E. A. Rog-Zielinska, P. Kohl, A. Galione, R. A. Burton, and D. A. Terrar. 2017. 'High resolution structural evidence suggests the Sarcoplasmic Reticulum forms microdomains with Acidic Stores (lysosomes) in the heart', *Sci Rep*, 7: 40620.

Atakpa, P., N. B. Thillaiappan, S. Mataragka, D. L. Prole, and C. W. Taylor. 2018. 'IP(3) Receptors Preferentially Associate with ER-Lysosome Contact Sites and Selectively Deliver Ca(2+) to Lysosomes', *Cell Rep*, 25: 3180-93.e7.

Ayagama, T., P. D. Charles, S. J. Bose, B. Boland, D. A. Priestman, D. Aston, G. Berridge, R. Fischer, A. P. Cribbs, Q. Song, G. R. Mirams, K. Amponsah, L. Heather, A. Galione, N. Herring, H. Kramer, R. A. Capel, F. M. Platt, U. Schotten, S. Verheule, and R. A. B. Burton. 2024. 'Compartmentalization proteomics revealed endolysosomal protein network changes in a goat model of atrial fibrillation', *iScience*, 27: 109609.

Ayagama, Thamali, Philip D. Charles, Samuel J. Bose, Barry Boland, David A. Priestman, Daniel Aston, Georgina Berridge, Roman Fisher, Adam P. Cribbs, Qianqian Song, Gary R. Mirams, Kwabena Amponsah, Lisa Heather, Antony Galione, Neil Herring, Holger Kramer, Rebecca A. Capel, Frances M. Platt, Ulrich Schotten, Sander Verheule, and Rebecca A. B. Burton. 'Compartmentalisation proteomics revealed endolysosomal protein network changes in a goat model of atrial fibrillation', *iScience*.

Azevedo, O., F. Cordeiro, M. F. Gago, G. Miltenberger-Miltenyi, C. Ferreira, N. Sousa, and D. Cunha. 2021. 'Fabry Disease and the Heart: A Comprehensive Review', *Int J Mol Sci*, 22.

Aziz, Q., Y. Li, and A. Tinker. 2018. 'Potassium channels in the sinoatrial node and their role in heart rate control', *Channels (Austin)*, 12: 356-66.

Bak, J., R. A. Billington, G. Timar, A. C. Dutton, and A. A. Genazzani. 2001. 'NAADP receptors are present and functional in the heart', *Curr Biol*, 11: 987-90.

Barker, C. J., and P. O. Berggren. 2013. 'New horizons in cellular regulation by inositol polyphosphates: insights from the pancreatic β-cell', *Pharmacol Rev*, 65: 641-69.

Beavo, J. A., N. L. Rogers, O. B. Crofford, C. E. Baird, J. G. Hardman, E. W. Sutherland, and E. V. Newman. 1971. 'Effects of phosphodiesterase inhibitors on cyclic AMP levels and on lipolysis', *Ann N Y Acad Sci*, 185: 129-36.

Benzoni, P., G. Campostrini, S. Landi, V. Bertini, E. Marchina, M. Iascone, G. Ahlberg, M. S. Olesen, E. Crescini, C. Mora, G. Bisleri, C. Muneretto, R. Ronca, M. Presta, P. L. Poliani, G. Piovani, R. Verardi, E. Di Pasquale, A. Consiglio, A. Raya, E. Torre, A. M. Lodrini, R. Milanesi, M. Rocchetti, M. Baruscotti, D. DiFrancesco, M. Memo, A. Barbuti, and P. Dell'Era. 2020. 'Human iPSC modelling of a familial form of atrial fibrillation reveals a gain of function of If and ICaL in patient-derived cardiomyocytes', *Cardiovasc Res*, 116: 1147-60.

Bernardes, T. P., R. D. Foresto, and G. M. Kirsztajn. 2020. 'Fabry disease: genetics, pathology, and treatment', *Rev Assoc Med Bras (1992)*, 66Suppl 1: s10-s16.

Berridge, M. J. 1984. 'Inositol trisphosphate and diacylglycerol as second messengers', *Biochem J*, 220: 345-60.

———. 2002. 'The endoplasmic reticulum: a multifunctional signaling organelle', *Cell Calcium*, 32: 235-49.

———. 2009. 'Inositol trisphosphate and calcium signalling mechanisms', *Biochim Biophys Acta*, 1793: 933-40.

———. 2016. 'The Inositol Trisphosphate/Calcium Signaling Pathway in Health and Disease', *Physiol Rev*, 96: 1261-96.

Berridge, M. J., and R. F. Irvine. 1989. 'Inositol phosphates and cell signalling', *Nature*, 341: 197-205.

Berridge, M. J., P. Lipp, and M. D. Bootman. 2000. 'The versatility and universality of calcium signalling', *Nat Rev Mol Cell Biol*, 1: 11-21.

Bers, D. M. 2002. 'Cardiac excitation-contraction coupling', *Nature*, 415: 198-205.

Bittihn, Philip. 2014. *Complex structure and dynamics of the heart* (Springer).

Blatter, L. A. 2017. 'The intricacies of atrial calcium cycling during excitation-contraction coupling', *J Gen Physiol*, 149: 857-65.

Bogdanov, K. Y., T. M. Vinogradova, and E. G. Lakatta. 2001. 'Sinoatrial nodal cell ryanodine receptor and Na(+)-Ca(2+) exchanger: molecular partners in pacemaker regulation', *Circ Res*, 88: 1254-8.

Bootman, M. D., and P. Lipp. 1999. 'Ringing changes to the 'bell-shaped curve'', *Curr Biol*, 9: R876-8.

Bose, S. J., M. J. Read, E. Akerman, R. A. Capel, T. Ayagama, A. Russell, D. A. Terrar, M. Zaccolo, and R. A. B. Burton. 2022. 'Inhibition of adenylyl cyclase 1 by ST034307 inhibits IP(3)-evoked changes in sino-atrial node beat rate', *Front Pharmacol*, 13: 951897.

Bose, Samuel J., Thamali Ayagama, and Rebecca A. B. Burton. 2022. 'Chapter 3 - Lysosomal proteases and their role in signaling pathways.' in André Zelanis (ed.), *Proteolytic Signaling in Health and Disease* (Academic Press).

Brailoiu, E., D. Churamani, X. Cai, M. G. Schrlau, G. C. Brailoiu, X. Gao, R. Hooper, M. J. Boulware, N. J. Dun, J. S. Marchant, and S. Patel. 2009. 'Essential requirement for two-pore channel 1 in NAADP-mediated calcium signaling', *J Cell Biol*, 186: 201-9.

Brailoiu, E., J. L. Hoard, C. M. Filipeanu, G. C. Brailoiu, S. L. Dun, S. Patel, and N. J. Dun. 2005. 'Nicotinic acid adenine dinucleotide phosphate potentiates neurite outgrowth', *J Biol Chem*, 280: 5646-50.

Brown, G. E., Y. D. Han, A. R. Michell, O. T. Ly, C. G. Vanoye, E. Spanghero, A. L. George, Jr., D. Darbar, and S. R. Khetani. 2024. 'Engineered cocultures of iPSC-derived atrial cardiomyocytes and atrial fibroblasts for modeling atrial fibrillation', *Sci Adv*, 10: eadg1222.

Brust, T. F., D. Alongkronrusmee, M. Soto-Velasquez, T. A. Baldwin, Z. Ye, M. Dai, C. W. Dessauer, R. M. van Rijn, and V. J. Watts. 2017. 'Identification of a selective small-molecule inhibitor of type 1 adenylyl cyclase activity with analgesic properties', *Sci Signal*, 10.

Bucchi, A., A. Tognati, R. Milanesi, M. Baruscotti, and D. DiFrancesco. 2006. 'Properties of ivabradine-induced block of HCN1 and HCN4 pacemaker channels', *J Physiol*, 572: 335-46.

Burgoyne, T., S. Patel, and E. R. Eden. 2015. 'Calcium signaling at ER membrane contact sites', *Biochim Biophys Acta*, 1853: 2012-7.

Burton, R. A. B., J. Tomek, C. M. Ambrosi, H. E. Larsen, A. R. Sharkey, R. A. Capel, A. D. Corbett, S. Bilton, A. Klimas, G. Stephens, M. Cremer, S. J. Bose, D. Li, G. Gallone, N. Herring, E. O. Mann, A. Kumar, H. Kramer, E. Entcheva, D. J. Paterson, and G. Bub. 2020. 'Optical Interrogation of Sympathetic Neuronal Effects on Macroscopic Cardiomyocyte Network Dynamics', *Iscience*, 23.

Burton, R. A., A. Klimas, C. M. Ambrosi, J. Tomek, A. Corbett, E. Entcheva, and G. Bub. 2015. 'Optical control of excitation waves in cardiac tissue', *Nat Photonics*, 9: 813-16.

Buxton, I. L., and L. L. Brunton. 1983. 'Compartments of cyclic AMP and protein kinase in mammalian cardiomyocytes', *J Biol Chem*, 258: 10233-9.

Calamaio, S., M. Serzanti, J. Boniotti, A. Fra, E. Garrafa, M. Cominelli, R. Verardi, P. L. Poliani, S. Dotti, R. Villa, G. Mazzoleni, P. Dell'Era, and N. Steimberg. 2023. 'Human iPSC-Derived 3D Hepatic Organoids in a Miniaturized Dynamic Culture System', *Biomedicines*, 11.

Calcraft, P. J., M. Ruas, Z. Pan, X. Cheng, A. Arredouani, X. Hao, J. Tang, K. Rietdorf, L. Teboul, K. T. Chuang, P. Lin, R. Xiao, C. Wang, Y. Zhu, Y. Lin, C. N. Wyatt, J. Parrington, J. Ma, A. M. Evans, A. Galione, and M. X. Zhu. 2009. 'NAADP mobilizes calcium from acidic organelles through two-pore channels', *Nature*, 459: 596-600.

Calejo, A. I., and K. Taskén. 2015. 'Targeting protein-protein interactions in complexes organized by A kinase anchoring proteins', *Front Pharmacol*, 6: 192.

Cang, C., Y. Zhou, B. Navarro, Y. J. Seo, K. Aranda, L. Shi, S. Battaglia-Hsu, I. Nissim, D. E. Clapham, and D. Ren. 2013. 'mTOR regulates lysosomal ATP-sensitive two-pore Na(+) channels to adapt to metabolic state', *Cell*, 152: 778-90.

Cannon, Walter Bradford, and CE Rosenberg. 1932. 'Homeostasis', *The wisdom of the body*: 263-86.

Capel, R. A., E. L. Bolton, W. K. Lin, D. Aston, Y. Wang, W. Liu, X. Wang, R. A. Burton, D. Bloor-Young, K. T. Shade, M. Ruas, J. Parrington, G. C. Churchill, M. Lei, A. Galione, and D. A. Terrar. 2015. 'Two-pore Channels (TPC2s) and Nicotinic Acid Adenine Dinucleotide Phosphate (NAADP) at Lysosomal-Sarcoplasmic Reticular Junctions Contribute to Acute and Chronic β-Adrenoceptor Signaling in the Heart', *J Biol Chem*, 290: 30087-98.

Capel, R. A., S. J. Bose, T. P. Collins, S. Rajasundaram, T. Ayagama, M. Zaccolo, R. B. Burton, and D. A. Terrar. 2021. 'IP(3)-mediated Ca(2+) release regulates atrial Ca(2+) transients and pacemaker function by stimulation of adenylyl cyclases', *Am J Physiol Heart Circ Physiol*, 320: H95-h107.

Capel, Rebecca A., Emily Akerman, Eva A. Rog-Zielinska, Annika Winbo, Daniel Aston, Razik Bin Abdul Mu-u-min, Matthew J. Read, Samuel J. Bose, Pawel Swietach, Jingyu Wang, Alexander D. Corbett, Andreas Koschinski, Johanna M. Montgomery, Florian Falter, Serena Calamaio, Dario Melgari, Rachele Prevostini, Ilaria Rivolta, Thamali Ayagama, Ifan Jenkin, Jillian N. Simon, Funsho E. Fakuade, Julius R. Pronto, Parveen Sharma, Qianqian Song, Martin J Booth, Frances M. Platt, Ming Lei, Svenja Hester, Roman Fischer, Niels Voigt, Ulrich Schotten, Sander Verheule, Antony Galione, Marco Keller, Franz

Bracher, Manuela Zaccolo, Derek A. Terrar, and Rebecca A. B. Burton. 2024. 'Lysosomal signalling pathways influence heart rhythm, and regulate atrial function', *bioRxiv*: 2024.06.10.597905.
Chandler, N. J., I. D. Greener, J. O. Tellez, S. Inada, H. Musa, P. Molenaar, D. Difrancesco, M. Baruscotti, R. Longhi, R. H. Anderson, R. Billeter, V. Sharma, D. C. Sigg, M. R. Boyett, and H. Dobrzynski. 2009. 'Molecular architecture of the human sinus node: insights into the function of the cardiac pacemaker', *Circulation*, 119: 1562-75.
Chao, Y. C., N. C. Surdo, S. Pantano, and M. Zaccolo. 2019. 'Imaging cAMP nanodomains in the heart', *Biochem Soc Trans*, 47: 1383-92.
Cheng, X., D. Shen, M. Samie, and H. Xu. 2010. 'Mucolipins: Intracellular TRPML1-3 channels', *FEBS Lett*, 584: 2013-21.
Christensen, K. A., J. T. Myers, and J. A. Swanson. 2002. 'pH-dependent regulation of lysosomal calcium in macrophages', *J Cell Sci*, 115: 599-607.
Churchill, G. C., and A. Galione. 2001. 'NAADP induces Ca2+ oscillations via a two-pool mechanism by priming IP3- and cADPR-sensitive Ca2+ stores', *Embo j*, 20: 2666-71.
Churchill, G. C., Y. Okada, J. M. Thomas, A. A. Genazzani, S. Patel, and A. Galione. 2002. 'NAADP mobilizes Ca(2+) from reserve granules, lysosome-related organelles, in sea urchin eggs', *Cell*, 111: 703-8.
Collins, T. P., R. Bayliss, G. C. Churchill, A. Galione, and D. A. Terrar. 2011. 'NAADP influences excitation-contraction coupling by releasing calcium from lysosomes in atrial myocytes', *Cell Calcium*, 50: 449-58.
Collins, T. P., and D. A. Terrar. 2012. 'Ca(2+)-stimulated adenylyl cyclases regulate the L-type Ca(2+) current in guinea-pig atrial myocytes', *J Physiol*, 590: 1881-93.
Conti, M., and J. Beavo. 2007. 'Biochemistry and physiology of cyclic nucleotide phosphodiesterases: essential components in cyclic nucleotide signaling', *Annu Rev Biochem*, 76: 481-511.
Cooper, D. M. 2003. 'Regulation and organization of adenylyl cyclases and cAMP', *Biochem J*, 375: 517-29.
Das, A., S. Banerjee, and S. C. Mandal. 2016. 'A simple method for Bachmann's bundle pacing with indigenous modification of J-stylet', *Indian Heart J*, 68: 678-84.
Davidson, S. M., K. Foote, S. Kunuthur, R. Gosain, N. Tan, R. Tyser, Y. J. Zhao, R. Graeff, A. Ganesan, M. R. Duchen, S. Patel, and D. M. Yellon. 2015. 'Inhibition of NAADP signalling on reperfusion protects the heart by preventing lethal calcium oscillations via two-pore channel 1 and opening of the mitochondrial permeability transition pore', *Cardiovasc Res*, 108: 357-66.
de Araujo, M. E. G., G. Liebscher, M. W. Hess, and L. A. Huber. 2020. 'Lysosomal size matters', *Traffic*, 21: 60-75.
De Duve, C., B. C. Pressman, R. Gianetto, R. Wattiaux, and F. Appelmans. 1955. 'Tissue fractionation studies. 6. Intracellular distribution patterns of enzymes in rat-liver tissue', *Biochem J*, 60: 604-17.
de Rooij, J., H. Rehmann, M. van Triest, R. H. Cool, A. Wittinghofer, and J. L. Bos. 2000. 'Mechanism of regulation of the Epac family of cAMP-dependent RapGEFs', *J Biol Chem*, 275: 20829-36.
de Rooij, J., F. J. Zwartkruis, M. H. Verheijen, R. H. Cool, S. M. Nijman, A. Wittinghofer, and J. L. Bos. 1998. 'Epac is a Rap1 guanine-nucleotide-exchange factor directly activated by cyclic AMP', *Nature*, 396: 474-7.
Delcarpio, J. B., W. C. Claycomb, and R. L. Moses. 1989. 'Ultrastructural morphometric analysis of cultured neonatal and adult rat ventricular cardiac muscle cells', *Am J Anat*, 186: 335-45.
Desplantez, T., E. Dupont, N. J. Severs, and R. Weingart. 2007. 'Gap junction channels and cardiac impulse propagation', *J Membr Biol*, 218: 13-28.
Devalla, H. D., V. Schwach, J. W. Ford, J. T. Milnes, S. El-Haou, C. Jackson, K. Gkatzis, D. A. Elliott, S. M. Chuva de Sousa Lopes, C. L. Mummery, A. O. Verkerk, and R. Passier. 2015. 'Atrial-like cardiomyocytes from human pluripotent stem cells are a robust preclinical model for assessing atrial-selective pharmacology', *EMBO Mol Med*, 7: 394-410.
DiFrancesco, D. 1991. 'The contribution of the 'pacemaker' current (if) to generation of spontaneous activity in rabbit sino-atrial node myocytes', *J Physiol*, 434: 23-40.
———. 1993. 'Pacemaker mechanisms in cardiac tissue', *Annu Rev Physiol*, 55: 455-72.
DiFrancesco, D., and P. Tortora. 1991. 'Direct activation of cardiac pacemaker channels by intracellular cyclic AMP', *Nature*, 351: 145-7.
Dodge-Kafka, K. L., L. Langeberg, and J. D. Scott. 2006. 'Compartmentation of cyclic nucleotide signaling in the heart: the role of A-kinase anchoring proteins', *Circ Res*, 98: 993-1001.
Dong, X. P., D. Shen, X. Wang, T. Dawson, X. Li, Q. Zhang, X. Cheng, Y. Zhang, L. S. Weisman, M. Delling, and H. Xu. 2010. 'PI(3,5)P(2) controls membrane trafficking by direct activation of mucolipin Ca(2+) release channels in the endolysosome', *Nat Commun*, 1: 38.
Du, C., X. Guan, and J. Yan. 2022. 'Two-pore channel blockade by phosphoinositide kinase inhibitors YM201636 and PI-103 determined by a histidine residue near pore-entrance', *Commun Biol*, 5: 738.
Eskelinen, E. L. 2006. 'Roles of LAMP-1 and LAMP-2 in lysosome biogenesis and autophagy', *Mol Aspects Med*, 27: 495-502.

Feske, S. 2007. 'Calcium signalling in lymphocyte activation and disease', *Nat Rev Immunol*, 7: 690-702.
Fischmeister, R., L. R. Castro, A. Abi-Gerges, F. Rochais, J. Jurevicius, J. Leroy, and G. Vandecasteele. 2006. 'Compartmentation of cyclic nucleotide signaling in the heart: the role of cyclic nucleotide phosphodiesterases', *Circ Res*, 99: 816-28.
Foskett, J. K., C. White, K. H. Cheung, and D. O. Mak. 2007. 'Inositol trisphosphate receptor Ca2+ release channels', *Physiol Rev*, 87: 593-658.
Frisk, M., J. T. Koivumäki, P. A. Norseng, M. M. Maleckar, O. M. Sejersted, and W. E. Louch. 2014. 'Variable t-tubule organization and Ca2+ homeostasis across the atria', *Am J Physiol Heart Circ Physiol*, 307: H609-20.
Froese, A., S. S. Breher, C. Waldeyer, R. F. Schindler, V. O. Nikolaev, S. Rinné, E. Wischmeyer, J. Schlueter, J. Becher, S. Simrick, F. Vauti, J. Kuhtz, P. Meister, S. Kreissl, A. Torlopp, S. K. Liebig, S. Laakmann, T. D. Müller, J. Neumann, J. Stieber, A. Ludwig, S. K. Maier, N. Decher, H. H. Arnold, P. Kirchhof, L. Fabritz, and T. Brand. 2012. 'Popeye domain containing proteins are essential for stress-mediated modulation of cardiac pacemaking in mice', *J Clin Invest*, 122: 1119-30.
Fye, W. B. 1994. 'A history of the origin, evolution, and impact of electrocardiography', *Am J Cardiol*, 73: 937-49.
Galione, A. 2011. 'NAADP receptors', *Cold Spring Harb Perspect Biol*, 3: a004036.
———. 2015. 'A primer of NAADP-mediated Ca(2+) signalling: From sea urchin eggs to mammalian cells', *Cell Calcium*, 58: 27-47.
Galione, A., A. M. Evans, J. Ma, J. Parrington, A. Arredouani, X. Cheng, and M. X. Zhu. 2009. 'The acid test: the discovery of two-pore channels (TPCs) as NAADP-gated endolysosomal Ca(2+) release channels', *Pflugers Arch*, 458: 869-76.
Galione, A., and O. H. Petersen. 2005. 'The NAADP receptor: new receptors or new regulation?', *Mol Interv*, 5: 73-9.
García-Rúa, V., S. Feijóo-Bandín, D. Rodríguez-Penas, A. Mosquera-Leal, E. Abu-Assi, A. Beiras, L. María Seoane, P. Lear, J. Parrington, M. Portolés, E. Roselló-Lletí, M. Rivera, O. Gualillo, V. Parra, J. A. Hill, B. Rothermel, J. R. González-Juanatey, and F. Lago. 2016. 'Endolysosomal two-pore channels regulate autophagy in cardiomyocytes', *J Physiol*, 594: 3061-77.
Garrity, A. G., W. Wang, C. M. Collier, S. A. Levey, Q. Gao, and H. Xu. 2016. 'The endoplasmic reticulum, not the pH gradient, drives calcium refilling of lysosomes', *Elife*, 5.
Georget, M., P. Mateo, G. Vandecasteele, J. Jurevicius, L. Lipskaia, N. Defer, J. Hanoune, J. Hoerter, and R. Fischmeister. 2002. 'Augmentation of cardiac contractility with no change in L-type Ca2+ current in transgenic mice with a cardiac-directed expression of the human adenylyl cyclase type 8 (AC8)', *Faseb j*, 16: 1636-8.
Gerndt, S., C. C. Chen, Y. K. Chao, Y. Yuan, S. Burgstaller, A. Scotto Rosato, E. Krogsaeter, N. Urban, K. Jacob, O. N. P. Nguyen, M. T. Miller, M. Keller, A. M. Vollmar, T. Gudermann, S. Zierler, J. Schredelseker, M. Schaefer, M. Biel, R. Malli, C. Wahl-Schott, F. Bracher, S. Patel, and C. Grimm. 2020. 'Agonist-mediated switching of ion selectivity in TPC2 differentially promotes lysosomal function', *Elife*, 9.
'Global, regional, and national age-sex-specific mortality for 282 causes of death in 195 countries and territories, 1980-2017: a systematic analysis for the Global Burden of Disease Study 2017'. 2018. *Lancet*, 392: 1736-88.
Gloerich, M., and J. L. Bos. 2010. 'Epac: defining a new mechanism for cAMP action', *Annu Rev Pharmacol Toxicol*, 50: 355-75.
Guellich, A., H. Mehel, and R. Fischmeister. 2014. 'Cyclic AMP synthesis and hydrolysis in the normal and failing heart', *Pflugers Arch*, 466: 1163-75.
Gul, R., D. R. Park, A. I. Shawl, S. Y. Im, T. S. Nam, S. H. Lee, J. K. Ko, K. Y. Jang, D. Kim, and U. H. Kim. 2016. 'Nicotinic Acid Adenine Dinucleotide Phosphate (NAADP) and Cyclic ADP-Ribose (cADPR) Mediate Ca2+ Signaling in Cardiac Hypertrophy Induced by β-Adrenergic Stimulation', *PLoS One*, 11: e0149125.
Hall, J.E. 2019. *Guyton and Hall Textbook of Medical Physiology (13th Edition)* (Beijing da xue yi xue chu ban she).
Hanoune, J., and N. Defer. 2001. 'Regulation and role of adenylyl cyclase isoforms', *Annu Rev Pharmacol Toxicol*, 41: 145-74.
Haug, L. S., A. C. Ostvold, R. F. Cowburn, A. Garlind, B. Winblad, N. Bogdanovich, and S. I. Walaas. 1996. 'Decreased inositol (1,4,5)-trisphosphate receptor levels in Alzheimer's disease cerebral cortex: selectivity of changes and possible correlation to pathological severity', *Neurodegeneration*, 5: 169-76.
Heijman, J., N. Voigt, S. Nattel, and D. Dobrev. 2014. 'Cellular and molecular electrophysiology of atrial fibrillation initiation, maintenance, and progression', *Circ Res*, 114: 1483-99.
Hellmich, M. R., and F. Strumwasser. 1991. 'Purification and characterization of a molluscan egg-specific NADase, a second-messenger enzyme', *Cell Regul*, 2: 193-202.

Hofmann, F., J. A. Beavo, P. J. Bechtel, and E. G. Krebs. 1975. 'Comparison of adenosine 3':5'-monophosphate-dependent protein kinases from rabbit skeletal and bovine heart muscle', *J Biol Chem*, 250: 7795-801.
Husser, Daniela, David S. Cannom, Anil K. Bhandari, Martin Stridh, Leif Sörnmo, S. Bertil Olsson, and Andreas Bollmann. 2007. 'Electrocardiographic characteristics of fibrillatory waves in new-onset atrial fibrillation', *EP Europace*, 9: 638-42.
Inui, M., A. Saito, and S. Fleischer. 1987. 'Purification of the ryanodine receptor and identity with feet structures of junctional terminal cisternae of sarcoplasmic reticulum from fast skeletal muscle', *J Biol Chem*, 262: 1740-7.
Ishibashi, K., M. Suzuki, and M. Imai. 2000. 'Molecular cloning of a novel form (two-repeat) protein related to voltage-gated sodium and calcium channels', *Biochem Biophys Res Commun*, 270: 370-6.
Iwasaki, Y. K., K. Nishida, T. Kato, and S. Nattel. 2011. 'Atrial fibrillation pathophysiology: implications for management', *Circulation*, 124: 2264-74.
Jackson, D. G., and J. I. Bell. 1990. 'Isolation of a cDNA encoding the human CD38 (T10) molecule, a cell surface glycoprotein with an unusual discontinuous pattern of expression during lymphocyte differentiation', *J Immunol*, 144: 2811-5.
Ji, Q., H. Liu, Y. Mei, X. Wang, J. Feng, and W. Ding. 2013. 'Expression changes of ionic channels in early phase of cultured rat atrial myocytes induced by rapid pacing', *J Cardiothorac Surg*, 8: 194.
Ji, T. H., M. Grossmann, and I. Ji. 1998. 'G protein-coupled receptors. I. Diversity of receptor-ligand interactions', *J Biol Chem*, 273: 17299-302.
Ju, Y. K., J. Liu, B. H. Lee, D. Lai, E. A. Woodcock, M. Lei, M. B. Cannell, and D. G. Allen. 2011. 'Distribution and functional role of inositol 1,4,5-trisphosphate receptors in mouse sinoatrial node', *Circ Res*, 109: 848-57.
Kalisch-Smith, Jacinta I., Nikita Ved, Dorota Szumska, Jacob Munro, Michael Troup, Shelley E. Harris, Helena Rodriguez-Caro, Aimée Jacquemot, Jack J. Miller, Eleanor M. Stuart, Magda Wolna, Emily Hardman, Fabrice Prin, Eva Lana-Elola, Rifdat Aoidi, Elizabeth M. C. Fisher, Victor L. J. Tybulewicz, Timothy J. Mohun, Samira Lakhal-Littleton, Sarah De Val, Eleni Giannoulatou, and Duncan B. Sparrow. 2021. 'Maternal iron deficiency perturbs embryonic cardiovascular development in mice', *Nature Communications*, 12: 3447.
Kannt, A., K. Sicka, K. Kroll, D. Kadereit, and H. Gögelein. 2012. 'Selective inhibitors of cardiac ADPR cyclase as novel anti-arrhythmic compounds', *Naunyn Schmiedebergs Arch Pharmacol*, 385: 717-27.
Kapoor, N., A. Tran, J. Kang, R. Zhang, K. D. Philipson, and J. I. Goldhaber. 2015. 'Regulation of calcium clock-mediated pacemaking by inositol-1,4,5-trisphosphate receptors in mouse sinoatrial nodal cells', *J Physiol*, 593: 2649-63.
Katz, Arnold M. 2010. *Physiology of the Heart* (Lippincott Williams & Wilkins).
Kawasaki, H., G. M. Springett, N. Mochizuki, S. Toki, M. Nakaya, M. Matsuda, D. E. Housman, and A. M. Graybiel. 1998. 'A family of cAMP-binding proteins that directly activate Rap1', *Science*, 282: 2275-9.
Keravis, T., and C. Lugnier. 2012. 'Cyclic nucleotide phosphodiesterase (PDE) isozymes as targets of the intracellular signalling network: benefits of PDE inhibitors in various diseases and perspectives for future therapeutic developments', *Br J Pharmacol*, 165: 1288-305.
Kirillova, A., L. Han, H. Liu, and B. Kühn. 2021. 'Polyploid cardiomyocytes: implications for heart regeneration', *Development*, 148.
Klarenbeek, J., J. Goedhart, A. van Batenburg, D. Groenewald, and K. Jalink. 2015. 'Fourth-generation epac-based FRET sensors for cAMP feature exceptional brightness, photostability and dynamic range: characterization of dedicated sensors for FLIM, for ratiometry and with high affinity', *PLoS One*, 10: e0122513.
Kockskämper, J., L. Seidlmayer, S. Walther, K. Hellenkamp, L. S. Maier, and B. Pieske. 2008. 'Endothelin-1 enhances nuclear Ca2+ transients in atrial myocytes through Ins(1,4,5)P3-dependent Ca2+ release from perinuclear Ca2+ stores', *J Cell Sci*, 121: 186-95.
Kockskämper, J., A. V. Zima, H. L. Roderick, B. Pieske, L. A. Blatter, and M. D. Bootman. 2008. 'Emerging roles of inositol 1,4,5-trisphosphate signaling in cardiac myocytes', *J Mol Cell Cardiol*, 45: 128-47.
Korhonen, Topi, Sandra L. Hänninen, and Pasi Tavi. 2009. 'Model of Excitation-Contraction Coupling of Rat Neonatal Ventricular Myocytes', *Biophysical Journal*, 96: 1189-209.
Koschinski, A., and M. Zaccolo. 2017. 'Activation of PKA in cell requires higher concentration of cAMP than in vitro: implications for compartmentalization of cAMP signalling', *Sci Rep*, 7: 14090.
Kottkamp, H., R. Bender, and J. Berg. 2015. 'Catheter ablation of atrial fibrillation: how to modify the substrate?', *J Am Coll Cardiol*, 65: 196-206.
Krupinski, J., F. Coussen, H. A. Bakalyar, W. J. Tang, P. G. Feinstein, K. Orth, C. Slaughter, R. R. Reed, and A. G. Gilman. 1989. 'Adenylyl cyclase amino acid sequence: possible channel- or transporter-like structure', *Science*, 244: 1558-64.

Lakatta, E. G., and D. DiFrancesco. 2009. 'What keeps us ticking: a funny current, a calcium clock, or both?', *J Mol Cell Cardiol*, 47: 157-70.
Lee, H. C., and R. Aarhus. 1995. 'A derivative of NADP mobilizes calcium stores insensitive to inositol trisphosphate and cyclic ADP-ribose', *J Biol Chem*, 270: 2152-7.
———. 2000. 'Functional visualization of the separate but interacting calcium stores sensitive to NAADP and cyclic ADP-ribose', *J Cell Sci*, 113 Pt 24: 4413-20.
Lehman, S. J., C. Crocini, and L. A. Leinwand. 2022. 'Targeting the sarcomere in inherited cardiomyopathies', *Nat Rev Cardiol*, 19: 353-63.
Levick, J Rodney. 2013. *An introduction to cardiovascular physiology* (Butterworth-Heinemann).
Lewis, A. M., P. K. Aley, A. Roomi, J. M. Thomas, R. Masgrau, C. Garnham, K. Shipman, C. Paramore, D. Bloor-Young, L. E. Sanders, D. A. Terrar, A. Galione, and G. C. Churchill. 2012. 'β-Adrenergic receptor signaling increases NAADP and cADPR levels in the heart', *Biochem Biophys Res Commun*, 427: 326-9.
Lezoualc'h, F., L. Fazal, M. Laudette, and C. Conte. 2016. 'Cyclic AMP Sensor EPAC Proteins and Their Role in Cardiovascular Function and Disease', *Circ Res*, 118: 881-97.
Lezoualc'h, F., M. Métrich, I. Hmitou, N. Duquesnes, and E. Morel. 2008. 'Small GTP-binding proteins and their regulators in cardiac hypertrophy', *J Mol Cell Cardiol*, 44: 623-32.
Li, P., M. Gu, and H. Xu. 2019. 'Lysosomal Ion Channels as Decoders of Cellular Signals', *Trends Biochem Sci*, 44: 110-24.
Li, X., N. Rydzewski, A. Hider, X. Zhang, J. Yang, W. Wang, Q. Gao, X. Cheng, and H. Xu. 2016. 'A molecular mechanism to regulate lysosome motility for lysosome positioning and tubulation', *Nat Cell Biol*, 18: 404-17.
Lievremont, J. P., G. S. Bird, and J. W. Putney, Jr. 2005. 'Mechanism of inhibition of TRPC cation channels by 2-aminoethoxydiphenylborane', *Mol Pharmacol*, 68: 758-62.
Lin, W. K., E. L. Bolton, W. A. Cortopassi, Y. Wang, F. O'Brien, M. Maciejewska, M. P. Jacobson, C. Garnham, M. Ruas, J. Parrington, M. Lei, R. Sitsapesan, A. Galione, and D. A. Terrar. 2017. 'Synthesis of the Ca(2+)-mobilizing messengers NAADP and cADPR by intracellular CD38 enzyme in the mouse heart: Role in β-adrenoceptor signaling', *J Biol Chem*, 292: 13243-57.
Lipp, P., M. Laine, S. C. Tovey, K. M. Burrell, M. J. Berridge, W. Li, and M. D. Bootman. 2000. 'Functional InsP3 receptors that may modulate excitation-contraction coupling in the heart', *Curr Biol*, 10: 939-42.
Lloyd-Evans, E., A. J. Morgan, X. He, D. A. Smith, E. Elliot-Smith, D. J. Sillence, G. C. Churchill, E. H. Schuchman, A. Galione, and F. M. Platt. 2008. 'Niemann-Pick disease type C1 is a sphingosine storage disease that causes deregulation of lysosomal calcium', *Nat Med*, 14: 1247-55.
Lloyd-Evans, E., and F. M. Platt. 2011. 'Lysosomal Ca(2+) homeostasis: role in pathogenesis of lysosomal storage diseases', *Cell Calcium*, 50: 200-5.
Logantha, S. J., S. F. Cruickshank, E. G. Rowan, and R. M. Drummond. 2010. 'Spontaneous and electrically evoked Ca2+ transients in cardiomyocytes of the rat pulmonary vein', *Cell Calcium*, 48: 150-60.
Macgregor, A., M. Yamasaki, S. Rakovic, L. Sanders, R. Parkesh, G. C. Churchill, A. Galione, and D. A. Terrar. 2007. 'NAADP controls cross-talk between distinct Ca2+ stores in the heart', *J Biol Chem*, 282: 15302-11.
Mackenzie, L., M. D. Bootman, M. Laine, M. J. Berridge, J. Thuring, A. Holmes, W. H. Li, and P. Lipp. 2002. 'The role of inositol 1,4,5-trisphosphate receptors in Ca(2+) signalling and the generation of arrhythmias in rat atrial myocytes', *J Physiol*, 541: 395-409.
Macquaide, N., H. T. Tuan, J. Hotta, W. Sempels, I. Lenaerts, P. Holemans, J. Hofkens, M. S. Jafri, R. Willems, and K. R. Sipido. 2015. 'Ryanodine receptor cluster fragmentation and redistribution in persistent atrial fibrillation enhance calcium release', *Cardiovasc Res*, 108: 387-98.
Maeda, N., T. Kawasaki, S. Nakade, N. Yokota, T. Taguchi, M. Kasai, and K. Mikoshiba. 1991. 'Structural and functional characterization of inositol 1,4,5-trisphosphate receptor channel from mouse cerebellum', *J Biol Chem*, 266: 1109-16.
Maltsev, V. A., and E. G. Lakatta. 2012. 'The funny current in the context of the coupled-clock pacemaker cell system', *Heart Rhythm*, 9: 302-7.
Maltsev, V. A., T. M. Vinogradova, and E. G. Lakatta. 2006. 'The emergence of a general theory of the initiation and strength of the heartbeat', *J Pharmacol Sci*, 100: 338-69.
Mattick, P., J. Parrington, E. Odia, A. Simpson, T. Collins, and D. Terrar. 2007. 'Ca2+-stimulated adenylyl cyclase isoform AC1 is preferentially expressed in guinea-pig sino-atrial node cells and modulates the I(f) pacemaker current', *J Physiol*, 582: 1195-203.
Meissner, G. 1986. 'Ryanodine activation and inhibition of the Ca2+ release channel of sarcoplasmic reticulum', *J Biol Chem*, 261: 6300-6.

Meng, Z., R. A. Capel, S. J. Bose, E. Bosch, S. de Jong, R. Planque, A. Galione, R. A. B. Burton, and A. Bueno-Orovio. 2023. 'Lysosomal calcium loading promotes spontaneous calcium release by potentiating ryanodine receptors', *Biophys J*, 122: 3044-59.

Michaud, M., W. Mauhin, N. Belmatoug, N. Bedreddine, R. Garnotel, F. Catros, O. Lidove, and F. Gaches. 2021. '[Fabry disease: A review]', *Rev Med Interne*, 42: 110-19.

Mizunami, M., Y. Nemoto, K. Terao, Y. Hamanaka, and Y. Matsumoto. 2014. 'Roles of calcium/calmodulin-dependent kinase II in long-term memory formation in crickets', *PLoS One*, 9: e107442.

Moen, J. M., M. G. Matt, C. Ramirez, K. V. Tarasov, K. Chakir, Y. S. Tarasova, Y. Lukyanenko, K. Tsutsui, O. Monfredi, C. H. Morrell, S. Tagirova, Y. Yaniv, T. Huynh, K. Pacak, I. Ahmet, and E. G. Lakatta. 2019. 'Overexpression of a Neuronal Type Adenylyl Cyclase (Type 8) in Sinoatrial Node Markedly Impacts Heart Rate and Rhythm', *Front Neurosci*, 13: 615.

Mons, N., L. Decorte, R. Jaffard, and D. M. Cooper. 1998. 'Ca2+-sensitive adenylyl cyclases, key integrators of cellular signalling', *Life Sci*, 62: 1647-52.

Morel, E., A. Marcantoni, M. Gastineau, R. Birkedal, F. Rochais, A. Garnier, A. M. Lompré, G. Vandecasteele, and F. Lezoualc'h. 2005. 'cAMP-binding protein Epac induces cardiomyocyte hypertrophy', *Circ Res*, 97: 1296-304.

Morgan, A. J., F. M. Platt, E. Lloyd-Evans, and A. Galione. 2011. 'Molecular mechanisms of endolysosomal Ca2+ signalling in health and disease', *Biochem J*, 439: 349-74.

Motiejunaite, J., L. Amar, and E. Vidal-Petiot. 2021. 'Adrenergic receptors and cardiovascular effects of catecholamines', *Ann Endocrinol (Paris)*, 82: 193-97.

Moulder, K. L., X. Jiang, C. Chang, A. A. Taylor, A. M. Benz, A. C. Conti, L. J. Muglia, and S. Mennerick. 2008. 'A specific role for Ca2+-dependent adenylyl cyclases in recovery from adaptive presynaptic silencing', *J Neurosci*, 28: 5159-68.

Muglia, L. M., M. L. Schaefer, S. K. Vogt, G. Gurtner, A. Imamura, and L. J. Muglia. 1999. 'The 5'-flanking region of the mouse adenylyl cyclase type VIII gene imparts tissue-specific expression in transgenic mice', *J Neurosci*, 19: 2051-8.

Musheshe, N., M. J. Lobo, M. Schmidt, and M. Zaccolo. 2018. 'Targeting FRET-Based Reporters for cAMP and PKA Activity Using AKAP79', *Sensors (Basel)*, 18.

Nakayama, H., I. Bodi, M. Maillet, J. DeSantiago, T. L. Domeier, K. Mikoshiba, J. N. Lorenz, L. A. Blatter, D. M. Bers, and J. D. Molkentin. 2010. 'The IP3 receptor regulates cardiac hypertrophy in response to select stimuli', *Circ Res*, 107: 659-66.

Nattel, S., and D. Dobrev. 2012. 'The multidimensional role of calcium in atrial fibrillation pathophysiology: mechanistic insights and therapeutic opportunities', *Eur Heart J*, 33: 1870-7.

Nattel, S., E. Guasch, I. Savelieva, F. G. Cosio, I. Valverde, J. L. Halperin, J. M. Conroy, S. M. Al-Khatib, P. L. Hess, P. Kirchhof, J. De Bono, G. Y. Lip, A. Banerjee, J. Ruskin, D. Blendea, and A. J. Camm. 2014. 'Early management of atrial fibrillation to prevent cardiovascular complications', *Eur Heart J*, 35: 1448-56.

Nattel, S., J. Heijman, L. Zhou, and D. Dobrev. 2020. 'Molecular Basis of Atrial Fibrillation Pathophysiology and Therapy: A Translational Perspective', *Circ Res*, 127: 51-72.

Nebel, M., A. P. Schwoerer, D. Warszta, C. C. Siebrands, A. C. Limbrock, J. M. Swarbrick, R. Fliegert, K. Weber, S. Bruhn, M. Hohenegger, A. Geisler, L. Herich, S. Schlegel, L. Carrier, T. Eschenhagen, B. V. Potter, H. Ehmke, and A. H. Guse. 2013. 'Nicotinic acid adenine dinucleotide phosphate (NAADP)-mediated calcium signaling and arrhythmias in the heart evoked by β-adrenergic stimulation', *J Biol Chem*, 288: 16017-30.

Noble, D. 1960. 'Cardiac action and pacemaker potentials based on the Hodgkin-Huxley equations', *Nature*, 188: 495-7.

Ogunbayo, O. A., J. Duan, J. Xiong, Q. Wang, X. Feng, J. Ma, M. X. Zhu, and A. M. Evans. 2018. 'mTORC1 controls lysosomal Ca(2+) release through the two-pore channel TPC2', *Sci Signal*, 11.

Ohkuma, S., Y. Moriyama, and T. Takano. 1982. 'Identification and characterization of a proton pump on lysosomes by fluorescein-isothiocyanate-dextran fluorescence', *Proc Natl Acad Sci U S A*, 79: 2758-62.

Patel, S. 2015. 'Function and dysfunction of two-pore channels', *Sci Signal*, 8: re7.

Patel, S., G. C. Churchill, T. Sharp, and A. Galione. 2000. 'Widespread distribution of binding sites for the novel Ca2+-mobilizing messenger, nicotinic acid adenine dinucleotide phosphate, in the brain', *J Biol Chem*, 275: 36495-7.

Patel, S., and R. Docampo. 2010. 'Acidic calcium stores open for business: expanding the potential for intracellular Ca2+ signaling', *Trends Cell Biol*, 20: 277-86.

Peiter, E., F. J. Maathuis, L. N. Mills, H. Knight, J. Pelloux, A. M. Hetherington, and D. Sanders. 2005. 'The vacuolar Ca2+-activated channel TPC1 regulates germination and stomatal movement', *Nature*, 434: 404-8.

Pereira, L., H. Cheng, D. H. Lao, L. Na, R. J. van Oort, J. H. Brown, X. H. Wehrens, J. Chen, and D. M. Bers. 2013. 'Epac2 mediates cardiac β1-adrenergic-dependent sarcoplasmic reticulum Ca2+ leak and arrhythmia', *Circulation*, 127: 913-22.

Pereira, L., M. Métrich, M. Fernández-Velasco, A. Lucas, J. Leroy, R. Perrier, E. Morel, R. Fischmeister, S. Richard, J. P. Bénitah, F. Lezoualc'h, and A. M. Gómez. 2007. 'The cAMP binding protein Epac modulates Ca2+ sparks by a Ca2+/calmodulin kinase signalling pathway in rat cardiac myocytes', *J Physiol*, 583: 685-94.

Pfleger, J., K. Gresham, and W. J. Koch. 2019. 'G protein-coupled receptor kinases as therapeutic targets in the heart', *Nat Rev Cardiol*, 16: 612-22.

Pinto, A. R., A. Ilinykh, M. J. Ivey, J. T. Kuwabara, M. L. D'Antoni, R. Debuque, A. Chandran, L. Wang, K. Arora, N. A. Rosenthal, and M. D. Tallquist. 2016. 'Revisiting Cardiac Cellular Composition', *Circ Res*, 118: 400-9.

Pitt, S. J., T. M. Funnell, M. Sitsapesan, E. Venturi, K. Rietdorf, M. Ruas, A. Ganesan, R. Gosain, G. C. Churchill, M. X. Zhu, J. Parrington, A. Galione, and R. Sitsapesan. 2010. 'TPC2 is a novel NAADP-sensitive Ca2+ release channel, operating as a dual sensor of luminal pH and Ca2+', *J Biol Chem*, 285: 35039-46.

Ponsioen, B., J. Zhao, J. Riedl, F. Zwartkruis, G. van der Krogt, M. Zaccolo, W. H. Moolenaar, J. L. Bos, and K. Jalink. 2004. 'Detecting cAMP-induced Epac activation by fluorescence resonance energy transfer: Epac as a novel cAMP indicator', *EMBO Rep*, 5: 1176-80.

Rall, T. W., and E. W. Sutherland. 1958. 'Formation of a cyclic adenine ribonucleotide by tissue particles', *J Biol Chem*, 232: 1065-76.

Reese, D. E., M. Zavaljevski, N. L. Streiff, and D. Bader. 1999. 'bves: A novel gene expressed during coronary blood vessel development', *Dev Biol*, 209: 159-71.

Rehfeld, Anders, Malin Nylander, and Kirstine Karnov. 2017. 'The Cardiovascular System.' in Anders Rehfeld, Malin Nylander and Kirstine Karnov (eds.), *Compendium of Histology: A Theoretical and Practical Guide* (Springer International Publishing: Cham).

Richards, M. A., J. D. Clarke, P. Saravanan, N. Voigt, D. Dobrev, D. A. Eisner, A. W. Trafford, and K. M. Dibb. 2011. 'Transverse tubules are a common feature in large mammalian atrial myocytes including human', *Am J Physiol Heart Circ Physiol*, 301: H1996-2005.

Ringer, S. 1883. 'A third contribution regarding the Influence of the Inorganic Constituents of the Blood on the Ventricular Contraction', *J Physiol*, 4: 222-5.

Ross, C. A., J. Meldolesi, T. A. Milner, T. Satoh, S. Supattapone, and S. H. Snyder. 1989. 'Inositol 1,4,5-trisphosphate receptor localized to endoplasmic reticulum in cerebellar Purkinje neurons', *Nature*, 339: 468-70.

Roy, A., M. J. Cumberland, C. O'Shea, A. Holmes, M. Kalla, K. Gehmlich, T. Geberhiwot, and R. P. Steeds. 2024. 'Arrhythmogenesis in Fabry Disease', *Curr Cardiol Rep*, 26: 545-60.

Ruas, M., L. C. Davis, C. C. Chen, A. J. Morgan, K. T. Chuang, T. F. Walseth, C. Grimm, C. Garnham, T. Powell, N. Platt, F. M. Platt, M. Biel, C. Wahl-Schott, J. Parrington, and A. Galione. 2015. 'Expression of Ca^{2+}-permeable two-pore channels rescues NAADP signalling in TPC-deficient cells', *Embo j*, 34: 1743-58.

Ruas, M., K. Rietdorf, A. Arredouani, L. C. Davis, E. Lloyd-Evans, H. Koegel, T. M. Funnell, A. J. Morgan, J. A. Ward, K. Watanabe, X. Cheng, G. C. Churchill, M. X. Zhu, F. M. Platt, G. M. Wessel, J. Parrington, and A. Galione. 2010. 'Purified TPC isoforms form NAADP receptors with distinct roles for Ca(2+) signaling and endolysosomal trafficking', *Curr Biol*, 20: 703-9.

Saez, J. C., V. M. Berthoud, M. C. Branes, A. D. Martinez, and E. C. Beyer. 2003. 'Plasma membrane channels formed by connexins: their regulation and functions', *Physiol Rev*, 83: 1359-400.

Sanchez-Quintana, D., V. Garcia-Martinez, V. Climent, and J. M. Hurle. 1995. 'Morphological changes in the normal pattern of ventricular myoarchitecture in the developing human heart', *Anat Rec*, 243: 483-95.

Sandow, Jarrod J, Giuseppe Infusini, Laura F Dagley, Rune Larsen, and Andrew I Webb. 2021. 'Simplified high-throughput methods for deep proteome analysis on the timsTOF Pro', *bioRxiv*: 657908.

Schlecker, C., W. Boehmerle, A. Jeromin, B. DeGray, A. Varshney, Y. Sharma, K. Szigeti-Buck, and B. E. Ehrlich. 2006. 'Neuronal calcium sensor-1 enhancement of InsP3 receptor activity is inhibited by therapeutic levels of lithium', *J Clin Invest*, 116: 1668-74.

Schotten, U., S. Verheule, P. Kirchhof, and A. Goette. 2011. 'Pathophysiological mechanisms of atrial fibrillation: a translational appraisal', *Physiol Rev*, 91: 265-325.

Scicchitano, P., S. Carbonara, G. Ricci, C. Mandurino, M. Locorotondo, G. Bulzis, M. Gesualdo, A. Zito, R. Carbonara, I. Dentamaro, G. Riccioni, and M. M. Ciccone. 2012. 'HCN channels and heart rate', *Molecules*, 17: 4225-35.

Seifert, R., G. H. Lushington, T. C. Mou, A. Gille, and S. R. Sprang. 2012. 'Inhibitors of membranous adenylyl cyclases', *Trends Pharmacol Sci*, 33: 64-78.

Setterberg, I. E., C. Le, M. Frisk, J. Li, and W. E. Louch. 2021. 'The Physiology and Pathophysiology of T-Tubules in the Heart', *Front Physiol*, 12: 718404.

Severs, N. J., A. F. Bruce, E. Dupont, and S. Rothery. 2008. 'Remodelling of gap junctions and connexin expression in diseased myocardium', *Cardiovasc Res*, 80: 9-19.
Seyama, I. 1976. 'Characteristics of the rectifying properties of the sino-atrial node cell of the rabbit', *J Physiol*, 255: 379-97.
Shah, J. S., D. A. Hughes, B. Sachdev, M. Tome, D. Ward, P. Lee, A. B. Mehta, and P. M. Elliott. 2005. 'Prevalence and clinical significance of cardiac arrhythmia in Anderson-Fabry disease', *Am J Cardiol*, 96: 842-6.
Sharma, A., G. Li, K. Rajarajan, R. Hamaguchi, P. W. Burridge, and S. M. Wu. 2015. 'Derivation of highly purified cardiomyocytes from human induced pluripotent stem cells using small molecule-modulated differentiation and subsequent glucose starvation', *J Vis Exp*.
Skalhegg, B. S., and K. Tasken. 2000. 'Specificity in the cAMP/PKA signaling pathway. Differential expression,regulation, and subcellular localization of subunits of PKA', *Front Biosci*, 5: D678-93.
Smith, G. L., and D. A. Eisner. 2019. 'Calcium Buffering in the Heart in Health and Disease', *Circulation*, 139: 2358-71.
Soubannier, V., G. L. McLelland, R. Zunino, E. Braschi, P. Rippstein, E. A. Fon, and H. M. McBride. 2012. 'A vesicular transport pathway shuttles cargo from mitochondria to lysosomes', *Curr Biol*, 22: 135-41.
States, D. J., T. F. Walseth, and H. C. Lee. 1992. 'Similarities in amino acid sequences of Aplysia ADP-ribosyl cyclase and human lymphocyte antigen CD38', *Trends Biochem Sci*, 17: 495.
Steinberg, S. F. 1999. 'The molecular basis for distinct beta-adrenergic receptor subtype actions in cardiomyocytes', *Circ Res*, 85: 1101-11.
Steinberg, S. F., and L. L. Brunton. 2001. 'Compartmentation of G protein-coupled signaling pathways in cardiac myocytes', *Annu Rev Pharmacol Toxicol*, 41: 751-73.
Streb, H., R. F. Irvine, M. J. Berridge, and I. Schulz. 1983. 'Release of Ca2+ from a nonmitochondrial intracellular store in pancreatic acinar cells by inositol-1,4,5-trisphosphate', *Nature*, 306: 67-9.
Südhof, T. C., C. L. Newton, B. T. Archer, 3rd, Y. A. Ushkaryov, and G. A. Mignery. 1991. 'Structure of a novel InsP3 receptor', *Embo j*, 10: 3199-206.
Sulke, N., F. Sayers, and G. Y. Lip. 2007. 'Rhythm control and cardioversion', *Heart*, 93: 29-34.
Supattapone, S., P. F. Worley, J. M. Baraban, and S. H. Snyder. 1988. 'Solubilization, purification, and characterization of an inositol trisphosphate receptor', *J Biol Chem*, 263: 1530-4.
Sutherland, E. W., and T. W. Rall. 1958. 'Fractionation and characterization of a cyclic adenine ribonucleotide formed by tissue particles', *J Biol Chem*, 232: 1077-91.
Swedberg, K., M. Komajda, M. Böhm, J. S. Borer, I. Ford, A. Dubost-Brama, G. Lerebours, and L. Tavazzi. 2010. 'Ivabradine and outcomes in chronic heart failure (SHIFT): a randomised placebo-controlled study', *Lancet*, 376: 875-85.
Taylor, C. W., A. A. Genazzani, and S. A. Morris. 1999. 'Expression of inositol trisphosphate receptors', *Cell Calcium*, 26: 237-51.
Ter Huurne, M., B. L. Parker, N. Q. Liu, E. L. Qian, C. Vivien, K. Karavendzas, R. J. Mills, J. T. Saville, D. Abu-Bonsrah, A. F. Wise, J. E. Hudson, A. S. Talbot, P. F. Finn, P. G. V. Martini, M. Fuller, S. D. Ricardo, K. I. Watt, K. M. Nicholls, E. R. Porrello, and D. A. Elliott. 2023. 'GLA-modified RNA treatment lowers GB3 levels in iPSC-derived cardiomyocytes from Fabry-affected individuals', *Am J Hum Genet*, 110: 1600-05.
Tinker, A., M. Finlay, M. Nobles, and A. Opel. 2016. 'The contribution of pathways initiated via the Gq\11 G-protein family to atrial fibrillation', *Pharmacol Res*, 105: 54-61.
Valks, D. M., S. A. Cook, F. H. Pham, P. R. Morrison, A. Clerk, and P. H. Sugden. 2002. 'Phenylephrine promotes phosphorylation of Bad in cardiac myocytes through the extracellular signal-regulated kinases 1/2 and protein kinase A', *J Mol Cell Cardiol*, 34: 749-63.
van Gorp, P. R. R., S. A. Trines, D. A. Pijnappels, and A. A. F. de Vries. 2020. 'Multicellular In vitro Models of Cardiac Arrhythmias: Focus on Atrial Fibrillation', *Front Cardiovasc Med*, 7: 43.
Verma, K. P., and M. Wong. 2019. 'Atrial fibrillation', *Aust J Gen Pract*, 48: 694-99.
Vinogradova, T. M., A. E. Lyashkov, W. Zhu, A. M. Ruknudin, S. Sirenko, D. Yang, S. Deo, M. Barlow, S. Johnson, J. L. Caffrey, Y. Y. Zhou, R. P. Xiao, H. Cheng, M. D. Stern, V. A. Maltsev, and E. G. Lakatta. 2006. 'High basal protein kinase A-dependent phosphorylation drives rhythmic internal Ca2+ store oscillations and spontaneous beating of cardiac pacemaker cells', *Circ Res*, 98: 505-14.
Wang, J., E. S. Allgeyer, G. Sirinakis, Y. Zhang, K. Hu, M. D. Lessard, Y. Li, R. Diekmann, M. A. Phillips, I. M. Dobbie, J. Ries, M. J. Booth, and J. Bewersdorf. 2021. 'Implementation of a 4Pi-SMS super-resolution microscope', *Nat Protoc*, 16: 677-727.
Wang, X., X. Zhang, X. P. Dong, M. Samie, X. Li, X. Cheng, A. Goschka, D. Shen, Y. Zhou, J. Harlow, M. X. Zhu, D. E. Clapham, D. Ren, and H. Xu. 2012. 'TPC proteins are phosphoinositide- activated sodium-selective ion channels in endosomes and lysosomes', *Cell*, 151: 372-83.
Wang, Y., Q. Shi, M. Li, M. Zhao, R. Reddy Gopireddy, J. P. Teoh, B. Xu, C. Zhu, K. E. Ireton, S. Srinivasan, S. Chen, P. J. Gasser, J. Bossuyt, J. W. Hell, D. M. Bers, and Y. K. Xiang. 2021. 'Intracellular β(1)-

Adrenergic Receptors and Organic Cation Transporter 3 Mediate Phospholamban Phosphorylation to Enhance Cardiac Contractility', *Circ Res*, 128: 246-61.
Wayman, G. A., S. Impey, Z. Wu, W. Kindsvogel, L. Prichard, and D. R. Storm. 1994. 'Synergistic activation of the type I adenylyl cyclase by Ca2+ and Gs-coupled receptors in vivo', *J Biol Chem*, 269: 25400-5.
Wijffels, M. C., C. J. Kirchhof, R. Dorland, and M. A. Allessie. 1995. 'Atrial fibrillation begets atrial fibrillation. A study in awake chronically instrumented goats', *Circulation*, 92: 1954-68.
Winbo, A., S. Ramanan, E. Eugster, S. Jovinge, J. R. Skinner, and J. M. Montgomery. 2020. 'Functional coculture of sympathetic neurons and cardiomyocytes derived from human-induced pluripotent stem cells', *Am J Physiol Heart Circ Physiol*, 319: H927-h37.
Wong, S. T., J. Athos, X. A. Figueroa, V. V. Pineda, M. L. Schaefer, C. C. Chavkin, L. J. Muglia, and D. R. Storm. 1999. 'Calcium-stimulated adenylyl cyclase activity is critical for hippocampus-dependent long-term memory and late phase LTP', *Neuron*, 23: 787-98.
Wu, Z. L., S. A. Thomas, E. C. Villacres, Z. Xia, M. L. Simmons, C. Chavkin, R. D. Palmiter, and D. R. Storm. 1995. 'Altered behavior and long-term potentiation in type I adenylyl cyclase mutant mice', *Proc Natl Acad Sci U S A*, 92: 220-4.
Xiao, R. P. 2001. 'Beta-adrenergic signaling in the heart: dual coupling of the beta2-adrenergic receptor to G(s) and G(i) proteins', *Sci STKE*, 2001: re15.
Xu, H., and D. Ren. 2015. 'Lysosomal physiology', *Annu Rev Physiol*, 77: 57-80.
Yamda, J., T. Ohkusa, T. Nao, T. Ueyama, M. Yano, S. Kobayashi, K. Hamano, K. Esato, and M. Matsuzaki. 2001. 'Up-regulation of inositol 1,4,5 trisphosphate receptor expression in atrial tissue in patients with chronic atrial fibrillation', *J Am Coll Cardiol*, 37: 1111-9.
Younes, A., A. E. Lyashkov, D. Graham, A. Sheydina, M. V. Volkova, M. Mitsak, T. M. Vinogradova, Y. O. Lukyanenko, Y. Li, A. M. Ruknudin, K. R. Boheler, J. van Eyk, and E. G. Lakatta. 2008. 'Ca(2+) - stimulated basal adenylyl cyclase activity localization in membrane lipid microdomains of cardiac sinoatrial nodal pacemaker cells', *J Biol Chem*, 283: 14461-8.
Yuan, Y., V. Arige, R. Saito, Q. Mu, G. C. Brailoiu, G. J. S. Pereira, S. R. Bolsover, M. Keller, F. Bracher, C. Grimm, E. Brailoiu, J. S. Marchant, D. I. Yule, and S. Patel. 2024. 'Two-pore channel-2 and inositol trisphosphate receptors coordinate Ca(2+) signals between lysosomes and the endoplasmic reticulum', *Cell Rep*, 43: 113628.
Yuan, Y., J. Zhao, Y. Gong, D. Wang, X. Wang, F. Yun, Z. Liu, S. Zhang, W. Li, X. Zhao, L. Sun, L. Sheng, Z. Pan, and Y. Li. 2018. 'Autophagy exacerbates electrical remodeling in atrial fibrillation by ubiquitin-dependent degradation of L-type calcium channel', *Cell Death Dis*, 9: 873.
Zaccolo, M. 2009. 'cAMP signal transduction in the heart: understanding spatial control for the development of novel therapeutic strategies', *Br J Pharmacol*, 158: 50-60.
———. 2011. 'Spatial control of cAMP signalling in health and disease', *Curr Opin Pharmacol*, 11: 649-55.
Zaccolo, M., A. Zerio, and M. J. Lobo. 2021. 'Subcellular Organization of the cAMP Signaling Pathway', *Pharmacol Rev*, 73: 278-309.
Zhang, F., G. Zhang, A. Y. Zhang, M. J. Koeberl, E. Wallander, and P. L. Li. 2006. 'Production of NAADP and its role in Ca2+ mobilization associated with lysosomes in coronary arterial myocytes', *Am J Physiol Heart Circ Physiol*, 291: H274-82.
Zhang, S. X., J. P. Zhang, D. L. Fletcher, R. T. Zoeller, and G. Y. Sun. 1995. 'In situ hybridization of mRNA expression for IP3 receptor and IP3-3-kinase in rat brain after transient focal cerebral ischemia', *Brain Res Mol Brain Res*, 32: 252-60.
Zhao, Z., G. J. Babu, H. Wen, N. Fefelova, R. Gordan, X. Sui, L. Yan, D. E. Vatner, S. F. Vatner, and L. H. Xie. 2015. 'Overexpression of adenylyl cyclase type 5 (AC5) confers a proarrhythmic substrate to the heart', *Am J Physiol Heart Circ Physiol*, 308: H240-9.
Zhao, Z. H., H. C. Zhang, Y. Xu, P. Zhang, X. B. Li, Y. S. Liu, and J. H. Guo. 2007. 'Inositol-1,4,5-trisphosphate and ryanodine-dependent Ca2+ signaling in a chronic dog model of atrial fibrillation', *Cardiology*, 107: 269-76.
Zhou, P., and W. T. Pu. 2016. 'Recounting Cardiac Cellular Composition', *Circ Res*, 118: 368-70.
Zhu, Y., and T. M. Nosek. 1991. 'Inositol trisphosphate enhances Ca2+ oscillations but not Ca(2+)-induced Ca2+ release from cardiac sarcoplasmic reticulum', *Pflugers Arch*, 418: 1-6.
Zong, X., M. Schieder, H. Cuny, S. Fenske, C. Gruner, K. Rötzer, O. Griesbeck, H. Harz, M. Biel, and C. Wahl-Schott. 2009. 'The two-pore channel TPCN2 mediates NAADP-dependent Ca(2+)-release from lysosomal stores', *Pflugers Arch*, 458: 891-9.